UCRL-53903
Distribution Category UC-412

UCRL--53903

DE89 013887

Effects of Trace Gases on Global Atmospheric Chemical and Physical Processes

Douglas Edward Kinnison

(Ph.D. Thesis)

Manuscript date: May 26, 1989

LAWRENCE LIVERMORE NATIONAL LABORATORY
University of California • Livermore, California • 94550

Effects of Trace Gases on Global Atmospheric Chemical and Physical Processes

By

Douglas Edward Kinnison

B.S. (Colorado State University) 1981

DISSERTATION

Submitted in partial satisfaction of the requirements for the degree of

DOCTOR OF PHILOSOPHY

in

CHEMISTRY

in the

GRADUATE DIVISION

of the

UNIVERSITY OF CALIFORNIA at BERKELEY

Approved: Harold Johnston April 25, 1989

Chair Date

April 25 1989

April 25 1989

****

To my parents,

Shirley and Edward,

for their love and support.

Acknowledgements

I would like to thank the many persons who supported my research at the University of California in Berkeley.

I am extremely appreciative of Professor Harold Johnston's guidance and support supplied in graduate school. Due to Professor Johnston's expanded research interests in many non-mainstream areas of physical chemistry, I had the opportunity to investigate the field of atmospheric chemistry.

I am also especially grateful to Dr. Donald Wuebbles for his support and encouragement in my research effort at Lawrence Livermore National Laboratory. His insight and comments were most helpful in writing this work.

I would also like to thank the following coworkers and friends for their support at Lawrence Livermore National Laboratory: Dr. Keith Grant for his patience in answering my many scientific and computer-related questions, Ray Tarp for his programming contributions and Julie Bagorio for her many hours of preparation on the manuscript. I also thank Dr. Peter Connell, Mabel Moore, and Mary Ann Mansigh for their assistance.

Special thanks to my colleagues at Berkeley, Phil Hunter, Ken Patten, Wade Sisk, Dr. Baek Oh, Dr. Anthony Young, Dr. Diane Swanson Waterman, Chip Miller, Bong Soo Kim, and Joel Burley, for their numerous contributions to my education.

The work at the University of California and Lawrence Berkeley was supported by the Director, Office of Energy Research, Office of Basic Energy Sciences, Chemical Sciences Division of the U.S. Department of Energy under Contract No. DE-AC03-76SF00098. Work at Lawrence Livermore National Laboratory

was performed under the auspices of the U.S. Department of Energy, under contract W-7405-ENG-48. and was supported in part by the Department of Energy Carbon Dioxide Research Division and by the National Aeronautics and Space Administration.

Table of Contents

Effects of Trace Gases on Global Atmospheric Chemical and Physical Processes

by

Douglas Edward Kinnison

Abstract

This study examines the effects that increased emissions of anthropogenic and naturally-occuring trace gases have on the chemical and physical processes in the global atmosphere. The Lawrence Livermore National Laboratory (LLNL) one- and two-dimensional chemical-radiative-transport models of the troposphere and stratosphere, are used to calculate the net effects that variations in these trace gases, either individually, or taken together have on the ozone distribution and temperature structure.

Using the LLNL one-dimensional model, calculations are made that include large changes of NO_x, Cl_x, and HO_x. The object was to see if any interesting or unexpected effects could be found. The nitrous oxide boundary value is varied from 1/4 to 8 times the reference (1960) value of 300 ppbv. Stratospheric Cl_x is varied from 0 to 22 ppbv. Special atmospheres are considered in which all HO_x, NO_x, and Cl_x, or combinations of these are omitted from the reference atmosphere.

A sensitivity study is carried out using the the LLNL one- and two-dimensional chemical-radiative-transport models to examine possible effects of future aircraft NO_x emissions on stratospheric ozone. A broad range in magnitude, altitude, and latitude of the assumed NO_x emissions is examined for various background Cl_x values. The change in column-ozone is calculated for each sensitivity scenario relative to a reference atmosphere. Comparisons between the one- and two-dimensional

models are discussed. The effect on the ozone-column due to variations in the eddy diffusion representation (K_{yy} and K_{zz}) is shown for one aircraft scenario.

The emissions and atmospheric concentrations of several trace gases (N_2O, CH_4, CO_2, $CFCl_3$, CF_2Cl_2, CCl_4, and CH_3CCl_3), plus the effect of both the 11 year solar sunspot cycle and NO_x produced from the nuclear test series of the late 1950's and early 1960's are examined using the LLNL two-dimensional model. Changes in ozone-column, local ozone, temperature profiles, and various other species distributions are compared to observations made from the ground, balloons, aircraft, rockets, and satellites. By modeling the emissions of these trace gases on the chemical and physical processes in the global atmosphere, the potential accuracy of the two-dimensional model can be estimated and the prospects of future perturbations can be more realistically assessed.

The effect of the eddy diffusion representation (K_{yy} and K_{zz}) on the two-dimensional transport of trace constituents is investigated, using analyzed carbon-14 and strontium-90 data from the nuclear test series in the late 1950's and early 1960's. Here various K_{yy} and K_{zz} values, as a function of latitude and altitude, were used to see what values best represented or corresponded with short and long term transport of the above two tracers. In addition, the model was used to help verify which of the two available estimates for bomb stabilization cloud height, Seitz [1968] or Peterson [1970], better represents the available data. The effect of varying the eddy transport is examined in terms of model-calculated change in O_3 column distributions. The best eddy diffusion representation derived from the tracer study gave the best ozone-column distribution relative to observational data.

Chapter 1: Introduction

The chemical composition of the global atmosphere is changing due to both natural and anthropogenic causes. Since the industrial revolution, mankind has injected increasingly large amounts of various trace gases. Currently, the most important of these trace gases, in respect to their effects on the global ozone distribution and the global temperature structure, include: carbon dioxide (CO_2); methane (CH_4); nitrous oxide (N_2O); and various chlorocarbons (ClC's) such as $CFCl_3$ (CFC-11), CF_2Cl_2 (CFC-12), carbon tetrachloride (CCl_4), and methyl chloroform (CH_3CCl_3) [WMO, 1985].

The largest relative increases of trace gas concentrations in recent decades are found in the ClC's, which have directly increased the total odd chlorine (Cl_y = $Cl + ClO + HCl + HOCl + ClONO_2 + ClNO_2$) in the upper stratosphere from a estimated 1950 values of 0.8 ppbv to a current level of 2.6 ppbv. This three fold increase in total chlorine is due completely to man-made sources. Present rates of increase for these gases per year are: CO_2 (0.4%), CH_4 (1–2%), N_2O (0.2–0.3%), $CFCl_3$ (5%), CF_2Cl_2 (5%), CCl_4 (1%), and CH_3CCl_3 (5%) [Wang et al. 1986; Watson et al., 1988; Wuebbles et al., 1989].

The complete chemical and physical effects of these traces gases on the ozone distribution, temperature structure, and consequently climate of the global atmosphere, are currently unresolved. In this investigation, Chapters 3, 4, 5, and 6 use both one- and two-dimensional chemical-radiative-transport models of the global atmosphere to calculate the net effects that variations in trace gases, either individually, or taken together have on the ozone distribution and temperature structure in the troposphere and stratosphere.

1.1 The Troposphere and Stratosphere

The Earth's atmosphere is a thin layer of gases, predominately made up of N_2 (78.1 percent) and O_2 (20.9 percent). In addition, there are many trace gases that contribute significantly to the temperature structure and climate of the atmosphere. It is convenient to divide the earths atmosphere into layers based on thermal characteristics [Figure 1.1]. The two lowest layers, the troposphere and stratosphere, are of primarily interest in this study. The troposphere is characteristic of convective motion, with a temperature gradient that decreases with altitude. The stratosphere, which extends up to approximately 50 km, has a temperature profile that increases with altitude from the tropopause up to the stratopause. This increase of temperature with height suppresses vertical mixing by convection. Ozone, through the absorption of ultraviolet radiation, acts as a heat source, which sets up the vertical temperature structure of the stratosphere. Ozone also absorbs infrared radiation and is therefore a greenhouse gas, which allows visible solar radiation to penetrate to the surface while absorbing long-wave emission from the surface. Therefore, understanding the stability of the ozone layer, which has a maximum concentration between 20 and 25 km (depending on latitude), is important in assessing the impact of anthropogenic emissions of trace gases on biological and climatic systems.

1.2 Biological Effects of Decreasing Ozone

Decreasing the total column of ozone due to natural or anthropogenic causes would increase the ultraviolet flux at the Earth's surface. This could have adverse effects on human health and aquatic and terrestrial ecosystems. Exposure to radiation, between 290 and 320 nanometers (UV-B), has been suggested to cause nonmelanoma type squamous cell and basal cell skin cancer. Currently there

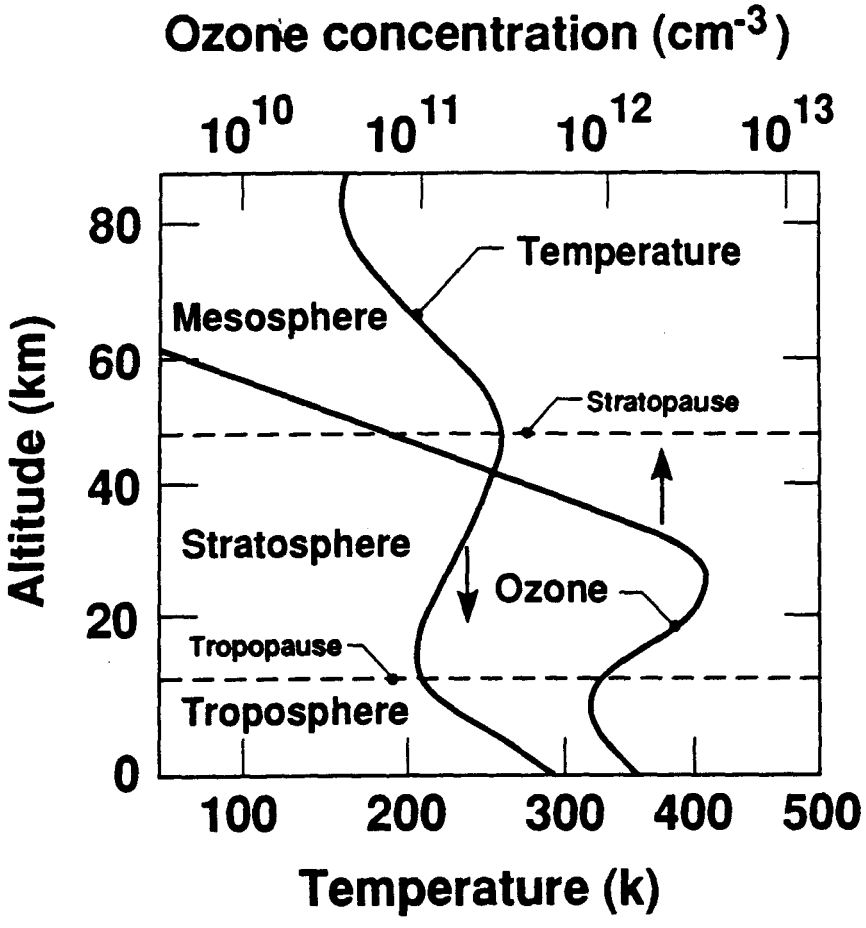

Figure 1.1. The ozone layer has a peak concentration in the lower stratosphere between about 20 to 25 kilometers altitude at mid-latitude. In the troposphere, temperature decreases with altitude. In the stratosphere, temperature increases with altitude. Source: WMO [1985].

are over 400,000 new cases of these skin cancers each year in the United States. Studies indicate that for every 1 percent increase in UV-B (which corresponds to less than 1 percent decrease in column ozone), nonmelanoma skin cancer cases would increase by about 1 to 3 percent, with the mortality for these forms of cancer corresponding to 1 percent of the total cases. A less common form of skin cancer, cutaneous malignant melanoma, is currently increasing at 25,000 cases

per year, with 5000 fatalities in the United States alone in 1987. Recent studies indicate that a decrease of 1 percent in UV-B could cause an increase from 0.5 to 1 percent in cutaneous malignant melanoma. In addition to skin cancer increases, cataracts on the eye may also increase due to increases in UV-B. Increases of UV-B have also shown in animals to depress the immune system. Studies indicate that phytoplankton, zooplankton, and the larvae of many fishes, are susceptible to harm from increases in UV-B. Since about one half of the world's protein is derived from marine species, the impact of a decrease in the species that make up the lower food chain, could cause detrimental effects on all forms of life. For a summary of the effects of increasing UV-B, see NAS [1982], NAS [1984], and EPA [1987].

1.3 Climatic Effects from Trace Gases

Since CO_2 and other radiatively active trace gases are increasing, changes in the tropospheric and stratospheric temperature distribution are expected. For doubling of CO_2, climate models estimate the increase of surface temperature to be 1.5–4.5° K [Charney, 1979; Smagorinsky, 1982; WMO, 1985]. In addition, the combined effects of the other trace gases may equal the estimated surface temperature increase due to CO_2 alone [Ramanathan et al., 1987]. In the stratosphere, cooling is expected from the greenhouse effect, which will impact ozone, by decreasing the rate at which temperature dependent ozone reducing processes occur, therefore tending to increase the concentration of ozone. However, since ozone is radiatively active in the visible region (Chappius band, 450–850 nanometers), increasing its concentration will have the opposite effect, decreasing the solar flux at the surface, therefore tending to decrease the temperature at the surface [Ramanathan et al., 1987]. These types of radiative interactions, in addition to

chemical and dynamical feedbacks, make simple prediction of increases in trace gases on climate difficult.

1.4 History of Trace Gases and their Effects on Ozone

The chemical mechanisms that influence the concentration of ozone due to trace gas variations have been examined and updated throughout the twentieth century with a large majority of theories being put forth in the last two decades.

Ozone was first measured accurately in the atmosphere by Fabry and Buisson [1913, 1921] and later by Dobson [1926]. Dobson developed an ultraviolet spectrometer that measured the total ozone column routinely. He established [1929] a network of stations at various latitudes; todays much expanded network still uses many of these same stations [NASA-WMO, 1989].

In 1930 Chapman [1930a,b,c] proposed that ozone was produced by photochemical processes. Specifically by the photolysis of molecular oxygen, producing oxygen atoms, which further react with molecular oxygen to produce ozone.

$$O_2 + h\nu(< 244 \text{ nm}) \rightarrow O + O \quad (1)$$

$$O + O_2 + M \rightarrow O_3 + M \text{ (twice)} \quad (2)$$

$$\text{Net : } 3O_2 \rightarrow 2O_3$$

Reactions (3) and (2), interconvert O and O_3, and (3) is generally not a destructive process with respect to O_3, since the O atom can rapidly produce O_3 by reaction (2).

$$O_3 + h\nu \rightarrow O + O_2 \quad (3)$$

$$O + O_2 + M \rightarrow O_3 + M \quad (2)$$

Net : Null Cycle

Odd oxygen loss reaction, (4) and (5) are:

$$O + O_3 \rightarrow 2O_2 \quad (4)$$

$$O + O + M \rightarrow O_2 + M \quad (5)$$

in the stratosphere reaction (5) is very slow, leaving reaction (4) as the primary odd oxygen loss reaction in the Chapman family.

Wulf and Deming [1936] calculated the ozone profile using a steady state photochemical model which assumed a solar intensity that corresponded to a black body temperature of 6000° K. They had one adjustable parameter, the ratio of the rate constants for reactions (2) and (4), which was varied to fit the experimentally observed column sum (obtained from the Dobson stations). Using this ratio and using the available absorption coefficient for O_2 (between 170 and 210 nm), they were able to calculate an ozone vertical profile. Three years earlier, Gotz [1934] developed the Umkehr method to measure the ozone vertical profile. The results of the Umkehr method showed ozone to have a vertical profile that peaked approximately at 25 km at mid-northern latitudes. Considering the uncertaintities in the rate constants, photo-absorption cross sections and solar irradiances, the calculated versus experimental ozone vertical profiles were in good agreement. In the 1950's, U-2 rockets were used for the first time to measure directly the solar intensities throughout the visible and ultraviolet. It was found that the solar

intensity could not be fit by a blackbody temperature profile of 6000° K. With this discrepancy in the blackbody temperature and additional changes in reaction coefficients and photolysis cross sections (for O_2 and O_3), experimentally observed vertical profiles of ozone were found to be less than the calculated values. In fact, the calculated ozone profile had twice as large an ozone column as that observed.

In the mean time, Bates and Nicolet [1950] introduced the photochemistry of water vapor.

$$H_2O + h\nu \longrightarrow OH + H \tag{6}$$

McGrath and Norrish [1960] experimentally showed that the hydroxyl radical could also be produced though the reactions of water vapor with excited oxygen atom.

$$O(^1D) + H_2O \longrightarrow 2OH \tag{7}$$

In laboratory experiments, the free radicals obtained from water vapor (H, OH, HO_2), were found to catalytically destroy ozone. Hampson [1964] and Hunt [1966] proposed that the following photochemical reactions by the free radicals based on water might be responsible for the observed low ozone.

$$HO + O_3 \rightarrow HO_2 + O_2 \tag{8}$$

$$HO_2 + O_3 \rightarrow HO + 2O_2 \tag{9}$$

$$\text{Net}: \quad 2\ O_3 \rightarrow 3\ O_2$$

$$HO + O_3 \rightarrow HO_2 + O_2 \quad (10)$$

$$HO_2 + O \rightarrow HO + O_2 \quad (11)$$

$$\text{Net : } O_3 + O \rightarrow 2\ O_2$$

$$HO + O \rightarrow H + O_2 \quad (12)$$

$$H + O_3 \rightarrow HO + O_2 \quad (13)$$

$$\text{Net : } O_3 + O \rightarrow 2\ O_2$$

Hunt [1966] modeled the atmosphere using twenty-eight photochemical reactions which corresponded to the Chapman mechanism plus the water reactions. He found that by adjusting the values for the rate constants of reaction (9) and (10), that a theoretical vertical ozone profile could be found to match an experimentally obtained profile. However, when more accurate values for the rate constants in the above mechanism became available, the theoretical value for both the ozone profile and total column still exceeded observational data.

Crutzen [1969] showed that Hunt's [1966] and Hampson's [1965] work did not adequately explain the ozone profile between 30 and 35 km.

Murcray et al. [1968] and Rhine et al. [1969] measured the concentration of nitric acid, HNO_3, as a few parts per billion in the stratosphere. Expanding on this, Crutzen [1970] reasoned that the observed HNO_3 implied enough NO and NO_2 to support a catalytic cycle that would reduce ozone more efficiently than the HO_x reactions:

$$NO + O_3 \rightarrow NO_2 + O_2 \quad (14)$$

$$NO_2 + O \rightarrow NO + O_2 \quad (15)$$

$$\text{Net}: \; O + O_3 \rightarrow NO + O_2$$

and Crutzen [1971], extending ideas of Bates and Hayes [1967] and Nicolet [1965], showed that tropospheric nitrous oxide, N_2O, could supply enough NO_x in the stratosphere to reduce ozone to about the observed value.

Johnston [1971] pointed out the potential threat of odd nitrogen injections from Super Sonic Transport's (SST's) flying in the stratospheric region of the atmosphere.

Stolarski and Cicerone [1974] realized that chlorine, if in high enough concentrations, also could be a important catalytic ozone destroyer.

$$Cl + O_3 \rightarrow ClO + O_2 \quad (12)$$

$$ClO + O \rightarrow Cl + O_2 \quad (13)$$

$$\text{Net}: \; O_3 + O \rightarrow 2\, O_2$$

Molina and Roland [1974] discovered that chlorocarbons, because of their atmospheric lifetimes, could penetrate into and dissociate within the stratosphere. The released chlorine could then react catalytically with ozone.

Wofsy et al. [1975] proposed that bromine, like chlorine, would be an effective catalytic ozone reducing agent in the stratosphere.

1.5 Brief Overview

Chapter 2: Atmospheric Models and Their Treatment of Physical and Chemical Processes

The chemical and physical structures of the LLNL two-dimensional chemical-radiative-transport models are described.

Chapter 3: Ozone Calculations with Large Nitrous Oxide and Chlorine Changes

The purpose of this study is broadly to reinvestigate total odd nitrogen ($NO + NO_2 + NO_3 + HNO_3 + HNO_4 + 2 \times N_2O_5 + HONO + ClONO_2$) and total odd chlorine ($Cl + ClO + HCl + HOCl + ClONO_2 + ClNO_2$) interactions relative to ozone control in the stratosphere, using the long-established LLNL one-dimensional model. This is accomplished by varying the surface boundary value of N_2O (by, 0.25, 0.50, 1, 2, 4, 8 times present value) for various odd chlorine conditions (1.1, 3.1, 7.9, 14.7 and 21.4 ppbv). In addition, "special atmospheres" were created that represented the Chapman reactions, O_x family, plus one or combinations of the following families: HO_x, NO_x, and Cl_x. From this approach, conclusions on the mechanisms that control ozone depletion in the stratosphere were suggested.

Chapter 4: Effects on Ozone from Aircraft Emissions

There recently has been renewed interest in the development of faster and more efficient aircraft for intercontiental passenger flights [e.g., First International Conference on Hypersonic Flight in the 21st Century, University of North Dakota, Grand Forks, ND, September 1988). A sensitivity study is carried out using the LLNL one- and two-dimensional chemical-radiative-transport models of the global atmosphere to examine possible effects of future aircraft NO_x (where NO_x is the amount of odd nitrogen injected at a given altitude in the form of NO_2) emissions on stratospheric ozone. Like Chapter 3, the NO_x emissions are injected

for the same background Cl_y values (one-dimensional model only) and the sensitivity towards ozone reduction is obtained. Using the two-dimensional model, a broad range in magnitude, altitude, and latitude of the assumed NO_x emissions is examined.

Chapter 5: Trends in Stratospheric Ozone

Based on a premise similar to the study by Wuebbles (1983, using the LLNL one-dimensional model), the trends in ozone are modeled using the LLNL two-dimensional chemical-radiative-transport model, from 1950 to present. The change in trace gases CO_2, N_2O, CH_4, $CFCl_3$, CF_2Cl_2, CCl_4, and CH_3CCl_3, plus the effect of both the 11 year solar sunspot cycle and NO_x from the nuclear test series of the late 1950's and and early 1960's are included. Changes in column (total number of molecules cm^2) ozone, local ozone (amount at a given altitude in molecules cm^3), temperature profiles, and various other species distributions (e.g., HCl, HNO_3, Cl_y, NO_y, CH_4, and N_2O) are compared to observations from ground, balloon, airplane, rocket, and satellite data bases. For one case, the model runs into the future, terminating on January 1, 1991.

Chapter 6: Tracer Study

The purpose of this study is to help clarify the understanding of transport processes in the LLNL two-dimensional chemical-radiative-transport model using recently reanalyzed carbon-14 and strontuim-90 data from the nuclear test series in the late 1950's and early 1960's. Variations in the eddy diffusion representation (K_{yy} and K_{zz}) are selected. The model calculated distribution of carbon-14 and strontium-90, using a particular eddy diffusion case, are compared to the observed carbon-14 and strontium-90 distributions, supplied by Johnston [1989], at given, times between 1963–1971, latitudes (typically four), and altitudes (from the surface

to 20–33 km). For six eddy diffusion representations, the column O_3 distribution (latitude versus time) is calculated. In addition, the sensitivity of an aircraft perturbation (1.8 Mt yr^{-1} as NO_2, injected globally at 19.5 km) is studied using two eddy diffusion representations.

Chapter 7: Summary and Conclusions

Chapter 8: References

Appendix A: For Chapter 5

Appendix B: For Chapter 6

Chapter 2: Atmospheric Models and Their Treatment of Physical and Chemical Process

2.1 Introduction

Atmospheric chemical-radiative-transport models, one- and two-dimensional, are used in this study to investigate the role trace gases have on both chemical and physical process that determine the distribution of global atmospheric ozone and other trace constituents. The models used at Lawrence Livermore National Laboratory are well recognized as important tools in the study of atmospheric chemical and physical processes. The one-dimensional model was initiated in the early 1970's [Chang et al., 1974] and, in its present state, is still a useful tool for studies of atmospheric processes [Wuebbles, 1983; Wuebbles et al., 1983; WMO, 1985; Hammitt et al., 1987; Kinnison et al., 1988b,c]. The two-dimensional model, which has supplanted the one-dimensional model as the primary atmospheric model for many research studies, because of its more detailed representation of atmospheric transport processes, was developed more recently [Wuebbles et al., 1987]. Three-dimensional chemical-radiative-transport models are generally not economically feasible at this time for such research because of the high computational expense. [WMO 1985, Chapters 6 and 12].

When describing the physical processes that make up these models, first consider a quasi-conserved constituent whose mixing ratio μ, satisfies the equation,

$$\frac{d\mu_i}{dt} = \Gamma_i \tag{1}$$

where Γ_i represents all sources and sinks, $\mu_i = c_i\rho^{-1}$, c_i is the concentration of species i, and ρ =concentration of air. After applying the total time derivative

or material derivative [e.g. see Brasser and Solomon, 1984], to equation (1), and assuming that species c_i is conserved, leaves what is generally called the trace constituent continuity equation:

$$\frac{\partial c_i}{\partial t} + \nabla \cdot \vec{F}_i(c_i, \vec{x}, t) = P_i\{c, J(\vec{x}, t, c), k\,T(\vec{x}, t), \rho]\} - L_i\{c, J(\vec{x}, t, c), k\,T(\vec{x}, t), \rho\}c_i - S_i(\vec{x}, t), \quad (2)$$

where $c_i = c_i(\vec{x}, t)$ is the concentration of the ith chemical constituent; $\vec{F}_i$ is the transport flux of c_i; P_i and $L_i c_i$ are the chemical and photochemical production and loss processes of c_i, respectively; S_i is other sources and sinks of c_i (e.g., aircraft emissions); J represents the photodissociation coefficients; k represents chemical reaction rate constants; ρ is the ambient air concentration. These variables are defined at a spatial position $\vec{x}$ at time t [e.g. see Chang and Duewer, 1979].

In the following description of the LLNL one- and two-dimensional chemical-radiative-transport models, the $\vec{F}$ term and the dimensionality are theoretically the only differences. For three dimensional models, the transport flux is derived in a self-consistent manner, without the uncertainties involved in parameterized transport coefficients.

2.2 One-Dimensional Model

Historically, one-dimensional models have been the principal theoretical tool used to study the effects that variations in trace gases have on both atmospheric composition and temperature structure. The details of the LLNL one-dimensional chemical-radiative-transport model of the troposphere and stratosphere have been presented previously [Chang et al., 1974; Luther et al., 1979; Wuebbles, 1981;

Wuebbles et al., 1983; Connell and Wuebbles, 1986]. Mathematically, the chemical and physical processes are represented in the following differential equation (continuity equation).

$$\frac{\partial c_i}{\partial t} = \frac{\partial}{\partial z}\left[K_z(z)\rho\frac{\partial}{\partial z}\left(\frac{c_i}{\rho}\right)\right] + P_i(c) - L_i(c)c_i + S_i \qquad (3)$$

where: z = vertical coordinate
c_i = atmospheric constitutent
ρ = air concentration
$K_z(z)$ = eddy diffusion coefficient
$P_i(c)$ = chemical and photochemical production rates
$L_i(c)\ c_i$ = chemical and photochemical loss rates
S_i = additional sources and sinks (e.g., aircraft emissions)

The one-dimensional model calculates the vertical distribution of 37 species [$O(^3P)$, O_3, NO, NO_2, N_2O, HNO_3, OH, HO_2, H_2O_2, Cl, $ClONO_2$, ClO, $ClNO_2$, HCl, NO_3, N_2O_5, HONO, HNO_4, HOCl, HCO, CH_2O, CH_3, CH_3OOH, CH_3O, CH_4, H_2, CO, H_2O, CH_3Cl, CCl_4, CH_3CCl_3, $CFCl_3$, CF_2Cl_2, CHF_2Cl, $CFCl_2CF_2Cl$, CF_2ClCF_2Cl, CF_2ClCF_3] as a function of boundary conditions and time. Three species (H, N, and $O(^1D)$) are assumed to be in instantaneous steady state. The vertical distribution of N_2, O_2, H_2O, and H_2 are assumed to be constant throughout the calculations. The lower boundary conditions for each specie are either fixed concentrations or fluxes at the surface. A constant flux boundary condition is assumed at the upper boundary of the model (zero flux corresponds to a fixed mixing ratio across the upper boundary).

The one-dimensional model atmosphere is divided up into 44 vertical layers which extend from the surface up to 56 km. There are 119 chemical reactions and 46 photochemical reactions included in the model. The chemical and photochemical rate constants are based on those recommended by the NASA Panel for Data Evaluation [DeMore et al., 1985, 1987].

The radiation submodel consists of absorption by O_2, O_3, and NO_2 in the ultraviolet and visible regions of solar spectrum, with longwave interaction of O_2, CO_2, and H_2O [see Wuebbles, 1983]. Multiple scattering effects are calculated in each layer [Luther et al., 1978]. The U.S. Standard Atmosphere [1976] temperature profile was used, except when the temperature feedback option was incorporated. Temperature feedback was included in the calculations presented in chapters 4 and 5.

The continuity equation for each individual species is solved using a variable time-step, variable order, implicit technique for solving stiff numerical systems with strict error control [Gear, 1968; Hindmarsh, 1972, 1976; and Chang, 1974]. The concentration of each species is calculated in each layer for every time step.

Transport of trace species is controlled by an empirically based eddy diffusion (K_z) representation (Figure 2.1). The K_z profile was developed by Wuebbles [1983], to represent hemispheric or globally-averaged transport in the vertical direction. This profile was based on various long-lived chemical tracers (e.g., N_2O, CF_2Cl_2, $CFCl_3$, and carbon-14).

A diurnally averaged version of the one-dimensional model was developed at LLNL [see Luther et al., 1979; Wuebbles, 1981] that is consistent with the full diurnal model. The diurnal model is used to generate species profiles (for a 24 hour period) for comparison with measurements and for short time perturbations (such as solar eclipse), and the diurnal-average model is used for perturbation and sensitivity studies involving long time integrations. For all applications in the following chapters, the diurnally averaged version of the model was used.

2.3 Two-Dimensional Model

Two-dimensional, zonally-averaged, models are quickly replacing the one-dimensional model in all but the extreme cases where large number of sensitiv-

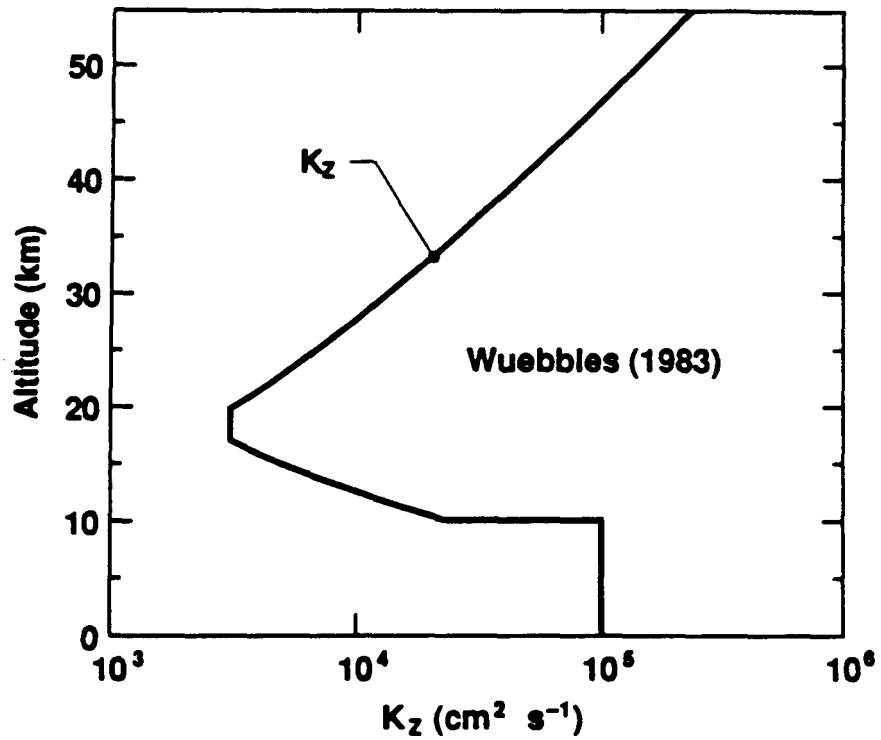

Figure 2.1. Vertical transport coefficient used in the one-dimensional model. Taken from Wuebbles, 1983.

ity scenarios are needed [e.g., Prabhakara, 1963; Shimazaki and Wuebbles, 1972; Harwood and Pyle, 1975; Cunnold, 1977; Pyle and Rogers, 1980; Holton, 1981; Garcia and Solomon, 1983; Guthrie et al., 1984; Ko et al., 1985; WMO, 1985; NASA-WMO, 1989].

By definition, two-dimensional models include transport in the meridonial direction that is not available in the one-dimensional approach. Therefore latitudinal and seasonal distribution of important trace specie like ozone can be compared with current ground based, balloon, aircraft, and satellite data which have global coverage (see WMO 1985 for a review of each of the above observational data that

are currently available for comparison purposes). In addition, two-dimensional models offer a more realistic representation of the feedbacks that dynamics can have on the distribution of constituents such as NO_x, HO_x and Cl_x. Since these constituents control ozone loss processes, the role of transport can be very important in determining the distribution of O_3 in the atmosphere. The temperature structure also is variable with season and latitude. Therefore reaction with temperature dependent rate constants will show variability with latitude and season.

One of the major difficulties in using a two-dimensional model representation of the global atmosphere is how to deal with the wave-driven eddy terms that appear in the solution to the dynamical portion of the continuity equation. These terms represent deviations from the mean motion, such as transport deriving from the effects of transient waves propagating in the stratosphere. In the atmosphere there are various types of waves that give rise to this deviation from zonally averaged conditions. The effects of these eddy terms are generally represented in diffusion-tensor form. There have been numerous studies that have tried to estimate or calculate the values for these terms [WMO 1985, Chapter 6; Plumb and Mahlman, 1987; Schneider et al., 1988; Smith et al., 1988; Newman et al., 1988; Jackman and Newman, 1988], but the problem is still unresolved.

The LLNL zonally-averaged two-dimensional chemical-radiative-transport model [Wuebbles et al., 1987; Grant and Wuebbles, 1987; Grant et al., 1987; Wuebbles and Kinnison, 1988; Connell and Wuebbles, 1988; Kinnison et al., 1988b,c; Johnston et al., 1989] currently determines the atmospheric distributions of 31 chemically active atmospheric trace constituents in the troposphere and stratosphere. The species include: N_2O, NO, NO_2, O_3, OH, HO_2, H_2O_2, H_2, NO_3, N_2O_5, HNO_3, HNO_4, Cl, ClO, HCl, HOCl, $ClONO_2$, CH_3Cl, CCl_4, CH_3CCl_3, $CFCl_3$, CF_2Cl_2, CO, CH_4, CH_2O, and CH_2O. $O(^1D)$, N, and H are considered to be in instantaneous steady state. Essentially all of the relevant atmospheric chemistry treated

in the one-dimensional model are also treated in the two-dimensional model. However, the methane oxidation series of reactions have been reformulated to account for very fast reactions.

The model domain extends from pole to pole, and from the ground to 0.56 mb (approximately 0 to 54 km). The sine of latitude is used as the horizontal coordinate with intervals of about 10°. The vertical coordinate corresponds to the natural logarithm of pressure ($z^* = -H_0 \ln(p/p_0)$, where H_0 is the assumed scale height of 7.2 km, and p_0 is the surface pressure, 1013 mb). The vertical resolution is $\ln(p/p_0) = 0.417$ or about 3 km.

Ninety-five chemical and photochemical reactions are included in the model. Reaction rates, solar flux data, absorption cross-sections, and quantum yields are based on the latest NASA panel recommendations [DeMore et al., 1985, 1987]. Photodissociation rates, including the effects of multiple scattering, are computed as a function of time at each zone, with optical depths consistent with calculated species distributions.

The diabatic circulation or residual circulation [Andrews and McIntyre, 1976, 1978a,b; Dunkerton, 1978] for the ambient atmosphere is determined using net heating rates calculated in an internally consistent way with the derived species distributions. The technique for deriving the diabatic circulation is similar to that used by Solomon et al. [1986b]. The zonally-averaged vertical velocity ($\bar{w}^*$) is determined from the zonally-averaged residual Eulerian thermodynamic equation [e.g. Holton, 1981] (also see Figure 2.2).

The thermodynamic equation is

$$\frac{\partial \bar{T}}{\partial t} + \bar{v}^* \frac{\partial \bar{T}}{\partial y} + \bar{w}^* \left(\frac{g}{C_p} + \frac{\partial \bar{T}}{\partial z} \right) = \bar{Q}. \qquad (4)$$

This can be rewritten to determine $\bar{w}^*$, the vertical velocity.

$$\bar{w}^* = \frac{\bar{Q} - \bar{v}^*(\partial\bar{T}/\partial y) - \partial\bar{T}/\partial t)}{(\frac{g}{C_p} + \partial\bar{T}/\partial z)}$$

where: z = vertical direction
y = horizontal direction
C_p = Heat capacity at constant pressure
g = graviational constant
$\bar{v}^*$ = zonally averaged meridional velocity
$\bar{w}^*$ = zonally averaged vertical velocity
$\bar{T}$ = zonally averaged temperature
t = time
$\bar{Q}$ = zonally averaged net heating rates

In equation (4), if the temperature distribution is provided, with $\bar{v}^*$ initially equal to zero, $\bar{w}^*$ can be obtained. The meridional velocity is determined using the equation for mass continuity (also see Figure 2.3).

$$\bar{v}^* = -\frac{1}{\cos\phi}\frac{1}{\rho_o}\frac{\partial}{\partial z}\rho_o\bar{\chi}^* \tag{5}$$

$$\bar{\chi}^* = \int \bar{w}^* \cos\phi dy \tag{6}$$

where: ρ_o = basic-state density
ϕ = latitude
$\bar{\chi}^*$ = zonally averaged mass meridional stream function
dy = a $d\phi$
a = radius of the Earth

With a value for $\bar{v}^*$, a new estimate of $\bar{w}^*$ in equation (4) is obtained, this time including the term $\bar{v}^*\frac{\partial\bar{T}}{\partial y}$. This process is continued until the values converge. The circulation shown in Figures 2.2, 2.3, and 2.4 compares well with zonally-averaged residual circulations derived from available satellite data [Solomon et al., 1986b; Kiehl and Solomon, 1986; Rosenfield et al., 1987]. The zonally-averaged mass meridional stream function ($\bar{\chi}^*$) is useful in showing the direction and magnitude

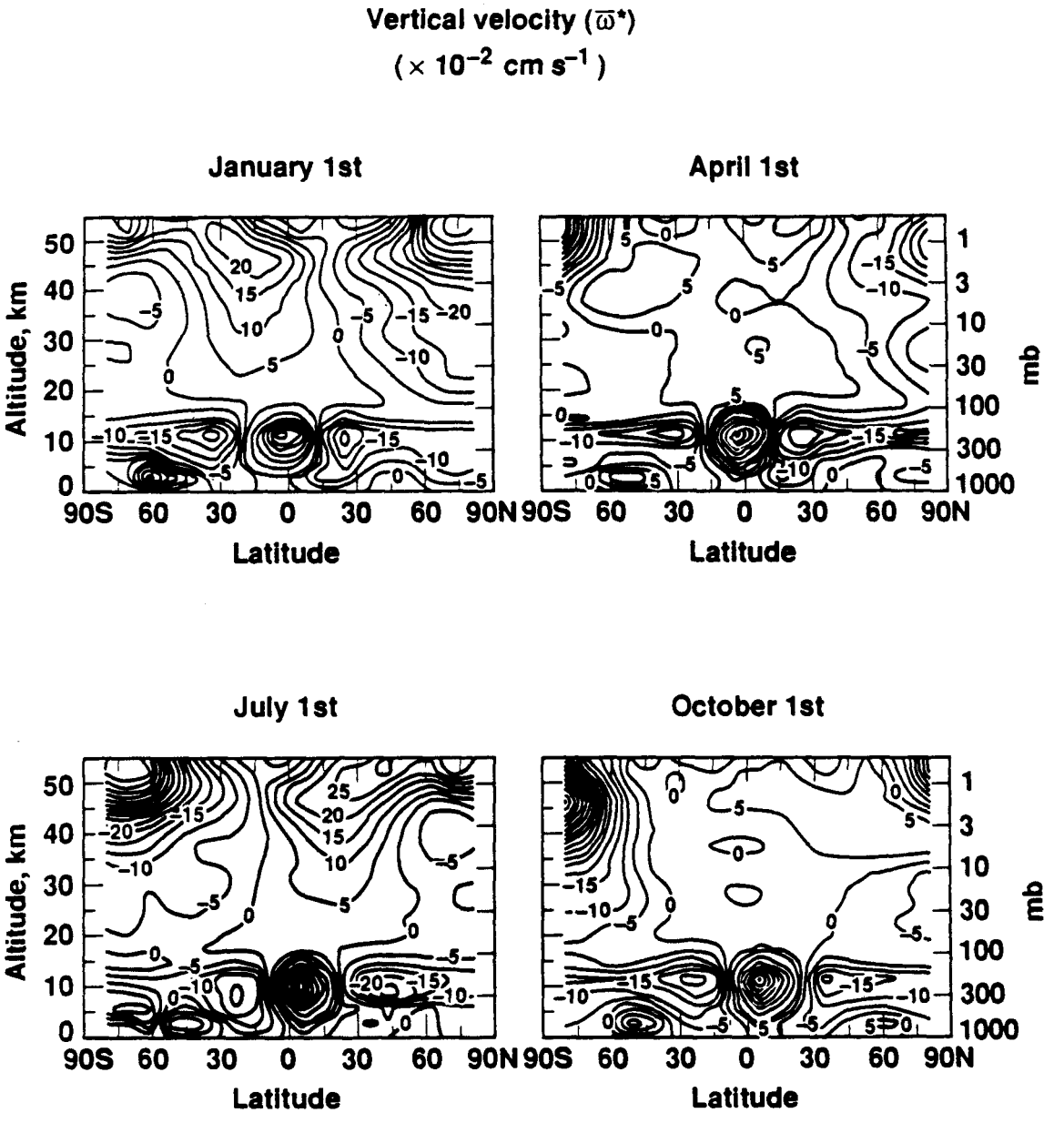

Figure 2.2. Vertical velocity component of advection ($\bar{w}^*$). Units are in cm s^{-1}, where negative and positive values correspond to motion toward the surface and space respectively. All values have been divided by a factor of 1.0×10^{-2}. Four figures are shown for the 1st of January, April, July, and October.

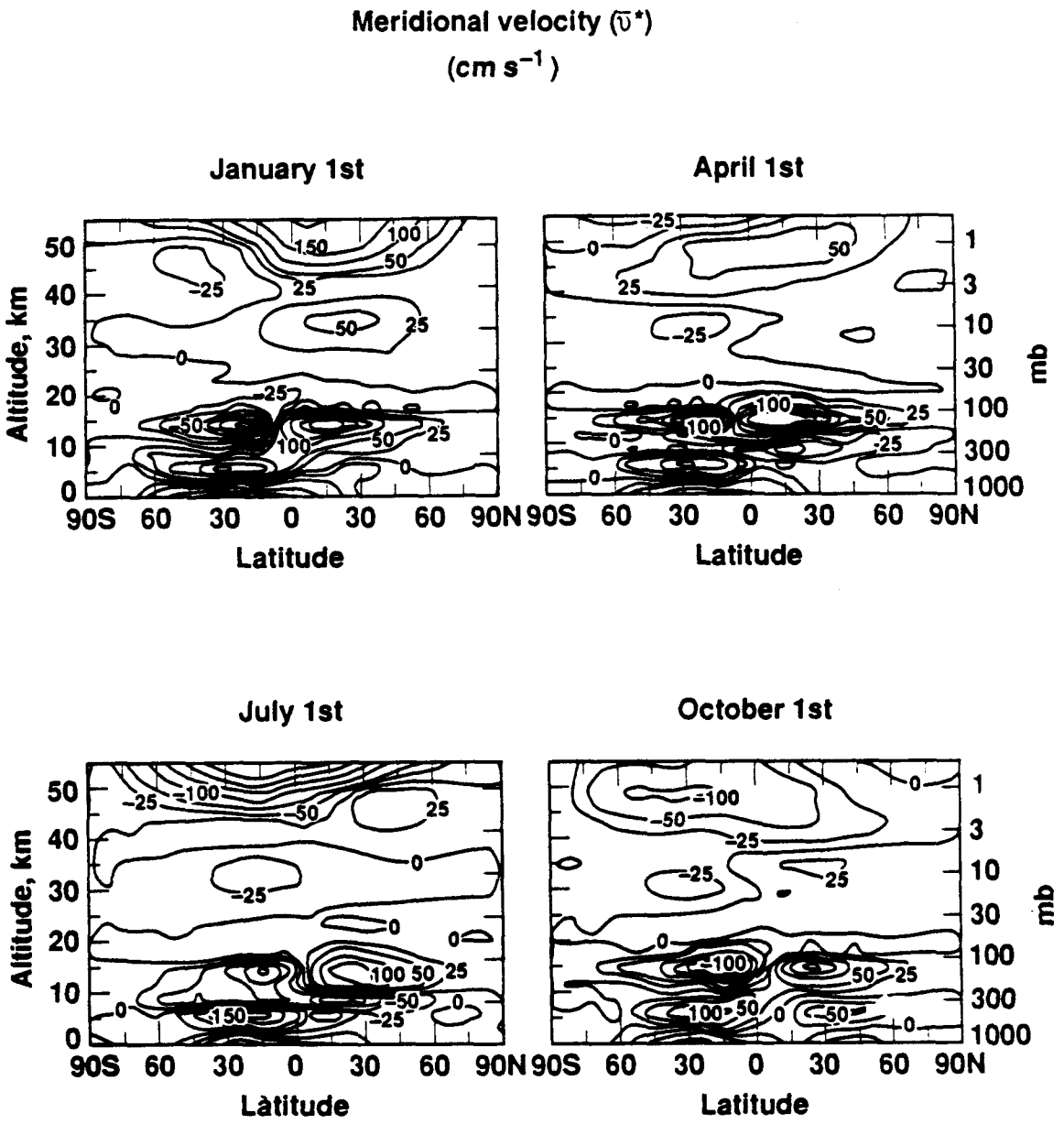

Figure 2.3. Horizontal velocity component of advection ($\bar{v}^*$). Units are in cm s^{-1}, where negative and positive values correspond to motion towards the south pole and north pole respectively. Four figures are shown for the months of January, April, July, and October. Here contour spacing varies as: $\pm$ 1000, 500, 250, 200, 150, 100, 50, 25, 0.

of the diabatic circulation (Figure 2.4). The closer the contour spacings, the more intense the circulation. Notice how the diabatic circulation has a strong downward motion during January in the northern hemisphere. This is consistent with Brewer [1949] suggestion that circulation exhibited a rising motion in the tropics and descending motion at the poles.

The net heating rates ($\bar{Q}$) are determined using accurate solar and infrared radiative submodels. In Figure 2.5. the contours of net heating and cooling are shown for January, April, July, and October. The values that are negative and positive imply cooling and heating respectively. In January, in the northern hemisphere there is pronounced cooling (maximum of -6.0 K day^{-1} at 55 km), while a net heating occurs in the southern hemisphere (maximum of 2.0 K day^{-1}). The same effect occures in July in the southern hemisphere. The solar submodel includes absorption and scattering effects of O_3, O_2, and NO_2 at ultraviolet and visible wavelengths, and for H_2O, CO_2, and O_2 in the near infrared. The longwave emission and absorption by O_3, CO_2, and H_2O are included in the infrared submodel [Grant et al., 1987].

Temperatures for the ambient atmosphere vary continuously, over the annual cycle, based on the reference model of Barnett and Corney [1985] (Figure 2.6). The derived diabatic circulation depends strongly on the temperature distribution; by using observed temperatures for the ambient atmosphere, a more accurate representation of the diabatic circulation can be derived.

For the perturbed atmosphere, a perturbation form of the thermodynamic equation is solved for the changes in stratospheric temperatures resulting from changes in the distribution of ozone and other radiatively active constituents. Using this approach, the diabatic circulation is assumed to be unchanged in the perturbed atmosphere from that calculated for the ambient.

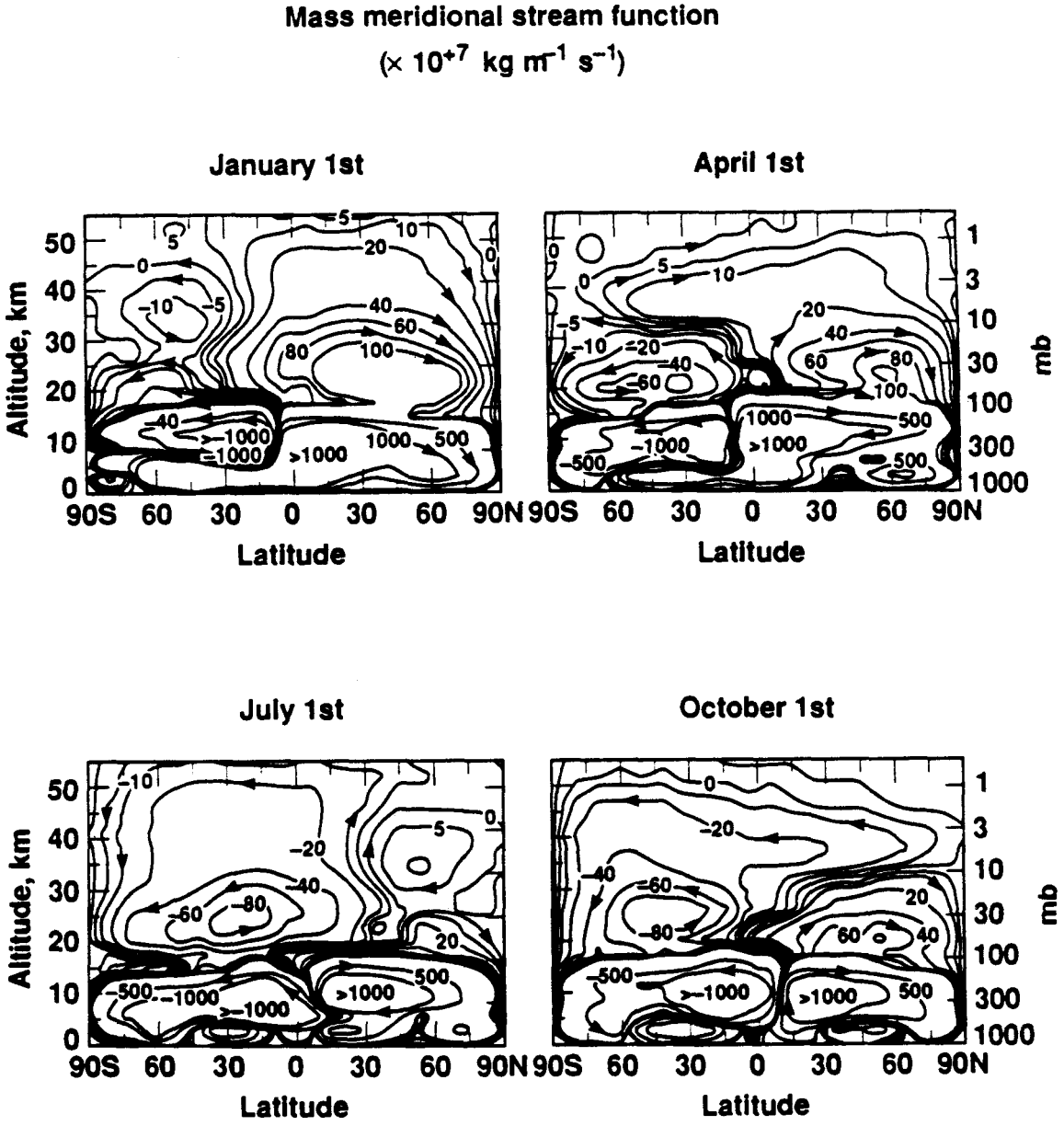

Figure 2.4. Calculated mass meridional stream function. Units are in kg m^{-1} s^{-2}. Negative values represent motion in the counterclockwise direction; positive value are in the clockwise direction. Four figures are shown for the 1st of January, April, July, and October.

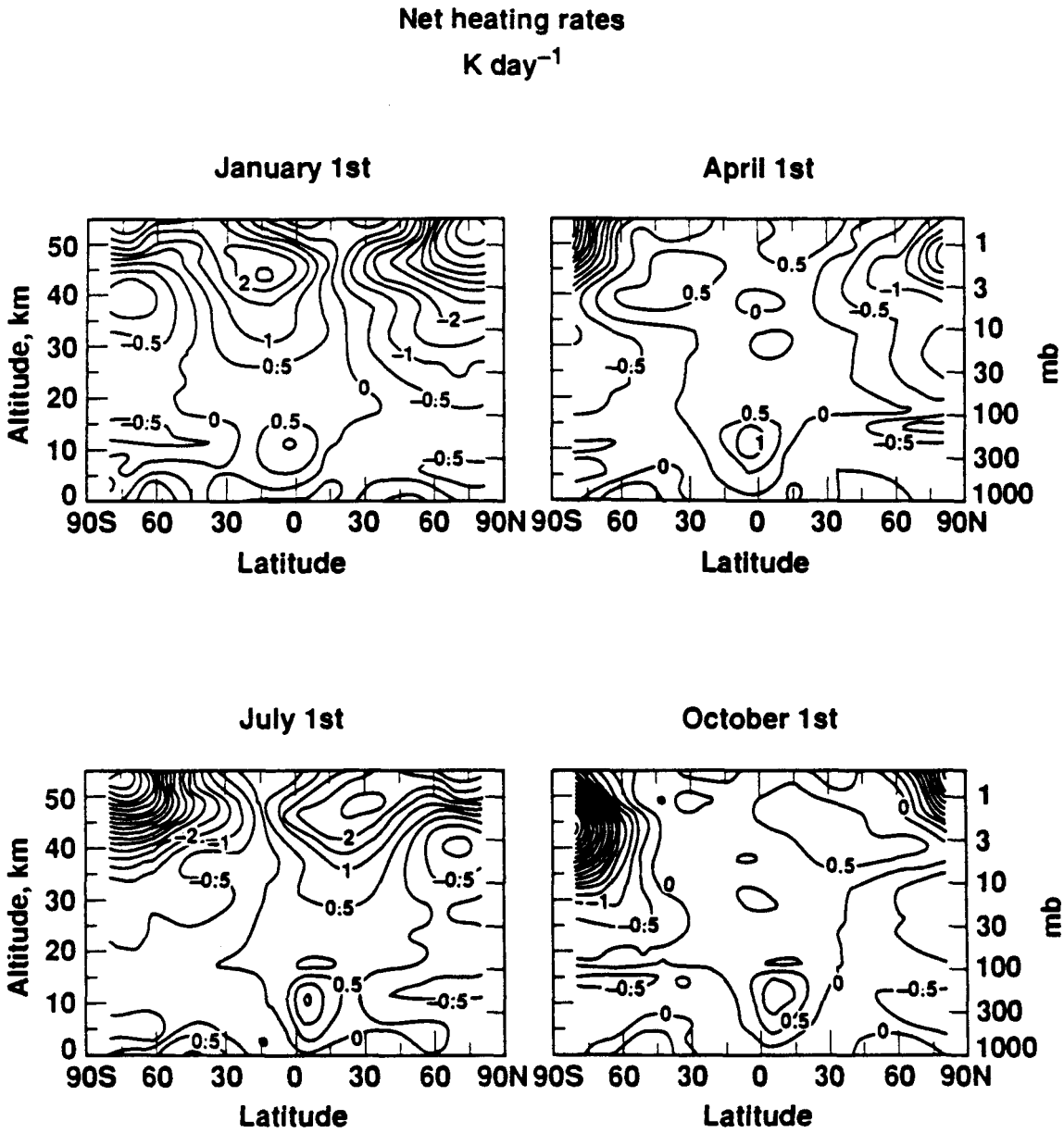

Figure 2.5. Calculated net heating rates. Units are in K day^{-1}, where negative and positive values correspond to net cooling and heating respectively. Four figures are shown for the 1st of January, April, July, and October.

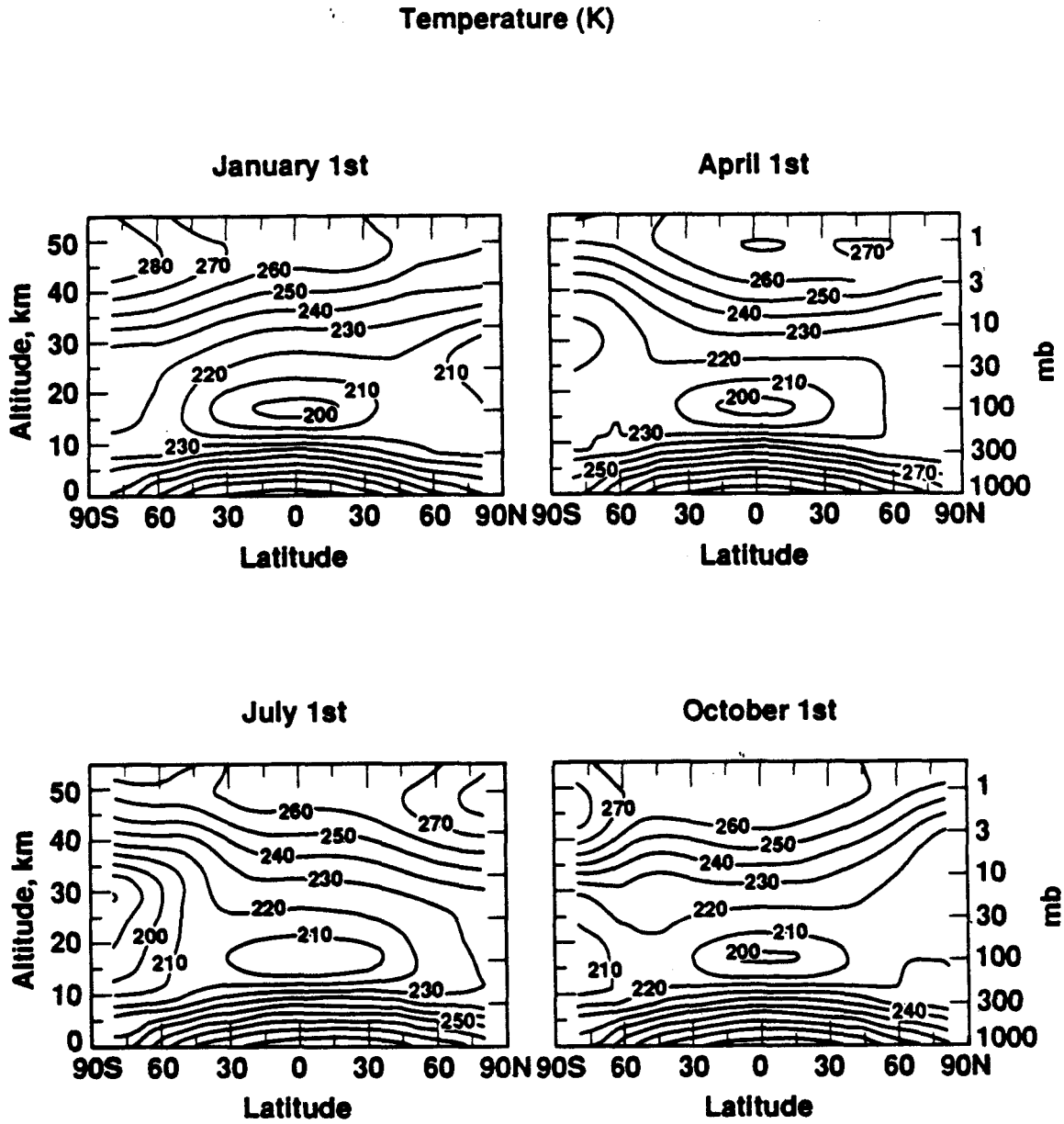

Figure 2.6. Temperature structure for the 1st of January, April, July, and October. Units are in degrees K.

After the horizontal and vertical winds are calculated, the chemical mass continuity equation can be solved.

$$\frac{\partial \bar{\mu}}{\partial t} + \bar{v}^* \frac{\partial \bar{\mu}}{\partial y} + \bar{w}^* \frac{\partial \bar{\mu}}{\partial z} = \bar{P} - \bar{L} + \bar{S} - \frac{1}{\rho \cos \phi} \frac{\partial}{\partial y} \left(\rho K_{yy} \cos \phi \frac{\partial \bar{\mu}}{\partial y} \right) - \frac{1}{\rho} \frac{\partial}{\partial z} \left(\rho K_{zz} \frac{\partial \bar{\mu}}{\partial z} \right) \quad (7)$$

On the left side of the partial differential equation, the zonally-averaged mixing ratio of each chemical specie ($\bar{\mu}$) is represented along with the advective part of the transport ($\bar{v}^*$ and $\bar{w}^*$). The right hand side represents the chemical and photochemical production and loss terms ($\bar{P}$ and $\bar{L}$), plus other sources and sinks ($\bar{S}$) in the model. In addition, eddy tranport must also be represented in order to represent the dispersive transport effects driven by waves and sub-grid scale phenomena and to consider deviations from the zonally averaged assumptions. Turbulent eddy transport is parameterized through diffusion coefficients K_{yy} and K_{zz}. In the current version of the model, a value of K_{yy} of 2×10^9 cm^2 s^{-1} is assumed at all stratospheric altitudes and latitudes; and values of 5×10^{10} cm^2 s^{-1} are assumed in the troposphere, with a transition region at the tropopause. Values of K_{zz} are 1×10^3 cm^2 s^{-1} in the lower stratosphere, increasing slowly with altitude based on gravity wave modeling studies [updated data from R. Garcia based on Garcia et al., 1985].

Advection terms are treated accurately using the two-dimensional transport algorithm of Smolarkiewicz [1984]. The diurnal-averaged concentrations for each species at each zone are calculated at each time step. Accurate diurnal calculations are used to derive time-varying factors for each chemical and photochemical reaction included in the diurnal-averaged version of the model (same method used in one-dimensional model).

The continuity equation for each species, at each latitude, altitude, and time step, is calculated using the accurate numerical method described previously in section 2.2.

*Chapter 3: Ozone Calculations with Large Nitrous Oxide and Chlorine Changes**

3.1 Introduction

In the stratosphere, ozone concentration is balanced by trace gases that makeup the NO_x, Cl_x, and HO_x families [Johnston and Podolske, 1978; Brasseur and Solomon, chapter 5, 1986]. The extent that these gases reduce the ozone concentration, relative to what it would be in a pure oxygen atmosphere, depends strongly on the strength of the coupling between families. In this chapter, the standard LLNL one-dimensional chemical-radiative-transport model was used to see if any interesting or unexpected effects could be found if large changes in NO_x, Cl_x, and HO_x were made.

There have been many model studies of how stratospheric ozone is affected by NO_x and Cl_x, both acting individually and taken together [for example, Chang and Duewer, 1977; WMO, 1981, 1985; Callis et al., 1983; Cicerone et al., 1983; Crutzen and Schmailzl, 1983; Wuebbles, 1983; Wuebbles et al., 1983; Prather et al., 1984; Herman and McQuillan, 1985; Brasseur et al., 1985; Owens et al., 1985; Isaksen and Stordal, 1986; Stolarski and Douglass, 1986]. As is well known, stratospheric chlorine is increasing from the release of chlorofluorocarbons [WMO, 1985].

To obtain new perspective on the effect of possible atmospheric perturbations, this study includes unrealistic conditions. The nitrous oxide boundary value is varied from one-quarter to eight times the reference ("1960") value of 300 ppbv. Stratospheric Cl_x is varied from 0 to 22 ppb [WMO, Chapter 3, 1985; Quinn et

* This chapter is based on an article by Kinnison, D. E., H. S. Johnston, and D. J. Wuebbles, *J. Geophys. Res.*, *93*, 14165–14175, 1988.

al.. 1985]. Special atmospheres are considered in which all HO_x, NO_x, Cl_x, or combinations of these are omitted from the reference atmosphere.

The reference atmosphere is designed to represent the pre-chlorocarbon (ClC) atmosphere, perhaps that of about 1960. It is made up of the following families of atmospheric species:

(A) The "Chapman model" atmosphere includes only the chemistry of O_2, O, O_3, and $O(^1D)$ [Chapman 1930a,b,c].

(B) The nitrogen oxides family, NO_x, is defined here as $NO_x = N + NO + NO_2 + NO_3 + 2N_2O_5 + (HNO_3 + HNO_4 + ClONO_2 + ClNO_2)$. The primary members are NO and NO_2, and the interaction species with the HO_x and Cl_x families are enclosed in parentheses. Its sources are the reaction in the stratosphere of singlet atomic oxygen with N_2O that rises from the troposphere, lightning, and cosmic rays [WMO Chapter 3, pp. 85–88, 1985].

(C) The free radicals derived from water and their important reservoir species are here called HO_x: $HO_x = H + HO + HO_2 + 2H_2O_2 + (HNO_3 + HNO_4 + HCl + HOCl + CHO_x)$. Water is specified by a tropopause boundary condition, and methane is transported from the troposphere. The sources of the HO_x free radicals are the reaction of H_2O with singlet atomic oxygen, photolysis of H_2O, and the reaction of CH_4 with singlet oxygen, with atomic chlorine, and with HO [WMO, Ch.3, pp. 88-100, 1985]. Methane and its derivatives (CHO_x) are included in the HO_x family in all cases except where noted to the contrary.

(D) The active chlorine family is represented as Cl_x, where

$$Cl_x = Cl + ClO + (HCl + HOCl + ClONO_2 + ClNO_2)$$

The maximum value of Cl_x is 1.1 ppbv at 55 km. In the reference model the source is tropospheric CH_3Cl and CCl_4 [WMO 1985, Chapter 3]. Cl_x perturbations are based on increases of CCl_4, $CFCl_3$, CF_2Cl_2, and CH_3CCl_3.

The vertical profile (10 to 55 km) of ozone concentration, calculated with the reference atmosphere, is shown in Figure 1-a. The profile, like most others in this article, is given as concentration (molecules cm^{-3}) versus altitude both with a linear scale. The ozone profile calculated from the reference atmosphere agrees reasonably well with the standard observed profile [WMO, 1985], and the calculated distributions of other species generally compare satisfactorily with observations [Wuebbles, 1983].

3.2. Sequences of Large NO_x and Cl_x Changes

The reference (1960) background of stratospheric chlorine is taken to be 1.1 ppbv. The 1988 level of stratospheric chlorine is about 3 ppbv [WMO, Chapter 3, 1985]. If the rate of chlorocarbon (ClC) production and release continues indefinitely at the present rate, stratospheric chlorine will reach about 8 ppbv by the middle of the next century. Assuming worldwide growth of the ClC industry, an increase of stratospheric chlorine to about 15 ppbv is regarded as possible [Quinn et al., 1985]. In a search for non-linear trends, an increase of stratospheric chlorine to about 22 ppbv is considered. The unrealistically large Cl_x increase assumed here is about fifty percent greater than the plausible extreme scenario. In this study, this targeted range of round numbers comes out to be 1.1, 3.1, 7.9, 14.7, and 21.4 ppbv of stratospheric chlorine, although at times these are referred to as the nominal values of 1, 3, 8, 15, and 22 ppbv.

Natural stratospheric NO_x is largely derived from tropospheric nitrous oxide, N_2O, which is broken down to NO, O_2, and N_2O in the stratosphere [Crutzen,

1971; Weiss, 1981; Prather, 1985]. A wide range of nitrous oxide was included in these model calculations: 1/4, 1/2, 1, 2, 4, and 8 times the reference amount of N_2O. The reference boundary value is 300 ppbv, and the corresponding maximum stratospheric NO_x is 19.4 ppbv, occurring at 37.5 km. Extrapolation of the current increasing trend in nitrous oxide indicates that it might increase by about 40 percent over the next century [Weiss, 1981; Prather, 1985; WMO, Ch. 3, p 84, 1985]. Large increases of stratospheric nitrogen oxides from stratospheric aircraft or nuclear bombs are conceivable, and these large changes of nitrous oxide provide some background for thinking about these perturbations.

3.3 Results of Model Calculations for N_2O and Cl_x Changes

Many results of this study are summarized in Table 3.1 and in Figures 3.1, 3.2, and 3.3. Figure 3.1-a gives the calculated ozone vertical profile for the reference model; on the same linear scale Figure 3.1-b shows the changes of ozone as the boundary value of nitrous oxide is increased by factors of 2, 4, and 8; and Figure 3.1-c shows the changes of ozone from the reference model as stratospheric Cl_x is increased from 1 to 3, 8, 15, and 22 ppbv. As N_2O increases in Figure 3.1-b, the successive curves show quantitatively increased ozone reductions, and they all show the same slightly asymmetrical bell-shape profile centered at about 22 kilometers. As Cl_x increases (with other boundary values of the reference model held constant), the ozone-change profiles show different qualitative features as well as quantitative changes: For small Cl_x increases, ozone reduction occurs over a narrow band between 35 and 45 kilometers and increases weakly in the 25 to 35 kilometer range. For large Cl_x increase, the ozone decrease spreads downward spanning the range from 25 to 45 kilometers (Figure 3.1-c).

The changes of the ozone column as a joint function of varied N_2O and Cl_x are shown by Figure 3.2.

Table 3.1 Calculated ozone vertical column for wide range of assumed N_2O boundary values and for five values of stratospheric Cl_x. The Reference conditions are 1.1 ppb Cl_x at 50 km. 7.645×10^{12} molecules cm^{-3} N_2O at the surface. The maximum NO_x mixing ratio occurs at altitudes between 31 and 37.5 km; in this discussion, NO_x includes all forms: N, NO, NO_2, NO_3, $2N_2O_5$, HNO_3, HNO_4, $ClNO_2$, $ClONO_2$, HONO, and Cl_x includes all forms: Cl, ClO, HCl, HOCl, $ClNO_2$, $ClONO_2$.

* From lightning and cosmic rays.

Cl_x ppbv	N_2O (reference)	Column O_3 ($\div 10^{18}$)	Percent Difference	Maximum NO_x, ppbv	Maximum Altitude km
0.0	0	10.99	−18.9	0	
1.1	0	9.535	− 3.1	1.9*	31
3.1	0	7.756	−16.1	1.9*	32
7.9	0	4.919	−46.8	1.9*	32
1.1	1/4	9.936	+ 7.5	7.8	40.0
3.1	1/4	9.235	− 0.1	7.6	37.5
7.9	1/4	7.351	−20.5	7.3	37.5
14.7	1/4	4.352	−52.9	6.6	37.5
21.4	1/4	3.436	−62.8	6.3	37.5
1.1	1/2	9.770	+ 5.7	12.3	37.5
3.1	1/2	9.417	+ 1.9	12.3	37.5
7.9	1/2	8.544	− 7.6	12.3	37.5
14.7	1/2	7.114	−23.0	12.3	37.5
21.4	1/2	4.016	−56.6	10.9	37.5
1.1	1	9.244	+ 0.0	19.4	37.5
3.1	1	9.116	− 1.4	20.0	35
7.9	1	8.775	− 5.1	20.7	35
14.7	1	8.121	−12.2	22.3	35
21.4	1	7.055	−23.6	22.9	35
1.1	2	8.282	−10.4	30.5	35
3.1	2	8.238	−10.9	31.2	35
7.9	2	8.097	−12.4	33.8	34
14.7	2	7.882	−14.7	37.8	34
21.4	2	7.684	−16.9	41.0	34
1.1	4	6.994	−24.3	47.1	33
3.1	4	6.954	−24.8	48.8	33
7.9	4	6.813	−26.3	53.6	33
14.7	4	6.615	−28.4	61.8	33
21.4	4	6.464	−30.1	67.6	33
1.1	8	5.660	−38.8	72.2	31
3.1	8	5.613	−39.3	74.8	31
7.9	8	5.455	−41.0	82.6	31
14.7	8	5.232	−43.4	95.1	31
21.4	8	5.077	−45.1	105.	31

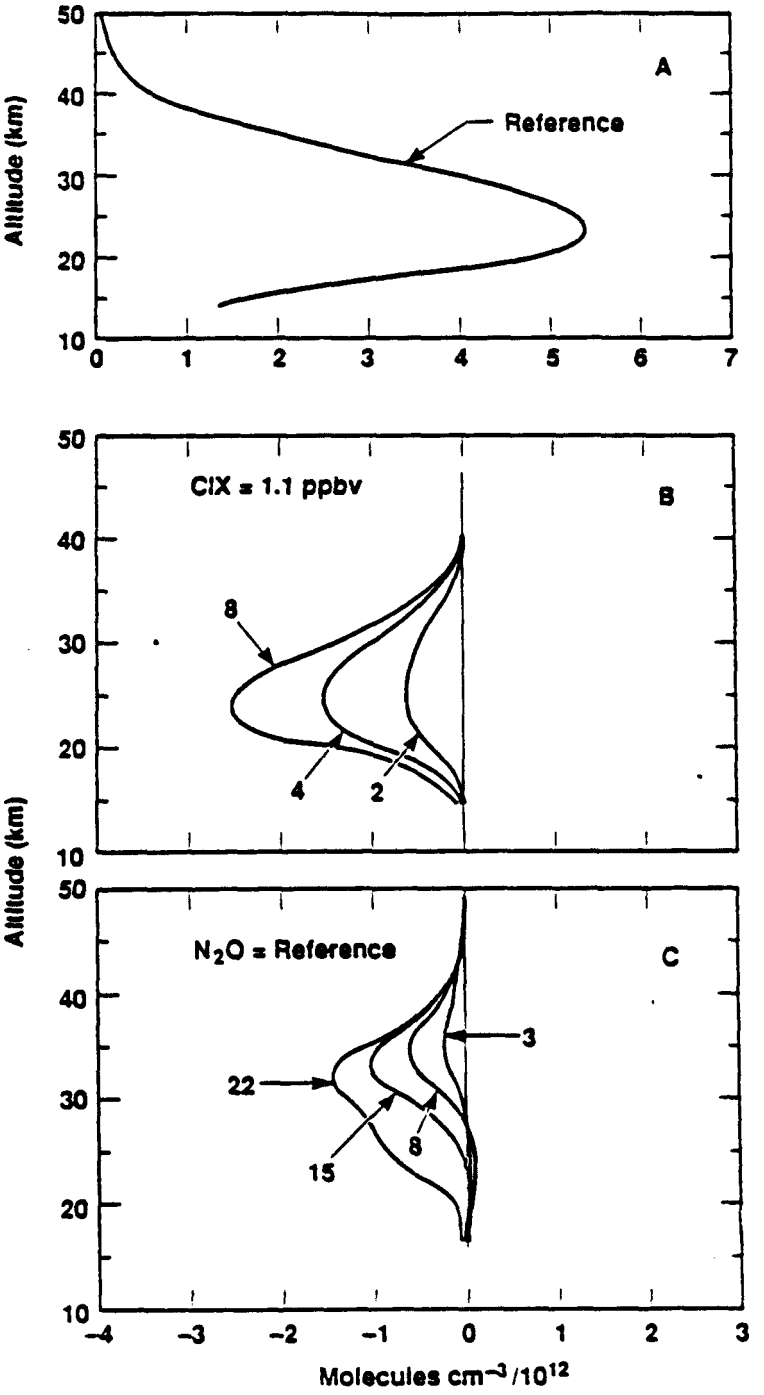

Figure 3.1-a. Calculated ozone vertical profile based on the reference model. Cl_x = 1.1 ppbv, N_2O = 300 ppbv. **3.1-b.** Calculated changes in the ozone vertical profile for Cl_x = 1.1 ppbv and for N_2O at 2, 4, and 8 times the reference value. **3.1-c.** Calculated changes in the ozone vertical profile for reference boundary value of N_2O and for 3, 8, 15, and 22 ppbv of Cl_x. The same concentration scale is used on all three panels.

Figure 3.2-a shows the percentage ozone-column change plotted against stratospheric Cl_x for various fixed boundary values of nitrous oxide. The pattern of these curves is varied and complex. (i) For the reference value of N_2O (300 ppbv), ozone decreases linearly with Cl_x up to about 10 ppbv, but above 15 ppbv it decreases in a non-linear, accelerating manner. At 22 ppbv Cl_x, the ozone reduction is 23 percent. (ii) At 1 ppbv Cl_x and for large amounts of NO_x, 2, 4, and 8 times the reference boundary condition of N_2O, there are large ozone reductions caused by NO_x. For these large amounts of NO_x, as Cl_x is increased to 3, 8, 15, and 22 ppbv, ozone decreases slowly and linearly. (iii) For the hypothetical case of one-half the reference value of N_2O and thus low NO_x, the decrease of ozone with increasing Cl_x is much faster and more non-linear than for the case of reference N_2O, reaching "56 percent" ozone reduction at 22 ppbv Cl_x. For one-quarter the reference boundary value of N_2O, the ozone decrease with increasing Cl_x is even faster, becoming "53 percent" at 15 ppbv Cl_x. With all NO_x removed from the model atmosphere, merely 8 ppbv Cl_x is calculated to reduce ozone by "48 percent". (These very large ozone reductions are put in quotation marks to acknowledge that such large perturbations would affect stratospheric temperature and dynamics, quantitative significance should not be ascribed to these numbers, but the trends should be noted). In no case does the ozone column increase with an increase of chlorine at constant boundary values of nitrous oxide (even though local ozone increases in some cases with increasing Cl_x, Figure 3.1-c).

Figure 3.2-b shows the percentage ozone-column change plotted against N_2O boundary values from zero to 8 times reference N_2O, at various values of fixed stratospheric Cl_x. The curves all show the same general shape. For a fixed amount of Cl_x, the ozone column is a maximum at a finite value of nitrous oxide, decreasing both for less and for more nitrous oxide. When nitrous oxide is low, increasing

nitrous oxide increases the ozone column. the degree of which depends on the amount of Cl_x.

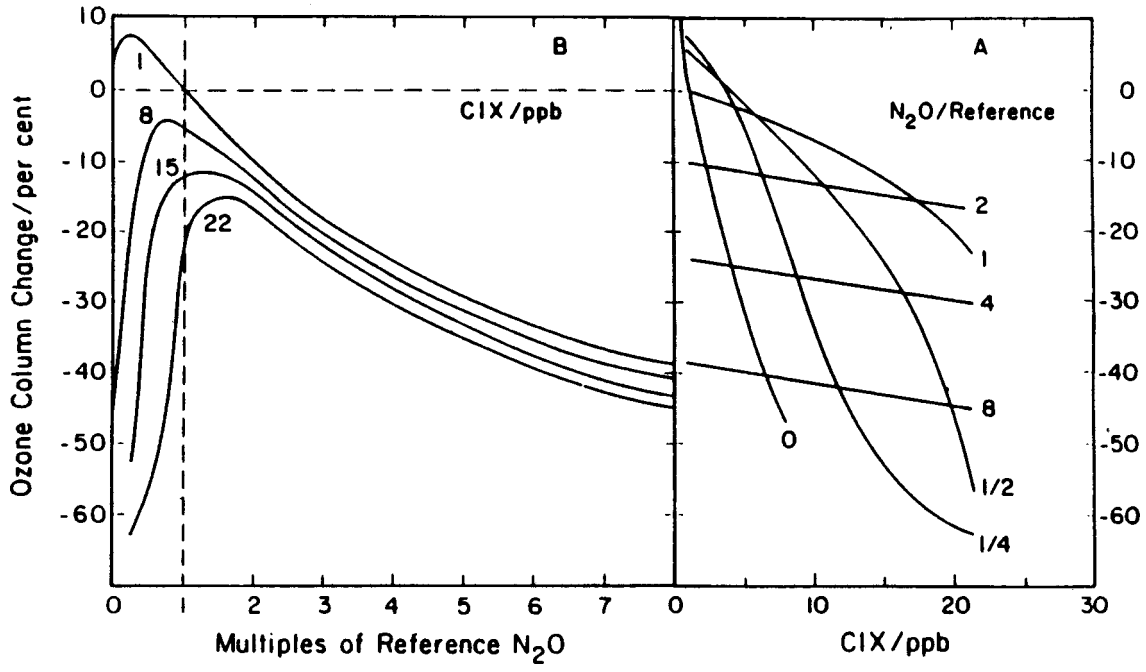

Figure 3.2-a. Steady-state ozone-column changes by increasing stratospheric chlorine for various assumed values of the nitrous oxide boundary values, spanning the range of 0, 1/4, 1/2, 1, 2, 4, and 8 times the reference amount, which is 300 ppbv. The stratospheric NO_x associated with these multiples of the reference boundary value of N_2O is: 1/4, 7.6 ppbv; 1/2, 12 ppbv; 1, 20 ppbv; 2, 31 ppbv; 4, 47 ppbv; 8, 72 ppbv. For large amounts of NO_x, ozone decreases linearly with increasing stratospheric chlorine; for small amounts of NO_x ozone changes very rapidly and non-linearly with increasing chlorine. **3.2-b.** Steady-state ozone column changes by increasing tropospheric nitrous oxide for various fixed values of stratospheric Cl_x.

The results shown in Figure 3.2 are re-expressed in Figure 3.3 with the independent variable taken to be the maximum mixing ratio of NO_x, which occurs between 35 and 40 km, instead of the multiple of the reference nitrous oxide. These values are included in Table 3.1. These data are expressed as a contour plot of percentage change of the ozone vertical column (relative to the reference model) as a joint function of stratospheric NO_x and Cl_x mixing ratios. The values of NO_x

for the reference boundary value of N_2O are indicated by an almost vertical solid line across Figure 3.3; this value increases slowly with increasing Cl_x. As Cl_x increases along the constant NO_x reference line, the ozone column decreases. Points on the contour lines where the tangent is parallel to the NO_x axis are connected by a dashed line to divide the contour plot into two areas, A and B. Anywhere in region B of Figure 3.3, (including the region to the left of the reference nitrous oxide line) an increase of NO_x at constant Cl_x reduces the ozone reduction, thus increasing ozone. Anywhere in region A, an increase of NO_x at constant Cl_x decreases ozone in addition to the reduction caused by chlorine. The A/B boundary line intersects the reference nitrous oxide line at about 10 ppbv Cl_x, where the ozone column reduction is about 7 percent; a small increase of stratospheric NO_x decreases ozone at lower amounts of Cl_x and increases ozone at larger amounts of Cl_x.

The contour map in Figure 3.3 is constructed from a relatively small number of points. The data for the fitting program have been extended by reading points off hand drawn curves similar to Figure 3.2. One should not expect Figure 3.3 to give quantitative results for all possible cuts through the figure.

A surprising feature of Figures 3.2 and 3.3 is that if the stratosphere had much less NO_x than the natural amount, a very small chlorine increase would cause a large reduction of ozone. An interesting feature is the region of high Cl_x where increasing NO_x in the stratosphere would increase the ozone column.

3.4 Interaction Mechanisms Between NO_x and Cl_x

Figures 3.1–3.3 show strong interactions between Cl_x and NO_x so far as ozone reduction is concerned. Some of these interactions can be identified, and such cases are given below.

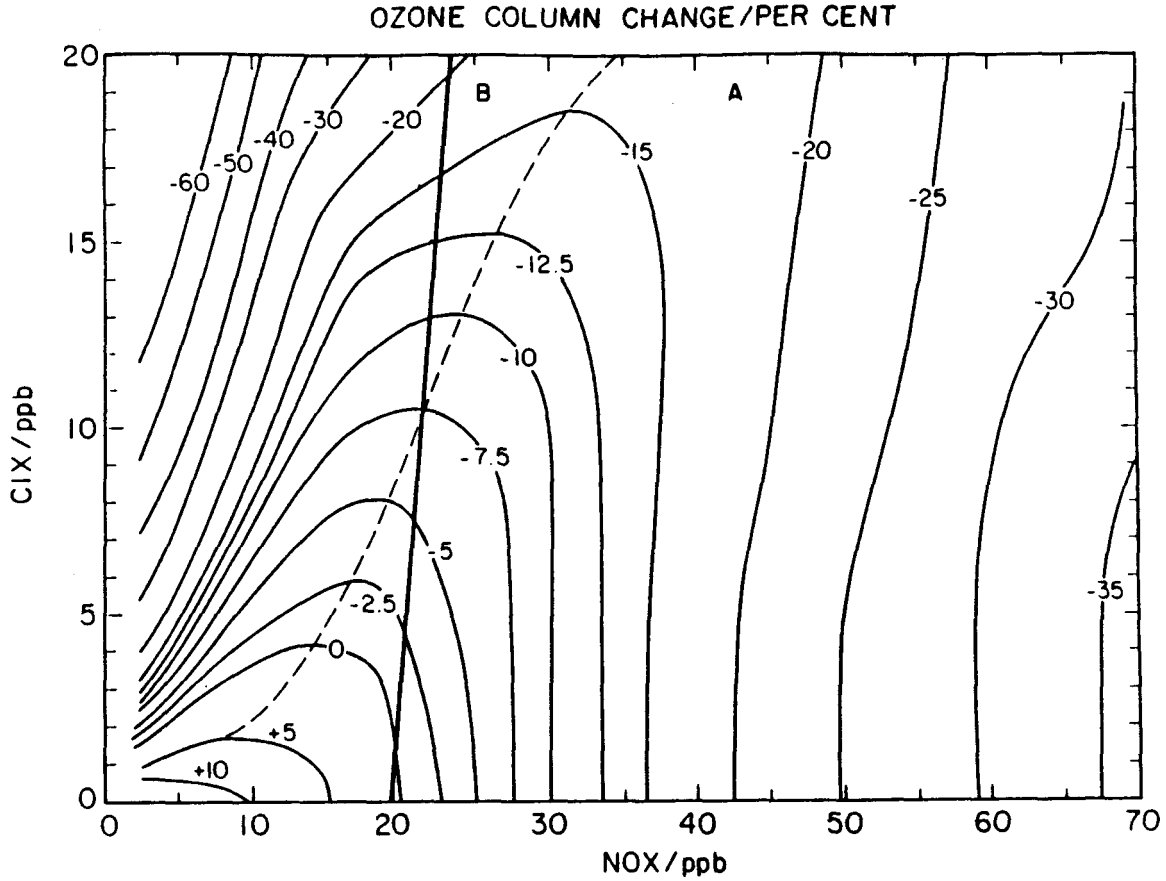

Figure 3.3. Contour plot of percentage ozone-column change (relative to reference atmosphere) as a function of stratospheric Cl_x and maximum stratospheric NO_x (which occurs between 30 and 35 km, see Table 3.1). This figure uses maximum stratospheric NO_x as independent variable. The region to the left of the almost vertical line contains less NO_x than the reference atmosphere. If ozone has reached steady state with respect to chlorine species, added NO_x increases ozone in region B and further decreases ozone in region A. The region to the left of the dashed line and to the right of the solid line represents possible future conditions where added NO_x would increase the ozone column.

3.4.1 Photochemical Self-Healing of Ozone

Ozone formation occurs through the reactions

$$O_2 + uv \rightarrow 2O \tag{1}$$

$$O + O_2 + M \rightarrow O_3 + M \text{ (twice)} \tag{2}$$

$$\text{Net}: \quad 3O_2 + uv \rightarrow 2O_3$$

and for the Chapman reactions the ozone destruction mechanism is

$$O + O_3 \rightarrow 2O_2 \tag{3}$$

In the stratosphere, solar radiation below 244 nm can either dissociate molecular oxygen to make two ozone molecules (1, 2) or dissociate ozone

$$O_3 + uv \rightarrow O_2 + O \tag{4}$$

which with rare exceptions is followed by (2), leading to no net chemical reaction. Ozone and oxygen compete for the same limited supply of radiation below 244 nm. In this way a reduction of the mixing ratio of ozone in a volume of air increases ozone production from (1, 2) relative to the null cycle (4, 2), which partially cancels the ozone reduction. This feedback is called the "self-healing effect". In the Chapman atmosphere, ozone destruction occurs primarily by the sequence (4, 3).

For NO_x and Cl_x, the predominant ozone-destroying catalytic cycles are respectively:

$$NO + O_3 \rightarrow NO_2 + O_2 \tag{5}$$

$$NO_2 + O \rightarrow NO + O_2 \tag{6}$$

$$\text{Net}: \quad O_3 + O \rightarrow 2O_2$$

$$Cl + O_3 \rightarrow ClO + O_2 \tag{7}$$

$$ClO + O \rightarrow Cl + O_2 \tag{8}$$

$$\text{Net}: \quad O_3 + O \rightarrow 2O_2$$

for which (6) and (8) are the rate determining steps.

Increasing stratospheric Cl_x up to 22 ppbv (at constant reference N_2O boundary value) decreases the column of ozone up to 21 percent (Figure 3.2-a), which increases the photolysis rate of molecular oxygen and thus increases the rate of ozone production, Figure 3.4-a. Increasing nitrous oxide up to 8 times the reference value (with Cl_x constant at 8 ppbv, for example) decreases the column of ozone by "40 percent" (Figure 3.2-b), which increases the photolysis rate of molecular oxygen and thus increases the rate of production of ozone, Figure 3.4-b.

Although the ozone column reduction by NO_x is almost twice as great as that caused by added Cl_x, the self-healing effect with increased Cl_x is much larger than that associated with NO_x, compare Figure 3.4-a with 3.4-b. This difference is general. For both NO_x and Cl_x this "self-healing effect" extends weakly down to 20 km.

3.4.2 Chlorine Nitrate

A strong interaction between the Cl_x and NO_x systems is the formation of chlorine nitrate [Rowland et al., 1976; WMO, 1985].

$$ClO + NO_2 + M \rightarrow ClONO_2 + M \qquad (9)$$

By this process the species occurring in the rate-determining step of both the Cl_x catalytic cycle (8) and the NO_x catalytic cycle (6) are tied up in a "reservoir species", chlorine nitrate. Vertical profiles of diurnally averaged concentrations of chlorine nitrate are shown in Figure 3.5. At a rate slightly faster than linearly, increasing Cl_x increases chlorine nitrate, Figure 3.5-a. However, as NO_x increases in a model of fixed Cl_x (8 ppmv, for example) the surprising result is that chlorine nitrate decreases, Figure 3.5-b. (This effect is general, observed for all levels of

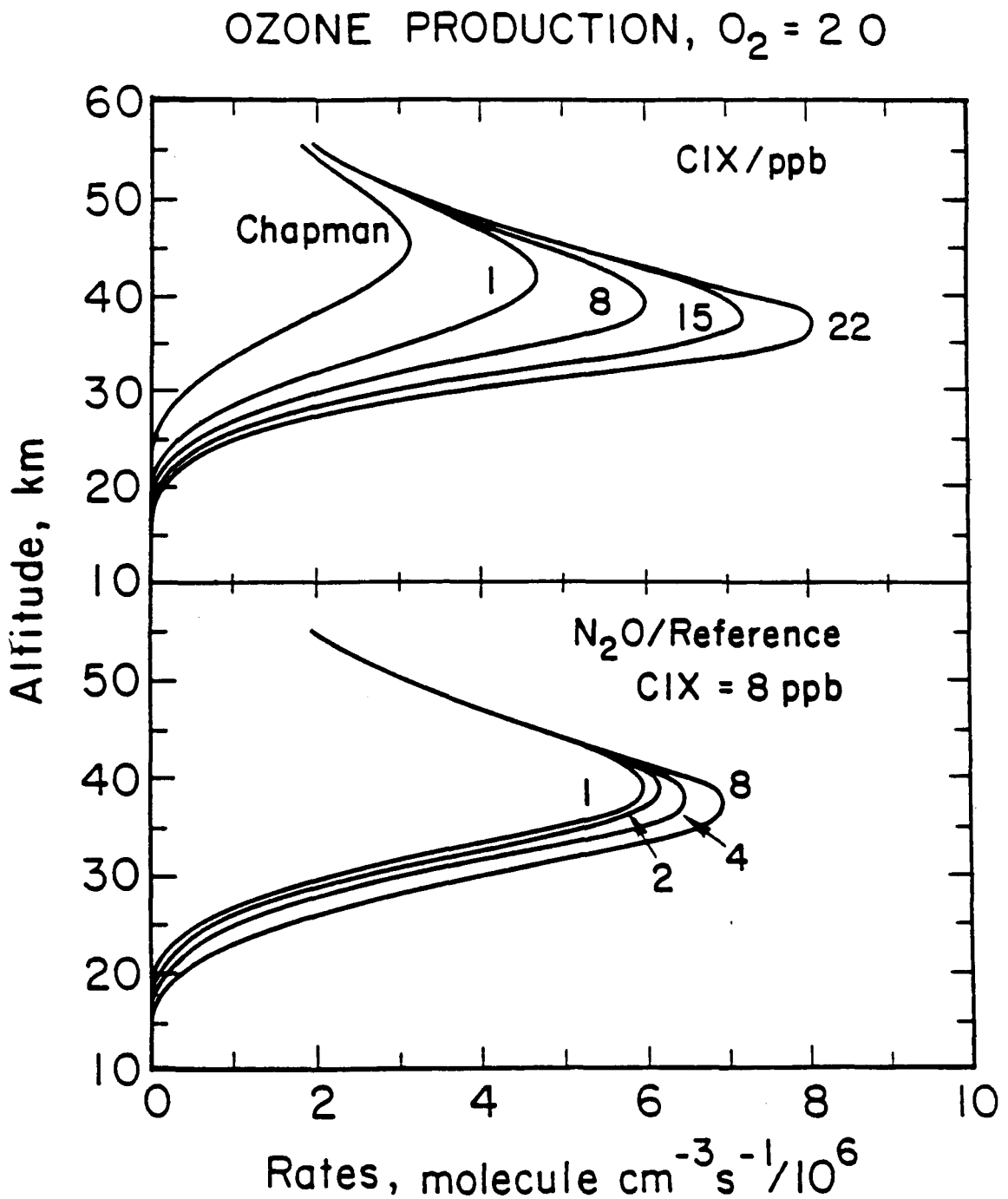

Figure 3.4. Profiles of the rate of production of atomic oxygen and thus ozone from the photolysis of molecular oxygen. (a) The first profile is for the Chapman model, the second is the reference atmosphere including 1.1 ppbv of Cl_x, and the other curves are the reference atmosphere plus ClC to give stratospheric Cl_x of 8, 15, and 22 ppbv. (b) With stratospheric Cl_x = 8 ppbv, this panel gives the rate of ozone production from oxygen photolysis with tropospheric N_2O multiplied by factors of 1, 2, 4, and 8.

Cl_x from 1.1 to 21.4 ppbv and for all amounts of N_2O equal to or greater than the reference model). The components of chlorine nitrate are ClO and NO_2. The vertical profiles of ClO concentration shows the same relation as chlorine nitrate, Figure 3.6. Increasing Cl_x increases ClO, but increasing N_2O decreases ClO. The vertical profiles of nitrogen dioxide are more complex than that for chlorine oxide. Figure 3.7. NO_2 is increased in the upper stratosphere by increasing Cl_x, but it is decreased in the lower stratosphere by increasing Cl_x. Nitrogen dioxide increases slightly faster than linearly with increasing NO_x, Figure 3.7-b.

3.4.3 Mechanism to Explain Some Major NO_x–Cl_x Interactions

The major features of Figures 3.5–3.7 are explained in terms of a simplified ten-reaction mechanism, given in Table 3.2. The steady-state approximation is made for the rapidly changing species (NO, NO_2, Cl, ClO, and $ClONO_2$), and a small additive term is neglected in one case. Five relations are derived and given in the upper part of the table, and the relations of ClO to Cl_x and of NO_2 to NO_x are given in the lower part of the table. For algebraic simplicity in this table, total Cl_x is approximated by the sum of the three species, HCl, ClO, and $ClONO_2$; and NO_x is approximated by $NO + NO_2 + HNO_3 - ClONO_2$; model calculations include all members of each family.

Chlorine nitrate (Figure 3.6) is formed by the third-body dependent reaction (g_M), $ClO + NO_2$, and destroyed by photolysis (h). The steady-state concentration of chlorine nitrate is

$$[ClONO_2] = g_M[ClO][NO_2]/h \qquad (10)$$

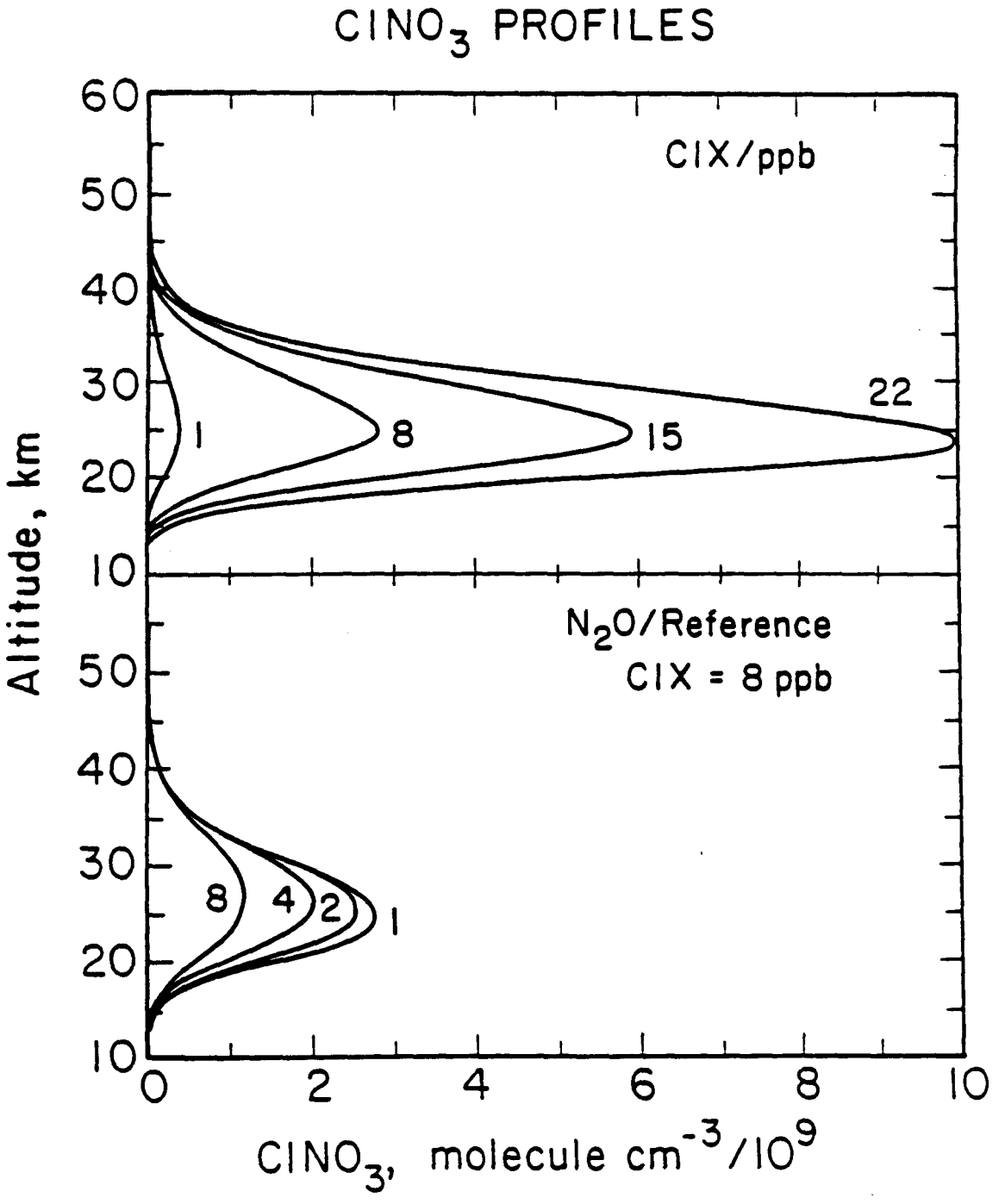

Figure 3.5. Profiles of the concentration of chlorine nitrate for the same model atmospheres as those in Figure 3.4. Note the expected increase of chlorine nitrate with increasing Cl_x but unexpected decrease of chlorine nitrate with increasing nitrogen oxides.

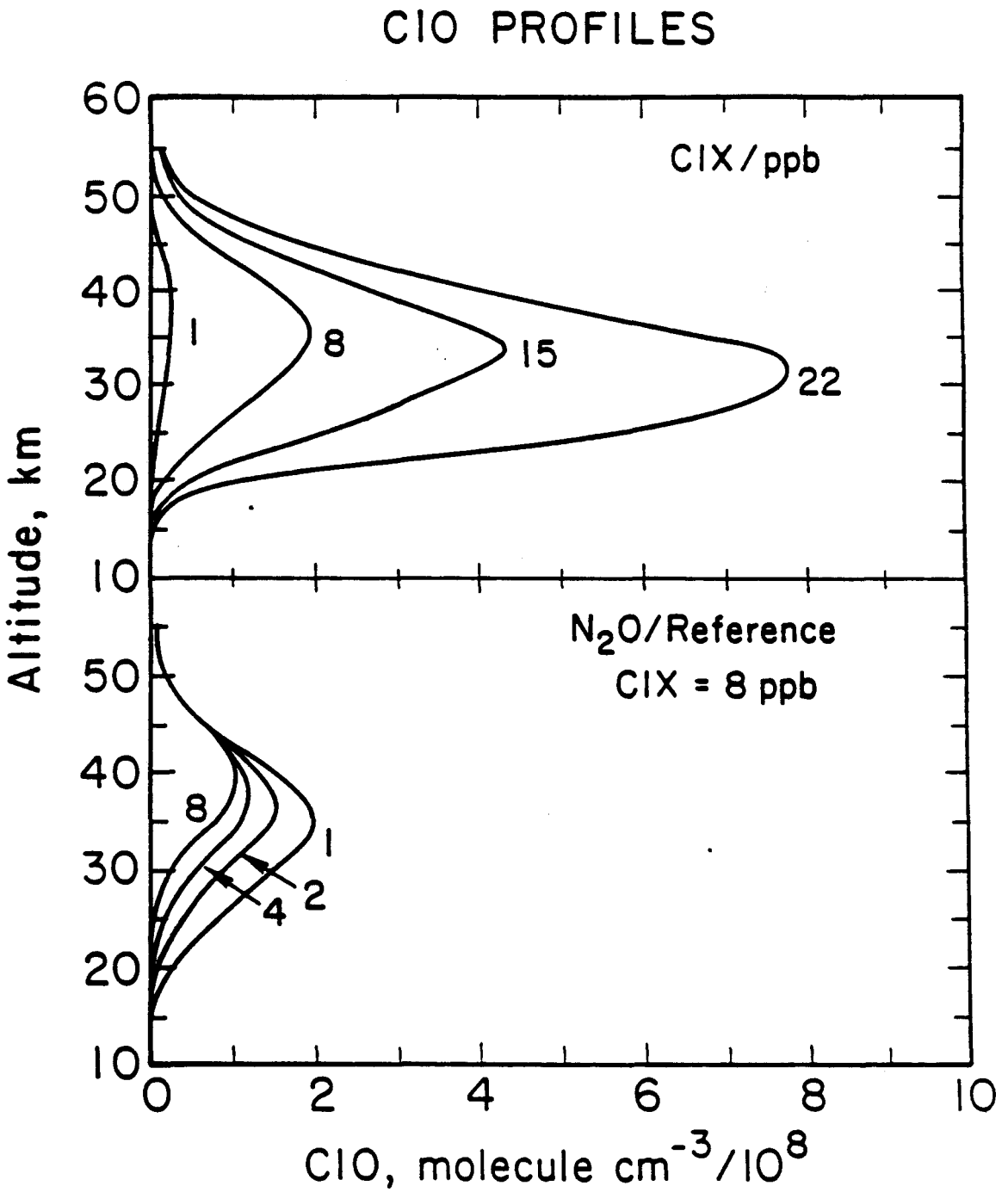

Figure 3.6. Profiles of the concentration of chlorine monoxide for the same model atmospheres as those in Figure 3.4. Note the decrease of ClO with increasing nitrogen oxides in panel B.

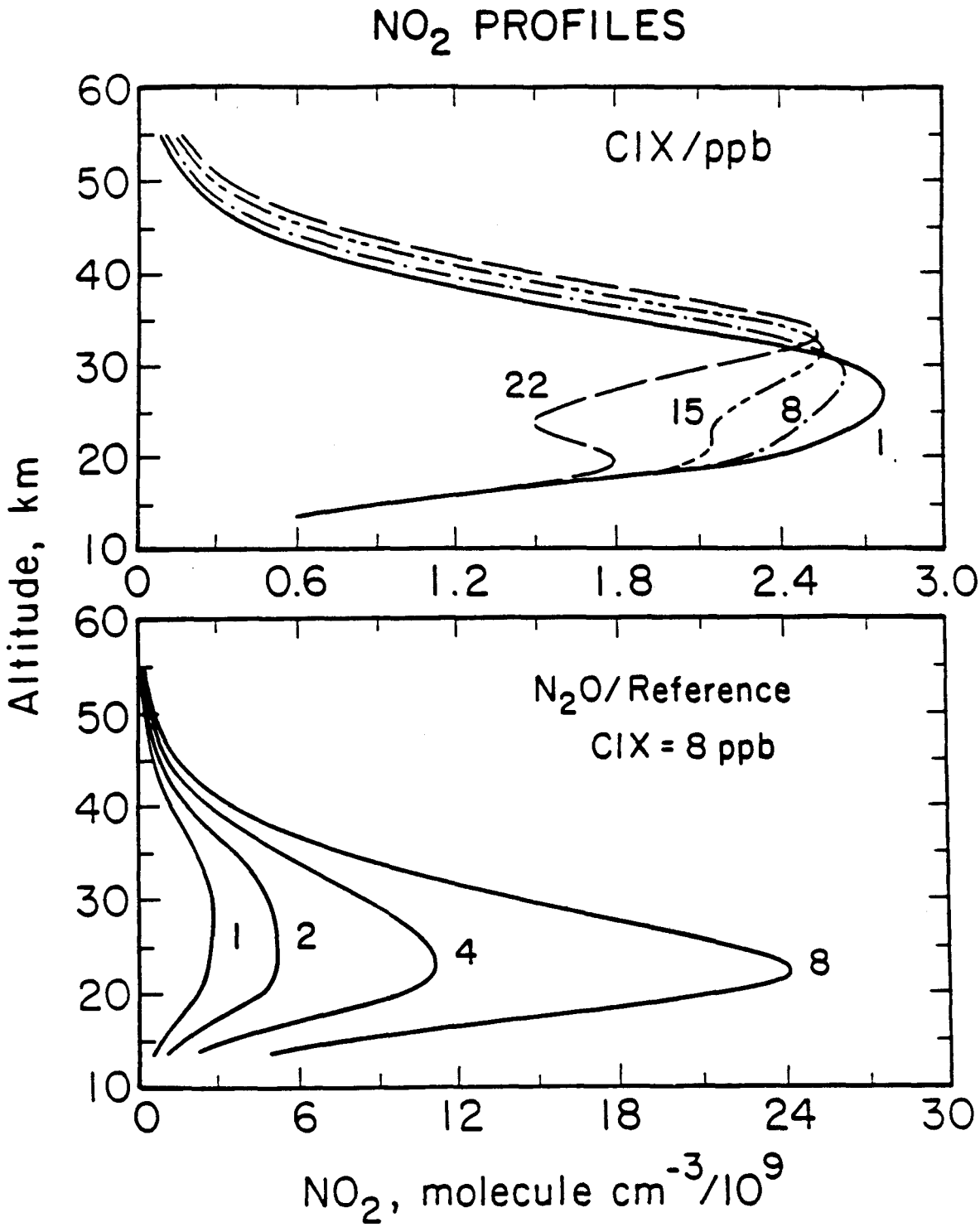

Figure 3.7. Profiles of the concentration of nitrogen dioxide for the same model atmospheres as those in Figure 3.4. In the upper panel (a) NO_2 decreases between 20 and 30 km but increases above 30 km upon increasing Cl_x. In the lower panel (b). NO_2 increases with increasing nitrous oxide.

Table 3.2 Abbreviated mechanism for major interactions between active NO_x and Cl_x species.

Reaction	Rate Constant	Approximate Steady Relation
$Cl - CH_4 \rightarrow HCl - CH_3$	a	
$HO - HCl \rightarrow H_2O - Cl$	b	$a[Cl][CH_4] = b[HO][HCl]$
$Cl - O_3 \rightarrow ClO - O_2$	c	
$ClO - NO \rightarrow Cl - NO_2$	d	$c[Cl][O_3] = d[ClO][NO]$
$NO + O_3 \rightarrow NO_2 + O_2$	e	
$NO_2 - h\nu \rightarrow NO - O$	f	$f[NO_2] = ([ClO] + e[O_3])[NO]$
$NO_2 + ClO \rightarrow ClONO_2$	g_M	
$CLONO_2 + h\nu \rightarrow Cl + NO_2 + O$	h	$g_M[NO_2][ClO] = h[ClONO_2]$
$HO + NO_2 \rightarrow HNO_3$	i_M	
$HNO_3 + h\nu \rightarrow HO + NO_2$	j	$i_M[HO][NO_2] = j[HNO_3]$

$[ClO] \approx C_1[Cl_x]/[NO] \qquad [NO_2] \approx C_2[NO_x]$ where:

$$\frac{[Cl_x]}{[ClO]} = \frac{ad[CH_4][NO]}{bc[HO][O_3]} + \frac{g(d[ClO] + e[O_3])[NO]}{f} - 1 = \frac{[NO]}{C_1}$$

$$\rightarrow \{ad[CH_4]/bc[HO][O_3] + ge[O_3]/f\}[NO], \text{ low stratosphere}$$

$$[NO_x]/[NO_2] = \{ 1 + f/(e[O_3] + d[ClO]) + i_M[HO]/j + g_M[ClO]/h \} = 1/C_2$$

$$\rightarrow \{1 + f/e[O_3] - i_M[HO]/j + g_M[ClO]/h\}, \text{ low stratosphere}$$

$$\rightarrow \{1 + f/d[ClO] + i_M[HO]/j\}, \text{ high stratosphere}$$

From this relation, we had assumed that chlorine nitrate increased with NO_x, but Figure 3.5 shows it to be otherwise. By virtue of reaction (d) between nitric oxide and chlorine oxide

$$NO + ClO \rightarrow NO_2 + Cl$$

the concentration of chlorine oxide is reduced by nitric oxide. As given in Table 3.2, ClO is approximately proportional to Cl_x and inversely proportional to NO in the lower stratosphere

$$[ClO] = C_1[Cl_x]/[NO] \tag{11}$$

The "constant" C_1 depends weakly on the concentrations of ozone, hydroxyl radicals, and methane, Table 3.2. Substitution of (11) into (10) gives the concentration of chlorine nitrate as

$$[ClONO_2] = (C_1 g_M/h)[Cl_x]([NO_2]/[NO]) \tag{12}$$

With NO_2 in the numerator and nitric oxide in the denominator of (12), it would appear that chlorine nitrate should be independent of NO_x. However, the ratio of nitrogen dioxide to nitric oxide depends on the concentration of ozone. In the lower half of the stratosphere where chlorine nitrate is important, the ratio of nitrogen dioxide to nitric oxide is approximately

$$[NO_2]/[NO] = e[O_3]/f \tag{13}$$

and the final expression for chlorine nitrate from this simplified mechanism is

$$[ClONO_2] = (C_1 g_M e/hf)[Cl_x][O_3] \qquad (14)$$

This expression agrees with and explains Figure 3.5. At constant (reference) N_2O boundary conditions, chlorine nitrate increases approximately linearly with $[Cl_x]$, Figure 3.5-a. At constant Cl_x (for example 8 ppbv in Figure 3.5-b, but also for any other value of Cl_x), as nitrous oxide increases ozone decreases in the lower stratosphere (Figure 3.1), the ratio of $[NO_2]/[NO]$ decreases (13), and chlorine nitrate decreases (12).

Profiles of chlorine oxide are given in Figure 3.6, and these follow the main features of the mechanism in Table 3.2. As indicated by (11), ClO increases with Cl_x at constant N_2O boundary condition (Figure 3.6-a). At constant Cl_x (8 ppbv, for example), chlorine oxide decreases with increasing nitric oxide, which increases with increasing N_2O (Figure 3.6-b).

Profiles of nitrogen dioxide are given in Figure 3.7. According to the simplified mechanism of Table 3.2, the ratio of nitrogen dioxide to total NO_x is the somewhat complicated expression C_2, which however takes on relatively simple forms in the upper and in the lower stratosphere. In the upper stratosphere, the reaction rate of nitric oxide with chlorine oxide (d) is very fast (Figure 3.8-a), becoming faster than the rate of nitric oxide with ozone (e). The increase of NO_2 with increasing Cl_x seen above 30 km in Figure 3.7-a is a result of reaction (d), as approximately given by the high stratosphere limit of C_2 in Table 3.2. The effect of reaction (d) falls off very rapidly below 30 km (Figure 3.8-a), and the rate of reaction of ozone with nitric oxide dominates in the region of maximum ozone concentration. The erosion of the NO_2 profile between 20 and 30 km with increasing Cl_x shown in

Figure 3.7-a is caused by the formation of chlorine nitrate, the term $g_M[ClO]$ in the low altitude form of C_2 in Table 3.2.

The rate of chlorine nitrate formation (Figure 3.8-b) reflects the trends of NO_2 concentrations above 30 km (Figure 3.7-a) and the trends of chlorine oxide concentrations below 30 km (Figure 3.6-b)

The explanations given above do not include the effect of atmospheric motions on the local concentrations of chemical species, and thus are not expected to be and are not fully quantitative. However, the simple mechanism of Table 3.2 does give a definite, semi-quantitative explanation of the major features of Figures 3.5–3.8.

3.4.4 Ozone Loss-Rate Profiles Over a Wide Range of NO_x and Cl_x

Reaction rate profiles for reaction (6), $NO_2 + O$, and for reaction (8), $ClO + O$, are given for a wide range of NO_x and Cl_x in Figure 3.9. These reaction-rate profiles should be studied in conjunction with Figure 3.2-a. From bottom to top, the three strips in Figure 3.9 correspond to the curves marked 2, 1, and 1/2 in Figure 3.2-a, for which the changes of ozone column with increasing Cl_x from 1 to 22 ppbv are linear, slightly non-linear, and extremely non-linear with strong downward curvature, respectively.

Nitrous oxide is given its reference value, and Cl_x changes from 1 to 22 ppbv across the center strip of Figure 3.9. At 1 ppbv Cl_x, ozone destruction by NO_x (6) is much faster than ozone destruction by Cl_x (8) at all altitudes; 8 ppbv Cl_x has overtaken NO_x at all altitudes above 35 km; 15 ppbv Cl_x has overtaken NO_x at all altitudes (Note: the curve of ozone reduction vs Cl_x is distinctly non-linear at and above this point in Figure 3.2-a); and 22 ppbv Cl_x dominates ozone destruction from 20 to 55 km.

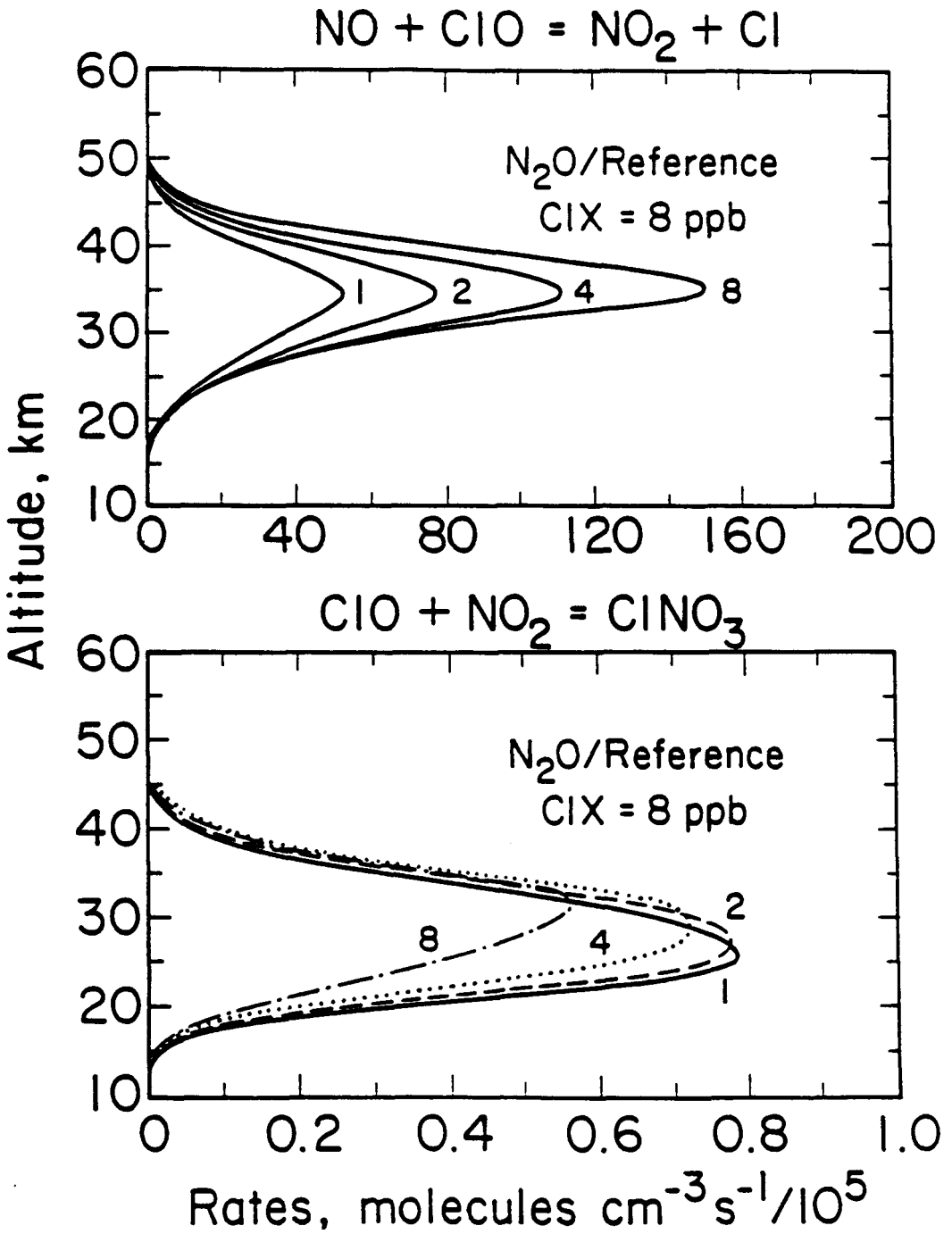

Figure 3.8. Profiles of rates of reaction for the same model atmospheres as those in Figure 3.4-b. (a) At fixed Cl_x, the fast reaction shown here between nitric oxide and chlorine monoxide reduces ClO upon increasing NO_x. (b) At fixed Cl_x, the rate of formation of chlorine nitrate decreases with increasing NO_x.

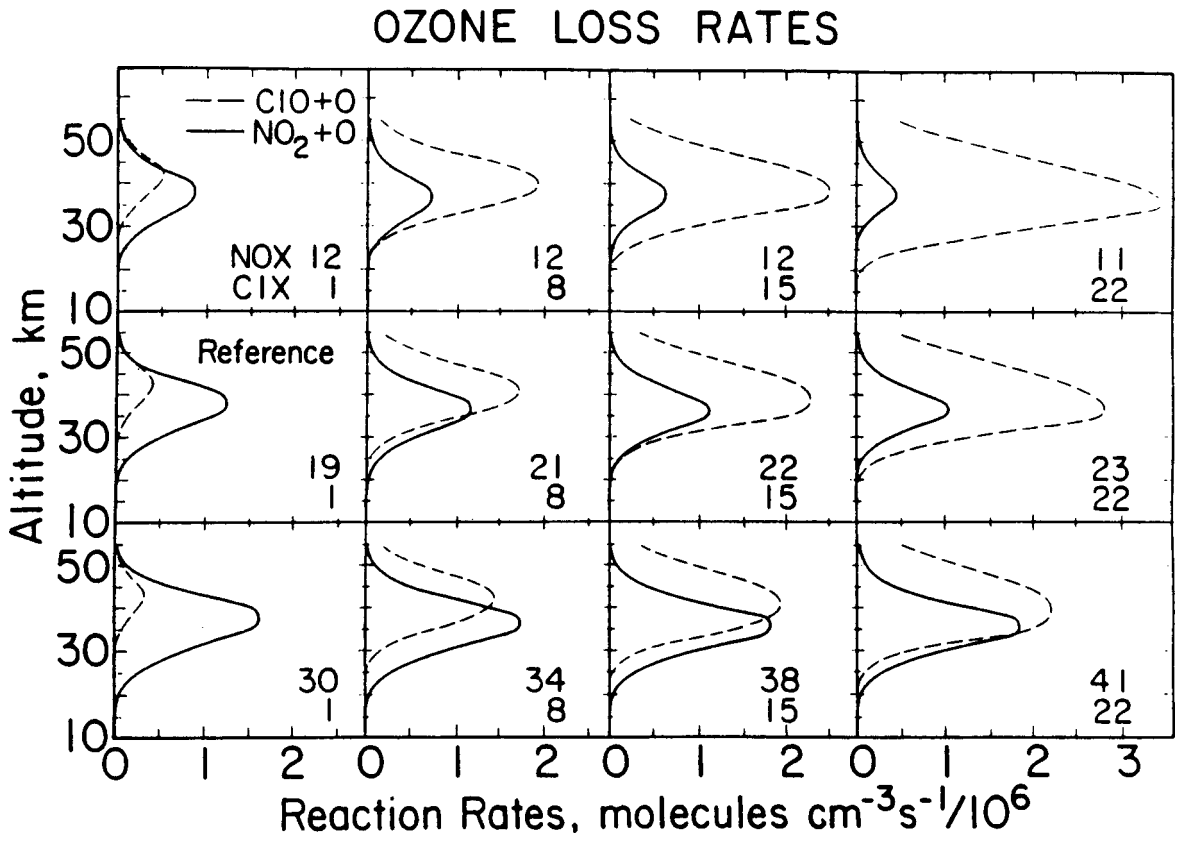

Figure 3.9. Profiles of ozone loss rates due to NO_x ($NO_2 - O \rightarrow NO + O_2$) and to Cl_x ($ClO + O \rightarrow Cl - O_2$) for a wide range of hypothetical atmospheres: (N_2O/reference = 1/2, 1, 2; Cl_x/ppbv = 1, 8, 15, 22). From top to bottom, the rows correspond to the cases in Figure 3.2-a where ozone reduction is, respectively, highly non-linear, slightly non-linear, and linear with increasing Cl_x. The onset of non-linearity in Figure 3.2-a occurs when stratospheric Cl_x has increased to the degree that the rate of ClO+O exceeds that of NO_2+O below about 35 km: panel 12,8 in the first row; panel 22,15 in the second row; and 41,22 in the last row.

When the boundary value of N_2O is twice the reference value (bottom strip of Figure 3.9), the NO_x ozone-destroying curve exceeds that for Cl_x at altitudes below about 30 km in all panels, and the reduction of the ozone column is linear in increasing Cl_x, Figure 3.2-a. The top strip of Figure 3.9 is based on the hypothetical scenario of one-half the reference value of nitrous oxide. In this case ozone

destruction is dominated by NO_x at 1 ppbv Cl_x, 8 ppbv or more Cl_x overwhelms NO_x, and total ozone changes non-linearly with added chlorine at and above 8 ppbv (Figure 3.2-a). These three cases suggest that total ozone changes linearly with Cl_x until the rate of ClO + O exceeds that of NO_2 – O below about 30 km, and then it becomes non-linear with downward curvature.

Objections can be raised to this statement, including inquiries about other ozone-destroying processes such as catalytic cycles closed by the reactions

$$HOCl + hv = HO + Cl \tag{15}$$

$$NO_3 + hv = NO + O_2 \tag{16}$$

$$NO_2 + NO_3 = NO + O_2 + NO_2 \tag{17}$$

$$ClO + ClO = O_2 + Cl_2 = O_2 + Cl + Cl \tag{18}$$

$$= ClOO + Cl = O_2 + Cl + Cl$$

The rates of (15) and (16) are significant relative to (8) and (6) only in the lowest stratosphere, where all of these rates are vanishingly slow. Even at the high values of NO_x or Cl_x, the rates that are bimolecular in radicals, (17) and (18), are very slow compared respectively to (6) and (8) at altitudes where the rates of (6) or (8) are important. Reactions (17) and (18) are not included in the model, and these statements are based on spot calculations.

For each of the horizontal strips of Figure 3.9, which represents a constant nitrous oxide boundary condition, as Cl_x increases from 1 to 22 ppbv the entire rate-profile of (6) O + NO_2 decreases. Likewise reading down any vertical column in Figure 3.9, one sees that the rate-profile of (8) O + ClO for constant ppbv Cl_x decreases as NO_x increases. Throughout this wide range of conditions, any

increase of stratospheric Cl_x tends to shrink the rate profile of ozone destruction by NO_x, and any increase of nitrous oxide tends to shrink the rate profile of ozone destruction by Cl_x.

Another interesting aspect of this study concerns the vertical spread of the rates of ozone destruction by the NO_x and Cl_x reactions. The "spread" of the plots of reaction-rate profiles in Figure 3.9 is defined as full altitude difference between the two points where the rate is half the maximum value. Over the 12 individual panels in Figure 3.9, the spread of the NO_x profiles covers the narrow range of 11 to 13 km, but the spread of the Cl_x profiles varies from 9 to 18 km.

3.5 Special Atmospheres

The calculations reported above concern large variations of NO_x and Cl_x, but no variation of HO_x was carried out, since a three-dimensional variation of parameters would involve a prohibitive amount of computer time. To explore effects of large changes of HO_x, calculations are given for "special atmospheres" with various inclusions and exclusions of the entire families, NO_x, HO_x, and Cl_x, from the model, Table 3.3.

3.5.1 Ozone Profiles Calculated With Different Model Atmospheres

Figure 3.10-a gives the ozone vertical profiles calculated by the reference model and the ozone profile calculated from the Chapman model. The Chapman model gives an ozone column 59 percent greater than the reference model.

The effects of deleting the individual NO_x, HO_x, and Cl_x families, one at a time, from the reference atmosphere are shown in Figures 3.10-c, 3.11-b and given in Table 3.3-b. In terms of the 1985 model, removal of all chlorine species from the reference atmosphere has almost no effect on the ozone column or the altitude

Table 3.3 Special Atmospheres

a) The effect of adding one family of ozone destroying catalysts at a time to the Chapman or O_x only atmosphere in terms of percentage ozone column (molecules cm^{-2}) change relative to the Chapman model and relative to the Reference model: 1.1 ppb Cl_x at 50 km as generated by CH_3Cl and CCl_4, and with other species corresponding to values appropriate to 1960.

O_x	NO_x	Cl_x	HO_x	HC HO_x	Column Ozone (÷ E18)	Percent Difference Relative to Reference Atmosphere	Percent Difference Relative to Chapman Model
X	O	O	O	O	14.72	+59.2	+ 0.0
X	X	O	O	O	7.425	−19.7	−49.6
X	O	X	O	O	8.442	− 8.4	−42.6
X	O	O	X	O	10.99	+18.9	−25.3
X	O	O	O	X	10.57	+14.3	−28.2
X	X	X	X	X	9.244	+ 0.0	−37.2

X = present, O = absent.
O_x = $O(^3P) + O(^1D) + O_3$.
NO_x = $N + NO + NO_2 + N_2O + NO_3 + 2N_2O_5$.
Cl_x = $Cl + ClO + CCl_4$.
HO_x = $H + HO + HO_2 + H_2O_2 + H_2 + H_2O$.
HC = $CH_4 + HCO + CH_2O + CH_3OOH - CH_3O + CH_3O_2 - CO + CH_3$.
Reference atmosphere includes HNO_3, $HOONO_2$, HOCl, $ClONO_2$, etc.

b) The effect of removing one family of ozone destroying catalysts at a time from the Reference (1960) model atmosphere in terms of percentage ozone column change relative to the Chapman model and relative to the Reference model.

Chapman Model	NO_x	Cl_x	HC HO_x	Column Ozone (÷ E18)	Percent Difference Relative to Reference Atmosphere	Percent Difference Relative to Chapman Model
X	X	X	X	9.244	+ 0.0	−37.2
X	O	X[a]	X[a]	7.449	−19.7	−49.4
X	X[b]	O	X[b]	9.348	+ 1.1	−36.5
X	X[c]	X[c]	O	7.416	−19.7	−49.6
X	O	O	O	14.72	+59.2	+ 0.0

a) Includes CH_3Cl, HCl, HOCl.
b) Includes $HONO_2$, HO_2NO_2, HONO.
c) Includes $ClONO_2$, $ClNO_2$.

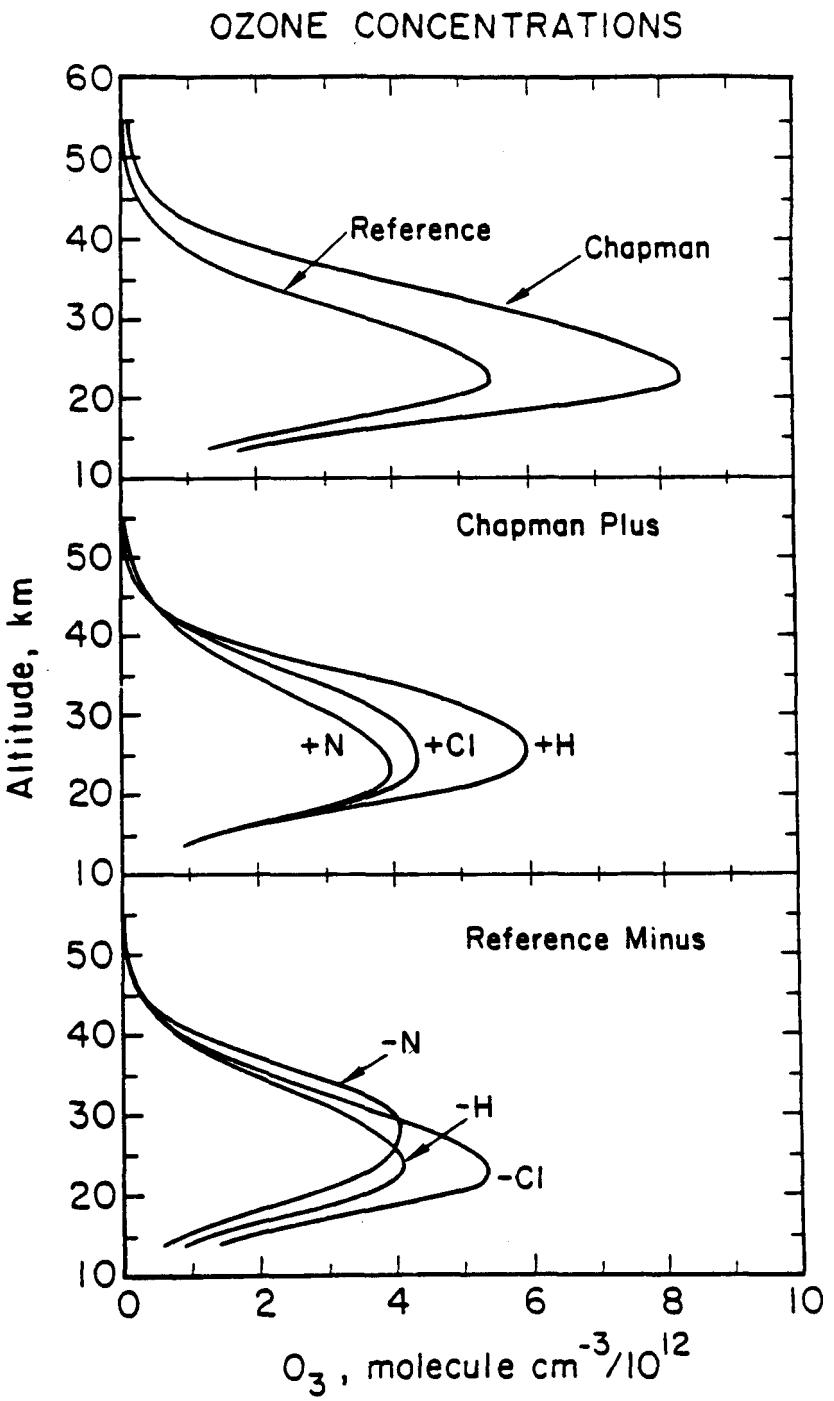

Figure 3.10. Calculated ozone vertical profiles for various special atmospheres. (a) Top panel: Chapman or O_x model with only O_2, O, and O_3 as reactive species; the reference atmosphere, presumably that existing in 1960, including 1.1 ppbv Cl_x and the amounts of NO_x, HO_x, and methane derivatives as given in Table 3.3. (b) The Chapman model plus either the NO_x family, the HO_x family, or the Cl_x family. (c) The reference model with the complete removal of either the NO_x family, the HO_x family, or the Cl_x family. The profile with all chlorine removed is almost identical with the reference profile of (a).

of the ozone profile, and thus the curve marked -Cl may be regarded as the ozone profile of the reference atmosphere. Removal of all NO_x, leaving hydrogen species and 1.1 ppbv Cl_x, gives a 19.4 percent ozone reduction and a substantial increase in the altitude of the ozone profile (Figure 3.10-c), relative to the reference model. Removal of all hydrogen species gives a 19.8 percent ozone reduction with little change in the ozone-profile altitude, relative to the reference atmosphere.

Using the 1985 atmospheric model, the effect of adding just the HO_x reactions (including methane) to the O_x reactions is given by Figure 3.10-b, 3.11-a and in Table 3.3-a. The ozone column is reduced 28 percent relative to the Chapman value (increased 14 percent relative to the reference atmosphere); with the exclusion of methane and its derivatives the reduction is 25 percent relative to the Chapman model. Adding only NO_x to the O_x family, the calculated ozone column is given in Figure 3.10-b, and Table 3.3-a. The ozone column is reduced 50 percent relative to the Chapman mechanism, it is about 20 percent lower than the reference column, and the calculated profile is similar in shape and in peak altitude compared to the observed ozone profile. In 1960 the amount of stratospheric chlorine, Cl_x, was about 1.1 ppbv. When this small amount is added to the Chapman model (with no NO_x or HO_x), the calculated ozone column is reduced 43 percent below the O_x model, the column is 8 percent less than that of the reference atmosphere (Table 3.3-a), and the ozone profile (Figure 3.10-b) and is similar to but slightly broader than that of the reference model. This calculation shows that chlorine in the absence of HO_x and NO_x is an extremely powerful destroyer of ozone (also see ozone difference profile, Figure 3.11-a). Similar calculations using then current stratospheric chemistry were made by Chang and Duewer [1979]; aside from some quantitative differences similar results were obtained in 1979 and in this study.

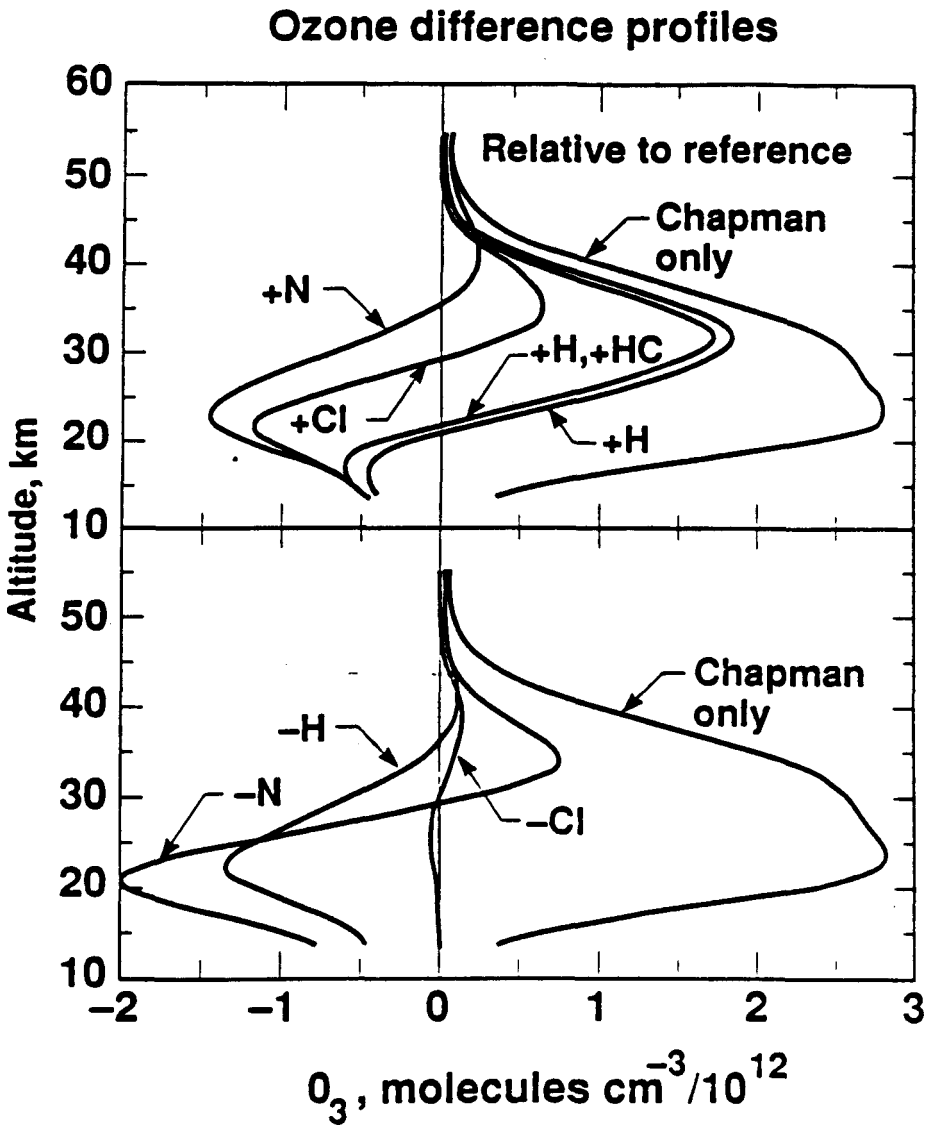

Figure 3.11. Ozone difference profiles for various special atmospheres. (a) The Chapman model plus either the NO_x family, the Cl_x family, the HO_x family, or the HO_x family plus methane chemistry. (b) The reference model with the complete removal of either the NO_x family, the HO_x family or the Cl_x family.

Adding 1.1 ppbv of Cl_x to the Chapman model reduces the ozone column by 43 percent relative to the O_x only atmosphere (Table 3.3-a, Figures 3.10-b, 3.11-a), but removing all (1.1 ppbv) chlorine from the reference model has virtually no effect on the ozone vertical column nor on the ozone vertical profile (Table 3.3-b.

Figures 3.10-c, 3.11-b). The contrast between the effect of 1.1 ppbv in Figure 3.10-c and Figure 3.10-b shows that the NO_x and HO_x families almost completely suppress the effect of 1 ppbv chlorine on ozone; but in the absence of NO_x and HO_x, even 1 ppbv chlorine is a powerful ozone destroying catalyst.

3.5.2 Ozone Destruction Rates in the Special Atmospheres

Ozone destruction by the reaction, $O + O_3 \rightarrow 2\ O_2$. Vertical profiles of the rates of ozone destruction are given by Figure 3.12. In the Chapman model, essentially the only chemical process that destroys ozone is (3) $O + O_3$, and this rate of odd oxygen destruction for the Chapman model is given in Figure 3.12-a. In the reference model, the ozone-destroying catalysts supplant this reaction, reducing its peak value by a factor of three, Figure 3.12-a. When HO_x is removed from the reference model, rate (3) increases especially above 45 km, the region previously dominated by HO_x. When NO_x is removed from the reference model, the rate, $O + O_3$, increases especially in the 35-45 km range. Removal of Cl_x from the reference model produces a very small increase in (3) between 40 and 45 km (not shown in Figure 3.12-a).

Ozone destruction by the reaction, $O + HO_2 \rightarrow HO + O_2$. There are at least five ozone destroying catalytic cycles based on the free radicals derived from water. The principal ozone destroying HO_x reaction in the middle and upper stratosphere is

$$HO + O_3 \rightarrow HOO + O_2 \qquad (19)$$

$$HOO + O \rightarrow HO + O_2 \qquad (20)$$

$$\text{Net}: \quad O_3 + O \rightarrow 2\ O_2$$

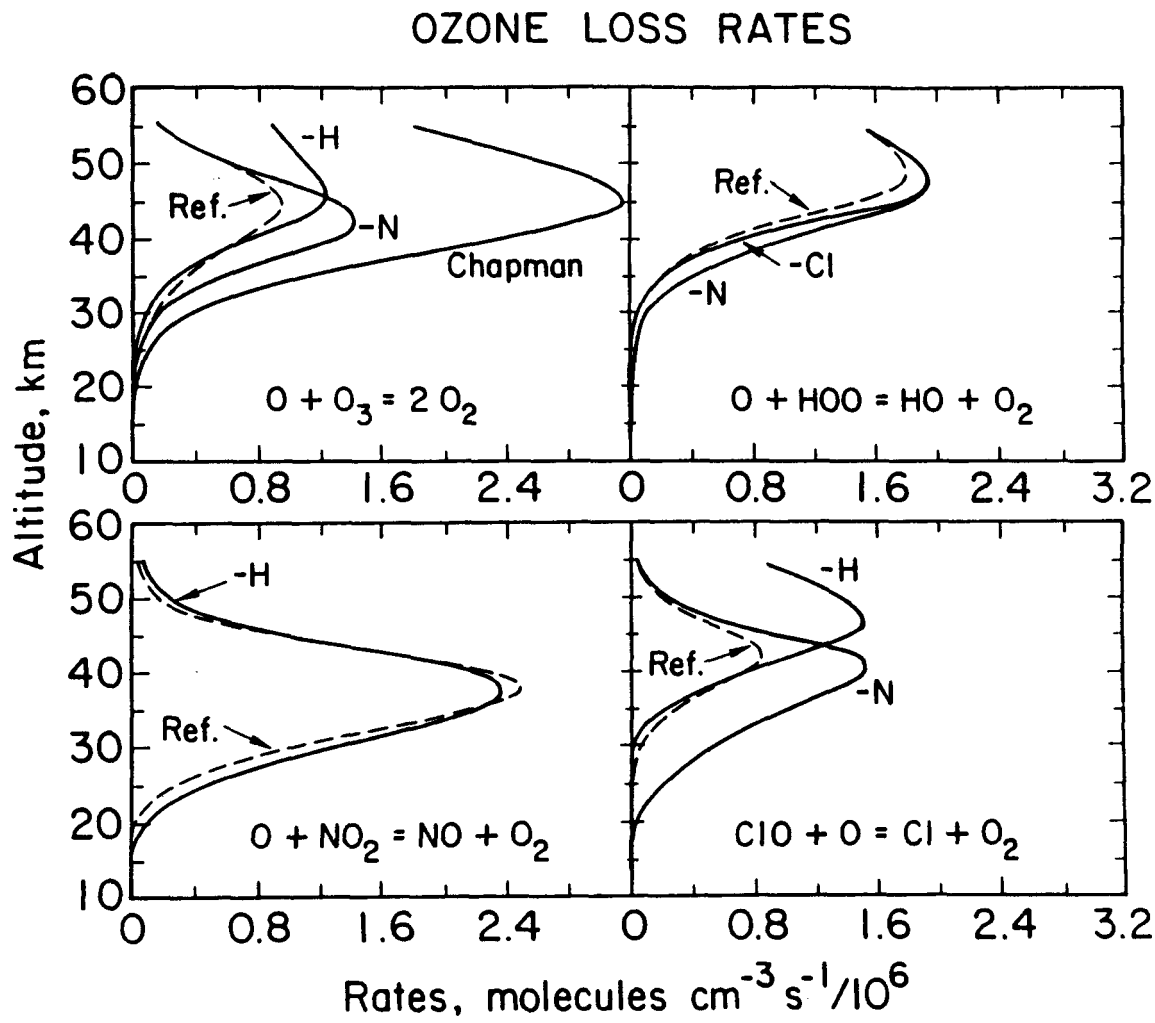

Figure 3.12. Profiles of ozone loss rates as caused by various chemical reactions and for various special atmospheres whose ozone profiles are given by Figure 3.10-a and c. (a) Reaction $O + O_3 = 2\ O_2$, as influenced by the presence or absence of H, N, or Cl species. (b) Reaction $O + HOO \rightarrow HO + O_2$, as influenced by the presence or absence of N or Cl species. (c) Reaction $O + NO_2 \rightarrow NO + O_2$, as influenced by the presence of absence of H or Cl species. (d) Reaction $O + ClO \rightarrow Cl + O_2$, as influenced by the presence or absence of H or N species. The ozone loss rates given in this figure are twice the rate of these reactions.

for which the rate-determining step is (20), O + HOO. The rate of (20) is shown as a function of altitude in Figure 3.12-b. Relative to the reference atmosphere, its rate is slightly increased between 25 and 50 km by omission of NO_x (about 19 ppbv), and it is slightly increased between 40 and 50 km by removal of Cl_x (1.1

ppbv), Figure 3.12-b. The principal feature of Figure 3.12-b is that the rate profile of (20) is only slightly changed by total removal of NO_x or Cl_x.

Ozone destruction by the reaction, $O + NO_2 \rightarrow NO + O_2$. The dominant ozone destroying mechanism in the reference model is the NO_x catalytic cycle (5, 6), with (6) as rate determining step. The rates of ozone destruction by NO_x for the reference atmosphere and for the reference atmosphere minus all hydrogen containing species are shown in Figure 3.12-c. Removal of Cl_x from the reference atmosphere has no detectable effect on the rate profile of (6), and it is not shown as a separate curve. Although removal of HO_x from the reference model causes a small increase of the rate of $O + NO_2$ below 34 kilometers and above 45 kilometers, it has little effect on the magnitude or altitude of this rate profile as a whole. This result is unexpected, since large amounts of nitrogen dioxide are tied up as nitric acid in the lower stratosphere, and elimination of HO_x releases the NO_2 from nitric acid and is expected to increase the rate of (6). When HO_x is omitted, nitrogen dioxide does increase, but ozone (Figure 3.10-c) and thus atomic oxygen decrease in the lower stratosphere. This increase of nitrogen dioxide and decrease of atomic oxygen very nearly balance, and there is no major change in the rate profile of reaction (6). Figure 3.12-c shows that the vertical profile of ozone destruction by NO_x is largely unmoved by total elimination of HO_x or Cl_x.

Ozone destruction by the reaction, $O + ClO \rightarrow Cl + O_2$. The reactions that destroy ozone in the chlorine system are primarily (7) and (8), the rate of ozone destruction being twice the rate of (8), $O + ClO$. In the reference model with 1.1 ppbv Cl_x, its rate of ozone destruction is much less than that for HO_x or NO_x (compare Figure 3.12-d with 3.12-b and 3.12-c), but it does have significant values between 35 and 50 km, Figure 3.12-d. Upon removal of NO_x, the rate of $O + ClO$ increases throughout the region where NO_x had been dominant, and it becomes

an important ozone destroying mechanism between 25 and 45 km (Figure 3.12-d). Upon removal of HO_x, chlorine reactions take over ozone destruction in the uppermost stratosphere, where HO_x had been dominant, Figure 3.12-d.

The strong increase in ozone destruction by Cl_x upon removal of HO_x and NO_x is examined in more detail in Figure 3.13. (This figure gives the rate of the reaction. ClO + O: Figure 3.12-d gives the rate of ozone destruction by this reaction , which is a factor of two greater). The role of 1.1 ppbv of stratospheric Cl_x is relatively small and vertically constrained in the reference model (Figure 3.12-d). Upon removal of NO_x, the upper boundary of the Cl_x ozone-destroying profile remains at about the same altitude, but Cl_x ozone destruction moves down into the stratosphere where NO_x had been dominant (Figure 3.13). Upon removal of NO_x and HO_x from the model, chlorine destruction of ozone becomes important from 18 km to the top of the stratosphere.

From studying model calculations for realistic scenarios, one may get the impression that the altitude region for ozone reduction by Cl_x is largely in the 35 to 50 km range; but if NO_x or HO_x should be unexpectedly low in some region, ozone would undergo a large destruction by chlorine (via reaction 8) from 20 km to well above 55 km, Figure 3.13. Figure 3.9 gives another aspect to this situation: even in the presence of HO_x and NO_x, at high Cl_x the rate of ozone destruction by the reaction, O + ClO, is important from 20 km to well above 55 km. In its altitude flexibility, chlorine destruction of ozone is qualitatively different from NO_x and HO_x destruction of ozone.

3.6 Conclusion

For some cases, effects present in the reference or in mildly perturbed atmospheres are amplified by the unrealistic conditions included in this study so that

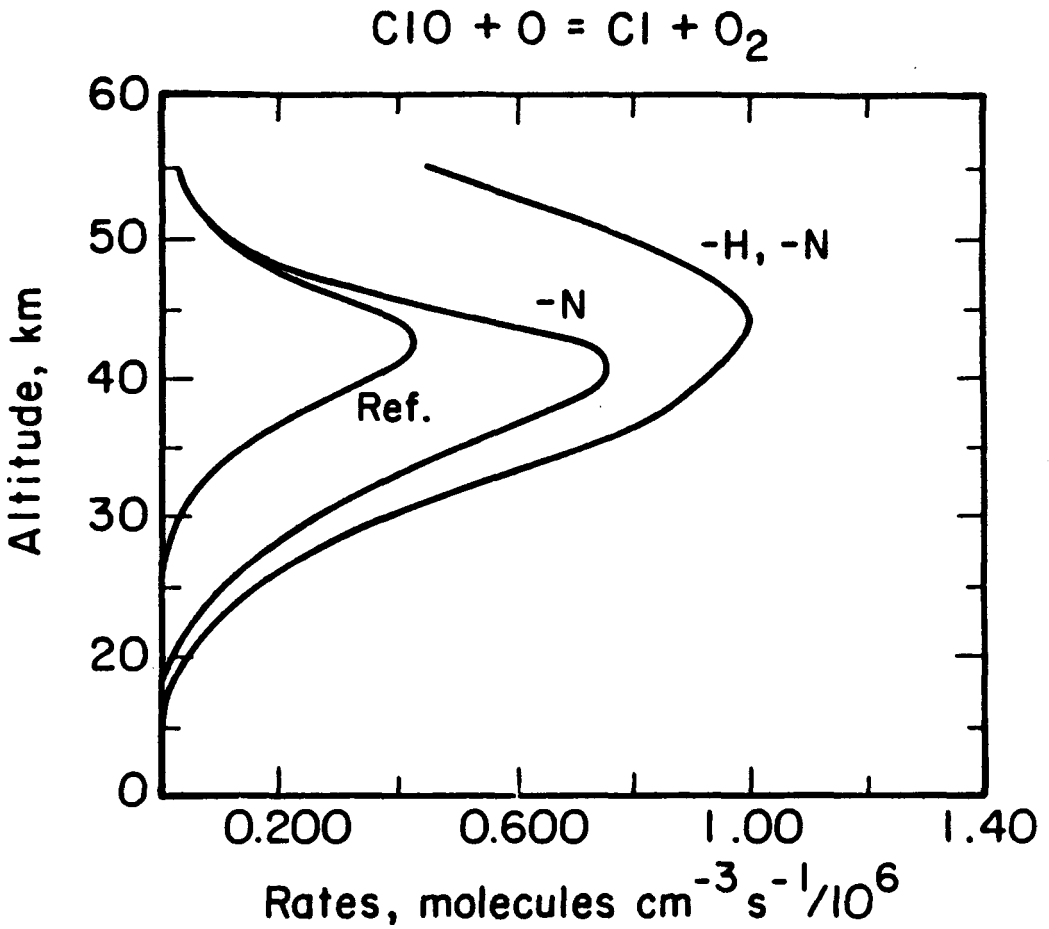

Figure 3.13. Increase in the reaction rate, $ClO + O \rightarrow Cl + O_2$, upon the assumed complete removal of all nitrogen species from the atmosphere and from the removal of both HO_x and NO_x species from the atmosphere (compare Figure 3.12-d). In this figure, the rate is that of the named reaction, not the rate of ozone loss, which is twice as great.

they become clearly visible on graphs. These effects should not be dismissed simply because unrealistic conditions are used to point them out. For other cases, the effects reported are properties of the large perturbations. They may be of interest to studies of primitive atmospheres, and perhaps they may be important at some latitudes in two-dimensional models. In any case, they are interesting in giving perspective to the real atmosphere.

*Chapter 4: Effects on Ozone from Aircraft Emissions**

4.1 Introduction

In the early to mid-1970s, there was concern about the potential effects of emissions of odd-nitrogen (NO_x) from commercial fleets of proposed supersonic transport (SST) aircraft. The concern was that these aircraft, if flying in large numbers, would produce exhaust emissions of NO_x sufficient to destroy a significant amount of stratospheric ozone [CIAP, 1975; NRC, 1975]. There recently has been renewed interest in the development of faster aircraft for intercontinental passenger flight (e.g., First International Conference on Hypersonic Flight in the 21st Century, University of North Dakota, Grand Forks, ND, September 1988). Such aircraft would probably spend a large fraction of their flight time in the stratosphere, perhaps at altitudes as high as 35 km. As a natural progression from studies that were done in the 1970s [Johnston, 1971; CIAP, 1975; Wuebbles and Chang, 1975; Cunnold et al., 1977; Luther et al., 1979] and as an extension of the sensitivity studies made in Chapter 3, this study investigates the sensitivity of stratospheric ozone to NO_x emissions in conjunction with current understanding of atmospheric chemical and physical processes.

---

* Kinnison, D. E., D. J. Wuebbles, and H. S. Johnston, "A study of the sensitivity of stratospheric ozone to hypersonic aircraft emissions," First International Conference on Hypersonics Flight in the 21st Century, Grand Forks, North Dakota, 1988b.

Kinnison, D. E., H. S. Johnston, and D. J. Wuebbles, "Sensitivity study of global ozone to NO_x emission from aircraft," International Quadrennial Ozone Symposium, Gottingen, Fed. Rep. of Germany, in press, 1988c.

Johnston, H. S., "Proposed use of excess carbon-14 data to test two-dimensional stratospheric models," in press, 1989.

Most prior analyses of the potential effects of aircraft emissions on ozone have depended on results from one-dimensional models of atmospheric processes, such as the one-dimensional model of the troposphere and stratosphere used at LLNL [Wuebbles, 1983]. These models, which determine the vertical distributions of important trace constituents, have the advantage of being computationally efficient while including detailed representations of atmospheric dynamical processes. However, the treatment of atmospheric dynamical processes in these models through an empirically based diffusion representation, has well recognized limitations [WMO, 1985, Chapter 12]. Nevertheless, the one-dimensional model remains a useful tool, particularly for sensitivity studies.

On the other hand, only a few limited studies of potential aircraft influences have been undertaken with two-dimensional, zonally averaged models of atmospheric chemical and physical processes [Cunnold et al., 1977; Widhopf et al., 1977, 1979]. Conceptually, the two-dimensional model has a number of advantages over the one-dimensional model, namely the inclusion of important effects from meridional motions in the stratosphere and the determination of latitudinal and seasonal variations in trace constituent distributions, as well as variations with altitude. A stronger theoretical basis for the treatment of dynamical processes in two-dimensional models has been developed in recent years through the residual mean or diabatic formulation of stratospheric transport [WMO, 1985, Chapter 12].

Many improvements in the model treatment of atmospheric chemical processes have been made over the last decade. Many chemical reaction rates and photodissociation parameters have been changed, and several chemical and photochemical reactions not recognized at the time of prior aircraft assessment studies have been included in current models, both based on more recent data from laboratory measurements [WMO, 1985, Chapter 2; DeMore et al., 1985, 1987].

Both the LLNL one- and two-dimensional chemical-radiative-transport models of the troposphere and stratosphere are used in this study. The one-dimensional model is used to examine the sensitivity of stratospheric ozone to varying amounts of NO_x injection amounts and flight altitudes for differing amounts of assumed stratospheric chlorine levels. This work is a continuation of chapter three, that examined the sensitivity of ozone changes in stratospheric nitrogen oxides as produced by varying tropospheric nitrous oxide (N_2O) over assumed large variations in stratospheric chlorine content. While in most cases the added NO_x reduced ozone, there were some situations, with large chlorine levels and small increased NO_x, where the added NO_x increased the total ozone column. In this study, we examine what conditions would be necessary for stratospheric aircraft emissions to lead to destruction of ozone, and what conditions would lead to an increase of ozone. Background chlorine is varied from 1.1 to 21.6 ppbv, assumed aircraft injections consider an eight-fold range in magnitude, and the altitude of NO_x injections are varied from 12 to 37.5 km.

The two-dimensional model (in a more limited sense, due to computational time limitations) is also used to examine the effects of nitrogen oxide emissions on ozone. Because of uncertainties in possible future emissions, it is necessary to examine the model sensitivity under a wide range in magnitude, altitude, and latitude of assumed NO_x emissions. As an initial study, the two-dimensional model is used to simulate a typical scenario from the CIAP era. These calculations are made for only one value of stratospheric Cl_y, 2.8 ppbv, that of about 1988; injection altitudes are varied from 16.5 to 34.5 kilometers; and injection rates are varied by a factor of three. Most injections are done for a narrow latitude band in the northern hemisphere (37 to 49 degrees), one is spread uniformly over the northern hemisphere, and another is spread uniformly over the globe. These calculations are sensitivity studies for the currently expected effects of injecting

nitrogen oxides, as if from aircraft, into the stratosphere. No consideration is given to any specific machines or scenarios. If these calculations were applied to any specific aircraft, one would have to consider such things as altitude and latitude flight patterns, rate of nitrogen oxide production in the exhaust, number of craft, and other details. The Climatic Impact Assessment Program (CIAP, 1975; Alyea et al., 1975) considered a rate of nitrogen oxides injection from a "large" fleet of commercial aircraft flying at 20 kilometer altitude as 1.8×10^9 (1.8 Mt) kg yr^{-1} of nitrogen oxides calculated as if NO_2. In the early 1970s, this injection rate was nominally that of 500 proposed U.S. supersonic aircraft flying at 20 kilometers 8 hours per day and with one estimate of the NO_x emission index and one estimate of the rate of fuel consumption. This injection rate is the upper limit considered by the two-dimensional model and the geometrical average of the range considered by the one-dimensional model.

4.2 Results from One-Dimensional Model

The LLNL one-dimensional chemical-radiative-transport model of the troposphere and stratosphere was used in this study, and references and boundary values are given in chapter three. Photochemical rate coefficients are from DeMore et al. [1985], except for a small number of special calculations that use DeMore et al. [1987]. The boundary values of the reference atmosphere were selected to reproduce the composition of about 1960, including 1.1 ppbv of Cl_y at 55 km and 300 ppbv of N_2O in the troposphere to give 19.4 ppbv of NO_y at 37.5 km. This article uses a slightly different notation from that of chapter 3 in that NO_x includes only the active radical species and their temporary reservoir ($N + NO + NO_2 + NO_3 + 2N_2O_5$) and NO_y includes these species and the interaction species ($HNO_3 + HNO_4 + ClONO_2 + ClNO_2$). Similarly, Cl_x includes only the active species ($Cl + ClO$), and Cl_y adds HCl, HOCl, $ClONO_2$, and $ClNO_2$.

Most of the one-dimensional model results of this study are presented in Table 4.1, which gives the percentage change of the ozone vertical column for 137 different assumed conditions. The CIAP [1975] injection rate of 1.8 Mt yr^{-1} as NO_2 is about the same as 1500 molecules $cm^{-3}s^{-1}$ over a one kilometer band. These one-dimensional calculations use 0, 500, 1000, 2000, and 4000 of these units, which thus spans from one-third to almost three times the CIAP reference value. Five values of stratospheric chlorine, 1.1, 3.1, 7.9, 14.7, and 21.6 ppbv, are included (often expressed as the nominal values of 1, 3, 8, 15, and 22 ppbv). The reference value of 1.1 ppbv corresponds to the stratosphere in about 1960, 3.1 ppbv is approximately that of 1988, 7.9 ppbv is the calculated future steady-state Cl_y value if ClC's (chlorocarbons) are produced and released indefinitely at the present (1988) rate, 14.7 ppbv is the calculated steady-state value if the use and release of ClC's should double, and 21.6 ppbv is an unrealistically large value for stratospheric Cl_y used to bracket the realistically expected range. These calculations are given in Table 4.1 for 8 altitudes. In terms of aircraft, these altitudes roughly correspond to current commercial aircraft (12 km), to the French-British Concorde (17 km), to the 1971 American-planned supersonic transport (20 km), and to possible future hypersonic aircraft (23 to 37 km).

Table 4.1 also includes calculated ozone changes for NO_x injected at 20 kilometers and with methane doubled. These results parallel those for 20 kilometers without doubling methane, but with doubled methane the ozone reductions are of somewhat lesser magnitude. Since the differences are so small, calculations with methane variations were not included at other altitudes.

Aircraft exhaust gases include much more water vapor than nitrogen oxides, and some calculations including 90 times as much water vapor as nitric oxide are shown in Table 4.2. For two widely different values of Cl_y, for one injection magnitude, and for three injection altitudes, the maximum changes in the ozone

Table 4.1 Percent change in column ozone as a result of various injection rates of nitric oxide from stratospheric aircraft at various altitudes and for various assumed constant background mixing ratios of Cl_y (ppbv) at 50 km. Injection rates are in units of molecules $cm^{-3}s^{-1}$ over a one kilometer band width centered at the stated altitude. LLNL one-dimensional model.

		NO_x Injection Altitude (km)							
Cl_y	Injection rate	12	17	20	23	27	30	34	37.5
1.1	0	−0.0	−0.0	−0.0	−0.0	−0.0	−0.0	−0.0	−0.0
	500	−0.1	−1.0	−3.0			−5.1		
	1000	−0.2	−2.2	−6.3			−9.4		
	2000	−0.2	−4.9	−13.1			−16.6		
	4000	−0.1	−10.8	−24.7			−26.5		
3.1	0	−1.4	−1.4	−1.4	−1.4	−1.4	−1.4	−1.4	−1.4
	500	−1.3	−2.1	−3.8	−5.4	−5.9	−5.6	−5.0	−3.6
	1000	−1.2	−3.1	−6.8	−9.8	−10.9	−9.7	−8.4	−7.3
	2000	−1.1	−5.5	−13.2	−18.3	−18.3	−16.3	−14.0	−11.8
	4000	−1.1	−11.0	−23.5	−30.3	−29.6	−25.7	−21.2	−18.5
7.9	0	−5.1	−5.1	−5.1	−5.1	−5.1	−5.1	−5.1	−5.2
	500	−4.9	−5.3	−6.3	−7.4	−7.7	−7.5	−7.1	
	1000	−4.8	−5.8	−8.5	−10.8	−11.4	−10.8	−9.8	−9.0
	2000	−4.6	−7.5	−13.9	−18.5	−17.0	−15.0	−13.1	
	4000	−4.4	−12.1	−24.7	−30.6	−29.5	−26.7	−23.0	−19.6
14.7	0	−12.2	−12.2	−12.2	−12.2	−12.2	−12.2	−12.2	−12.2
	500	−11.9	−11.3	−11.1			−11.2		
	1000	−11.7	−10.9	−11.7			−13.0		
	2000	−11.3	−11.3	−15.5			−18.4		
	4000	−10.7	−14.3	−25.2			−27.7		
21.6	0	−23.6	−23.6	−23.6	−23.6	−23.6	−23.6	−23.6	−23.6
	500	−23.1	−20.5	−17.8			−16.2		
	1000	−22.7	−18.5	−16.2			−15.7		
	2000	−21.8	−16.7	−17.5			−19.6		
	4000	−20.4	−17.2	−25.7			−28.5		

column caused by the added exhaust water vapor varied between −0.005 and −0.08 percent. Over this range of conditions, the injected nitrogen oxides gives a calculated ozone column change between −11 and −14 percent. In this model, the effect on ozone of water vapor in the aircraft exhaust is extremely small compared to the effect of the nitrogen oxides in the exhaust. On the basis of these studies, the water boundry value was not varied in any of the sensititivity scenarios in Table 4.1.

Table 4.2 Effect of injecting water vapor at 90 times the rate of injecting nitric oxide. The table gives the value of the vertical ozone column in multiples of 10^{18} molecules cm^{-2}. Injection rates are in units of molecules $cm^{-3}s^{-1}$ over one kilometer band, centered at the stated altitude. The reference atmosphere depends on the background Cl_y value. LLNL one-dimensional model.

Altitude (km)	Cl_y/ppbv	NO inj. rate	H_2O inj. rate	Ozone Column ($\div 10^{18}$)	% change (by H_2O)
20	1.1	0	0	9.2439	
	1.1	2000	0	8.0351	
	1.1	2000	1.8×10^5	8.0355	+0.005
30	1.1	2000	0	7.7063	
	1.1	2000	1.8×10^5	7.7043	−0.03
20	7.9	0	0	8.7747	
	7.9	2000	0	7.9566	
	7.9	2000	1.8×10^5	7.9567	+0.001
30	7.9	2000	0	7.6592	
	7.9	2000	1.8×10^5	7.6565	−0.04
37.5	7.9	2000	0	7.1923	
	7.9	2000	1.8×10^5	7.1869	−0.08

Figure 4.1 gives a straight-forward presentation of changes in the ozone column for NO_x injections at 20 kilometers and for stratospheric chlorine varying from 1 to 22 ppbv. At large NO_x injection rates, 2000 to 4000 molecules $cm^{-3}s^{-1}$, the ozone column is reduced by about 15 to 25 percent, almost regardless of the amount of chlorine in the stratosphere. At small NO_x injection rates, the effect on the ozone

column is strongly dependent on the amount of chlorine present. If Cl_y is 1 or 8 ppbv, small NO_x injections decrease ozone; if Cl_y is 15 or 22 ppbv, small NO_x injections increase the ozone column relative to the ozone reduction caused by the chlorine. This "buffering effect" that occurs when background Cl_x varies with the five NO_x injection cases can also be seen in Table 4.3. Here the percent change in total ozone is relative to the background Cl_y (1.1, 3.1, 7.9, 14.7, and 21.6 ppbv) and not the "1960" Reference atmosphere. For example, when considering background values of Cl_y of 3.1 and 7.9 ppbv, injecting at 20 km with an injection rate of 2000, ozone is reduced by 11.8 percent with 3.1 ppbv Cl_y and 8.8 percent with 7.9 ppbv Cl_y. This "buffering effect" amounts to a total saving of 3 percent. A major motive behind this chapter is to generalize the conditions of Cl_y background and NO_x injection magnitude and altitude that decrease or increase the ozone column.

For 20 kilometer injection altitude, Figure 4.2 gives vertical profiles of ozone changes by added Cl_y and by injected NO_x. For 1.1 ppbv background Cl_y, injected nitrogen oxides in any amount reduces ozone at all altitudes from 12 to 42 km, and the maximum ozone reduction occurs at 21 km (top panel). For 14.7 ppbv Cl_y, there is a large ozone reduction centered at 34 km and extending from 21 to about 50 km, and there is a small local ozone increase below 20 km (the solid line in the middle panel). For the relatively small NO_x injection of 500 units, there is no effect on the peak ozone reduction by Cl_y, and there is a slight local ozone increase below about 30 km. For 2000 injection units, the ozone reduction profile shows two peaks, one at 34 km due to Cl_y and one at 20 km due to injected NO_x. For 21.6 ppbv Cl_y (lower panel), the ozone reduction profile shows a large peak at 33 km and a secondary shoulder at 25 km; a small injection of NO_x reduces the ozone reduction caused by chlorine below 34 km and thus increases ozone by action of a double negative; and a large NO_x injection increases local ozone between 35 and 25 km and decreases local ozone between 25 and 15 km. Although the ozone column

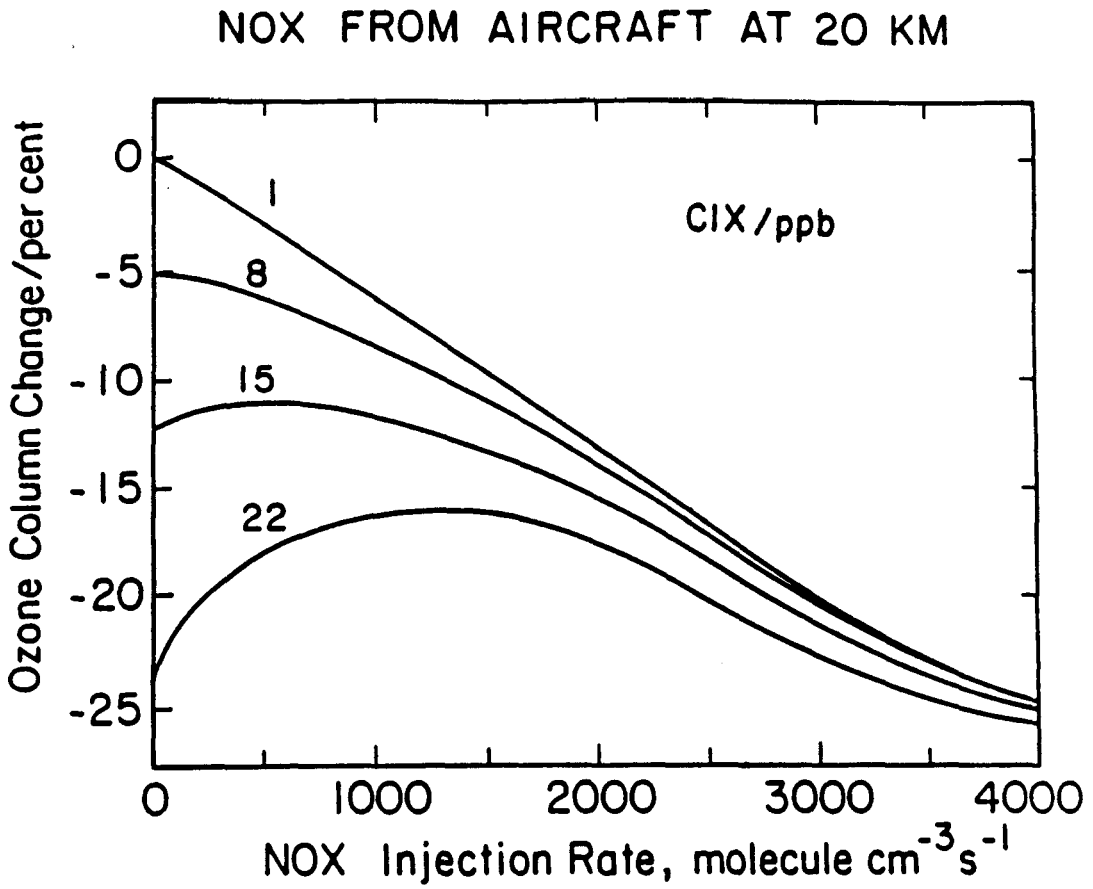

Figure 4.1. Percentage change of the ozone vertical column as calculated by the one-dimensional model, where the reference conditions include upper boundary value of stratospheric Cl_y at 1.1 ppbv, and the lower boundary value of nitrous oxide is 300 ppbv. For each value of Cl_y at 1.1, 7.9, 14.7, and 21.6 (nominally 1, 8, 15, and 22) ppbv, nitric oxide injection rates of 0, 500. 1000, 2000, and 4000 molecules $cm^{-3}s^{-1}$ at 20 kilometers are considered.

reduction is about the same for 0 or 4000 injection units of NO_x (Figure 4.1), the vertical profile of ozone is strongly modified by 4000 injection units (lower panel, Figure 4.2). Figure 4.2 explains many aspects of Figure 4.1. For a discussion of the chemical mechanisms for these effects, see chapter three.

Ozone-difference profiles for three agents that strongly change the model-calculated stratospheric ozone are given by Figure 4.3. These ozone differences are relative to a stratosphere with 1.1 ppbv Cl_y, but it is more instructive to compare the effect of large additions of Cl_y, N_2O, or injected NO_x against the profile

Table 4.3 Percent change in column ozone as a result of various injection rates of nitric oxide from stratospheric aircraft at various altitudes and for various assumed constant background mixing ratios of Cl_y (ppbv) at 50 km. Injection rates are in units of molecules $cm^{-3}s^{-1}$ over a one kilometer band width centered at the stated altitude. The reference atmosphere depends on the background Cl_y value. LLNL one-dimensional model.

		NO_x Injection Altitude (km)							
Cl_y	Injection rate	12	17	20	23	27	30	34	37.5
1.1	0	−0.0	−0.0	−0.0	-0.0	-0.0	−0.0	−0.0	−0.0
	500	−0.1	-1.0	-3.0			-5.1		
	1000	−0.2	-2.2	-6.3			-9.4		
	2000	−0.2	-4.9	-13.1			-16.6		
	4000	-0.1	-10.8	-24.7			-26.5		
3.1	0	−0.0	+0.0	+0.0	+0.0	-0.0	+0.0	+0.0	+0.0
	500	−0.1	-0.7	-2.4	-4.0	-4.5	-4.2	-3.6	-2.2
	1000	−0.2	-1.7	-5.4	-8.4	-9.5	-8.3	-7.0	-5.9
	2000	+0.3	-4.1	-11.8	-16.9	-16.9	-14.9	-12.6	-10.4
	4000	−0.3	-9.6	-22.1	-28.9	-28.2	-24.3	-19.8	-17.1
7.9	0	−0.0	+0.0	+0.0	+0.0	+0.0	+0.0	+0.0	+0.0
	500	+0.2	+0.2	-1.2	-2.3	-2.6	-2.4	-2.0	
	1000	+0.3	-0.7	-3.4	-5.7	-6.3	-5.7	-4.7	-3.8
	2000	+0.5	-2.4	-8.8	-13.4	-11.9	-9.9	-8.0	
	4000	+0.7	-7.0	-19.6	-25.5	-24.4	-21.6	-17.9	-12.4
14.7	0	+0.0	+0.0	+0.0	−0.0	+0.0	+0.0	+0.0	+0.0
	500	+0.3	+0.9	+1.1			+1.0		
	1000	+0.5	+1.3	-0.5			-0.8		
	2000	+0.9	+0.9	-3.3			-6.2		
	4000	+1.5	-2.1	-13.0			-15.5		
21.6	0	+0.0	+0.0	+0.0	+0.0	+0.0	+0.0	+0.0	+0.0
	500	−0.5	+3.1	+5.8			+7.4		
	1000	−0.9	+5.1	+7.4			+7.9		
	2000	−1.8	+6.9	+6.1			+4.0		
	4000	−3.2	+7.4	-2.1			-4.9		

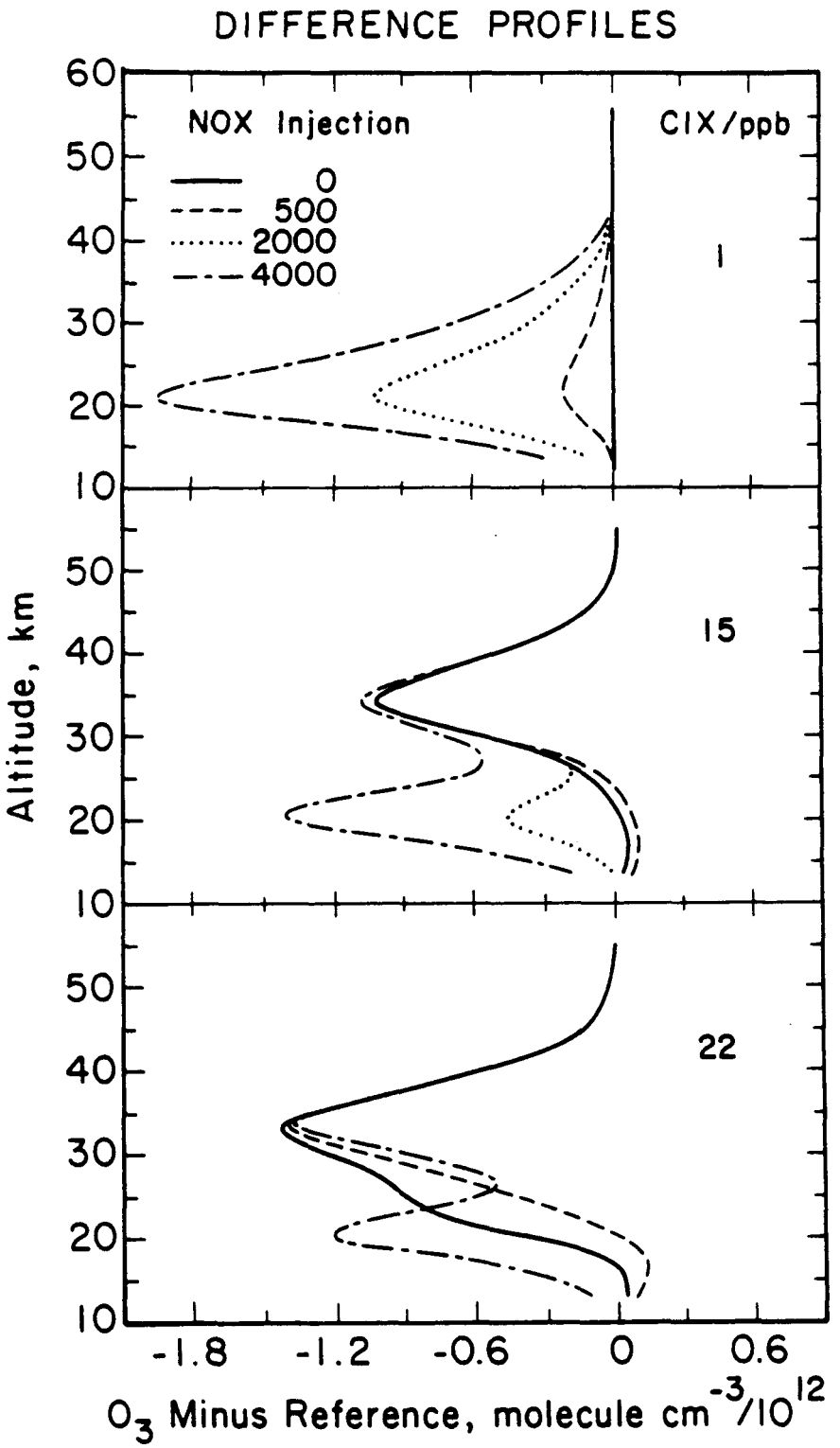

Figure 4.2. Vertical profiles of ozone changes caused by nitric oxide injections at 20 kilometers for various Cl_y background mixing ratios: 1.1 ppbv in top panel. 14.7 ppbv in middle panel. and 21.6 ppbv in lowest panel.

for 8 ppbv Cl_y which is included on each panel. This mixing ratio of Cl_y is that expected at steady state for long-term ClC releases at the current level. Further increases of Cl_y beyond 8 ppbv causes additional reduction of ozone at all altitudes (upper panel). Increase of nitrous oxide beyond the reference value causes additional ozone reduction relative to 8 ppbv Cl_y (middle panel) [see chapter 3]. All injections of NO_x from aircraft at 20 km causes additional ozone reduction at all altitudes relative to 8 ppbv Cl_y (lower panel). Since these ozone changes are given in concentration units (molecules cm^{-3}), the three panels of Figure 4.3 may be compared in terms of equal areas give equal changes in the ozone vertical column. In terms of the ozone vertical column (relative to that with 8 ppbv Cl_y), the ozone reduction caused by an NO_x injection of 2000 molecules $cm^{-3}s^{-1}$ over a 1 km band is comparable to an increase of Cl_y from 8 to 15 ppbv or to doubling the value of tropospheric nitrous oxide.

Figure 4.4 demonstrates the effect of NO_x injection altitude on the ozone-column reduction, including two chlorine backgrounds and five rates of NO_x injection (including zero). In 1988 the value of stratospheric Cl_y is about 3 ppbv (top panel), and the vertical line of 1.4 percent ozone reduction corresponds to no NO_x injection. NO_x injections at 12 km increase the ozone column relative to the reduced value caused by ClC's, but the increase is not sufficient to restore the ozone column to its "1960" value. At 17 km, the ozone column is reduced by injected NO_x, the amount of the reduction increases with altitude of injection up to about 25 km, and for a given rate of injection the amount of ozone-column reduction decreases with injection height above about 25 km. The same pattern is shown by 7.9 ppbv Cl_y as background (lower panel). The chlorine alone reduces ozone by 5.1 percent relative to the standard atmosphere; at 12 km injection altitude, NO_x increases the ozone column by 0.7 percentage point; and the altitude of maximum ozone reduction by NO_x injection is 25 ± 2 km. There is a weak tendency for the

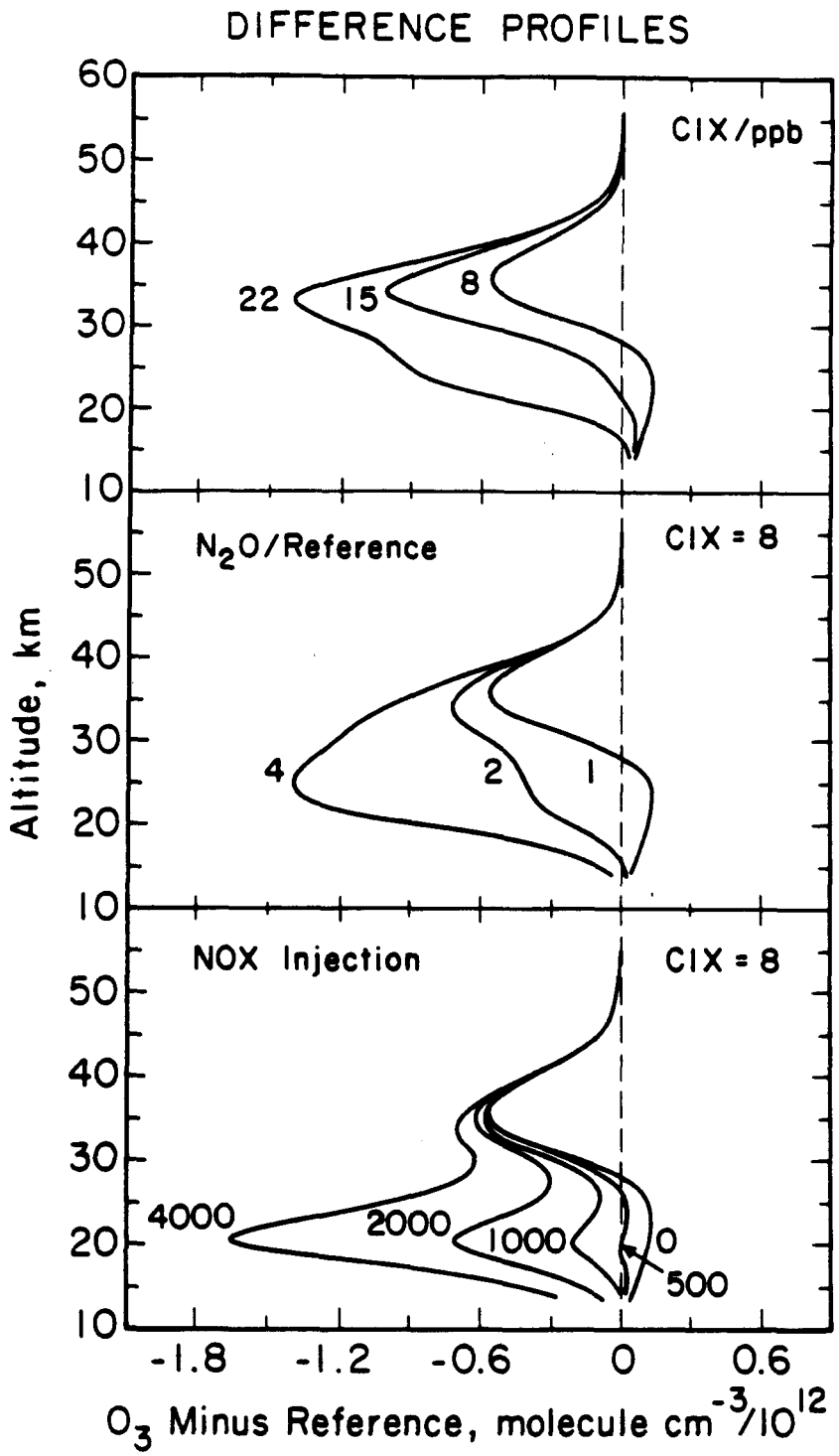

Figure 4.3. Vertical profiles of ozone changes caused by (i) large increases in stratospheric Cl_y (top panel), (ii) large multiple increases of the boundary value of nitrous oxide with Cl_y fixed at 7.9 ppbv (middle panel), and (iii) large injections of nitric oxide at 20 kilometers as if by stratospheric aircraft with Cl_y fixed at 7.9 ppbv (lowest panel).

injection altitude of maximum ozone-reduction efficiency to become lower as the magnitude of the NO_x injection increases. In Figure 4.5, the altitude of injection for NO_x (12–33 km) versus nitric oxide injection rate (0–3000 molecules $cm^{-2}s^{-1}$) is shown, where percent change in total ozone is relative to a 3.1 ppbv reference atmosphere (see Table 4.3). Again, two major results are obvious, (i) at a given altitude, increasing NO_x, decreases O_3, and (ii) at a given injection rate, column O_3 decreases up to 25 ± 2 km, the altitude of maximum ozone-reduction efficiency, and becomes less above this altitude.

For all background values of Cl_y above the reference value, NO_x injected at 12 km increases the ozone column relative to the ozone reduction caused by chlorine, but the increase is never enough to restore ozone to the value it had in the reference model, Table 4.1. For other injection altitudes, the pattern of ozone increase and decrease upon injecting NO_x is more complicated, and it is well demonstrated by contour plots. Figure 4.6 gives the percentage change of the ozone vertical column as a function of stratospheric Cl_y and NO_x injection rate at 17 km. Where the slope of a contour line is negative, increasing the rate of NO_x injection decreases the ozone column. Where the slope is positive, increasing NO_x injection increases the ozone column. Where the contour line is parallel to the nitric oxide axis, the ozone column is neither increased nor decreased upon an increase of the NO_x injection rate. The dashed line in Figure 4.6 divides the figure into two zones, A and B. In zone A, increasing the rate of NO_x injection decreases the ozone column; and in zone B, increasing the rate of NO_x injection increases the ozone column. For 9 to 12 ppbv Cl_y, the contour lines in Figure 4.6 are very nearly parallel for small to moderate injection rates, and according to this model NO_x from aircraft would have only a very small effect on the ozone column under these high chlorine conditions.

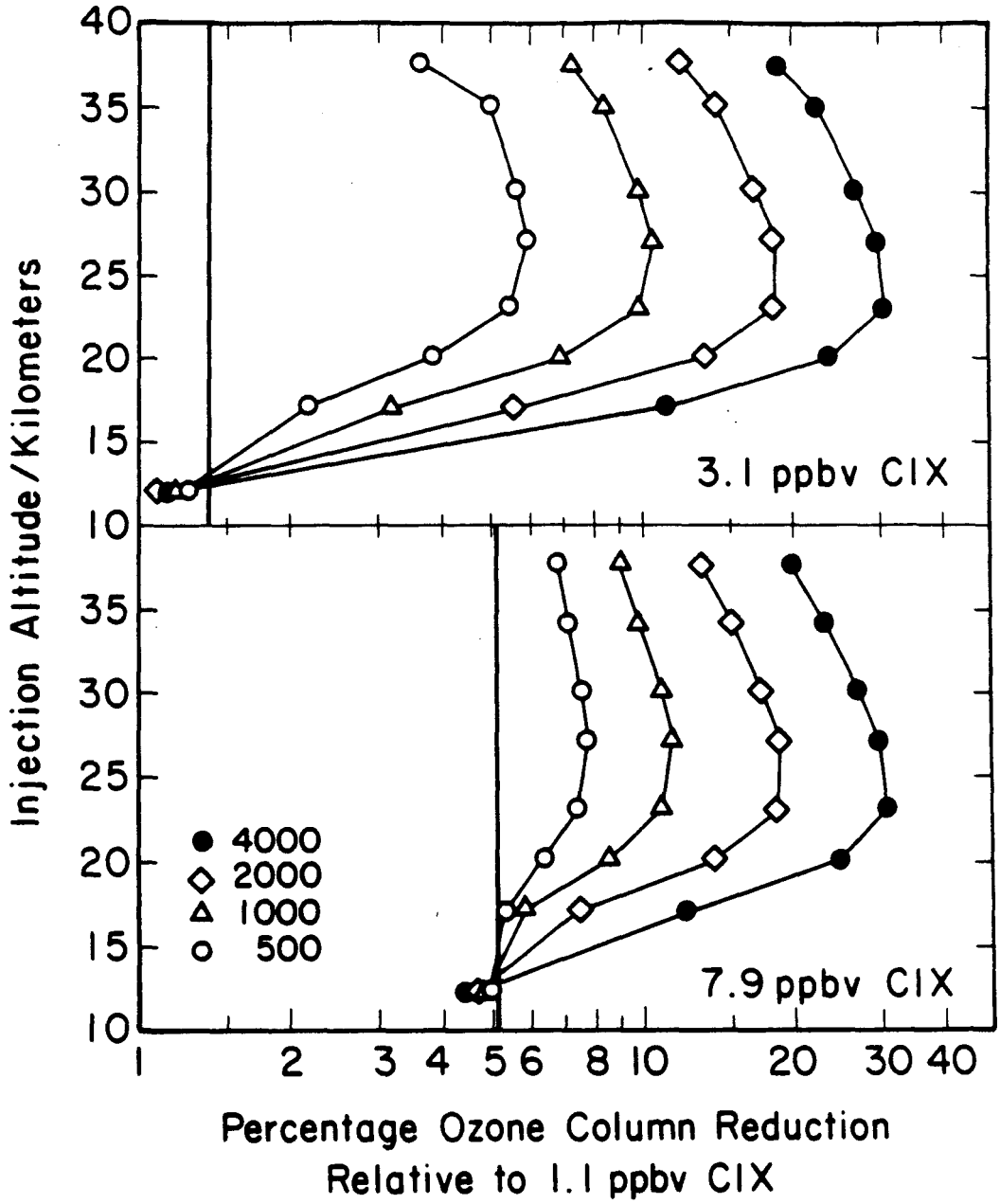

Figure 4.4. Percentage reduction of the ozone vertical column as a function of altitude and magnitude of NO injections. The ozone reduction is calculated relative to the reference atmosphere with 1.1 ppbv of Cl_y. The background of Cl_y is 3.1 ppbv in the upper panel, and the vertical line on the left-hand side is the ozone reduction caused by 3.1 ppbv of Cl_y. The background of Cl_y is 7.9 ppbv in the lower panel, and the vertical line in the center of the panel is the ozone reduction brought about by 7.9 ppbv of Cl_y. For a given Cl_y background and a given NO injection rate, the injection altitude that produces the maximum ozone reduction is 25 $\pm$ 2 kilometers. For injections at 12 kilometers, added nitric oxide decreases the ozone reduction caused by Cl_y, giving a relative increase of ozone.

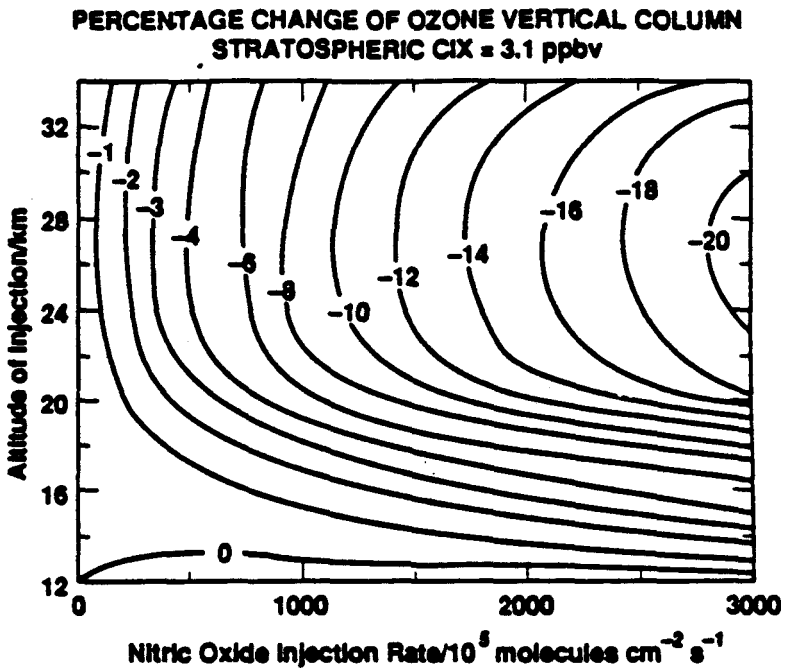

Figure 4.5. Percentage change of the ozone vertical column as calculated by the one-dimensional model as a function of altitude on NO_x injection and magnitude of NO_x injection in units of molecules $cm^{-3}s^{-1}$ over a one kilometer band centered at the stated altitude. The ozone reduction is calculated relative to the reference atmosphere with 3.1 ppbv Cl_y (approximately the 1988 value). An injection of 1500 in these units corresponds to a global injection of 1.8×10^{12} g yr^{-1} (as NO_2). Photochemical coefficients are from DeMore et al. (1985).

Figure 4.7 gives a contour plot similar to Figure 4.6, but the injection altitude is 20 km. It, too, has a region B where injection of NO_x increases ozone, but the area is much less than it is for 17 km injection altitude. In general, the contour lines in the figure for 20 km injection altitude are much steeper than those for 17 km injection. Figure 4.8 gives a contour plot of the same sort, where the injection altitude is 30 km. This contour plot is similar to that at 20 km, and there appears to be no new effect for altitudes above 20 km. (The ripples on the right hand side of Figures 4.7 and 4.8 are artifacts of the computerized plotting method).

To summarize Figures 4.6-4.8: at very large Cl_y mixing ratios, NO_x injections in the stratosphere partially counteract the chlorine reductions of ozone, but this

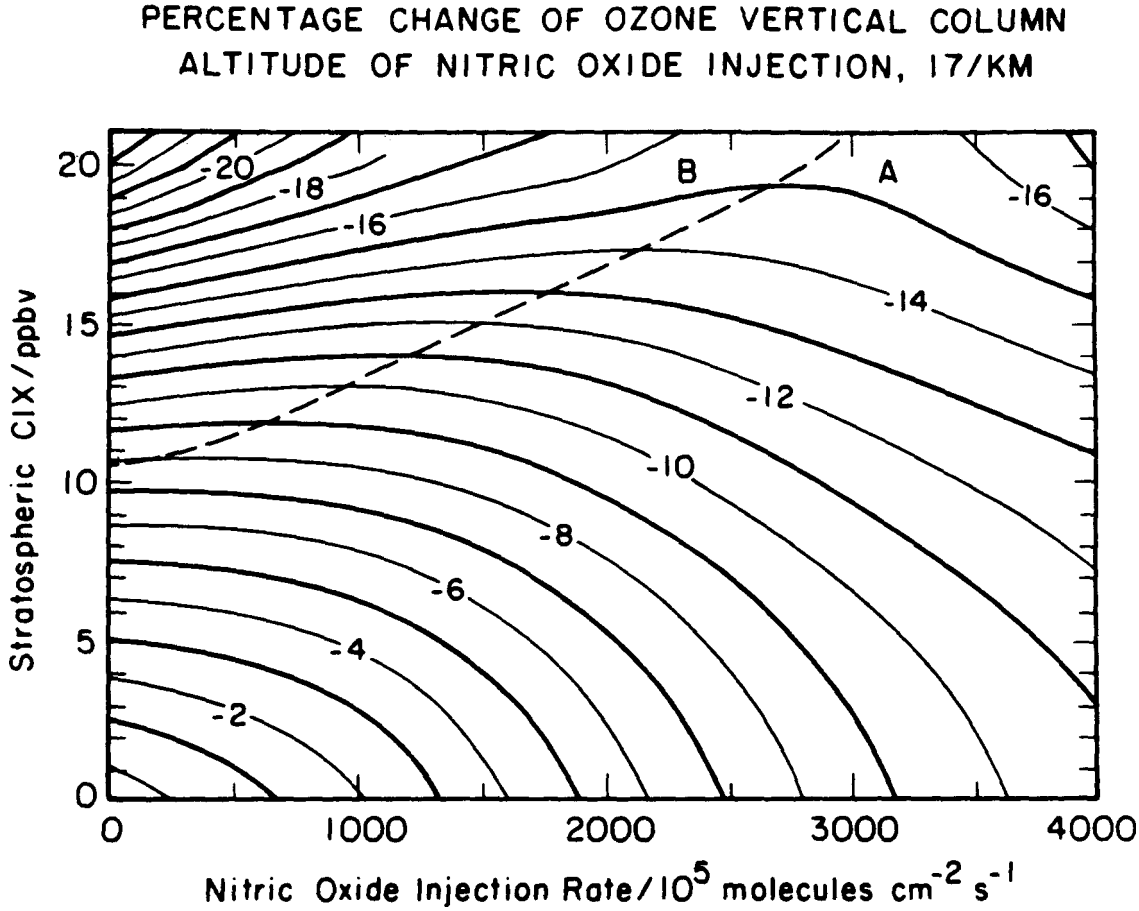

Figure 4.6. Contour plot of percentage change of the ozone vertical column as a joint function of nitric oxide injection rate at 17 kilometers and stratospheric Cl_y mixing ratio. The ozone reduction is calculated relative to the reference atmosphere with 1.1 Cl_y. To the left of the dashed line (at high values of Cl_y and low nitric oxide injection rates), an increase in nitric oxide injection rate (as if by stratospheric aircraft) decreases the ozone reduction caused by Cl_y, giving a relative increase of ozone.

effect occurs only in a highly chlorine-perturbed atmosphere where ozone is already greatly depleted.

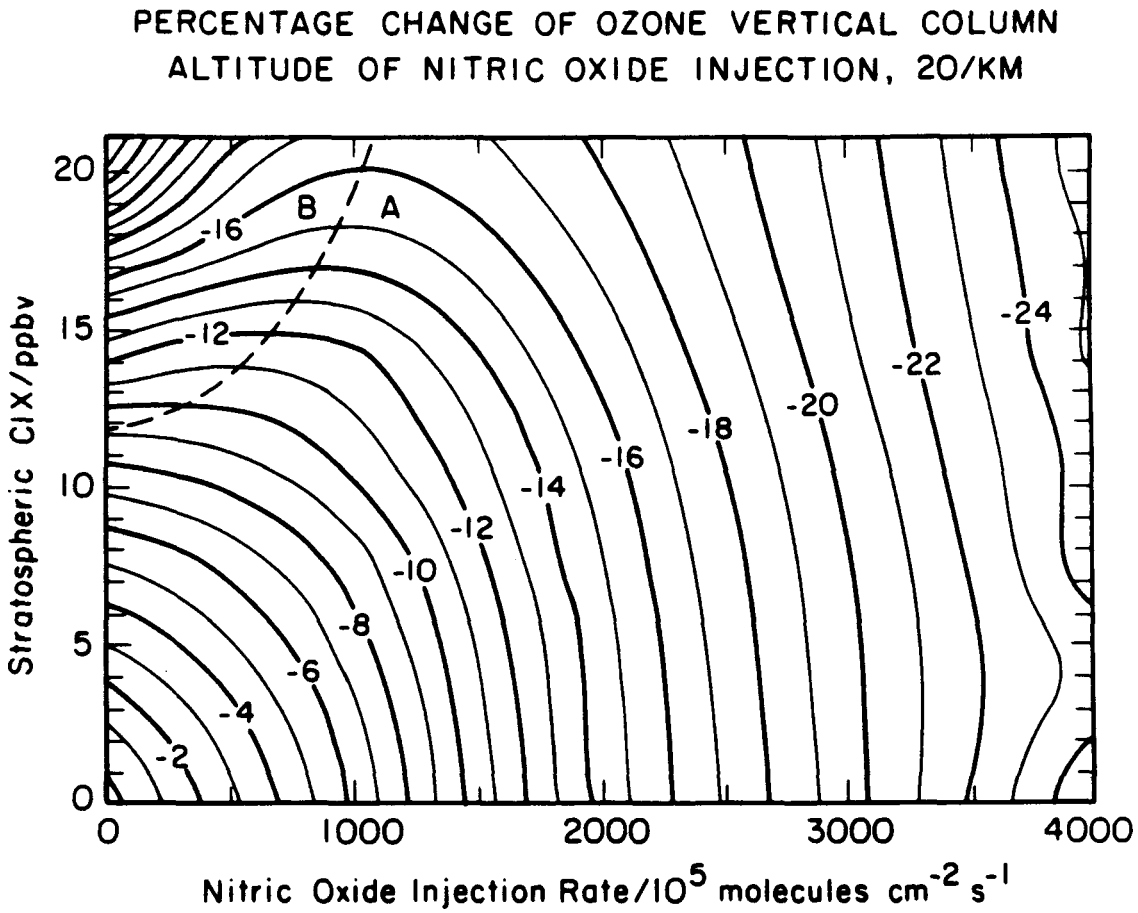

Figure 4.7. Same as Figure 4.6, except that nitric oxide injection from stratospheric aircraft occurs at 20 kilometers.

4.3 Results from Two-Dimensional Model

The reference atmosphere (300 ppbv nitrous oxide in the troposphere, 1.6 ppbv methane, and enough ClC to produce 2.8 ppbv of Cl_y in the stratosphere) was run to steady state, and nine NO_x injections as given by Table 4.4-a were also run to steady state. Percentage ozone-column changes relative to the reference atmosphere are given in Table 4.4-a for the northern hemisphere, the southern hemisphere, and for the globe. Steady-state residence times for odd nitrogen are calculated from the relation:

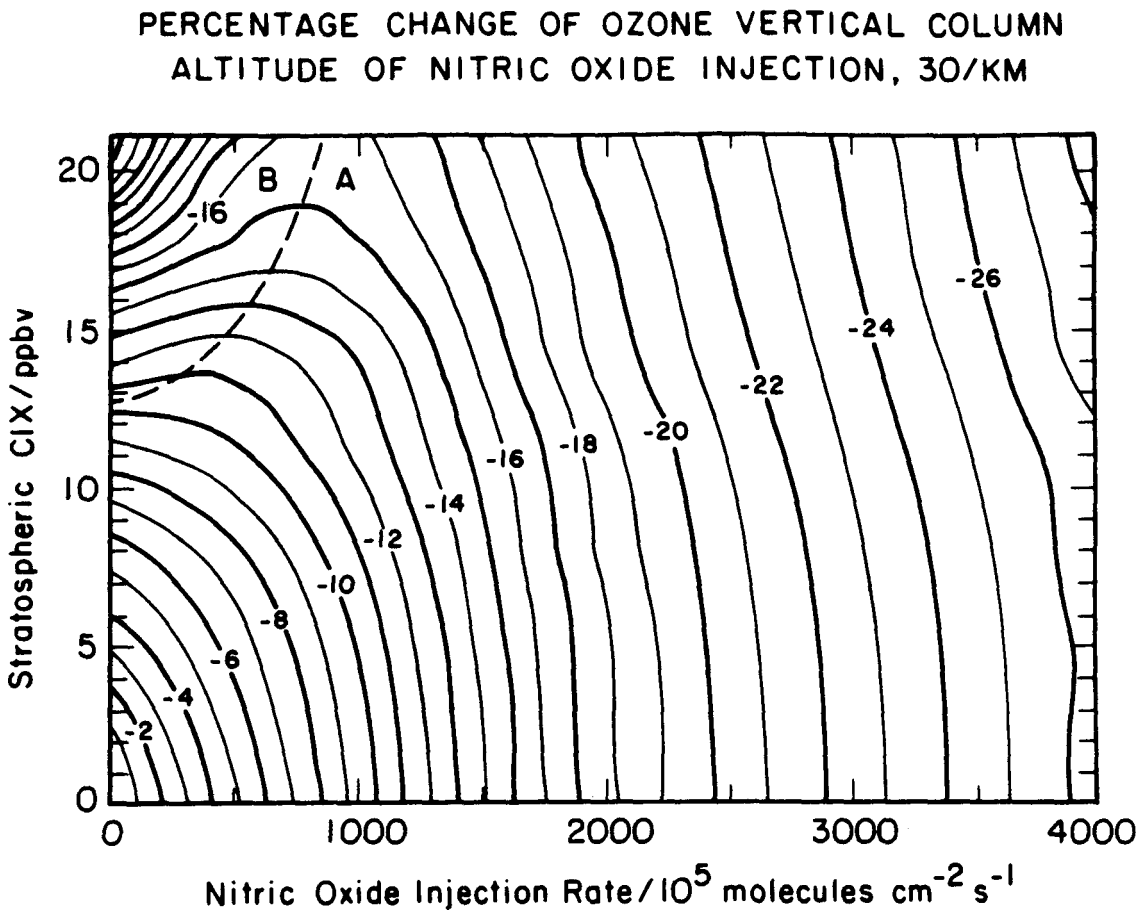

Figure 4.8. Same as Figure 4.6, except that nitric oxide injection from stratospheric aircraft occurs at 30 kilometers.

$$\text{lifetime} = t(NO_y) = \frac{\text{global excess global } NO_y \text{ at steady state}}{\text{global } NO_x \text{ injection rate}}$$

and these times are entered as the last column in Table 4.4-a. These stratospheric NO_y residence times are 0.3 years at 16.5 km, 1.2 years at 19.5 km, and 1.8 years above 30 km.

Additional one-dimensional model calculations were made to correspond to the reference atmosphere and injection rates used by the two-dimensional model. These results are given in Table 4.4-b.

The latitudinal and altitudinal NO_y distribution for the reference atmosphere in January is given as the top panel of Figure 4.9. The maximum value is 20

Table 4.4 Calculated changes in global and hemispheric ozone vertical columns as a result of NO_x injections by stratospheric aircraft.

a. LLNL two-dimensional model. The boundary values include 300 ppbv of nitrous oxide and enough chlorofluorocarbons to give 2.8 ppbv of stratospheric chlorine at 50 km. JPL 1987.##.

NO_x Injection as NO_2			% Ozone Change			$t(NO_y)$*
km	Lat. N	MT/yr	Global	N.H.	S.H.	yr
16.5	37–49	1.8	+0.01	−0.02	+0.04	0.3
19.5	37–49	1.8	−3.3	−5.0	−1.6	1.2
31.5	37–49	1.8	−8.0	−13.8	−2.2	1.8
34.5	37–49	1.8	−7.2	−12.4	−1.8	1.8
34.5	37–49	1.8	−7.7**	−13.1	−2.3	
34.5	N.H.	1.8	−7.1	−11.3	−2.9	1.8
34.5	Global	1.8	−8.0	−7.5	−9.6	1.9
34.5	37–49	0.9	−4.0	−6.9	−1.0	
34.5	37–49	0.45	−2.1	−3.6	−0.5	

b. One-dimensional model results. 3.1 ppbv Cl_y.**

		JPL (DeMore et al.)			$t(NO_y)$*
km	Mt yr^{-1}	1985	1987##	1987	yr
12	1.8		+0.2		
17	1.8	−2.9	−2.9	−3.5	1.5
20	1.8	−8.6	−8.7	−10.0	2.7
30	1.8	−12.1	−12.5	−13.4	3.9
34	1.8	−10.1	−10.5	−11.4	3.6

* Stratospheric residence time of excess NO_y calculated as ratio of steady-state excess inventory of NO_y over injection rate of NO_x.

** Temperature feedback is not included in this case.

Old, slower rate for reaction $O + NO_2$.

ppbv at about 40 km in the equatorial stratosphere. For a uniform global NO_2 injection rate of 1.8 Mt yr^{-1} at 33 to 36 km, the distribution of excess nitrogen oxides is given by the middle panel of Figure 4.9. The maximum local increase of NO_y is 20 ppbv at mid-latitude in the northern hemisphere, and the total global increase of NO_y is 53 percent. For the same injection between 37 and 49 degrees north, the distribution of excess NO_y is given by the lower panel of Figure 4.9. The maximum local mixing ratio of excess NO_y is 40 ppbv in temperate and polar regions of the northern hemisphere. There is less than 5 ppbv added NO_y in the southern hemisphere stratosphere.

For the uniform global injection of nitrogen oxides at 34.5 $\pm$ 1.5 km (conditions shown by the center panel of Figure 4.9), the percent changes of the ozone column are shown as a function of season and latitude in the upper panel of Figure 4.10, and the vertical profiles of percentage ozone changes (January) is given as the lower panel of Figure 4.10. The ozone column reductions are as high as 18 percent during spring in polar regions, are about 10 percent in mid-latitudes, and are about 4 percent at equatorial latitudes. The global average ozone change is -8 percent . In the one-dimensional model, the ozone column is calculated to be reduced by 10.5 percent (Table 4.4-b). In this case the ozone-column reduction in the one-dimensional model corresponds to the ozone-column reduction at 45 degrees north or south in the two-dimensional model, and there are larger ozone-column reductions than the one-dimensional model in polar regions and lower ozone-column reductions in equatorial zones.

Ozone changes are given in Figure 4.11 for the case of NO_x injection distributed uniformly over the northern hemisphere; otherwise the conditions are the same as those of Figure 4.10. The maximum ozone-column reduction is 28 percent at 75°N in the spring, compared to 18 percent for the globally uniform injection. The year-around ozone reduction at 45°N is 15 $\pm$ 2 percent, compared to 10 $\pm$ 1 percent

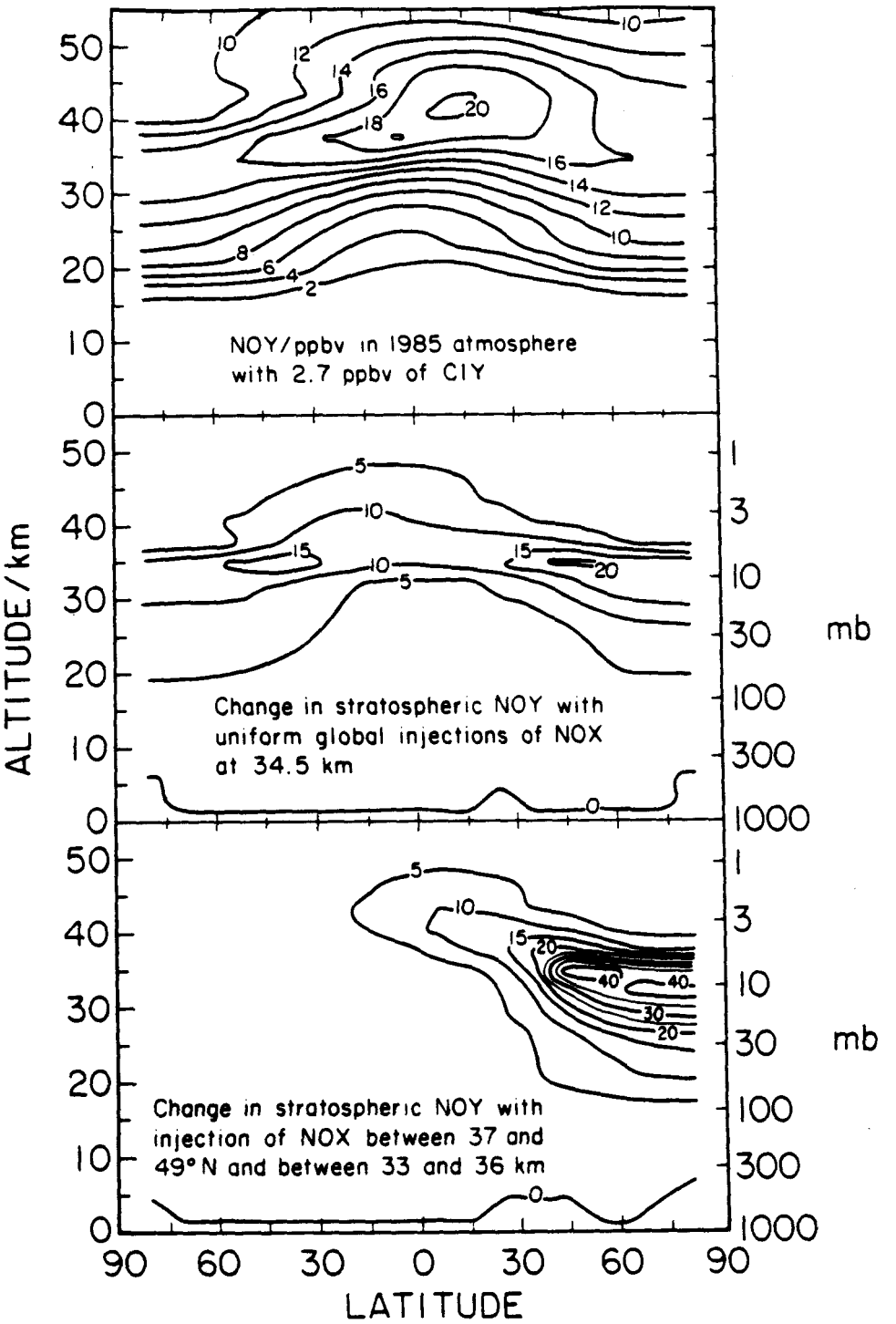

Figure 4.9. Two-dimensional distributions of nitrogen oxides during January: (top panel), background mixing ratios in reference atmosphere, which includes 2.7 ppbv Cl_y; (middle panel), steady-state increase of stratospheric nitrogen oxides with injection of 1.8 Mt NO_2 yr^{-1} spread uniformly over the globe between 33 and 36 km; and (lower panel), the same amount of nitrogen oxides injected between 37 and 49 degrees north.

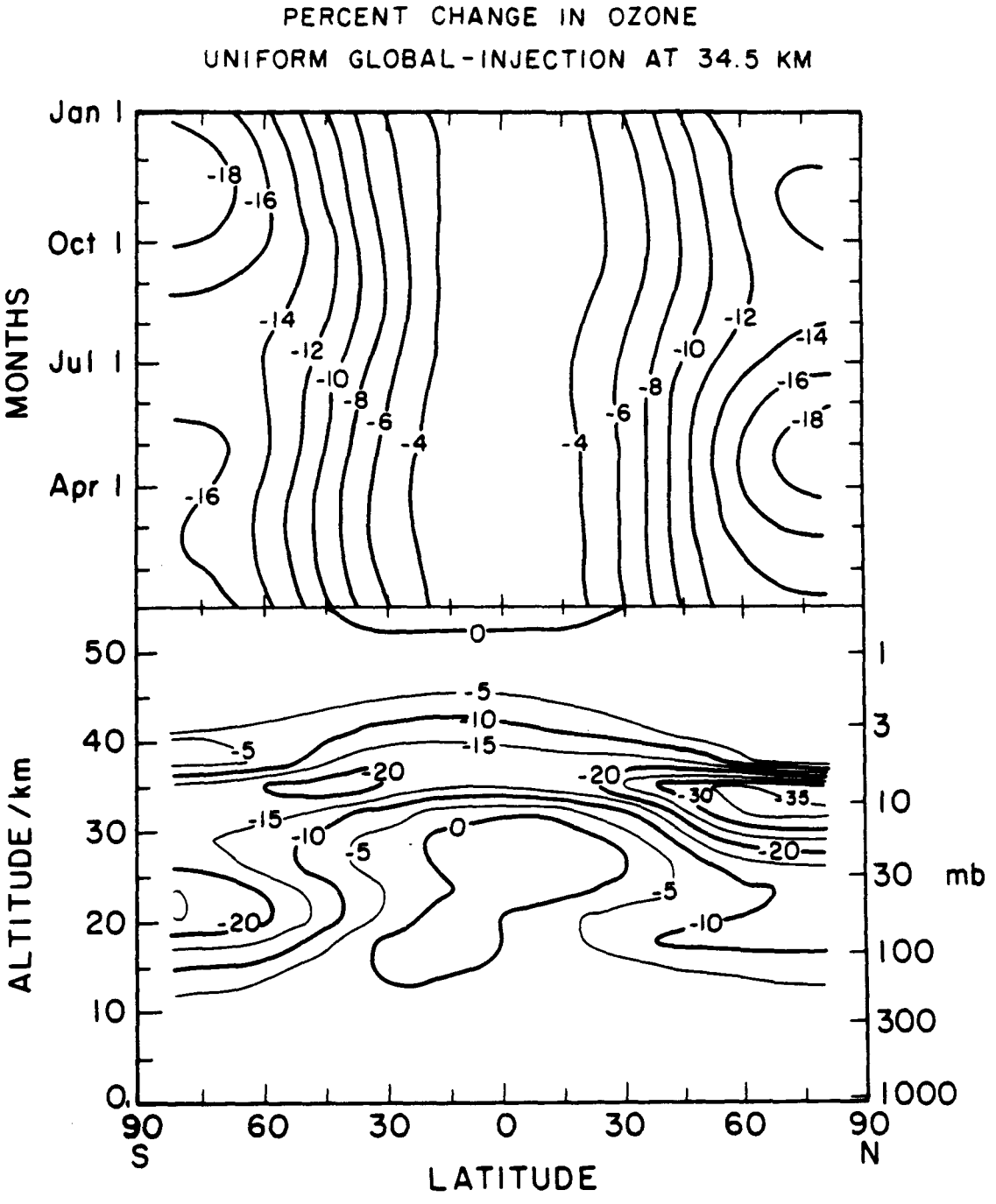

Figure 4.10. Percent change in ozone for the uniform global injection of 1.8 Mt NO_2 yr^{-1} between 33 and 36 km: (upper panel), change in ozone vertical column as a function of latitude and season: and (lower panel), change in local ozone during January as a function of latitude and altitude. Compare middle panel of Figure 4.9.

for the uniform global injection. Ozone reduction in the southern hemisphere is about 4 percent . The maximum local ozone reduction (January, lower panel) is 50 percent at 35 km between 60°N and 80°N.

For the same NO_x injection shown in Figures 4.10 and 4.11 but restricted between 37°N and 49°N (compare the lower panel of Figure 4.9), the calculated ozone changes are given by Figure 4.12. With minor differences, Figure 4.12 and Figure 4.11 (uniform northern hemisphere injection) are the same. Figure 4.12 shows a maximum ozone-column reduction of 32 percent, compared to 28 percent for Figure 4.11. The maximum local ozone reduction are 60 percent and 50 percent, respectively. The narrow corridor of injection in the northern hemisphere gives an ozone reduction of about 2 percent in mid-latitudes of the southern hemisphere, compared to 4 percent in Figure 4.11.

In Figure 4.13, the difference between having the change in net heating rates feeding back into temperature (temperature feedback) or holding temperature constant is compared. Since decreasing ozone cools the stratosphere which slows down the catalytically important ozone destruction reactions, temperature feedback should be important. When injecting at 42.5 degrees north, at 34.5 km, and 1.8 Mt per year of NO_2, the amount of total ozone saved between having temperature feedback on compared to off is a maximum of 3.5 percent.

For the standard NO_x injections of Figures 4.10–4.12, the global average ozone reduction is nearly the same, regardless of latitude spread of the injection: 8.0 percent, uniform global; 7.1 percent, uniformly over the northern hemisphere; and 7.2 percent, restricted to 37°N to 49°N (Table 4.4-a). The global ozone reductions are nearly the same whether temperature feedback is included (7.2 percent) or not included (7.7 percent).

For NO_x injection at 34.5 km and between 37 and 49 north, the global ozone reduction increases somewhat slower than linearly with the global rate of NO_x

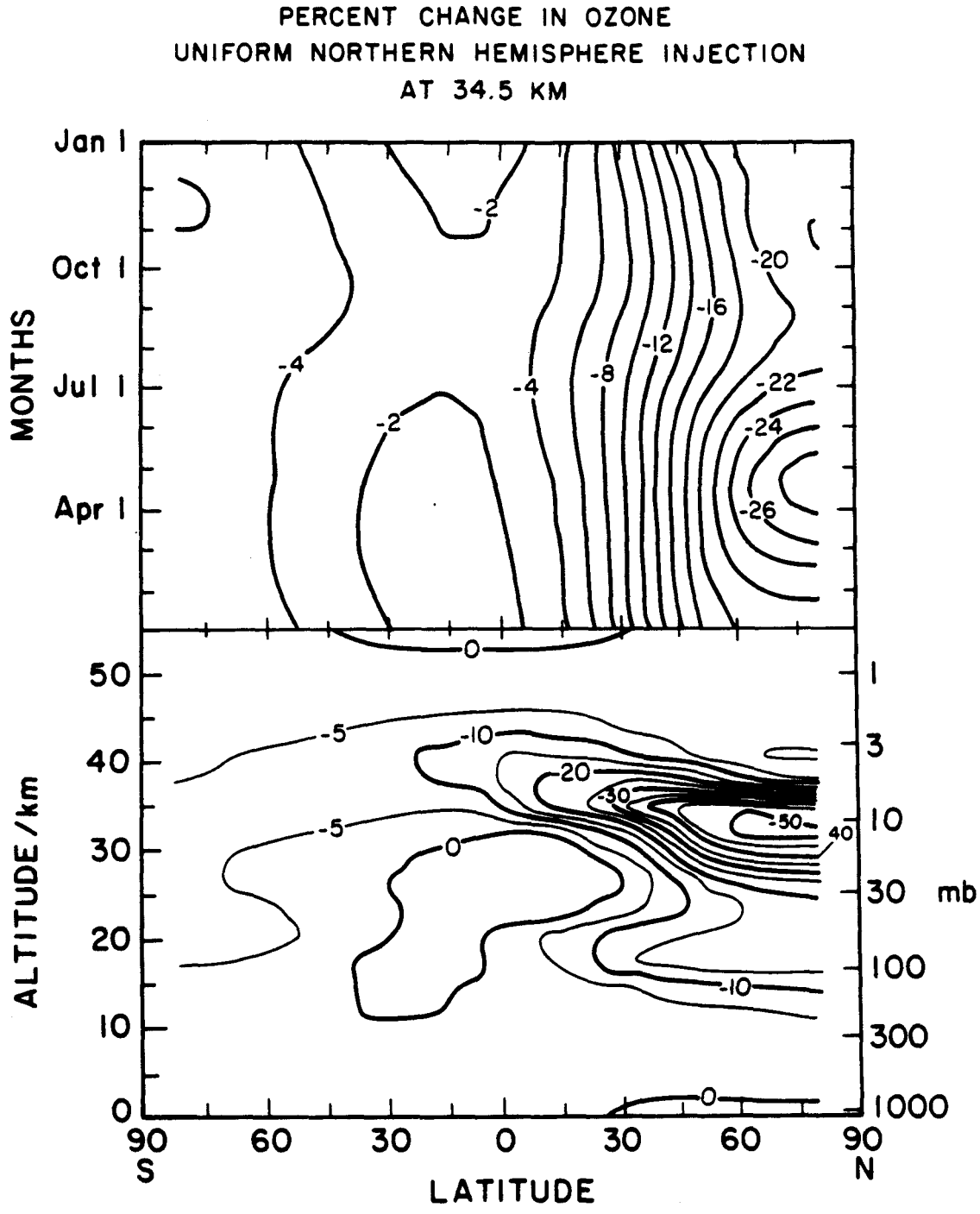

Figure 4.11. Same as Figure 4.10, except for uniform injection over the northern hemisphere.

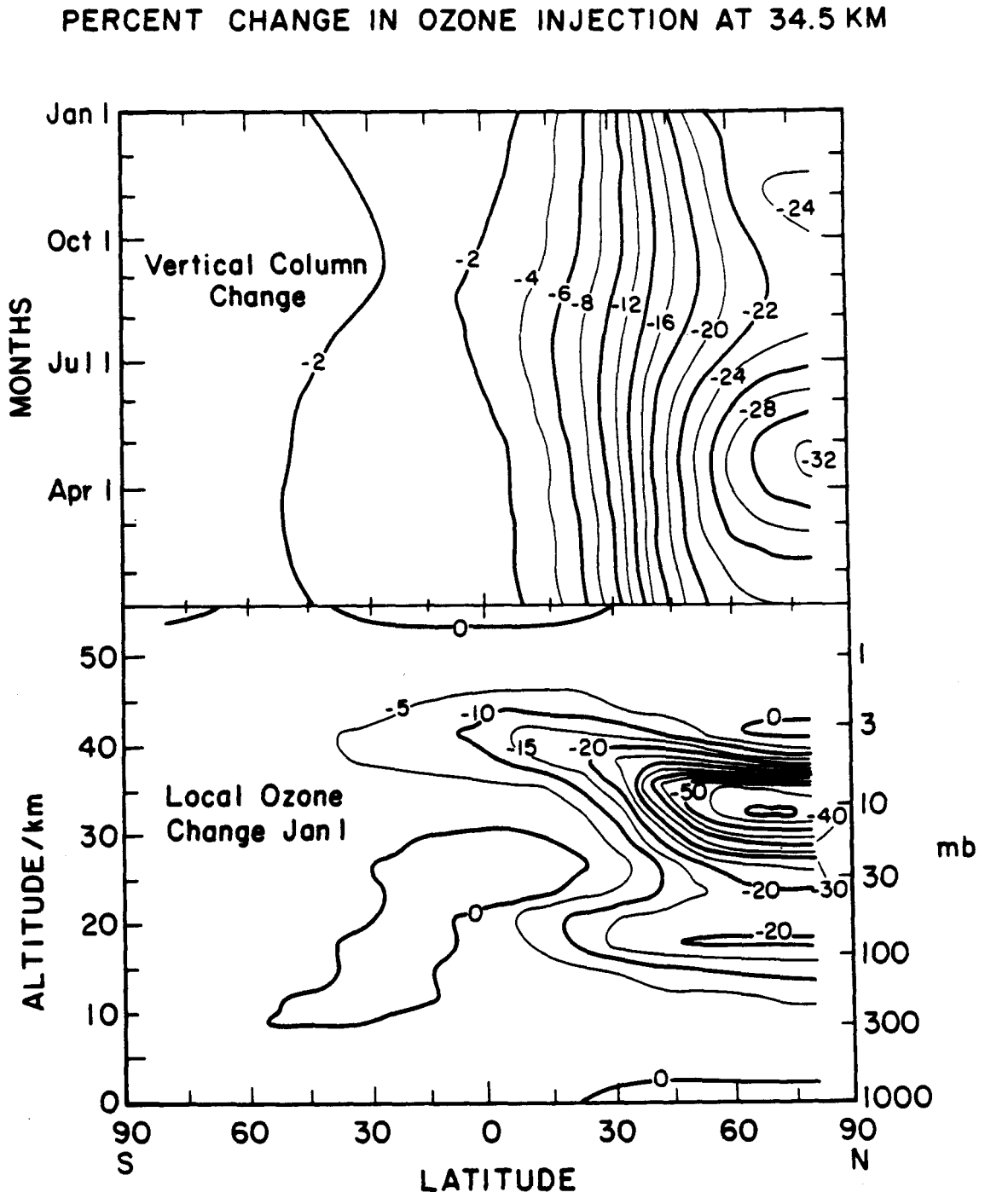

Figure 4.12. Same as Figure 4.10, except for injection only between 37 and 49 degrees north. Compare lower panel of Figure 4.9.

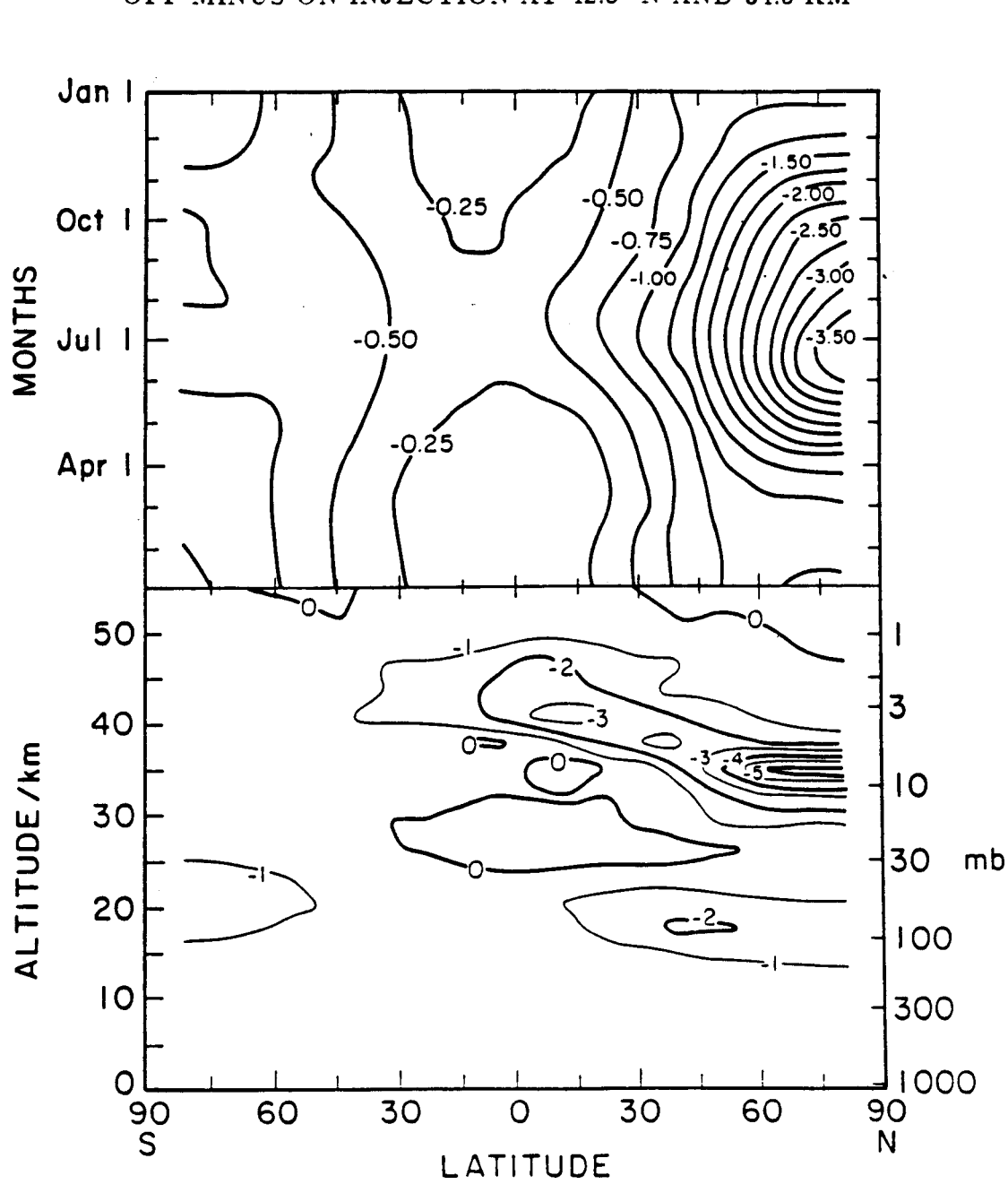

Figure 4.13. The percent change in ozone with temperature being adjusted during the perturbation relative to no adjustment. Here 1.8 Mt NO_2 is injected between 37 and 49 degrees north. The altitude of injection is between 33 and 36 km.

injection: 2.1 percent for 0.45 Mt yr^{-1},4.0 percent for 0.90 Mt yr^{-1}, and 7.2 percent for 1.8 Mt yr^{-1} (Table 4.4-a).

In Figures 4.14, 4.15 and 4.16, the percent change in ozone is plotted for both column ozone (top panel) and local ozone (bottom panel) for the three additional altitude cases at 16.5, 19.5 and 31.5 km respectively.

4.4 Comparison of One-Dimensional and Two-Dimensional Models

The one-dimensional model gives larger ozone reductions than the two-dimensional model by a factor of 1.3 for NO_x injection at 34.5 km, by a factor of 1.5 for NO_x injection at 31.5 km, and by a factor of 2.6 at 19.5 km. (This is only true for two-dimensional model scenarios that use the eddy diffusion representation (K_{yy} and K_{zz}) of Table 4.4 and Figures 4.9 through 4.17 (case A, in Chapter 6). Later in this section, results from a different choice for the eddy diffusion representation, based off the carbon-14 tracer studies of chapter 6, will be discussed.) For globally uniform NO_x injection of 1.8 Mt yr^{-1} at 34.6 $\pm$ 1.5 km in the two-dimensional model, the global average ozone reduction is 8.0 percent; for the equivalent injection in the one-dimensional model at 34 $\pm$ 0.5 km, the ozone-column reduction is 10.5 percent, For the same magnitude injection at 19.5 $\pm$ 1.5 km in the two-dimensional model, the global ozone reduction is 3.3 percent; for the equivalent injection at 20 $\pm$ 0.5 km in the one-dimensional model, the ozone-column reduction is 8.6 percent (Table 4.4).

For the same global-average NO_x injection rate at 34.5 km, the global-average ozone reduction is almost the same, 7.1 to 8.0 percent, regardless of whether the injection was globally uniform, was only over the northern hemisphere, or was confined to a narrow latitudinal band (37 to 49 degrees) in the northern hemisphere.

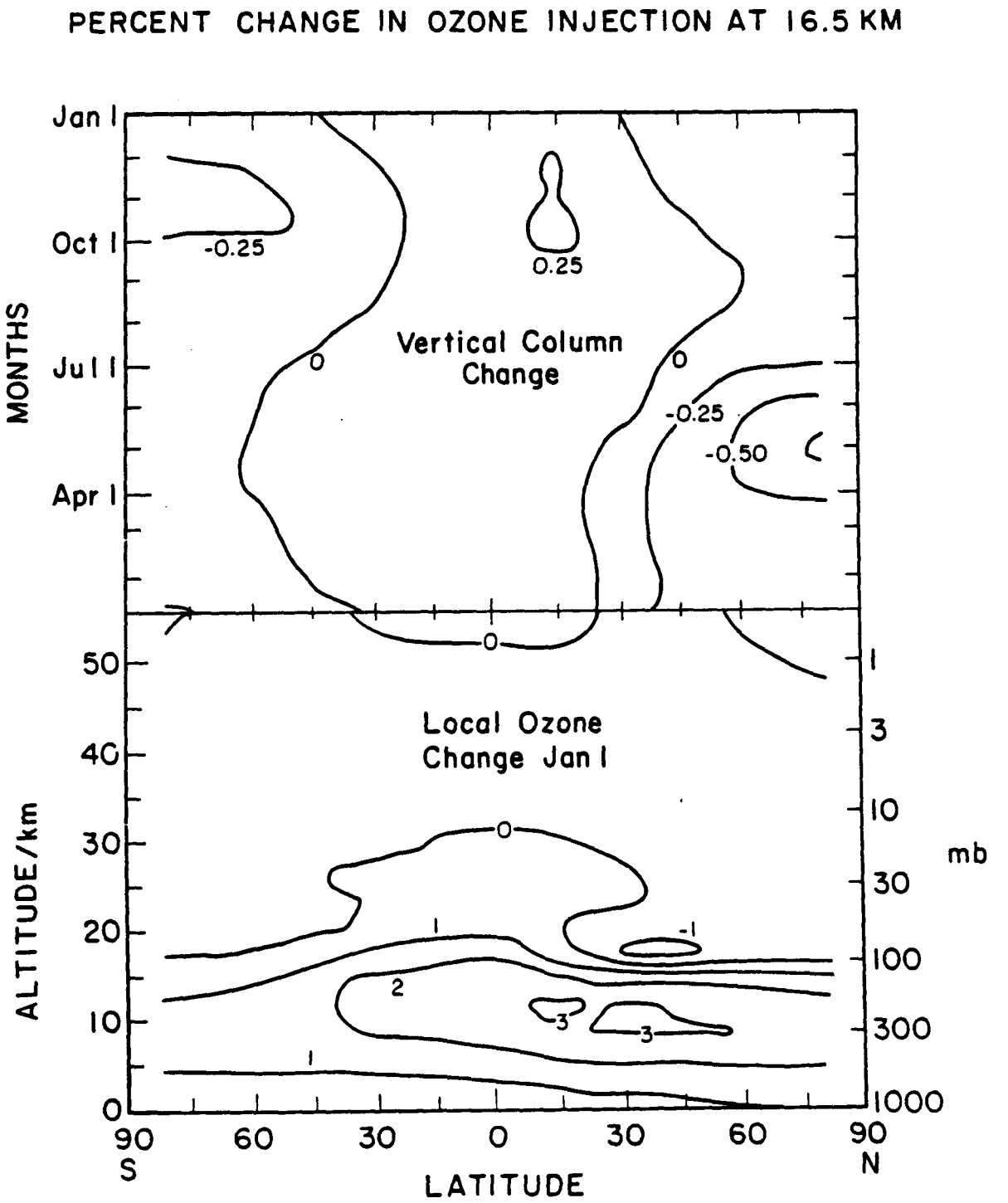

Figure 4.14. Same as Figure 4.10, except for injection only between 37 and 49 degrees north and between 15 and 18 km (centered at 16.5 km).

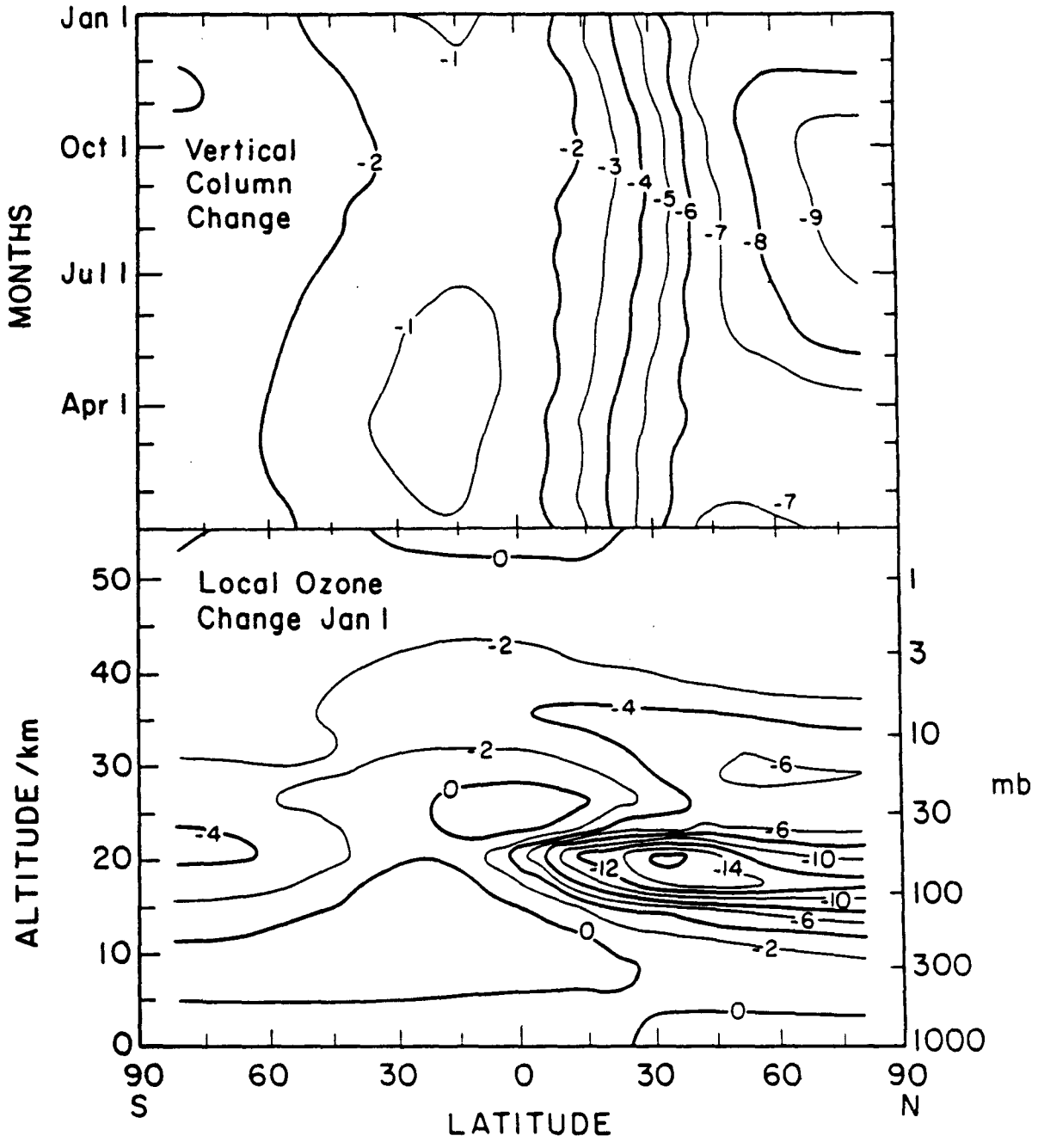

Figure 4.15. Same as Figure 4.10. except for injection only between 37 and 49 degrees north and between 18 and 21 km (centered at 19.5 km).

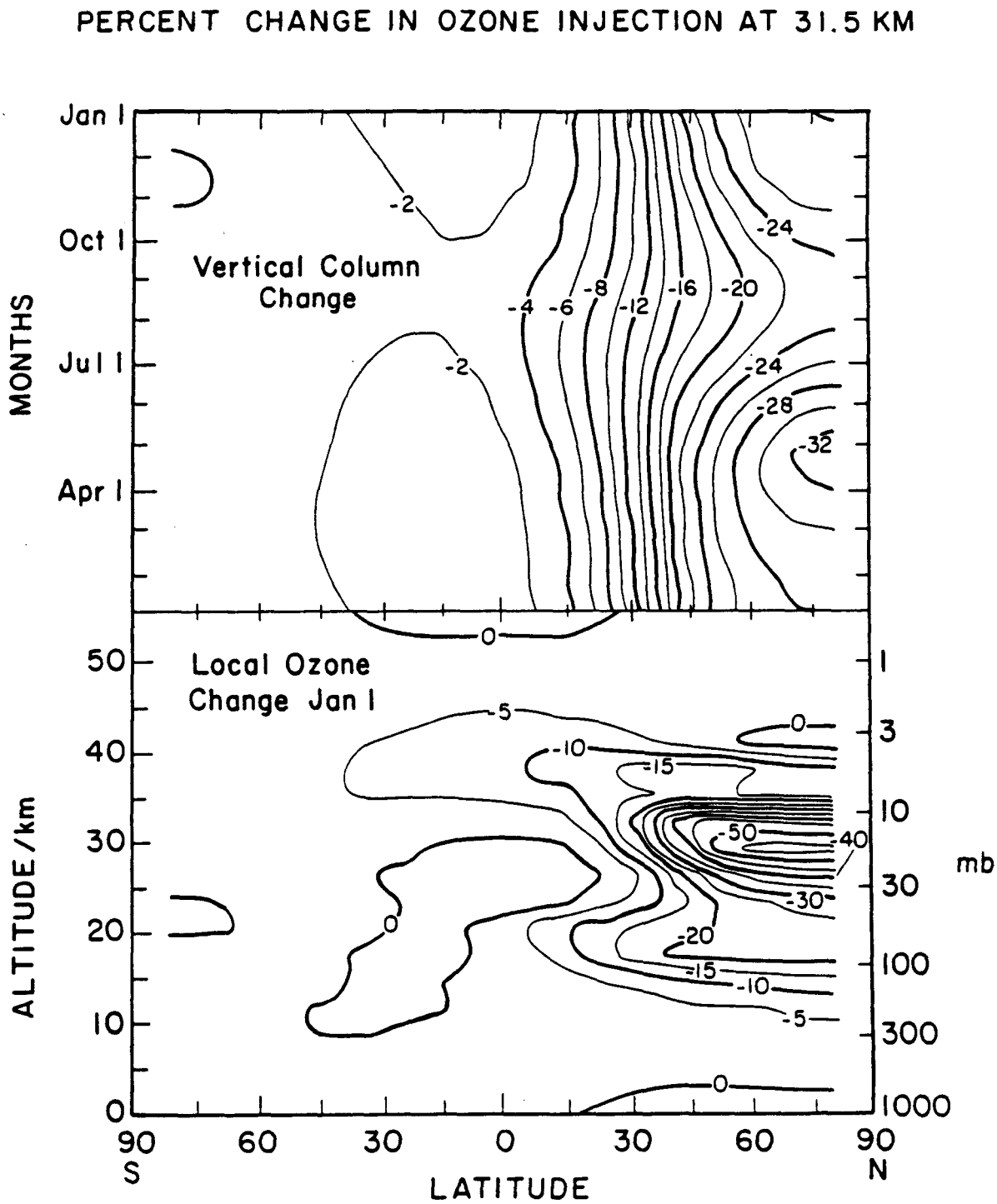

Figure 4.16. Same as Figure 4.10, except for injection only between 37 and 49 degrees north and between 30 and 33 km (centered at 31.5 km).

There is a small difference in the chemical model used by the one-dimensional and the two-dimensional models. The main body of calculations using the one-dimensional model were completed before the 1987 tabulation was published [DeMore et al., 1985, 1987]. The two-dimensional model calculations were made with the 1987 tabulation. However, both models used the 1985 value for the rate of the reaction, $NO_2 + O = NO + O_2$. For injection altitudes of 17, 20, 30, and 24 km, spot calculations were (1) with the one-dimensional model using 1987 chemistry and (2) with 1987 chemistry and the newer faster value of this reaction. The calculated ozone reduction is slightly greater (10 to 20 percent) when we use the new [DeMore et al., 1987] temperature dependent value for the rate coefficients for the reaction $O + NO_2$, relative to that for the constant value, 9.3×10^{-12} cm^3s^{-1}, Table 4.4-a.

The lifetime of excess NO_x injected into the stratosphere was calculated from the relation

$$\text{lifetime} = t(NO_y) = \frac{\text{global excess } NO_y \text{ at steady state}}{\text{global } NO_x \text{ injection rate}}$$

for both one- and two-dimensional models, and these values are included as the last column in Table 4.4. For NO_x injection at 30 to 35 km, the one-dimensional lifetime of excess NO_y is twice that for the two-dimensional model; at 17 km injection altitude the one-dimensional lifetime is almost five times as long as that for the two-dimensional model.

The build up and decay of excess NO_y in the stratosphere upon injection of nitrogen oxides at 34 km is given for the one-dimensional model and for the globally uniform injection by the two-dimensional model in Figure 4.17. For the same tropospheric nitrous oxide boundary values, the NO_y steady state in the reference atmosphere is 1.7×10^{16} molecules cm^{-2} for the two-dimensional model,

and it is the larger value 2.4×10^{16} for the one-dimensional model (This factor is 1.4). For the 8 years after the injections start, the increase to NO_y steady state is faster for the two-dimensional model than the one-dimensional model. For the 8 years after the injections cease, the excess NO_y decreased with an average relaxation time of 3.4 years for the one-dimensional model and 2.0 years for the two-dimensional model.

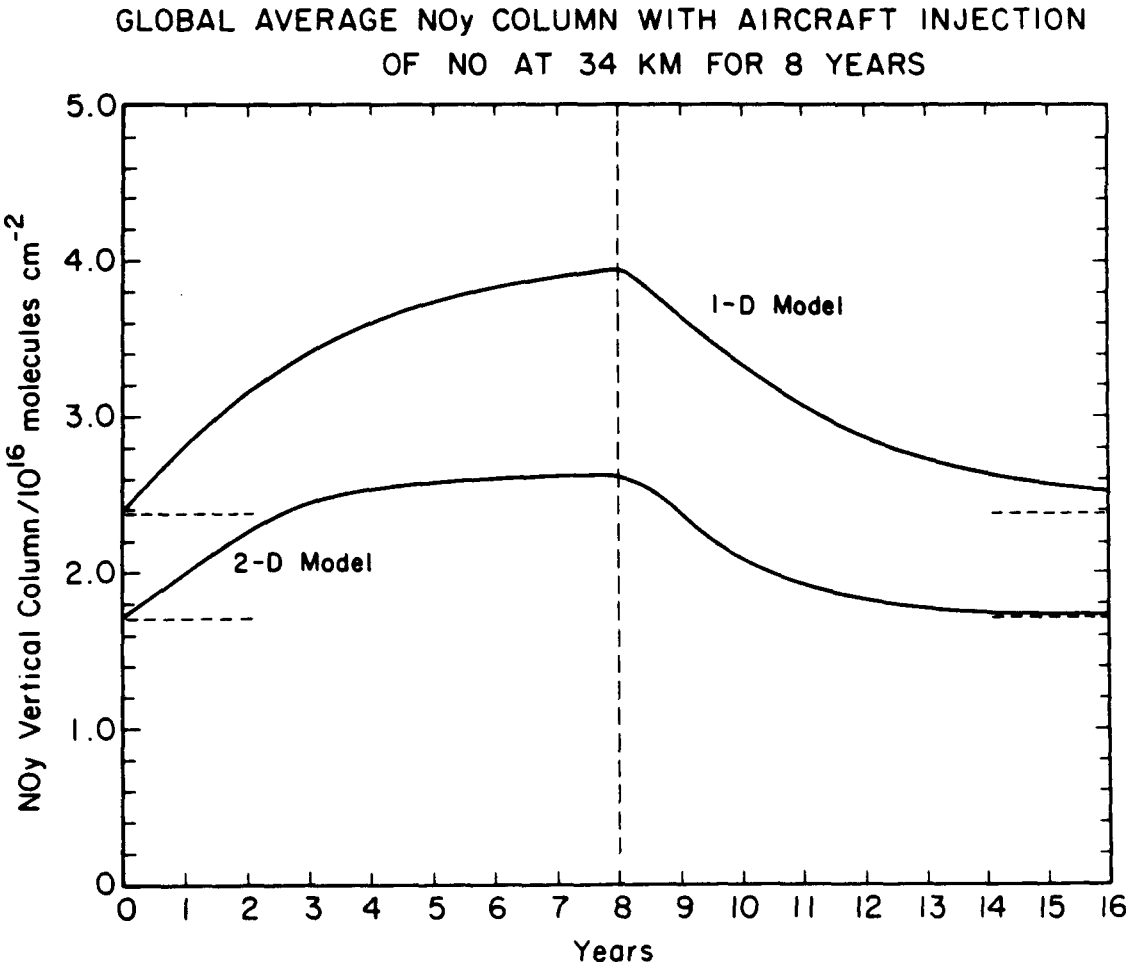

Figure 4.17. Comparison of global average nitrogen oxides column according to LLNL one-dimensional model and LLNL two-dimensional model with uniform global injection pattern (compare middle panel of Figure 4.9). Each model was operated to steady state with respect to its reference atmosphere, at time zero on the figure each model injected 1.8 Mt yr^{-1} NO_2, this injection continued for 8 years, and after stopping the injection the models were run for another 8 years.

From these considerations of relaxation times. it is clear that the differences between the models in calculating ozone changes are due to differences in transport properties, and the two-dimensional model sweeps excess NO_y out of the stratosphere much faster than the one-dimensional model. Clearly, the two-dimensional model is much more realistic than the one-dimensional model in representing the effects of atmospheric circulation on global trace gas transport, however. both models use empirical eddy diffusion functions, K_{zz} and K_{yy} for the two-dimensional model and K_z for the one-dimensional model. Although these functions represent a small additive part of the transport in the two-dimensional model and the K_z function represents all the transport in the one-dimensional model, one should conservatively keep open the possibility that the difference between the two models may be due in part to incomplete calibration of the K_{zz} and K_{yy} functions in the two-dimensional model.

In Chapter 6, recent reanalysis of the carbon-14 distribution produced from nuclear bomb tests in the late 1950's and early 1960's [Johnston, 1989] was used to choose more representative values for both K_{yy} and K_{zz} eddy diffusion coefficients in the LLNL two-dimensional model. This study concluded that the eddy diffusion representation of case B, compared the best to the observed carbon-14 distributions supplied by Johnston [1989]. The major differences between cases A and B are the magnitudes of K_{yy} and K_{zz} in the troposphere and the sharpness of the cutoff at the tropopause (case B is sharper than case A, which has the effect of lowering the tropopause height for case B relative to case A). In the stratosphere for both cases A and B, the magnitudes of K_{yy} and K_{zz} are the same. In Table 4.5, both cases A and B are shown for a global injection of 1.8 Mt yr^{-1} of NO_x at 19.5 km. The net result of using case B as the eddy diffusion representation, increases the lifetime of NO_y from 1.0 to 1.9 years relative to case A. This increase in NO_y is directly connected to the tropopause height, since after transition into

the troposphere, deposition to the surface or destruction by chemical processes is rapid. Therefore, increasing the lifetime of NO_y, will increase the reduction efficiency of ozone (e.g., case A, 2.6 percent and case B, 7.2 percent, for globally averaged conditions). It is interesting to point out that the one-dimensional model still calculates a higher column ozone reduction (−10 percent, Table 4.4-b) than the two-dimensional model using case B. In this aircraft scenario, the injection altitude was 19.5 km, which should be very sinsitive to the tropopause height. For a higher altitude injection, the difference in NO_y lifetimes between cases A and B should be less. Therefore, when considering the impact of high altitude aircrafts, or any other perturbation, it is important to understand and express the uncertainties in the eddy diffusion representation.

Table 4.5 Calculated changes in global and hemispheric ozone vertical columns as a result of NO_x injections by stratospheric aircraft. Two different eddy diffusion representation (K_{yy} and K_{zz}) are compared. Case A, is used in all scenarios in Table 4.4, while case B is based off of carbon-14 tracer studies (see Chapter 6). The boundary values include 300 ppbv of nitrous oxide and enough chlorofluorocarbons to give 2.8 ppbv of stratospheric chlorine at 50 km. The reaction set is based off of JPl-87. The scenario for both cases A and B, inject NO_x globally at 19.5 km, with a magnitude of 1.8 Mt yr^{-1}.

NO_x injected as NO_2	% of Ozone change			$t(NO_y)$*
Diffusion Case	Global	N.H.	S.H.	yr
A	−2.7	−2.7	−2.6	1.0
B	−7.2	−7.2	−7.1	1.9

* Stratospheric residence time of excess NO_y calculated as ratio of steady-state excess inventory of NO_y over injection rate of NO_x.

4.5 Conclusion

(1) These calculations find that significant decreases in the total ozone column and in global ozone result from stratospheric NO_x emissions.

(2) Larger reductions of total ozone are expected as the altitude of emission increases, until a maximum effect is calculated near an injection altitude of about 25 kilometers. Above this injection altitude, effects on ozone decrease slowly with altitude.

(3) For 1, 3, or 8 ppbv of stratospheric Cl_y the one-dimensional model finds that small injections of NO_x decrease the ozone-column beyond the decrease caused by the atmospheric chlorine; but at 15 or 22 ppbv of stratospheric Cl_y, small injections of NO_x partially cancel the ozone-column reduction caused by Cl_y.

(4) The effects of water vapor emission at a factor of 90 greater than the NO_x emissions has a negligible effect on ozone, compared to the effects of the assumed NO_x emissions. Doubling methane weakly diminishes the effect of injected NO_x on ozone.

(5) Two different eddy diffusion representation based off of calculations in Chapter 6 (K_{yy} and K_{zz}) were compared for a global injection of NO_x (1.8 Mt yr^{-1}) at 19.5 km. It was found that case B, smaller diffusion in troposphere and a sharper transitions at the tropopause, increased the lifetime of NO_y from 1.0 to 1.9 years compared to case A. The column ozone reduction increase from 2.6 percent percent (case A) to 7.2 percent (case B).

Chapter 5: Trends in Stratospheric Ozone

5.1 Introduction

Within the last three decades, atmospheric concentrations of some important trace constituents have been increasing at a alarming rate [WMO, 1985; Wang et al., 1986; Ramanathan et al., 1987; Wuebbles, 1987; Wuebbles and Edmonds, 1988]. These gases include carbon dioxide (CO_2), methane (CH_4), nitrous oxide (N_2O) and several chlorocarbons ($CFCl_3$, CF_2Cl_2, CCl_4, and CH_3CCl_3) (see Table 5.1-a).

Carbon dioxide has continuously been measured since 1958 at Mauna Loa, Hawaii, and for shorter time at many other worldwide locations. The mixing ratio of CO_2 has increased from 315 ppmv in 1958, to 345 ppmv in 1985 (9.5 percent increase) [Keeling et al., 1982]. The increase in CO_2 in the atmosphere is thought to be entirely related to anthropogenic sources (e.g., fossil fuel combustion) [Wuebbles and Edmonds, 1988]. CO_2 is not chemically active in the troposphere and stratosphere, but poses a threat as a greenhouse gas. It has been estimated from climate models that a doubling of CO_2 would increase the global average surface temperature by 1.5–4.5° C [Charney, 1979; Smagorinsky, 1982; WMO, 1985]. In addition, the absorption and reemision of infrared radiation by CO_2 decreases stratospheric temperatures, therefore slowing down the reactivity of chemical processes that destroy ozone.

Methane has been observed to be increasing by about one percent per year since 1977 [Rasmussen and Khalil, 1981; Fraser et al., 1982; Blake et al., 1982; Ehhalt et al., 1985; Blake and Rowland, 1986, 1988]. Before 1977, the data record is sparse. Rinsland et al., 1985, analysed the ground-based solar infrared spectra

recorded in 1951, and found CH_4 to be increasing at a rate of 1 percent per year. Ice core measurements imply an pre-industrial mixing ratio of less than half (0.7 ppmv) the current value of 1.7 ppmv in the northern hemisphere and 1.6 ppmv in the southern hemisphere [Robbins et al., 1973; Craig and Chou, 1982; Khalil and Rasmussen, 1982]. Methane is important to atmospheric chemistry and climate in many ways. It produces O_3 through the CH_4-NO_x smog reactions in troposphere. It affects O_3 in the stratosphere through HO_x production and by decreasing the effectiveness of Cl_x and NO_x catalytic reactions. CH_4 is also a greenhouse gas. Doubling the concentration of CH_4 is predicted by climate models to increase the surface temperature by 0.2–0.4° C [Ramanathan et al., 1987]. Man-made sources of methane are enteric fermentation (cattle etc.), rice paddies, biomass burning, natural gas and mining losses, and solid waste [Cicerone and Shetter, 1981; Khalil and Rasmussen, 1983; WMO, 1985; Ehhalt, 1985; McElroy and Wofsy, 1987; Matthews and Fung, 1987].

Nitrous oxide is currently increasing at 0.2–0.3 percent per year [Weiss, 1981]. The rate of increase for N_2O is significant, since the odd nitrogen production in the stratosphere occurs primarily from the reaction of $O(^1D)$ with N_2O. The current concentration of N_2O in the troposphere is 300 to 305 ppbv [WMO, 1985]. The pre-industrial concentration may have been as low as 285 ppbv [Wang et al., 1986]. N_2O is considered to be a strong greenhouse gas. Doubling of N_2O could raise the equilibrium surface temperature by 0.3–0.4° C [Ramanathan et al., 1987]. Man-made source are from combustion of fossil fuels, biomass burning, fertilized soils, and cultivated natural soils [Crutzen, 1983; WMO, 1985; McElroy and Wofsy, 1987].

The chlorocarbons are increasing exclusively from anthropogenic emissions. These gases are used as solvents, refrigerants, foam blowing agents, and spray

propellants. They have long atmospheric lifetimes ($CFCl_3$, 75 years; CF_2Cl_2, 110 years; CCl_4, 50 years; CH_3CCl_3, 10 years) [e.g. see WMO, 1985] due to their chemical inertness in the troposphere. The current increase per year for $CFCl_3$, CF_2Cl_2, and CH_3CCl_3 is between 4 and 8 percent; with CCl_4 increasing at 1-3 percent [WMO, 1985; Wang et al., 1986]. These gases can, and are having, major effects on chemistry and climate [Solomon, 1988]. First, they are greenhouse gases like N_2O and CH_4. For example, for both $CFCl_3$ and CF_2Cl_2, changing the tropospheric concentration from 0 to 2 ppbv, would increase the surface temperature by 0.3° C [Ramanathan et al., 1985]. Second, since they are inert in the troposphere, they eventually are photolyzed in the stratosphere, where the reactive chlorine released can chemically reduce the concentration of ozone. In the transition from winter to spring, in the Antarctic region, the effects of these gases may already be evident. Farman et al. [1985], first reported O_3 column decreases of 40 percent, using a Dobson spectrophotometer at Halley Bay (75° S, 64° W). Halley's Bay and other ground based observation have been confirmed by data from the Total Ozone Mapping Spectrometer (TOMS) and Solar Backscattering Ultraviolet instruments on the polar-orbiting Nimbus 7 satellite [Stolarski et al., 1986]. There are numerous chemical and dynamical theories why O_3 has decrease in the Antarctic [Farman et al., 1985; Solomon et al., 1986a; McElroy et al., 1986; Tung et al., 1986; Molina and Molina, 1986; Crutzen and Arnold, 1986; Callis and Natarajan, 1986; Austin et al., 1986a; Mahlman and Fels, 1986]. In some of the above theories, increased Cl_y plays in important role in the mechanism that is responsible for O_3 destruction [see Solomon, 1988, for a review of the Antarctic Hole]. Due to an increasing awareness of the ClC problem, many governments are calling for a ban on the ClC's that pose a environmental or health risk [Montreal Protocol, 1988].

This study was conducted to better understand the chemical interactions that the above trace gases have on O_3. In addition, the solar flux variability due to variances in the 11 year sunspot cycle and the nuclear test serie of the late 1950's and early 1960's (explained below) were modeled. This study follows up on previous one-dimensional analysis [Wuebbles, 1983] and a less complete two-dimensional anaylsis by the NASA-WMO Ozone Trends Panel Report [1989].

The LLNL two-dimensional chemical-radiative-transport model of the troposphere and stratosphere has been applied to analyzing the effects that these natural and anthropogenic influences may have had on global ozone concentration since 1950. The LLNL one-dimensional model was also used for comparison. With both models, temperature feedback was included for each scenario, with transport terms being held constant (see chapter 2). The eddy diffusion representation was case A (see Chapter 6 and Appendix B).

There were three scenario runs conducted with both models.

1. Trace gas only: CO_2, N_2O, CH_4, and ClC's were allowed to vary from 1950–1987.

2. Trace gas + solar variability: Here the solar cycle variability was added in addition to the trace gas only case. This scenario ran from 1950–1990.

3. Trace gas + solar variability + nuclear test series: The NO_x produced from the nuclear bombs between 1958–1968 were input during this scenario.

The one-dimensional model was started in 1850 (pre-industrial atmosphere) and ran up to 1950 using the trace gas only scenario. By starting in 1850, the total anthropogenic effect on atmospheric ozone can be obtained [Wuebbles, 1983]. In all cases, the chemistry reaction set was based on DeMore et al. [1987].

5.2 Modeling Historical Emissions

Modeling past trends require estimates of the historical changes in trace gas emission and concentrations, variations in solar ultraviolet radiation, and NO_x produced from nuclear tests. Possible effects from other influences such as the El Chichon eruption, the Antarctic ozone hole, or possible changes in climate or atmospheric dynamics, were not included. As much as possible, available measurements and emissions evaluations were used in the development of the historical scenarios.

The historical emissions for the chlorocarbons $CFCl_3$, CF_2Cl_2, CCl_4 and CH_3CCl_3 were based on the expressions developed by Wuebbles et al. [1984] from available Chemical Manufacturing Association data and other databases. The time history of CH_4 concentrations were based on measurements made since 1978 indicating a 1 percent per year increase in methane concentrations [WMO, 1985; Blake and Rowland, 1988] and data for earlier periods (e.g., spectral data and ice core data). Historical changes in N_2O surface mixing ratios were based on the data and analysis of Weiss [1981]. The expression for increase in CO_2 concentrations developed by Wuebbles et al. [1984] was used: this was based on observations at Mauna Loa since 1958 and assumes a pre-industrial concentration of 270 ppmv.

Many uncertainties remain regarding the variations in ultraviolet radiation during the 11-year solar sunspot cycle. The variations assumed here are derived form the analyses of Heath and Schlesinger [1984, 1986]. Their analyses was based on the Solar Backscattered Ultra Violet (SBUV) instrument on board the Nimbus-7 satellite. It assumed that the spectrum of solar rotation-induced variations are preserved over the solar cycle and that the irradiance variation are linearly related to the ratio of the core to wing variations in the ultraviolet flux from solar minimum to maximum of 9 percent at 205 nm, 4 percent at 250 nm, and 1 percent at 270

nm. Since wavelengths that are less than 242 nm favor ozone production, the maximum ozone concentration throughout the 1950–1990 period is always at solar flux maximum. For the model studies presented here, the solar cycle flux changes are assumed to have a sinusoidal variation with time. Magnitudes of respective solar cycles are based on F10.7 solar radio flux data [Heath and Schlesinger, 1984], with the magnitude of solar cycle 21 (1974–1985) taken to be 1.0 (i.e., same solar flux variations from solar minimum to solar maximum as given above).

Past modeling studies [e.g., Chang et al., 1979; Wuebbles, 1983] have indicated that nitrogen oxides produced from atmospheric nuclear tests could have had significant effects on stratospheric ozone during the early 1960s. In the calculations presented here, all reported tests are included [see Appendix A, and Table 5.1-B], with the timing and yield of the various test devices based on Bauer [1979]. The altitude for the bottom and top of the stabilized cloud are taken from two sources. One scenario was run using the empirically-based analysis of Peterson [1970], who analyzed only the U.S. tests at equatoral latitudes and inferred the cloud bases and tops at higher latitudes. The other scenario was taken from Seitz et al. [1968], who estimated cloud bases and tops from measurement of radioactive debris during the 1961–1962 test. For the larger tests (>10 Mt), the high latitude values for both cloud bases and tops of Peterson were higher than those of Seitz. The distribution of NO_x formed within the cloud is based on Peterson [1970]. There still remains uncertainty regarding the amount of NO produced per megaton of explosive energy: this study assumed 0.67×10^{32} NO molecules/Mt based on the discussion in Chang et al. [1979].

5.3 1985 Atmosphere

When attempting to assess the accuracy of two-dimensional chemical-radiative-transport models in studies where trace gases are varied, both past and future,

Table 5.1. (a) Lower boundary value mixing ratios for species N_2O, CH_4, CO_2, $CFCl_3$, CF_2Cl_2, CCl_4, and CH_3CCl_3 for the years of 1950, 1960, and 1986. Cl_y is representative of an altitude of 52.5 km. (b) Estimated total yield of nuclear tests for each year from 1958 to 1963 [taken from Bauer, 1979].

A. Trace Gases

	1950	1960	1986
N_2O (ppbv)	290	293	304
CH_4 (ppmv)	1.24	1.35	1.73
CO_2 (ppmv)	311	316	346
$CFCl_3$ (pptv)	0.49	9.26	218
CF_2Cl_2 (pptv)	5.92	30.4	392
CCl_4 (pptv)	47.6	66.4	125
CH_3CCl_3 (pptv)	0.0	3.24	147
Cl_y (ppbv)	0.80	0.93	2.6

B) Nuclear Test Series

Year	Mt
1958	39
1959	0
1960	0
1961	112
1962	233
1963	0

it is important first to compare species distributions obtained from the present atmosphere (i.e., 1985) to that of ground based, satellite, balloon, and aircraft measured data. For a review of each experimental technique, see WMO [1985], Chapters 8, 9, 10, and 11; and Houghton et al. [1984].

In Figure 5.1, the observed total ozone taken from the Dobson network [Dütsch, 1971] and the Total Ozone Mapping Spectrometer, TOMS, on the Nimbus 7 satellite (normalized to Dobson network), is compared to the ozone distribution calculated by the LLNL two-dimensional model. The two observed column ozone distributions show the same general shape and magnitude, 440 Dobson units in the

northern hemisphere winter, decreasing equatorially. At the equator, the ozone-column reaches a minimum of approximately 260 Dobson units. In the southern hemisphere both SAMS and the Dobson network observe the ozone-column spring-time maximum off the pole (between 50° S and 60° S). The LLNL two-dimensional model calculates the magnitude of the northern hemispherical maximum to be 400 Dobson units, 20 to 40 less than the observed data. In the equatorial region, 280 Dobson units are calculated, which is 20 Dobson units higher than the observed column ozone distributions. The LLNL two-dimensional model does not reproduce the southern hemisphere spring time maximum between 50° and 60° S. This latter effect may be due to the inadequacies of how the zonally-averaged meridional diffusive component of transport in the southern hemisphere is handled in the model. The dynamical variations between hemispheres arises from the different amount of continental land mass, which induce wave structure that effects transport of trace species. In Chapter 6, the effect of weaker meridional eddy diffusion (K_{yy}) in the southern hemisphere, which will affect the distribution of ozone, is addressed. In addition, the model does not represent any "Antarctic Hole" processes (i.e., heterogenous chemistry or polar vortex dynamics), that would tend to decrease ozone at the South pole.

In Figure 5.2, the O_3 profile calculated for an ambient atmosphere, for January 1, 1985, is compared to the observed profile obtained from the Solar Backscattering Ultraviolet Spectrometer on the Nimbus 7 satellite (SBUV). The maximum mixing ratio of O_3 calculated by the model is slightly lower than that observed (1 ppmv). In general, this is a very good agreement. At altitudes greater than 34 km (10 mb), the LLNL two-dimensional model underestimates the mixing ratio of O_3 by greater than 20 percent (Figure 5.3). This effect is a general problem with one and two-dimensional models [Froidevaux et al., 1985; Frederick and Cicerone, 1985;

WMO 1985, Chapter 8]. Either a new source(s) of O_3 in the upper stratosphere is missing (e.g. as proposed by Slanger et al., 1988), or there exist interferences to loss processe(s) that currently are not being modeled. It is also interesting to plot the concentration of O_3 for January and July 1st (Figure 5.4 a,b), to show where the largest magnitude of O_3 resides for a given time (January and February), altitude, and latitude. As expected (see Figure 5.1), the concentration in the northern hemisphere is larger than the southern hemisphere. The altitude of maximum concentration in O_3 is between 20 and 21 km at the pole (winter hemisphere) and 24–27 km at the equator.

In Figure 5.5, the N_2O profiles are compared. The observed profile obtained from Stratospheric and Mesospheric Sounder instrument on the Nimbus 7 satellite (for a description of SAMS, see Drummond et al., 1980; Jones and Pyle, 1984) agrees with the N_2O profile calculated by the model above 35 km, in the equatorial region. There are major differences between 30–35 km at all latitudes. The distribution (altitude versus latitude) for the observed N_2O profile shows a steeper slope at the poles for any given altitude than that calculated by the model. In addition, the observed profile in the equatorial region shows a larger magnitude for the mixing ratio of N_2O, 300 ppbv, at 30 km, compared to 200 ppbv calculated by the two-dimensional model. For mid-latitudes, northern hemisphere, comparison of *in situ* and SAMS data indicate that SAMS is bias 20–30 percent high [WMO, 1985]. At higher altitudes, SAMS measurements agree well with other *in situ* measurements both in terms of vertical gradient and absolute amount [WMO 1985, Chapter 10]. It is also possible that the diabatic circulation in the LLNL two-dimensional model is not strong enough in the tropics, therefore not transporting N_2O high enough into the stratosphere.

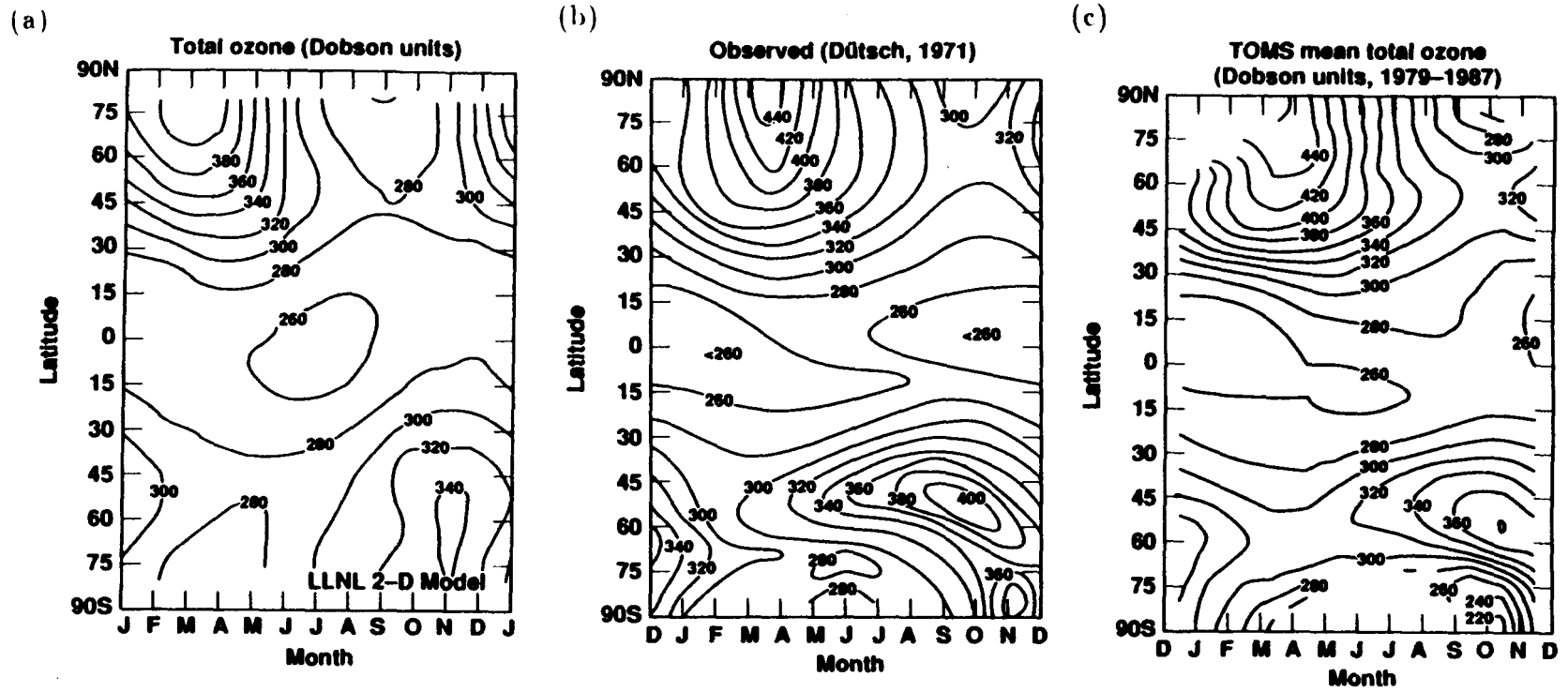

Figure 5.1. Column-ozone as function of latitude and time of the year (Dobson units). (a) The 1985 reference atmosphere is calculated from a 1950–1985 run using the LLNL two-dimensional model (Case A eddy diffusion representation, see Chapter 6). (b) Taken from Dütsch [1971], using data from the global Dobson network. (c) TOMS mean 1979-1987 data, normalized to the Dobson network.

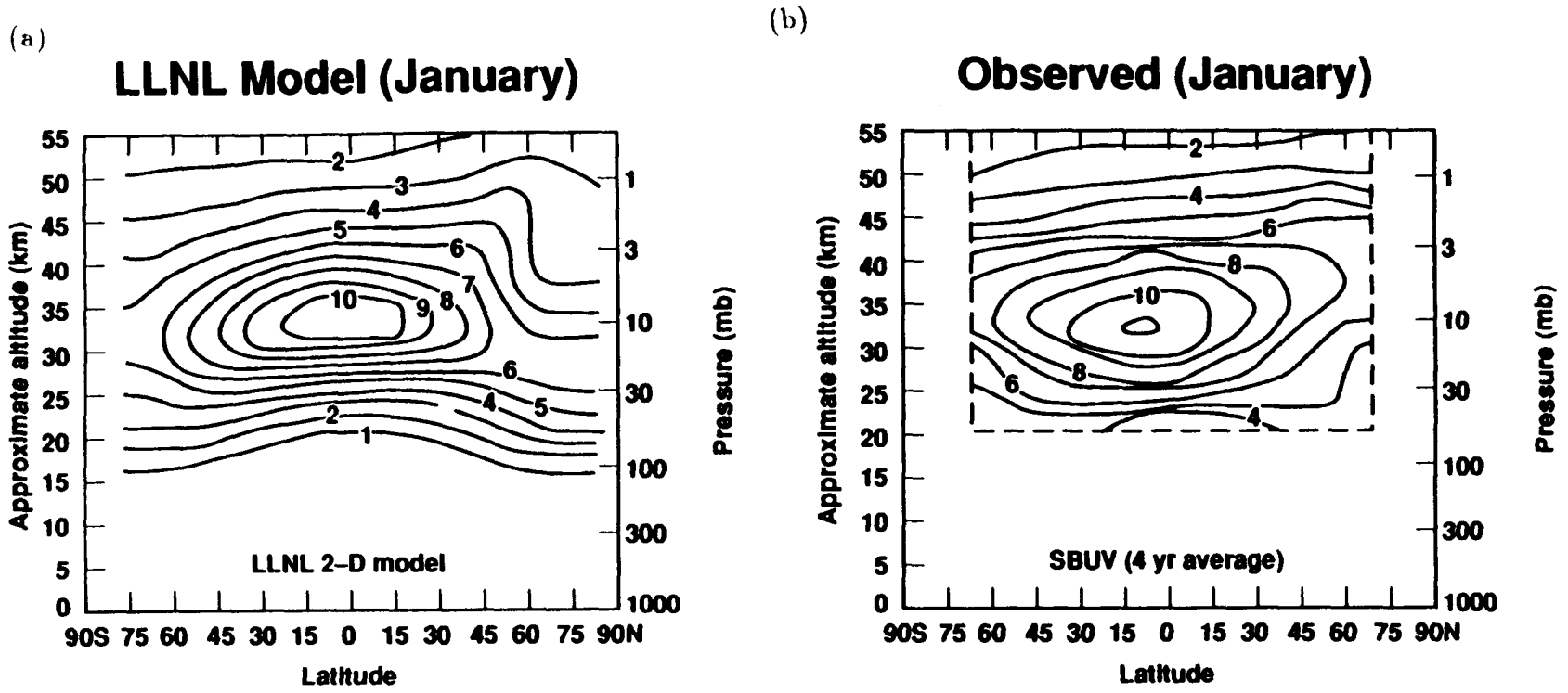

Figure 5.2. Local ozone mixing ratio (ppbv) as function of altitude and latitude. (a) The January 1, 1985 reference atmosphere is calculated from a 1950–1985 run using the LLNL two-dimensional model. (b) Obtained from the SBUV instrument on the Nimbus 7 satellite (month of January, 4 year averaged).

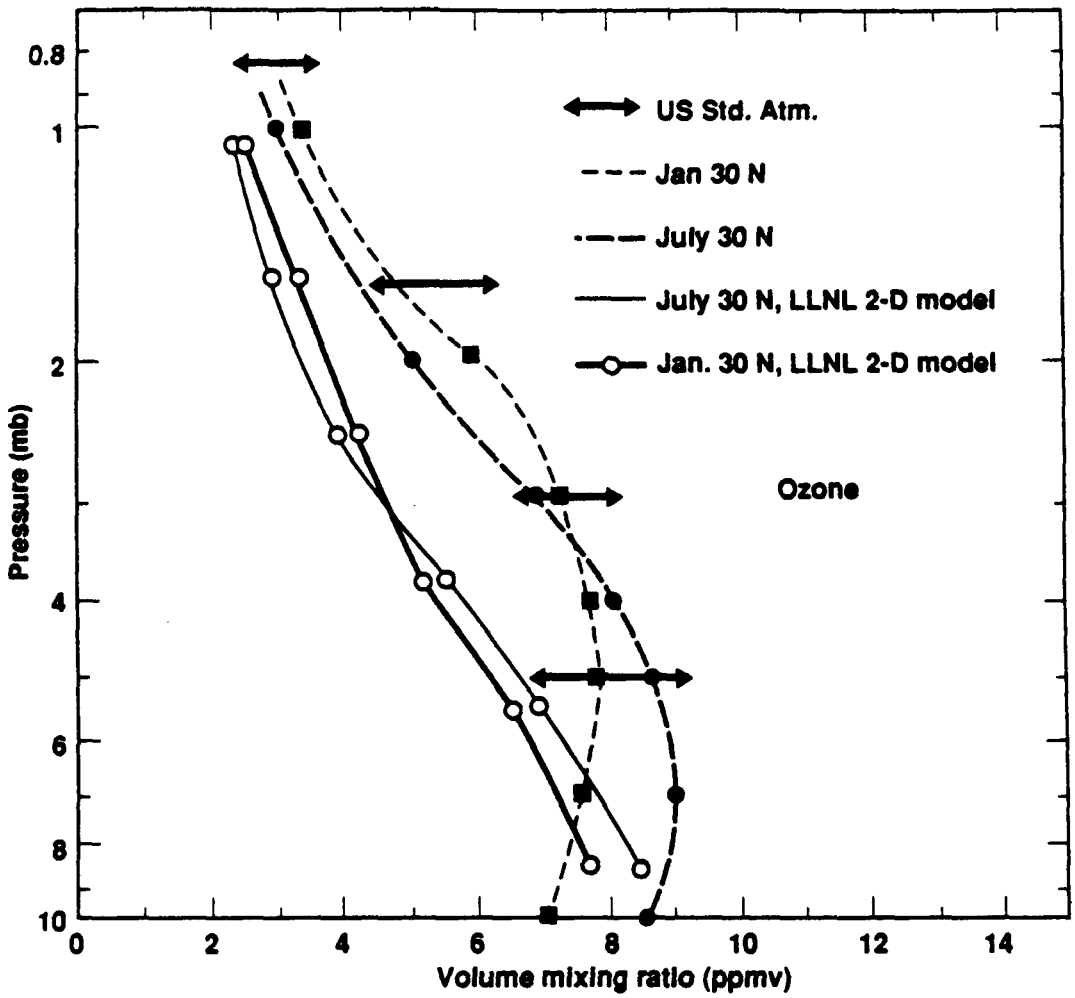

Figure 5.3. Ozone vertical distribution in the stratosphere (taken from WMO, 1985). Units are in ppmv. Observational data at 30° N for January and July, is a composite based on SME (UV and IR), SBUV and balloon ozonesondes. For historical purposes, the US Standard Atmosphere is shown at various levels. The LLNL two-dimensional chemical-radiative-transport model is shown for a 1985 reference atmosphere (calculated from a 1950–1985 run).

In Figure 5.6, total odd nitrogen, NO_y is plotted for three different pressure levels; 3 mb, 40 km; 16 mb, 29 km; and 30 mb, 24 km. The NO_y calculated by the LLNL two-dimensional model compares moderately well with the magnitude and shape of the Limb Interferometer Monitor of the Stratosphere, LIMS, data

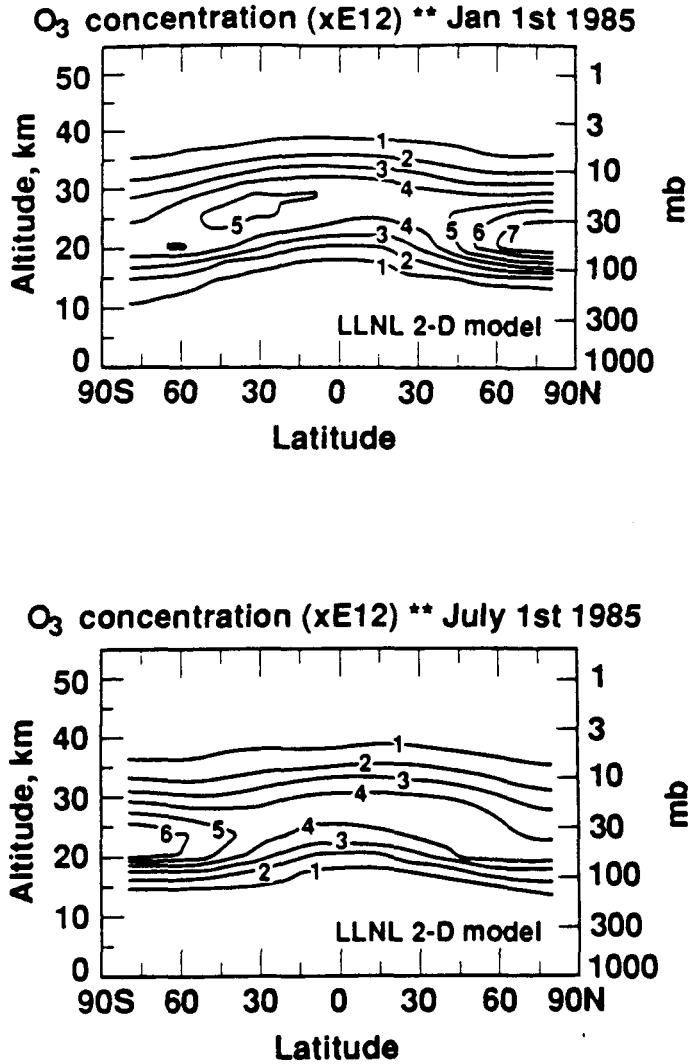

Figure 5.4. Using the LLNL two-dimensional model, O_3 distributions for January and July 1, 1985 are calculated from a 1950–1985 run. Concentration units are in molecules cm^{-3}.

at each pressure level (for comparison of LIMS to other two-dimensional models, see WMO [1985], Chapter 10). If the strength of the "Brewer Circulation" were increased to match the N_2O profile, the altitude profile of total odd nitrogen would rise, leaving a poor match with the LIMS data. The NO_y altitude versus latitude contour plot for July 1, 1985 is shown in Figure 5.7. The model calculates the maximum magnitude of NO_y to be 23 ppbv, which compares fairly well with the inferred maximum abundance of NO_y of 21 ppbv from LIMS [Solomon et al., 1985].

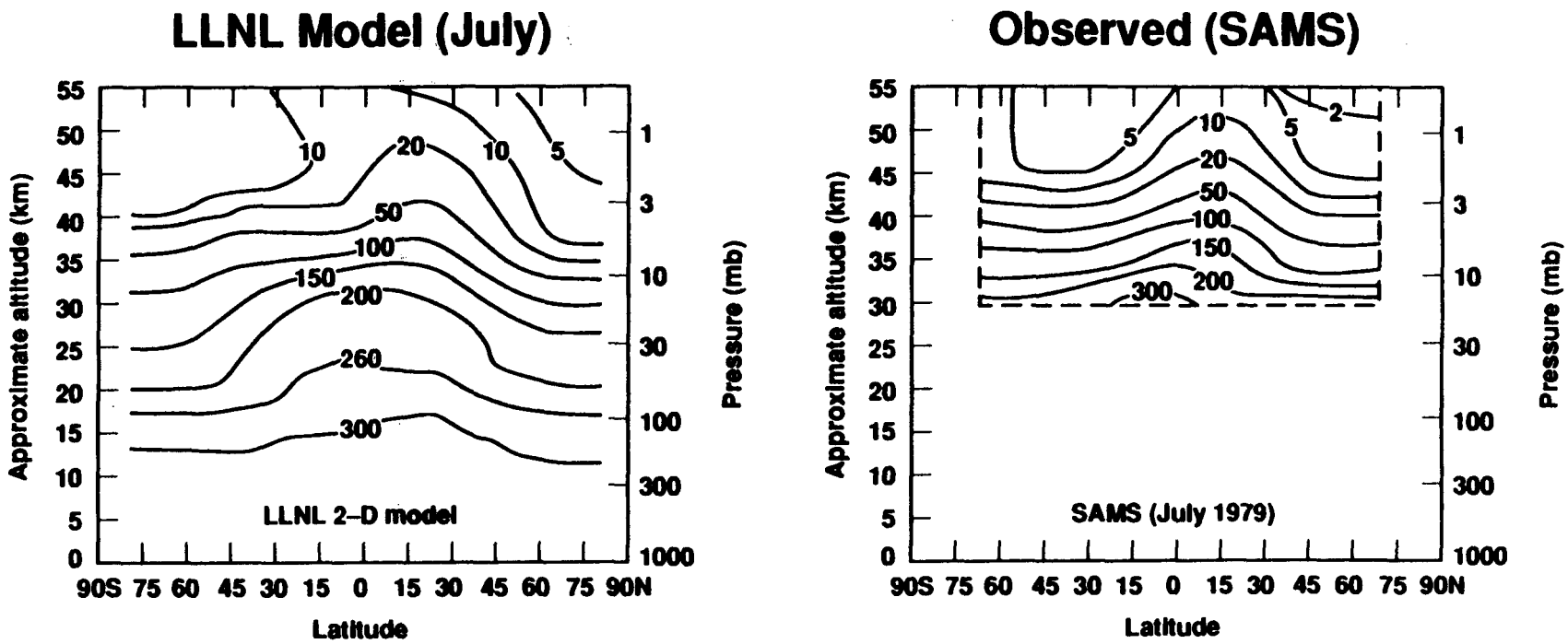

Figure 5.5. N_2O altitude versus latitude distribution for July. Units are in ppbv. (a) The July 1, 1985 reference atmosphere is calculated from a 1950–1985 run using the LLNL two-dimensional model. (b) Obtained from SAMS on the Nimbus 7 satellite.

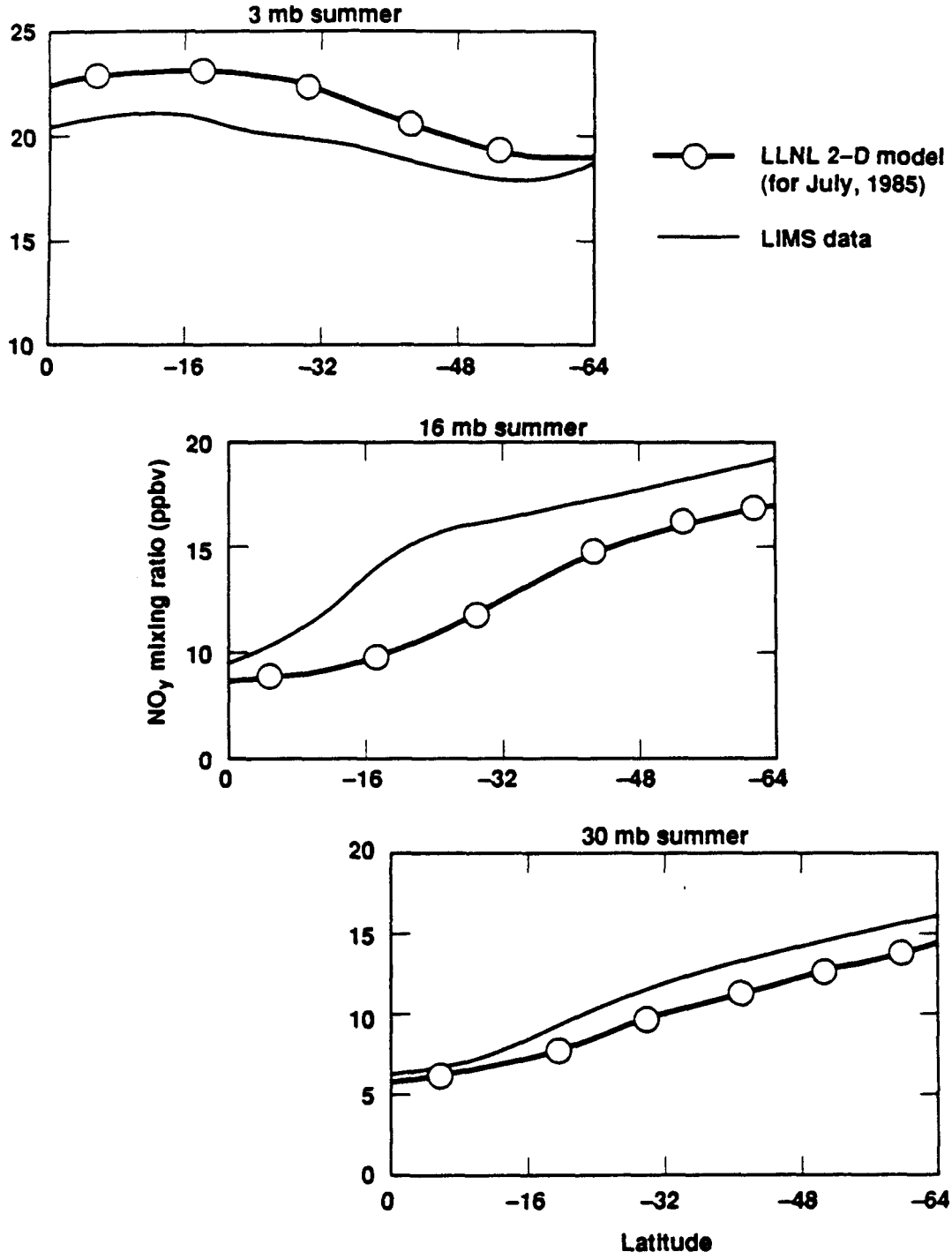

Figure 5.6. Latitudinal gradients in total odd nitrogen (NO_y) obtained from LIMS (plot taken from WMO 1985, Chapter 10). The July 1, 1985 reference atmosphere is calculated from a 1950–1985 run using the LLNL two-dimensional model.

Figure 5.8 presents the HNO_3 mixing ratio near 45° N as measured by balloon profiles and LIMS [WMO, 1985]. The LLNL two-dimensional model shows good agreement with both balloonsondes and satellite data below 35 km. Above 35 km. the two-dimensional model's mixing ratio is larger than observations would suggest. This same effect was observed with the Garcia and Solomon model [Austin et al., 1986b]. In Figure 5.9. an altitude versus latitude contour plot for HNO_3. for the LLNL two-dimensional model. exhibits a maximum at both poles. with the summer season (8 ppbv) showing a larger magnitude than the winter season (6.5 ppbv). HNO_3 distributions observed by LIMS [Austin et al., 1986b; Jackman et al., 1987] show a maximum mixing ratio in the winter polar region. Two dimensional models calculate a HNO_3 maximum in the summer polar region. Austin et al. [1986b], suggest that heteogenous processes like: $N_2O_5 + H_2O \rightarrow 2HNO_3$, are important in the HNO_3 balance at high latitudes, in the winter hemisphere. They feel the reaction rate should be about 2×10^{-20} for such a heterogeneous reaction in order to increase the mixing ratio of HNO_3, making it more comparible with the LIMS data. Jackman et al. [1987], found (using NASA Goddard two-dimensional model) that this rate only made the mixing ratios equal, and suggest a reaction rate of 2.0×10^{-19} would be more appropriate. Comparison between total column HNO_3 calculated from the LLNL two-dimensional model ($6.0 - 6.7 \times 10^{15}$ molecules cm^{-2}, minimum to maximum) and that observed at Mauna Loa Hawaii (5.9×10^{15} molecules cm^{-2}), are in good agreement [Rinsland et al., 1989]. Other measured column amounts of HNO_3 at the same latitude of Mauna Loa range from 4 to 6×10^{15} molecules cm^{-2} [Murcray et al., 1987].

In Figure 5.10, the altitude versus latitude contour of CH_4 as calculated by the LLNL two-dimensional model is plotted with data collected by SAMS. In the upper stratosphere, the single "hump" that is observed in the satellite data set is observed

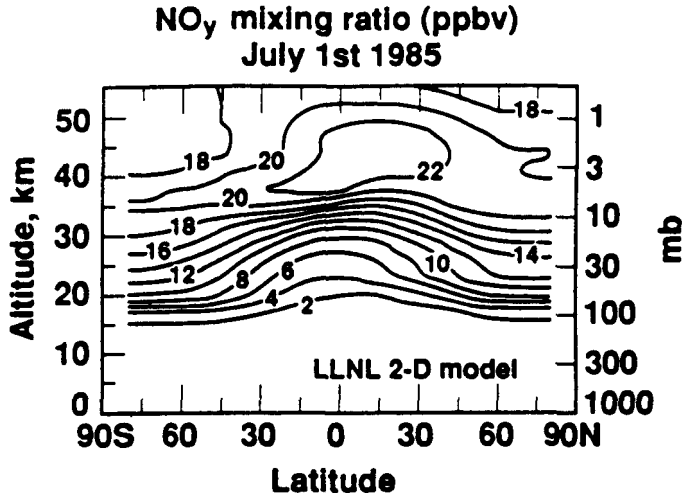

Figure 5.7. Total odd nitrogen (NO_y). The July 1, 1985 reference atmosphere is calculated from a 1950–1985 run using the LLNL two-dimensional model. Mixing ratio units are in ppbv.

in the model calculations, however, the model does not duplicate the "double hump" seen in the spring or fall, due to semi-annual oscillations not included in the model. The magnitude of CH_4 in the two-dimensional model compares well with that given by SAMS at all altitudes above 30 km in the equatorial region. At higher latitudes, the observed CH_4 mixing ratio decreases more rapidly than that calculated by the model. In the troposphere, the model exhibits the gradient between hemispheres [Blake et al., 1986] that exists due to the strong northern hemispherical sources. In Figure 5.11, the experimental profile of CH_4 obtained from balloon sounding at 44° N [Fabian et al., 1981; Schmidt et al., 1984] is compared to that calculated by the LLNL two-dimensional model at 42.5° N. In the upper troposphere and lower stratosphere the CH_4 profile calculated by the two-dimensional model compares well with the balloon sounding, but above 22 km, the model calculates a larger mixing ratio than the observational data would suggest.

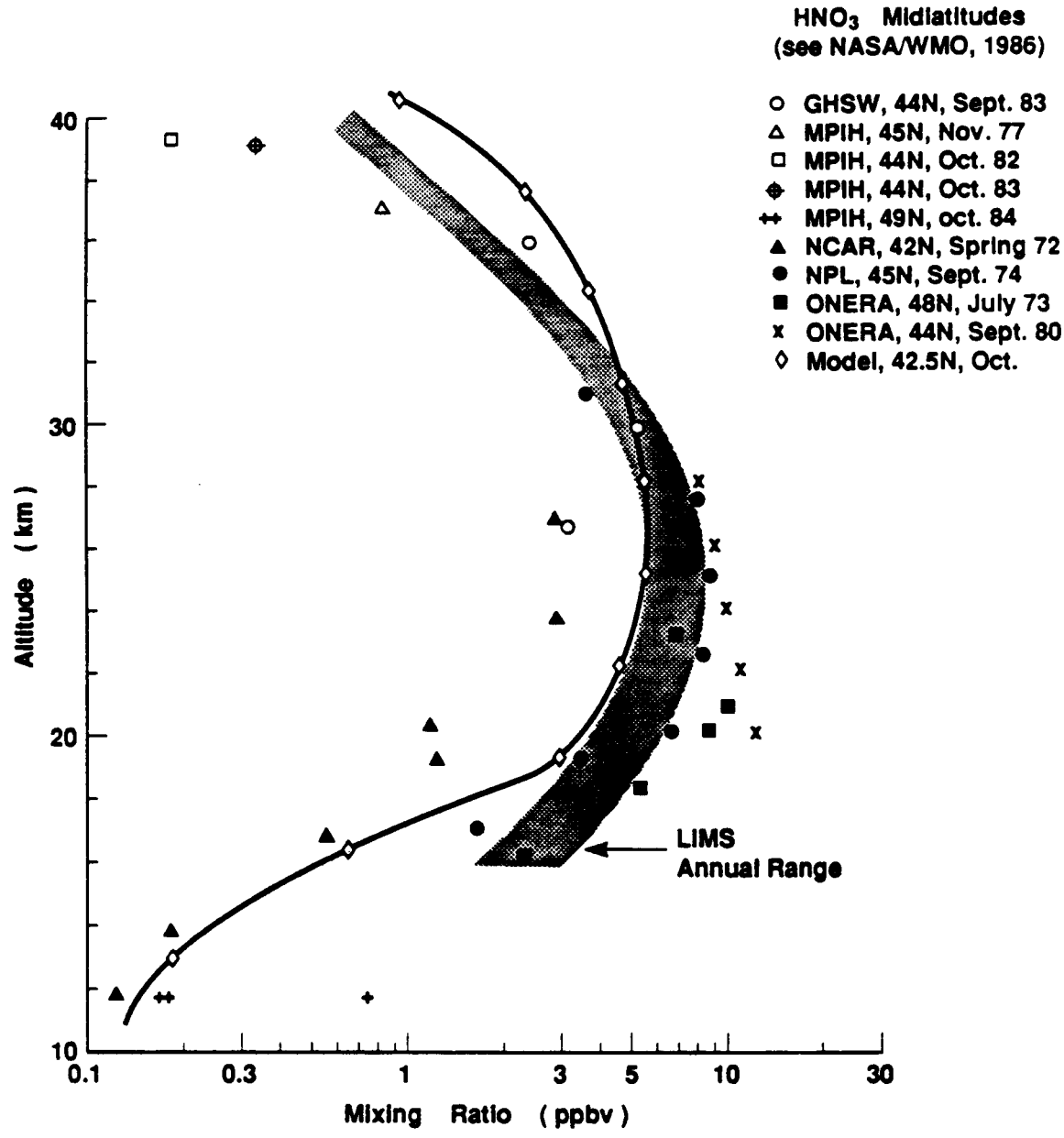

Figure 5.8. HNO_3 mid-latitude mixing ratio profile [based on Austin et al., 1986b]. Units are in ppbv. GHSW, MPIH, NCAR, NPL, and ONERA are initials of various research groups. For references on the data of each group, see WMO [1985], Table 10.3.

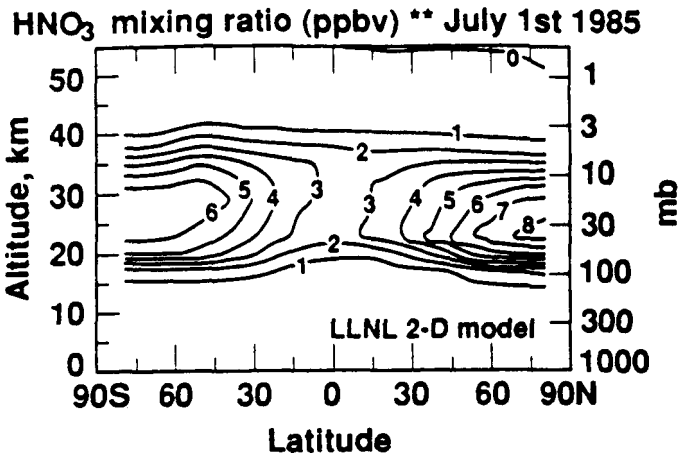

Figure 5.9. HNO_3 mixing ratio distribution. The July 1, 1985 reference atmosphere is calculated from a 1950–1985 run using the LLNL two-dimensional model.

HCl is primarily produced in the stratosphere from anthropogenic chlorine emitted from ClC's. In Figure 5.12, the HCl profile calculated by the LLNL two-dimensional model at 30° N, is compared with many observational measurements at 32° N, during the Balloon Intercomparison Campaign in 1982 and 1983 [WMO, 1985]. At all altitudes the model calculated HCl profile compares very well with the observed data. Figure 5.13 shows the calculated distribution of HCl in a contour plot. In Figure 5.14, the percent change in HCl from 1985 to 1986 for the LLNL two-dimensional model is shown for column HCl (latitude versus time) and local HCl (altitude versus latitude, January 1st). The column abundance of HCl over the PEL Lauder site in New Zealand (45° S) shows a column HCl value of 2.0×10^{15} molecules cm^{-2} and a annual trend of 10 percent [Matthews et al., 1989]. The HCl column amount calculated by the model is 3.0×10^{15} molecules cm^{-2}, with a annual trend of 2.3 percent (Figure 5.15). The model calculates the

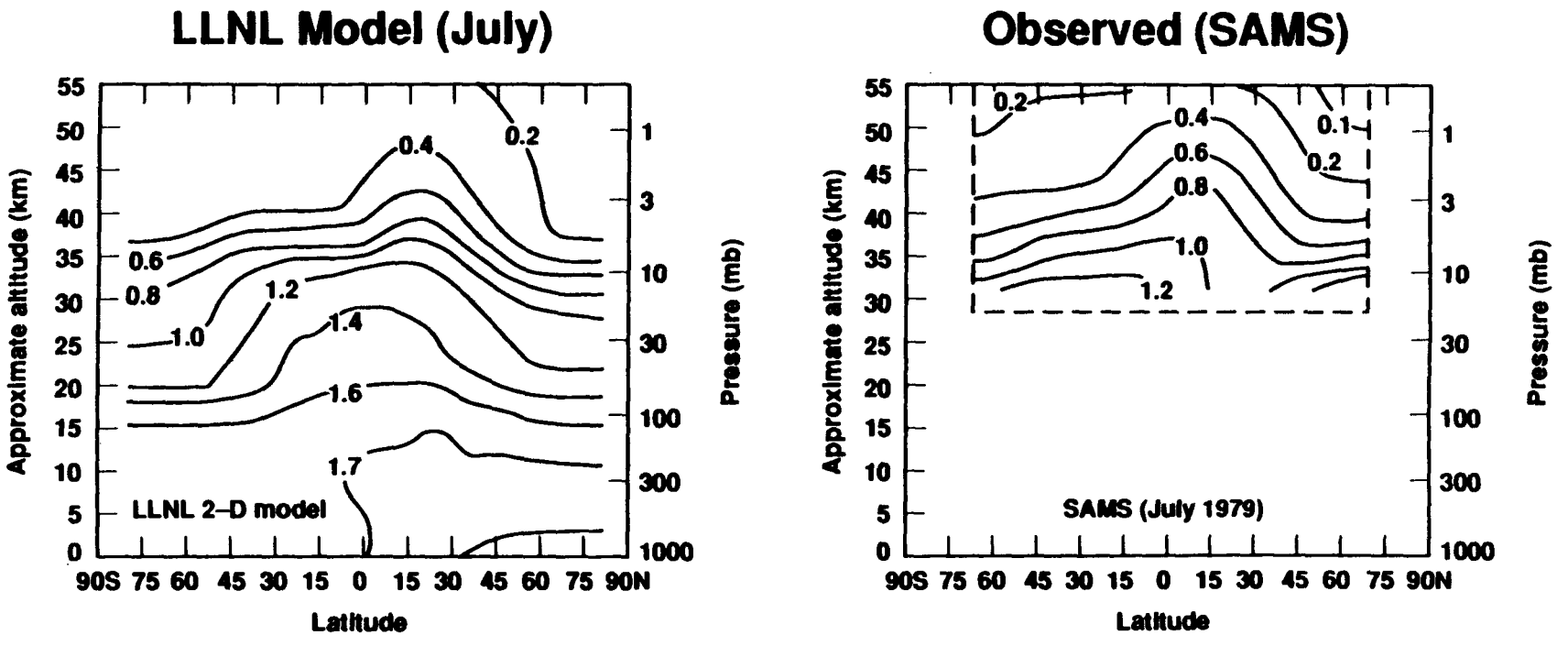

Figure 5.10. CH_4 mixing ratio distribution in units of ppmv. (a) The July 1, 1985 reference atmosphere is calculated from a 1950 1985 run using the LLNL two-dimensional model. (b) Monthly mean zonal mean cross-sections of CH_4 for May 1979 measured by SAMS instrument on the Nimbus 7 satellite [taken from Jones and Pyle, 1984].

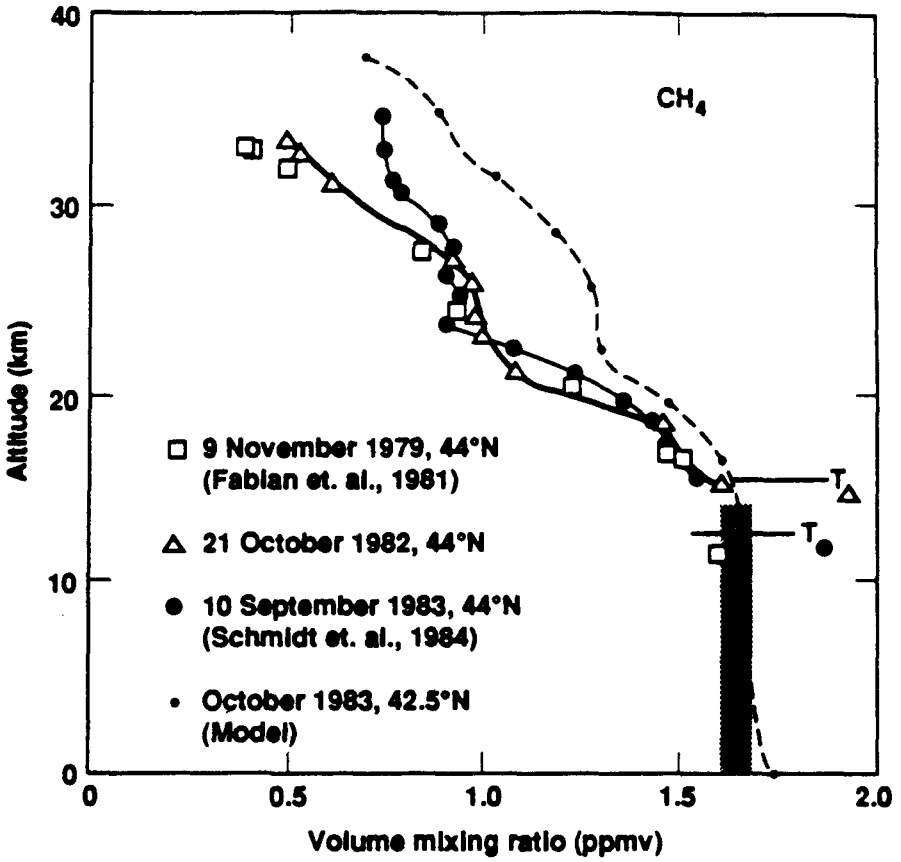

Figure 5.11. CH_4 mixing ratio (ppmv) distribution as measured by balloons. Taken from WMO [1985], Chapter 9. The October 1, 1983 reference atmosphere is calculated from a 1950–1985 run using the LLNL two-dimensional model.

change in column HCl from 1970 to 1986, to be 60 percent, with much larger local HCl changes over the same period (e.g., at 40.5 km, 130 percent).

In Figure 5.16, the LLNL two-dimensional model's total burden of odd chlorine (Cl_y) is shown for July 1, 1985. The maximum mixing ratio at the top of the atmosphere is 2.5–2.6 ppbv. In 1950, this value was on the order of 0.7–0.8 ppbv. Experimentally, Berg et al. [1980], measured total chlorine at approximately 20 km at various latitudes, using activated charcoal traps and neutron activation analysis. They obtained values ranging between 2.7 ± 0.9 and 3.2 ± 0.7 ppbv total chlorine. Gallagher et al. [1985], used cryogenic whole air samplers to measure

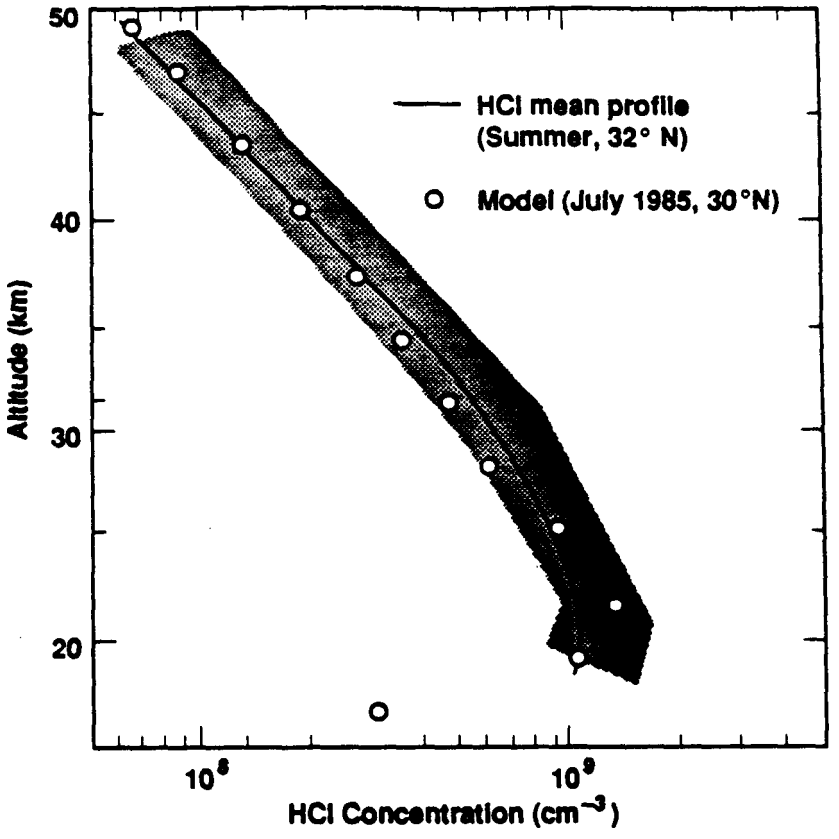

Figure 5.12. HCl concentration (molecules cm^{-3}) profile. Taken from WMO [1985], Chapter 11. The shaded area is a composite of data collected at 32° N during the Balloon Intercomparison Campaigns in 1982 and 1983. The July 1, 1985 reference atmosphere, at 30° N, is calculated from a 1950–1985 run using the LLNL two-dimensional model.

individual halogenated hydrocarbons, and filter samplers to measure acidic an particulate chlorine. Their analysis measured the total chlorine mixing ratio to be 2.6 ppbv at 15 km, decreasing to 2.2–2.5 ppbv for higher altitudes. At present rates of emission of ClC's, it is estimated that the total burden of odd chlorine in the atmosphere, at steady state, will produce a Cl_y mixing ratio maximum of 8 ppbv [WMO, 1985; EPA, Future Concentrations of Stratospheric Chlorine and Bromine, 1988].

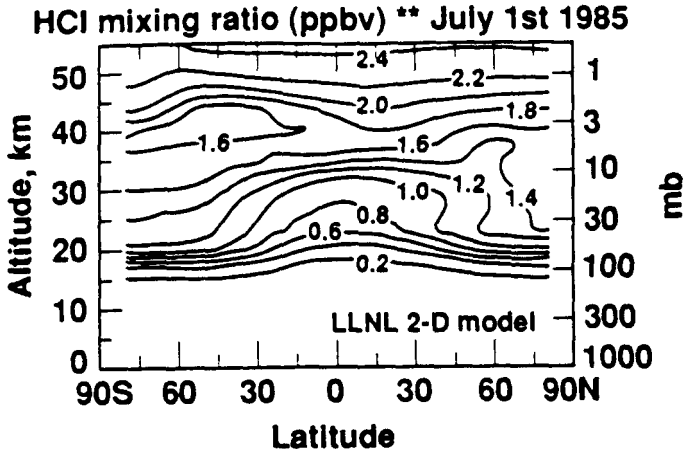

Figure 5.13. HCl mixing ratio (ppbv) distribution. The July 1, 1985 reference atmosphere is calculated from a 1950–1985 run using the LLNL two-dimensional model.

5.4 Result

In the following five sections, the LLNL one- and two-dimensional models results are compared (if possible) to experimentally obtained data. The first section, 5.4.1. deals with the effects on O_3 from injections of NO_x due to the nuclear test series of the late 1950's and early 1960's. The remaining four sections examine individual time frames; 1970–1980, 1970–1986, 1979–1986, and 1986–1990, in order to extract out trends for O_3 and temperature in the data record.

5.4.1 Nuclear Test Series

Foley and Ruderman [1973] suggested that the nuclear tests during the 1950's and 1960's should have caused a reduction in stratospheric ozone. Chang and Duewer [1973], used a one-dimensional chemical-radiative-transport model and found a northern hemispherical reduction of 4 percent for 1963. Chang et al. [1979] and later Wuebbles [1983] using the LLNL one-dimensional model, reinvestigated the effects that a NO_x pulsed injection have on O_3 with updated models and revised

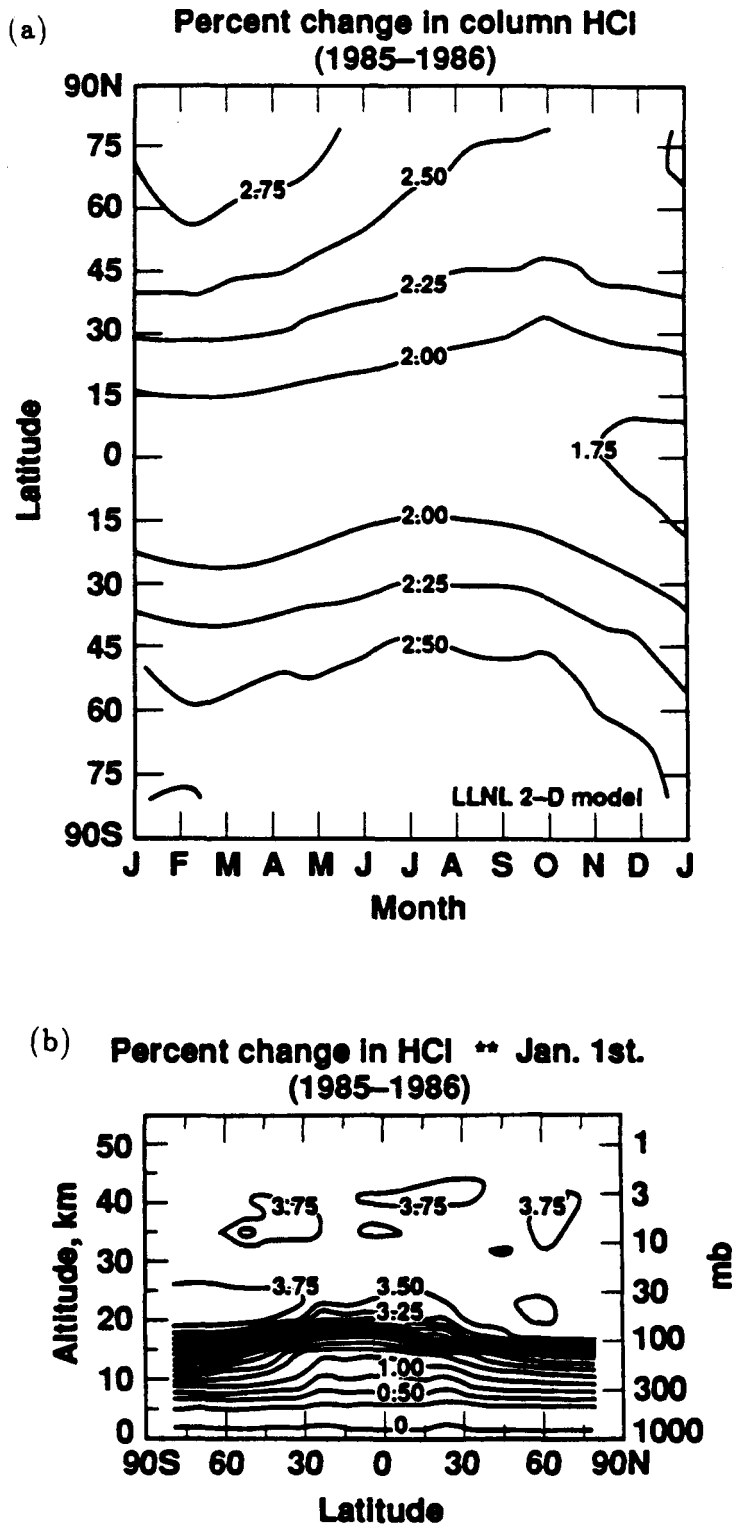

Figure 5.14. Percent change in HCl, between 1985–1986, using the LLNL two-dimensional model, for, (a) column HCl, and (b) local HCl (January 1st).

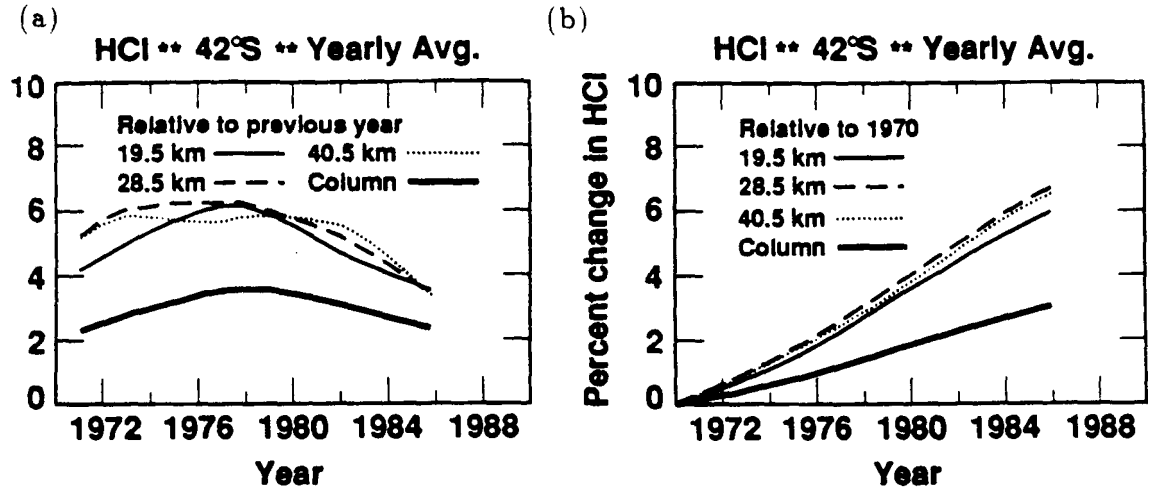

Figure 5.15. Percent change in HCl, using the LLNL two-dimensional model. Data is yearly and globally averaged. (a) Relative to previous years value. (b) Relative to 1970.

chemistry sets. Wuebbles [1983] considered the seasonal and latitudinal timing of the injection of NO_x and calculated the effects on O_3, by parameterizing the losses due to downward transport in the polar region, during winter, and the mixing of NO_x from equatorial explosion into the southern hemsphere. His analysis showed a maximum decrease of 2.5 percent in O_3, where Chang's [1979] approach, showed a much larger decrease of 4.5 percent (using 1983 chemistry).

In this study, both one and two-dimensional chemical-radiative-transport models were used to investigate the effect of NO_x on the distribution of O_3 and other trace species from 1958–1968. The scenarios are described in section 5.1 and 5.2.

In Figure 5.17-a, the results of the LLNL one-dimensional model are shown for the periods 1850–1990. Total column O_3 increased by 1.6 percent from 1850 to 1950 due to anthropogenic effects. The increase in O_3 over this time period is due to both the CH_4-NO_x smog reaction that produce O_3 in the troposphere. and temperature feedback from increasing CO_2. Wuebbles [1983], conducted the

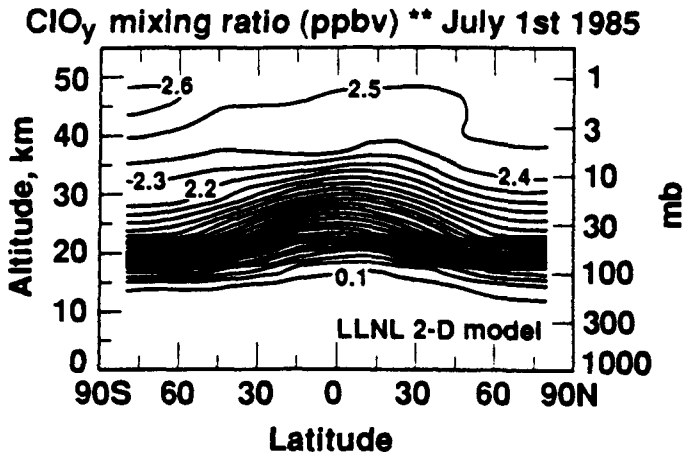

Figure 5.16. Total odd chlorine (Cl_y). The July 1, 1985 reference atmosphere is calculated from a 1950–1985 run using the LLNL two-dimensional model. Mixing ratio units are in ppbv.

same scenario and found O_3 to increase by 1.1 percent. The change in O_3 between this study and Wuebbles [1983] is due to changes in chemistry (the physics of the model is practically the same).

Figure 5.17-b, shows the three different scenarios spanning 1950 through 1990. The maximum real time effect from the nuclear test series (Table 5.2) for the one-dimensional model is −3.2 percent (January 1963). This is larger than Wuebbles [1983] by 0.7 percent. This increase can be directly connected with a change in the rate for $NO_2 + O$ in 1983 of 9.3×10^{-12} (not temperature dependent), to a temperature dependent rate constant, where the pre-exponential factor (A) is 6.5×10^{-12} and temperature dependent exponential factor (B) is 120 ± 120 [where

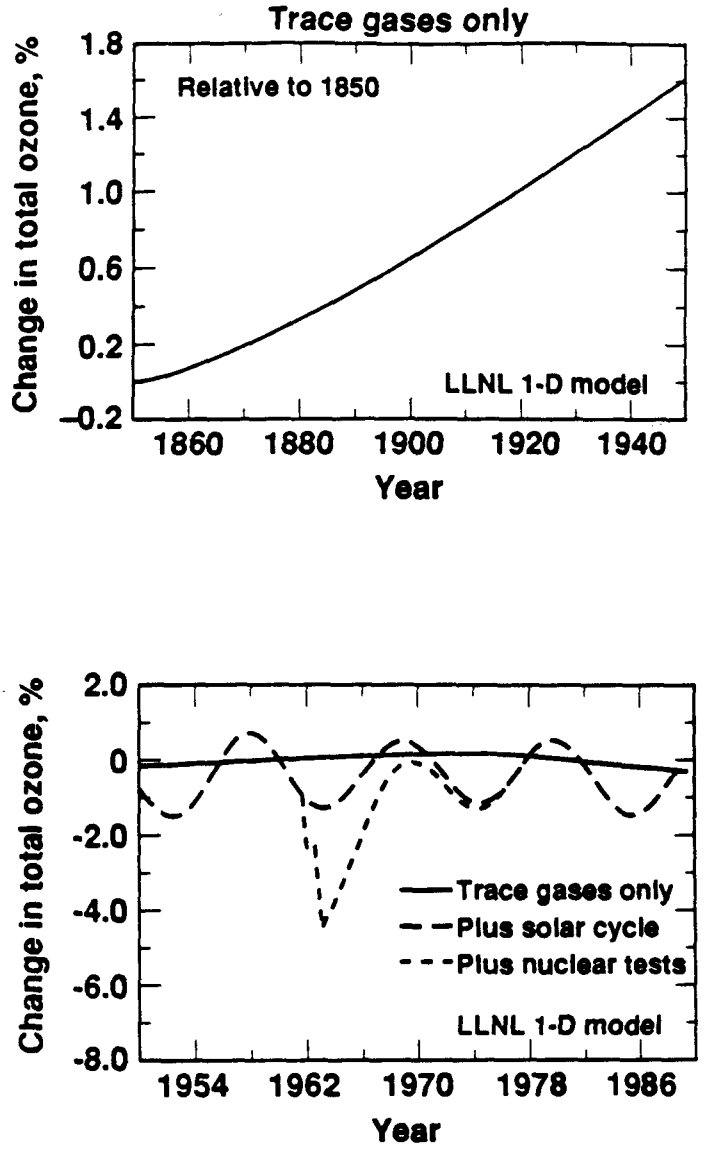

Figure 5.17. Calculated change in total O_3 by the one-dimensional model.

$k = Ae^{B/T}$, DeMore et al., 1987]. This gives a rate constant of 9.7×10^{-12} and 1.1×10^{-11} for 298 K and 250 K respectively.

The two-dimensional model calculates a real time maximum northern hemispherical average effect of -4.28 and -3.50 for Peterson and Seitz bomb cloud stabilization heights respectively. In Figure 5.18, the trend series is plotted for the three scenarios calculated with the LLNL two-dimensional model. The data are averaged yearly for global, northern hemispherical, and southern hemispherical

Table 5.2. Calculated northern hemispherical average effect on O_3 from the nuclear test series for both Peterson [1970] and Seitz [1968] bomb stabilization cloud heights.

Year	1-D Peterson Real Time (%)	2-D Peterson Real Time (%)	2-D Peterson Yearly Aver. (%)	2-D Seitz Real Time (%)	2-D Seitz Yearly Aver. (%)
1958.0	0.00	0.00	−0.06	0.00	−0.06
1958.5	0.00	−0.06		−0.06	
1959.0	−0.05	0.00	−0.11	0.00	−0.11
1959.5	−0.05	−0.12		−0.12	
1960.0	−0.04	−0.11	−0.08	−0.11	−0.08
1960.5	−0.04	−0.08		−0.08	
1961.0	−0.03	−0.06	−0.18	−0.06	−0.08
1961.5	−0.03	−0.04		−0.04	
1962.0	−1.41	−0.95	−2.29	−0.33	−1.41
1962.5	−1.10	−1.62		−0.65	
1963.0	−3.22	−4.28	−3.52	−3.50	−2.56
1963.5	−2.78	−3.69		−2.60	
1964.0	−2.48	−2.72	−1.72	−1.94	−1.22
1964.5	−2.22	−1.65		−1.17	
1965.0	−1.96	−1.21	−0.83	−0.88	−0.61
1965.5	−1.72	−0.80		−0.59	
1966.0	−1.49	−0.63	−0.43	−0.46	−0.32
1966.5	−1.28	−0.42		−0.31	
1967.0	−1.10	−0.31	−0.22	−0.24	−0.17
1967.5	−0.94	−0.21		−0.16	
1968.0	−0.81	−0.18	−0.12	−0.13	−0.09

changes in total O_3 relative to 1960 values. In Table 5.2, the northern hemisphere yearly averaged data are listed for both bomb stabilization heights. The maximum northern hemispherical yearly average effect is −3.5 and −2.6 for Peterson and Seitz respectively. In all cases Seitz shows a smaller O_3 reduction than Peterson. Since Peterson injects the NO_x at a higher altitude, it has a longer stratospheric lifetime, and therefore a larger effect on O_3. In Figures 5.19 and 5.20, the percent change in column O_3 for years 1962 and 1963 are shown for Peterson and Seitz respectively. Column O_3 is reduced approximately by 3 percent more (depending

on latitude) for Peterson (−12 percent maximum) than Seitz (−9 percent maximum). In both cases, there is little reduction of O_3 (less than 1 percent) in the southern hemisphere. In Figures 5.21-a and 5.21-b, an altitude versus latitude contour plot, for percent change in O_3 due to the nuclear test series, is shown for November 1, 1962 (also see Appendix A, for percent O_3 change every two months, up to January 1, 1964). This is right after the large tests in October of 1962. One can see that the Seitz (−15 percent local change) versus Peterson scenario (−18 percent local change) is more concentrated to a narrower altitude band and shows a smaller magnitude change in O_3.

Experimentally, there have been many authors that have investigated the nuclear series and its effect on O_3. Komhyr et al. [1971], found an increasing average trend between 2 and 10 percent during 1961 through 1970 . Johnston et al. [1973], proposed the increase was recovery from the nuclear test series. They found a statistically insignificant decrease in the northern hemisphere of 2.2 percent in the early 1960's, followed by a statistically significant (5.1 ± 1.2 percent) increase from 1961-1970 for the error-weighted average from 93 Dobson stations with 169,000 observation days. They suggested, depending on the amount of NO_x per megaton ($0.17 - 1.0 \times 10^{32}$), that the expected ozone reduction due to the nuclear test series, is between 1–6 percent. Birrer [1974], went back through the oldest Dobson record (Arosa Switzerland, 1961–1971) and pointed out that ozone showed increases and decreases that lasted several years and were comparable to or larger than the trend observed in the 1960's. Therefore, the long-term record did not support the theory that O_3 was destroyed by NO_x from nuclear bombs. Goldsmith et al. [1973], examined the noisy record of Arosa and Oxford, and concluded that the failure of these records to show a significant O_3 depletion positively disproved the theory that NO_x reduced O_3 in the stratosphere. Angell and Korshover [1976], concluded

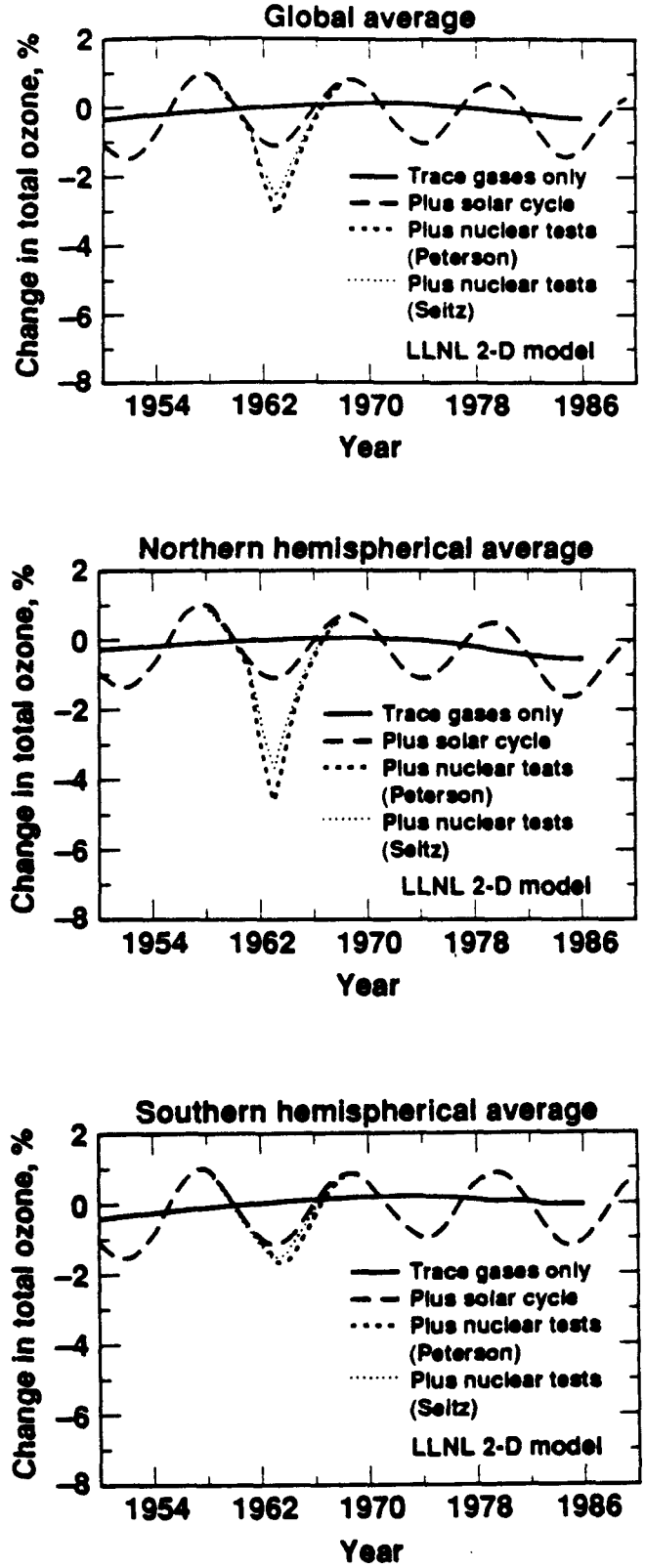

Figure 5.18. Calculated change in total O_3 by the two-dimensional model.

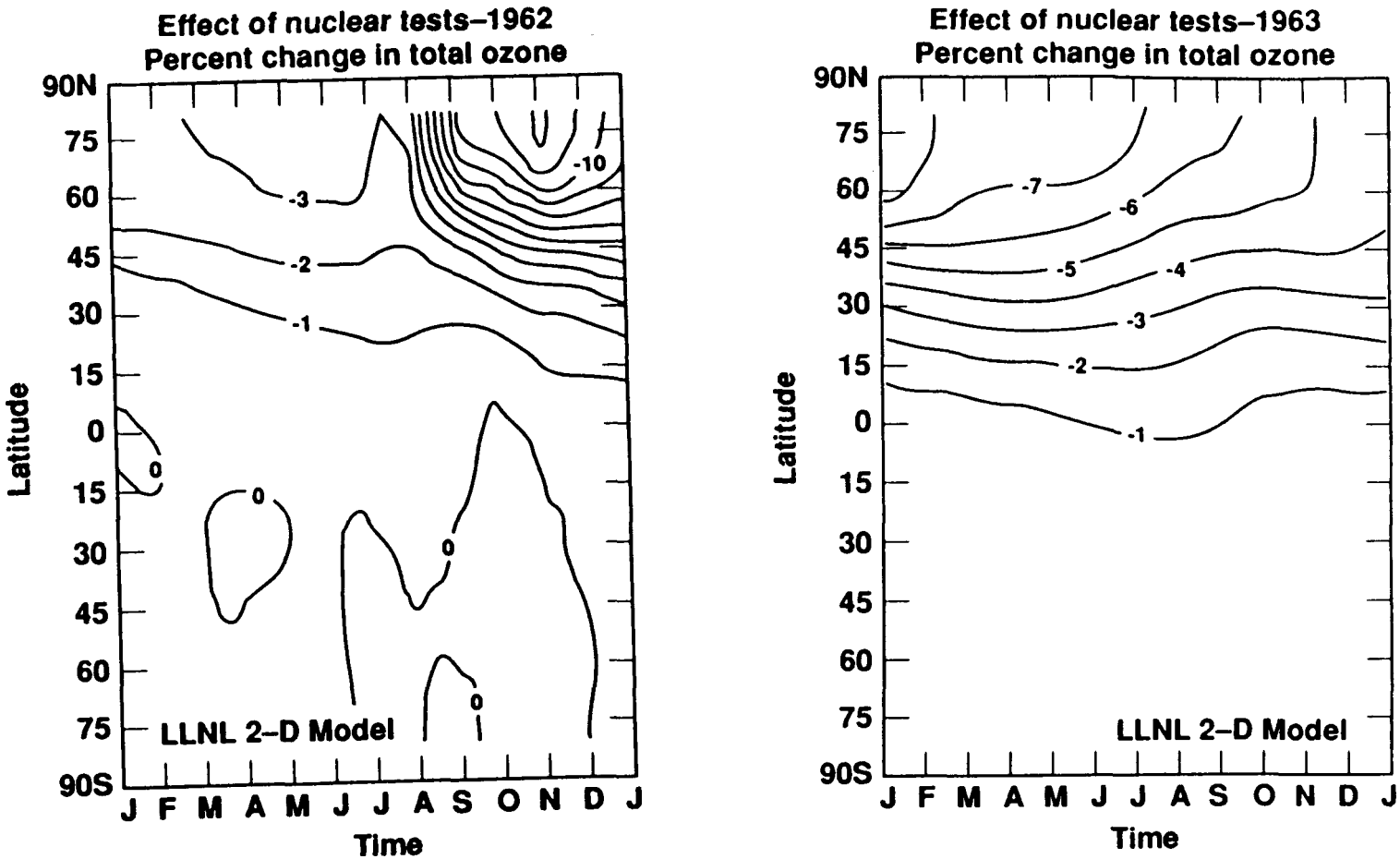

Figure 5.19. Percent change in total O_3 for the years of 1962 and 1963, using Peterson [1970] bomb cloud stabilization heights.

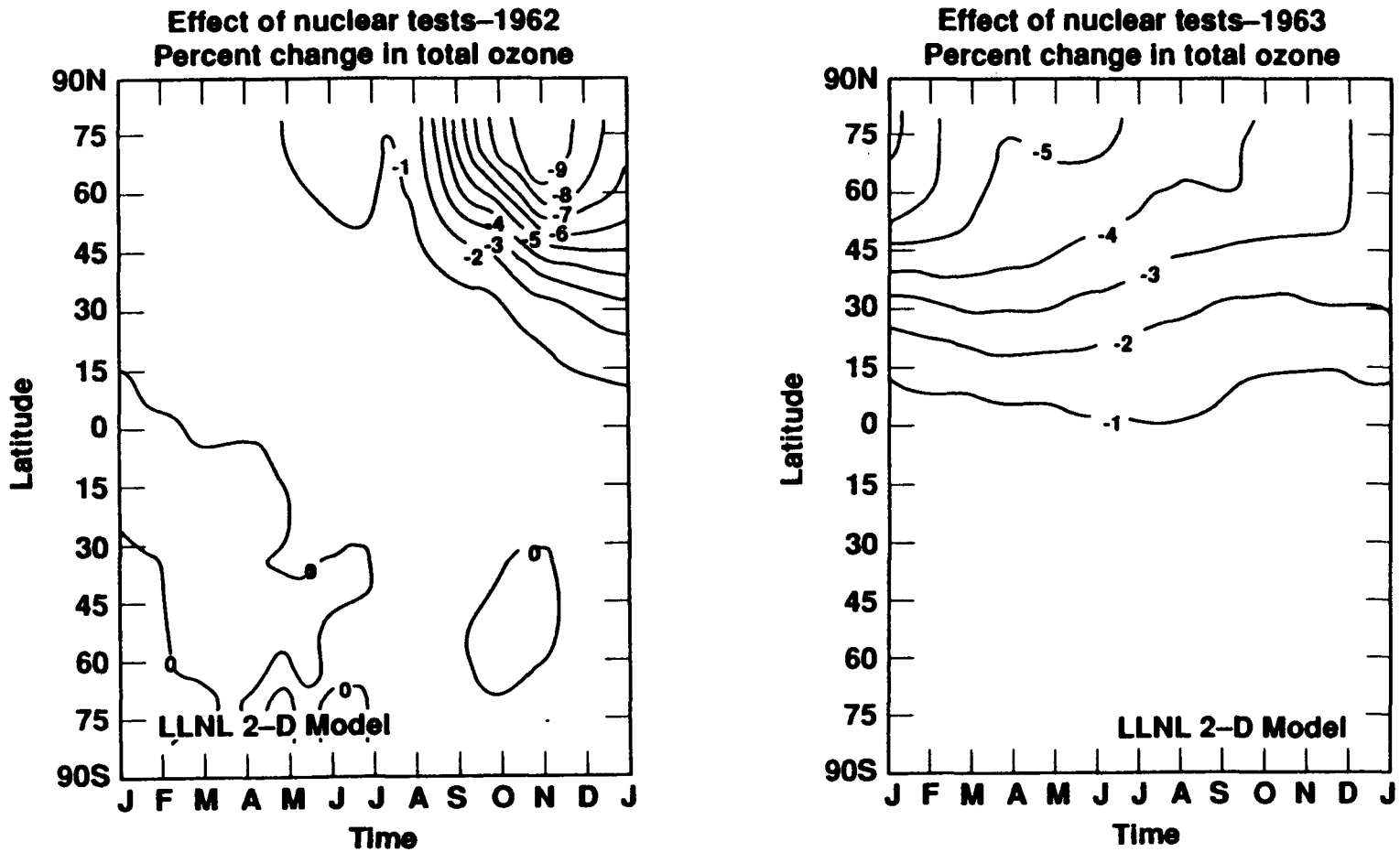

Figure 5.20. Percent change in total O_3 for the years of 1962 and 1963, using Seitz [1968] bomb cloud stabilization heights.

(a)

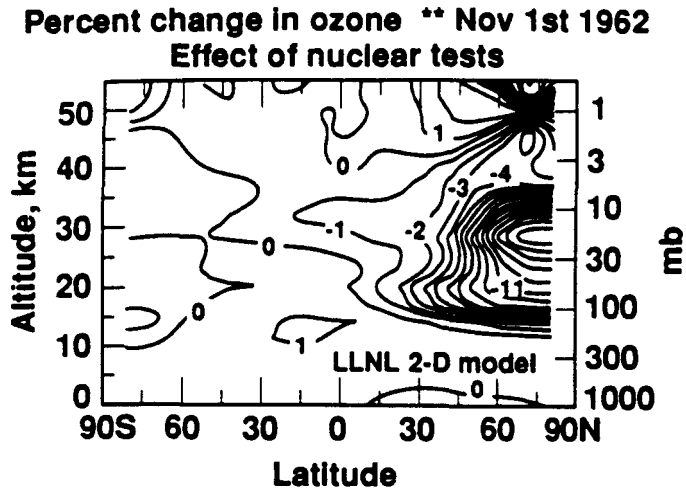

(b)

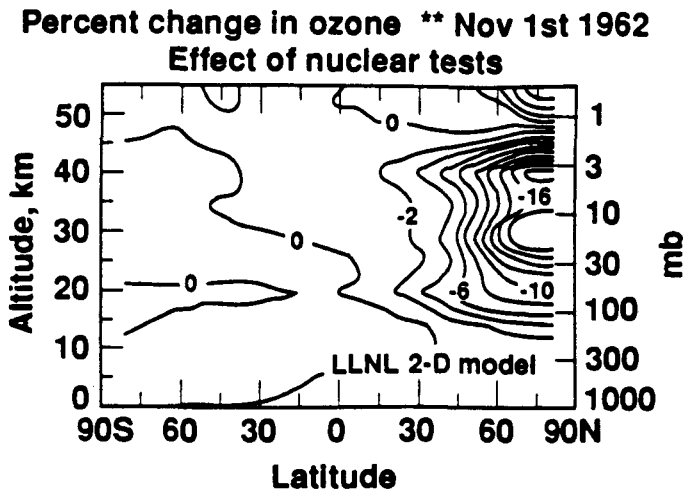

Figure 5.21. Percent change in O_3 for November 1, 1962. (a) Peterson [1970] bomb cloud stabilization heights. (b) Seitz [1968] bomb cloud stabilization heights.

that any ozone reduction caused by the nuclear test series must have been less than 1–2 percent. Johnston [1982] showed that using the techniques of Angell and Korshover [1976], that a 5 percent or greater decrease would be undeterminable by their method. Reinsel [1981], using the method of time series analysis, examined the O_3 data from a network of stations between 1959 and 1979. He concluded that a 2–4.5 percent decrease in the northern hemisphere would be consistent with his

analysis of the Dobson network. In Table 5.2, the LLNL one- and two-dimensional model seems to show good agreement with Reinsel's analysis. Recently, Harris et al. [see NASA-WMO, 1989], reanalyzed the Dobson network data, using time series analysis, like Reinsel [1981], but with a different technique in handling the seasonal cycle (monthly averages instead of using a sine curve and its harmonics to describe the seasonal cycle). They also used a function supplied by the LLNL two-dimensional model, that showed allowance for possible latitudinal and seasonal variation in reponse to the nuclear tests [Reinsel, 1981, used a function derived from a one-dimensional model]. Harris et al. [see NASA-WMO, 1989] divided the northern hemisphere into three latitude zones 30–39° N, 40–52° N, and 53–64° N. In Table 5.3, the results calculated by the LLNL two-dimensional model that correspond to the nearest latitude zone are listed every half year between 1959 and 1965. In most cases, results calculated by the model show a larger decrease in column O_3 than the observed data. Harris [private communication, 1989] believes that the technique used in calculating the results of the band approach can lower the actual observed effect. Therefore it is better to compare to individual stations. In Table 5.4, seven stations whose record started before 1960, are shown for January 1, 1963 (approximately the time of maximum O_3 reduction). At high latitudes (Lerwick and Edmonton), the decrease in O_3 is much larger than the 53–64° N band would suggest (Table 5.3). There are also longitudinal effects in the results of the analysis by Harris (e.g., Sapporo versus Rome), which may arise from regional meteorological conditions. For example, Sapporo (43° N) has a smaller correlation coefficient, -0.18 ± 0.31, than either Arosa (47° N), -0.60 ± 0.25, or Rome (42° N), -0.55 ± 0.33, which are at similiar latitudes. They find that the the error estimates get larger as latitude decreases due to the signal being smaller at lower latitudes. At Tateno (36° N), the corrolation coefficient is actually positive, -0.65 ± 0.46, which would imply a increasing trend during 1963. In general,

Harris et al. conclude from their reanalysis of the Dobson network of stations, that "there was a decrease of several per cent in total ozone in the early 1960s which is consistent with the hypothesis of an effect from the atmospheric testing of nuclear weapons." and "the observed decrease is smaller than that calculated by the LLNL two-dimensional model, however, neither the significance of the desparity nor its possible causes are clear." To be published in NASA-WMO, Ozone Trends Panel Report 1989.

In Figure 5.22, two latitudes (80 and 42.5° N) are shown for the percent change in O_3 (altitude versus time) during years 1962 and 1963. The large change in O_3 is expected for late 1962, but, at first thought, not in the spring of 1963. One would expect the percent change in local O_3 to decrease with time and show no seasonal behavior, due to the nuclear test ban treaty, which outlawed the testing of nuclear weapons above ground (for the USSR and USA) after December, 1962. In Figure 5.23, excess NO_y (all odd nitrogen species) in ppbv is plotted for the same latitudes as Figure 5.22. Here NO_y decreases with time, as one would expect, since NO_y is transported to other latitudes within the stratosphere and from the stratosphere, and then removed from the atmosphere by rainout in the water soluble form of HNO_3 or HNO_4. In Figure 5.24, excess NO_x is plotted in ppbv, again for the same conditions as Figure 5.23. At high latitudes (80° N), excess NO_x (NO and NO_2) increase by 11 ppbv for October 1st, and by December 1st, decreased to zero. It is known that at high latitudes, during polar night, that NO and NO_2 are converted to either N_2O_5 or HNO_3, therefore removing NO_x from the active species. The same effect on NO_x was calculated at lower latitudes (42.5° N), but not to the same extent. At 80° N, in the spring time of 1963, the reservoir species N_2O_5 and HNO_3 are photolyzed and NO_x is released and O_3 reduction occurs. The reduction in spring of 1963 is at a lower altitude, therefore NO_x, tied up in HNO_3

Table 5.3 Ozone column change due to nuclear test series for three latitude bands; 30 39° N, 40 52° N, and 53 64° N. Statistical analysis of Dobson network taken from Harris et al. [NASA-WMO, 1989], between 1962 and 1965 (real time). Model data are shown for three latitudes; 30° N, 42° N, and 62° N. Both Peterson [1970] and Seitz [1968] bomb stabilization cloud heights are shown.

Time	Harris 30-39 N	2-D (Peterson) 30 N	2-D (Seitz) 30 N	Harris 40-52 N	2-D (Peterson) 42 N	2-D (Seitz) 42 N	Harris 53-64 N	2-D (Peterson) 62 N	2-D (Seitz) 62 N
1959.0	—	0.41	0.41	—	-0.06	-0.06		0.15	0.15
1960.0	—	-0.10	-0.10	—	-0.15	-0.15		0.18	0.18
1961.0	—	-0.05	-0.05	—	-0.08	-0.08		0.10	0.10
1961.5	—	-0.03	-0.03	—	-0.03	-0.03		0.04	0.07
1962.0	-0.05 ± 0.16	-0.17	-0.16	-0.69 ± 0.42	-0.98	-0.49	-1.14 ± 0.45	2.65	0.74
1962.5	-0.10 ± 0.34	-1.33	-0.53	-0.74 ± 0.44	-1.97	-0.78	-0.89 ± 0.35	3.04	1.12
1963.0	-0.24 ± 1.10	-2.85	-2.55	-2.67 ± 1.60	-5.20	-4.38	-3.49 ± 1.38	8.74	6.76
1963.5	-0.25 ± 0.8	-3.25	-2.34	-1.86 ± 1.12	-4.55	-3.17	2.02 ± 0.80	6.32	4.26
1964.0	-0.20 ± 0.70	-2.76	-1.99	-1.40 ± 0.84	-3.73	-2.61	-1.54 ± 0.53	4.04	2.73
1965.0	-0.12 ± 0.37	-1.12	0.80	0.72 ± 0.43	1.62	1.17	0.81 ± 0.32	1.89	1.38

and N_2O_5, is transported by advection downward in the wintertime stratosphere. This is consistent with current dynamic theory. In Figure 5.25, both excess HNO_3 and N_2O_5 increase in the late winter of 1962. For excess N_2O_5, it is obvious that during the winter, high latitude, and polar night conditions (80° N), N_2O_5 builds up and decays as the seasonal cycle progresses.

Table 5.4 Dobson stations for January 1963 whose record started before 1960.

Station	Latitude	Δ D.U.	D.U.	Correlation Coefficient	O_3 Percent Difference Due to Nuclear Tests
Lerwick	60° N	28.6	336	-0.71 ± 0.27	-6.04 ± 2.30
Edmonton	54° N	28.6	373	-0.62 ± 0.27	-4.75 ± 2.07
Arosa	47° N	20.0	342	-0.60 ± 0.25	-3.51 ± 1.46
Sapporo	43° N	20.0	422	-0.18 ± 0.31	-0.85 ± 0.15
Rome	42° N	20.0	349	-0.55 ± 0.33	-3.15 ± 1.89
Cagliari	39° N	12.6	342	-0.38 ± 0.63	-1.40 ± 2.32
Tateno	30° N	12.6	335	$+0.65 \pm 0.46$	$+2.44 \pm 1.73$

In Figure 5.26, the excess column NO_2, in the year of 1962 (latitude versus time), shows a September maximum of 5.0×10^{15} molecules cm^{-2}. Since NO_2 has a large visible cross section centered at 400 nm, the direct solar flux should be attenuated. In fact, a -4.0 and -2.0 percent change in the direct solar flux is calculated to occur at the surface and at 28.5 km respectively (Figures 5.27). Also notice the increase in the direct solar flux at wavelengths of 600 nm, where the O_3 Chappuis bands reside. Since O_3 is reduced, the direct solar flux increases at this wavelength. Kondratyev and Nikolsky [1988], comment that in the USSR, after some of the large nuclear tests in 1962, decreases of 6 to 8 percent in the direct solar flux, at wavelengths that corrospond to NO_2, were observed. If their

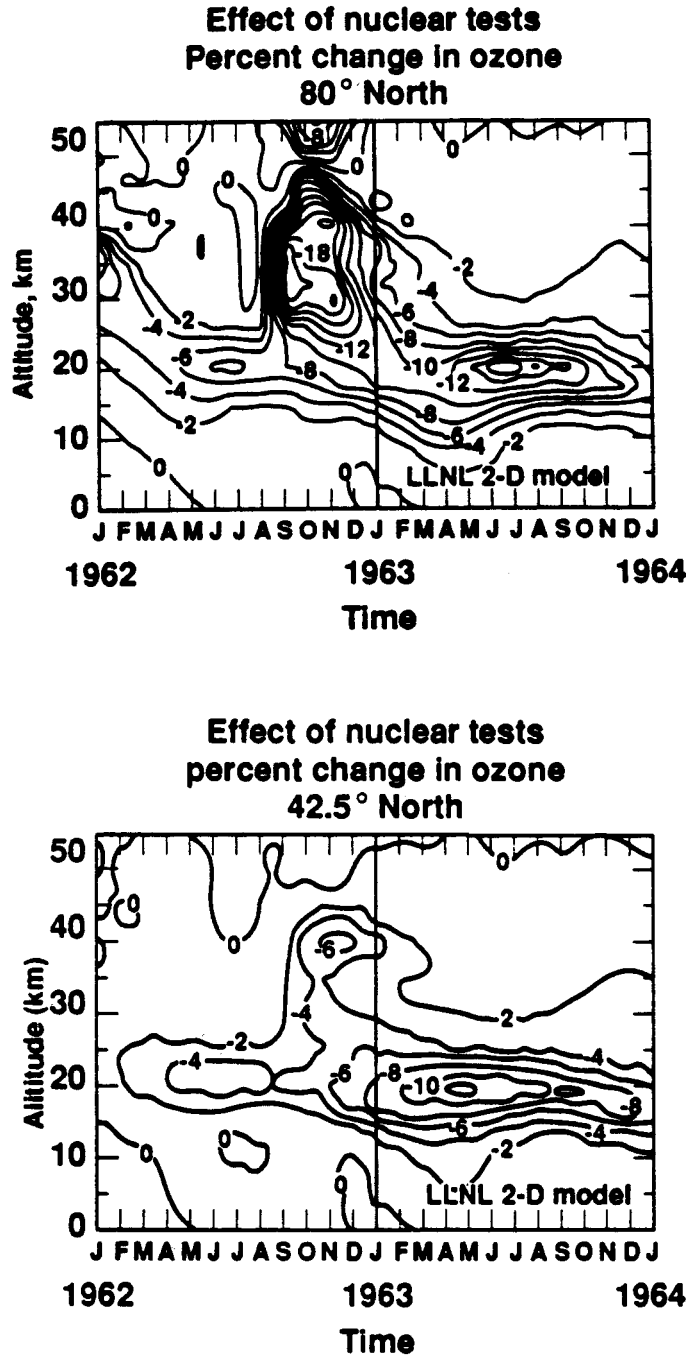

Figure 5.22. Percent change in ozone due to the nuclear test series. Peterson [1970] bomb cloud stabilization heights were used.

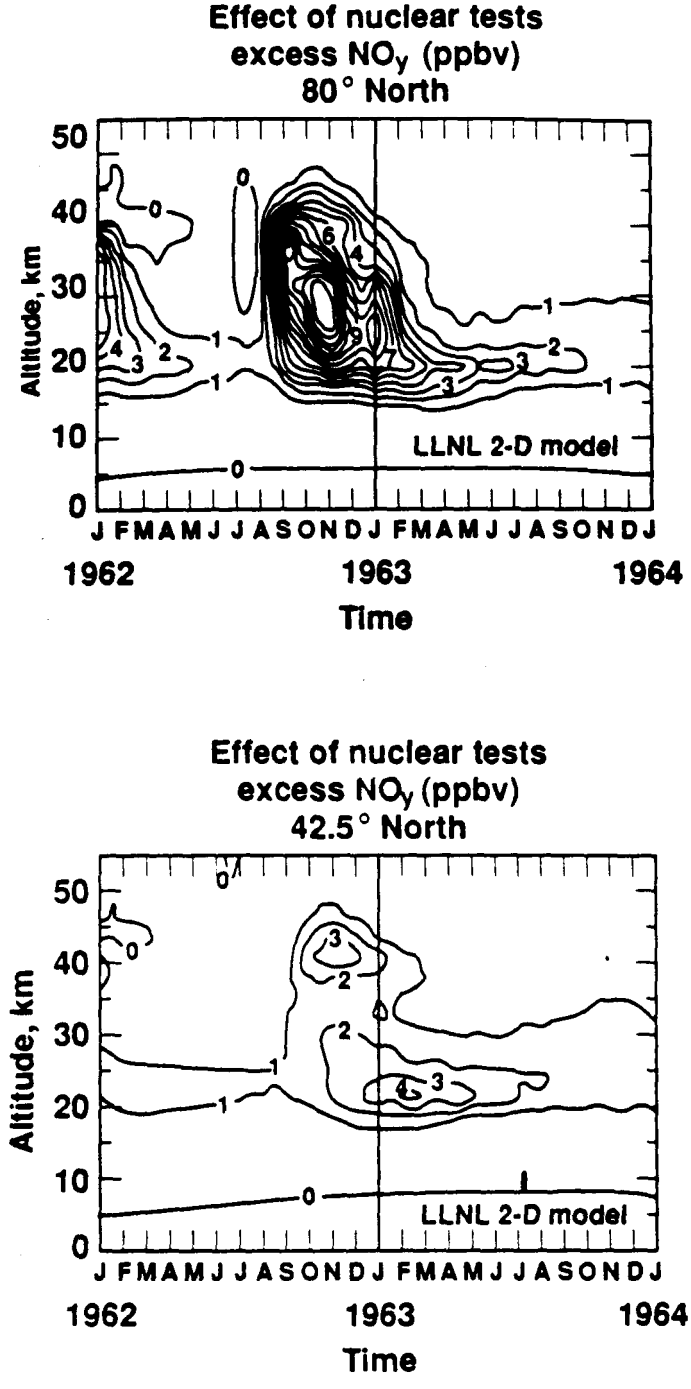

Figure 5.23. Change in NO_y due to the nuclear test series. Peterson 1970 bomb cloud stabilization heights were used.

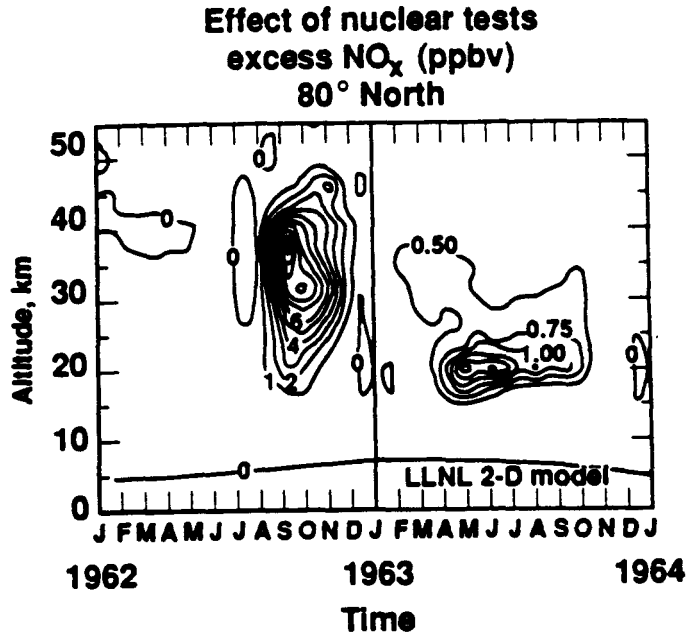

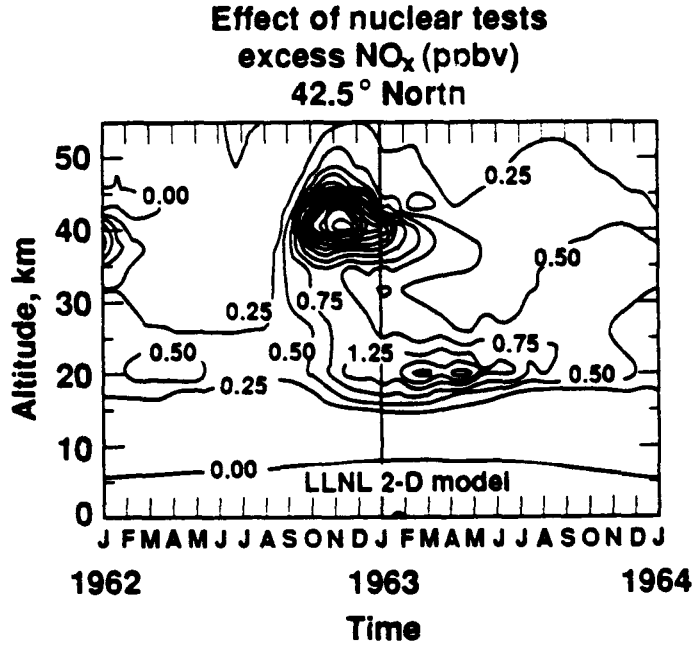

Figure 5.24. Change in NO_x due to the nuclear test series. Peterson 1970 bomb cloud stabilization heights were used.

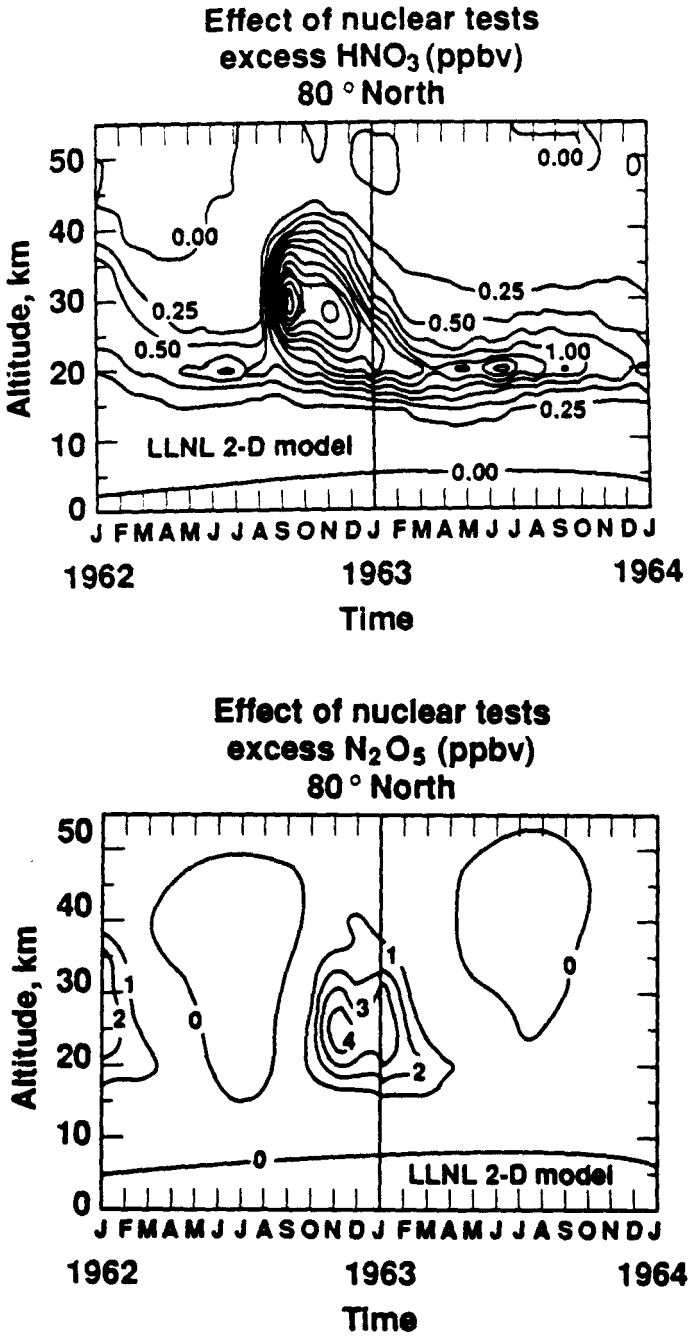

Figure 5.25. Change in HNO_3 due to the nuclear test series. Peterson [1970] bomb cloud stabilization heights were used.

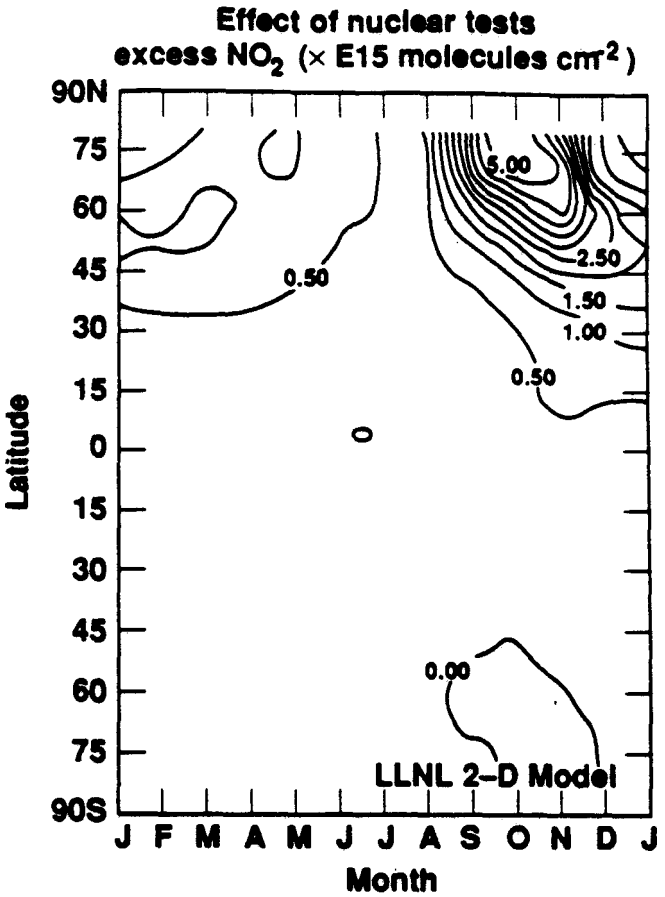

Figure 5.26. Change in column NO_2 due to the nuclear test series. Peterson [1970] bomb cloud stabilization heights were used.

observations are correct, it suggests a larger magnitude of NO_x was injected. This implies a larger O_3 change relative to current two-dimensional model calculations.

5.4.2 Trends between 1970–1980

Column O_3, using the LLNL one-dimensional model, was calculated to have increased by 0.3 percent per decade for the time period of 1970 to 1980 [Wuebbles, 1983]. Although the O_3 column was calculated to have increased during the 1970s, this increase was a result of a summation between an increase in the troposphere (CH_4-NO_x smog reactions and temperature feedback from increased CO_2) and a decrease in the upper stratosphere (Cl_y chemistry) [Wang et al., 1986].

Reinsel [1981], calculated an increase of 0.28 ± 0.67 percent in total column O_3 for the period of 1970 through 1978. St. John et al. [1982], found an increase of 1.5 ± 0.5 percent between 1970 and 1979, while Bloomfield et al. [1983], calculated an increase of 0.1 ± 0.55 percent during the same time period. Updating analysis through 1983. Reinsel et al., as reported in WMO [1985], determined a statistically insignificant tend in total ozone of -0.17 ± 1.1 percent per decade, while Oehlert 1986 , reports a change of -1.1 ± 0.47 percent per decade. In all the above cases, the data and statistical approach were slighty different, and yet, when the error bars are considered, there is little evidence of a statistically significant trend [WMO, 1985]. In Figure 5.28, the LLNL two-dimensional model calculates a decreasing trend at mid-latitudes in the northern hemisphere, which is not inconsistent with both Wuebbles [1983] and the statistical analysis described above. For the trace gas only scenario, the trend is between -0.75 and -0.25, depending on the time of year at 45° N. When the solar cycle is included, the trend is between -0.50 and 0.0 at 45° N. At high latitudes in the northern hemisphere winter, the trend can be as high as -1.0 percent between 1970–1980. In Table 5.5, the period of 1970–1980 is given for global (Gl), northern (NH) and southern (SH) hemispherically yearly averaged data. The comparison to both Wuebbles [1983] and the three statistical studies given above are more consistent when comparing the two-dimensional models NH yearly averaged trend for the period of 1970–1980 (-0.02 percent per decade).

In Figures 5.29 and 5.30, the percent change in O_3 and change in temperature is shown for July 1st. The maximum change of -8.0 percent between 40–45 km is shown in Figure 5.30-a. For Umkehr levels 7 and 8 (2–8 mb or about 34–43 km), Reinsel et al. [1984] determined a trend of -3 to -4 percent per decade.

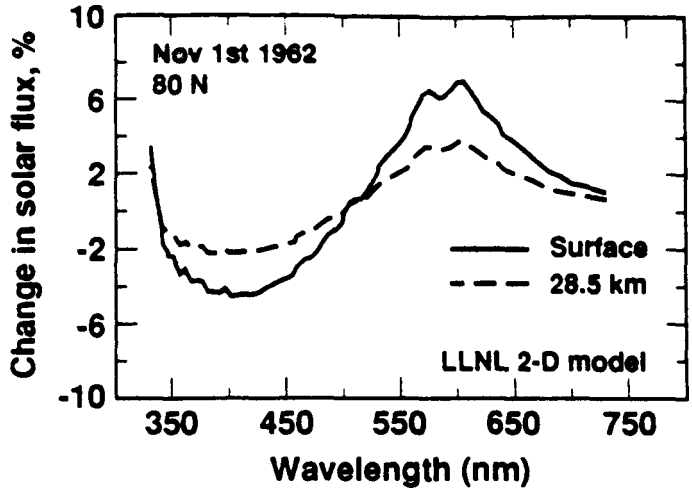

Figure 5.27. Percent change in Direct Solar Flux due to excess NO_2 produced by the nuclear test series.

Table 5.5 Percent change in yearly averaged column O_3 for global, northern, or southern hemispherically averaged trends.

Period	Scenario	Global Average	NH Average	SH Average
1970–1980	T	−0.27	−0.40	−0.13
1970–1980	T + S	+0.12	−0.02	+0.26
1970–1986	T	−0.46	−0.66	−0.25
1970–1986	T + S	−1.78	−1.93	−1.60
1979–1986	T	−0.22	−0.31	−0.13
1979–1986	T + S	−1.98	−2.01	−1.94

T = Trace gas only
T + S = Trace gas and solar variability

The LLNL two-dimensional model calculates a 3–8 percent change, depending on latitude.

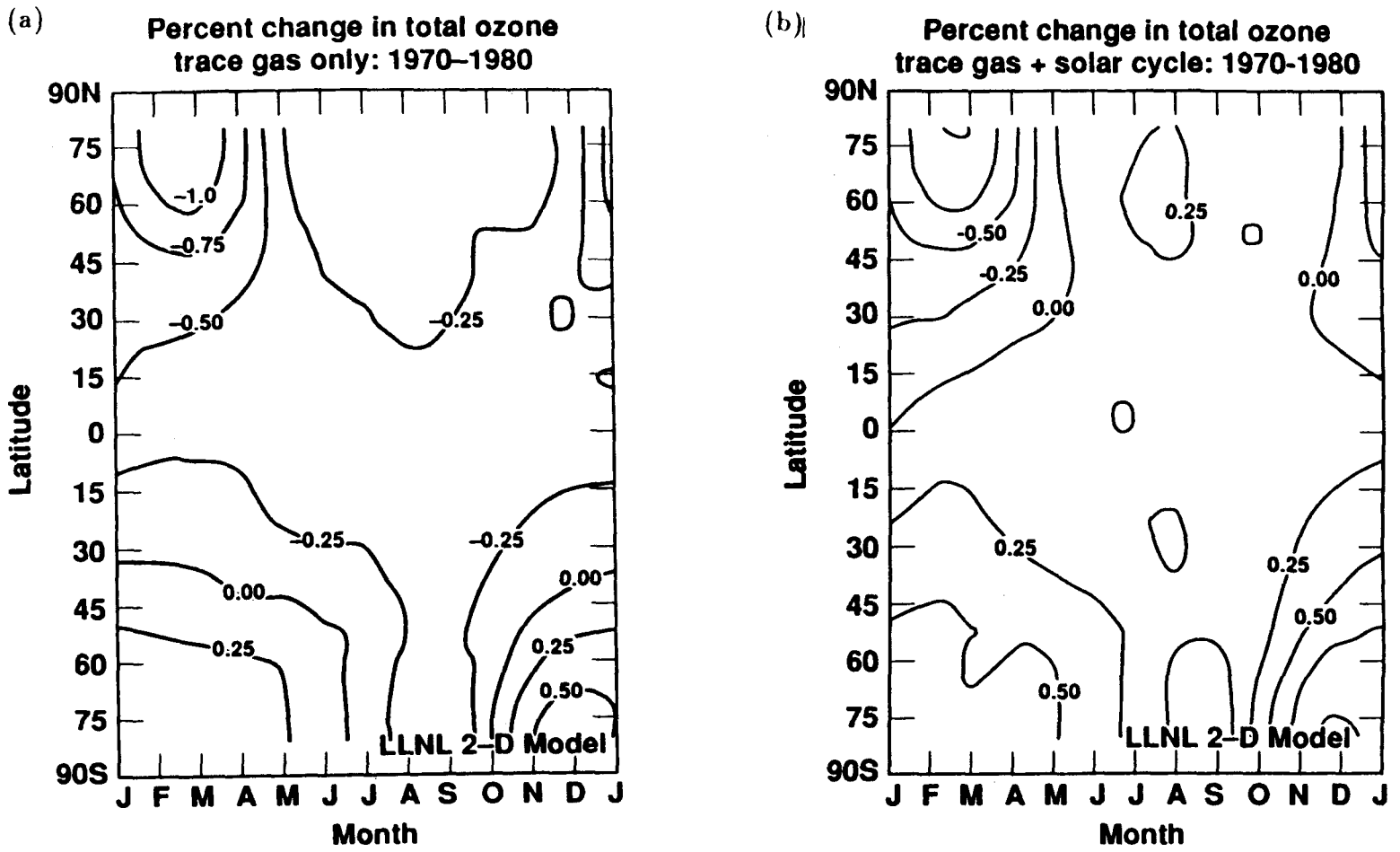

Figure 5.28. Percent change in total O_3, between 1970-1980, for scenarios, (a) trace gas only, and (b) trace gas plus solar variability.

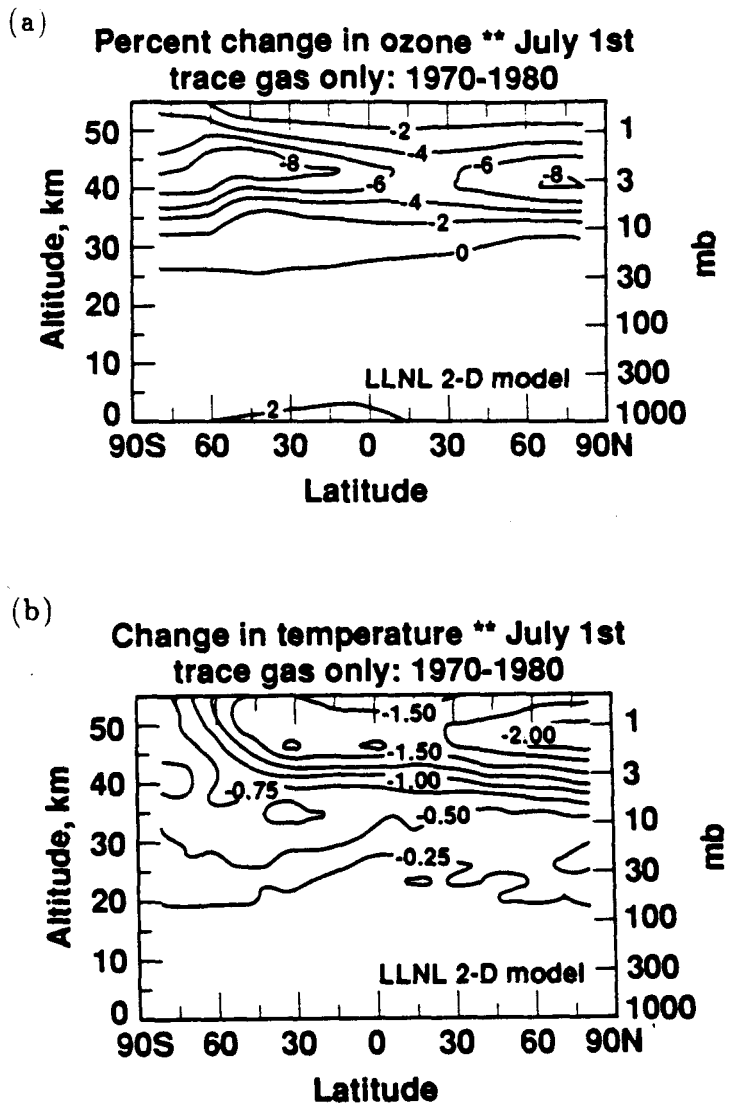

Figure 5.29. Trace gas only scenario, between 1970–1980, on July 1st, for, (a) percent change in O_3, and (b) change in temperature (K).

The corresponding temperature change for the model, during this period, is shown in Figure 5.30-b. The maximum effect (-1.75 K) occurs between 45–50 km, at high latitude in the northern hemisphere. Angell [1982] analyzed rocketsonde data and observed a temperature change of; -1.5 to -3.0 K, between 26–35 km: -2.5 to -3.5 K, between 38–45 km; and -3.5 to -5.0 K, between 48–55 km. The

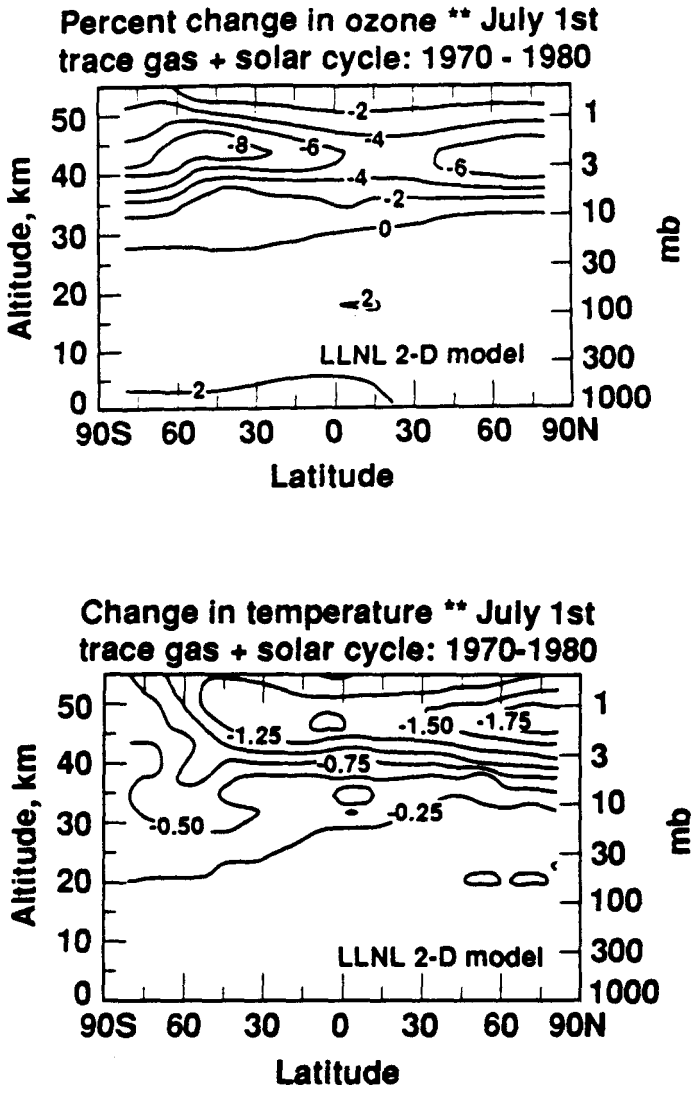

Figure 5.30. Trace gas plus solar variability scenario, between 1970–1980, on July 1st, for, (a) percent change in O_3, and (b) change in temperature (K).

disagreement between calculated and observed temperature trend during 1970 to 1980 is unresolved [Wang et al., 1986].

5.4.3 Trends between 1970–1986

In Figure 5.31, the percent change in column ozone is shown for the period between 1970 to 1986. The additional six years (see Figure 5.28-b), exhibit a much larger trend than during the decade of the 1970's. The mid-latitude trend in the

northern hemisphere is −3.0 percent, three time as large (see Figure 5.31-b) as that observed during 1970–1980. Figures 5.31-a and 5.31-b (trace gas only and trace gas plus solar variability respectively) are very different, unlike Figures 5.28-a and 5.28-b. This difference is due to the minimum in sunspot activity in 1986. Recent analysis by Harris et al. see NASA-WMO, 1989], investigated this time period, using the method of time series analysis, and found significant decreases in the northern hemisphere (Figure 5.32). They observed a large seasonal difference that the model does not produce. For example, in the latitude zone between 53° and 64° N, they see a -6.2 ± 1.5 and -0.4 ± 0.8 winter and summer average decrease respectively in O_3 between 1969–1986. The two-dimensional model, in this latitude band, calculates approximately −3.5 and −1.5 for winter and summer seasons respectively. This may be a signature that the model is either not sensitive enough to the inputed trace gases, or other process (i.e., heterogenous chemistry) are reducing O_3.

The percent local ozone change for July 1st in Figures 5.33-a and 5.34-a, show large decreases in local O_3 between 40–45 km (−14 and −16 maximum for Figures 5.33-a and 5.34-b respectively). The solar variability effect on ozone amounts to approximately 2 percent down to 20 km and the reduction in O_3 due the solar cycle is constant across latitude. In Table 5.5, the solar variability effect on total O_3 can be obtained by subtracting out the trace gas only from the trace gas plus solar variability rows. In all cases, the change due to the addition of solar variability, is constant across latitude (approximately 1.3 percent for 1970–1986). The solar variability fingerprint on O_3 is different from the Cl_y fingerprint, in that, odd chlorine tends to decrease O_3 predominately between 35–45 km and shows a larger effect at high latitudes. These differences should aid future investigators on trends in O_3 due to multiple effects.

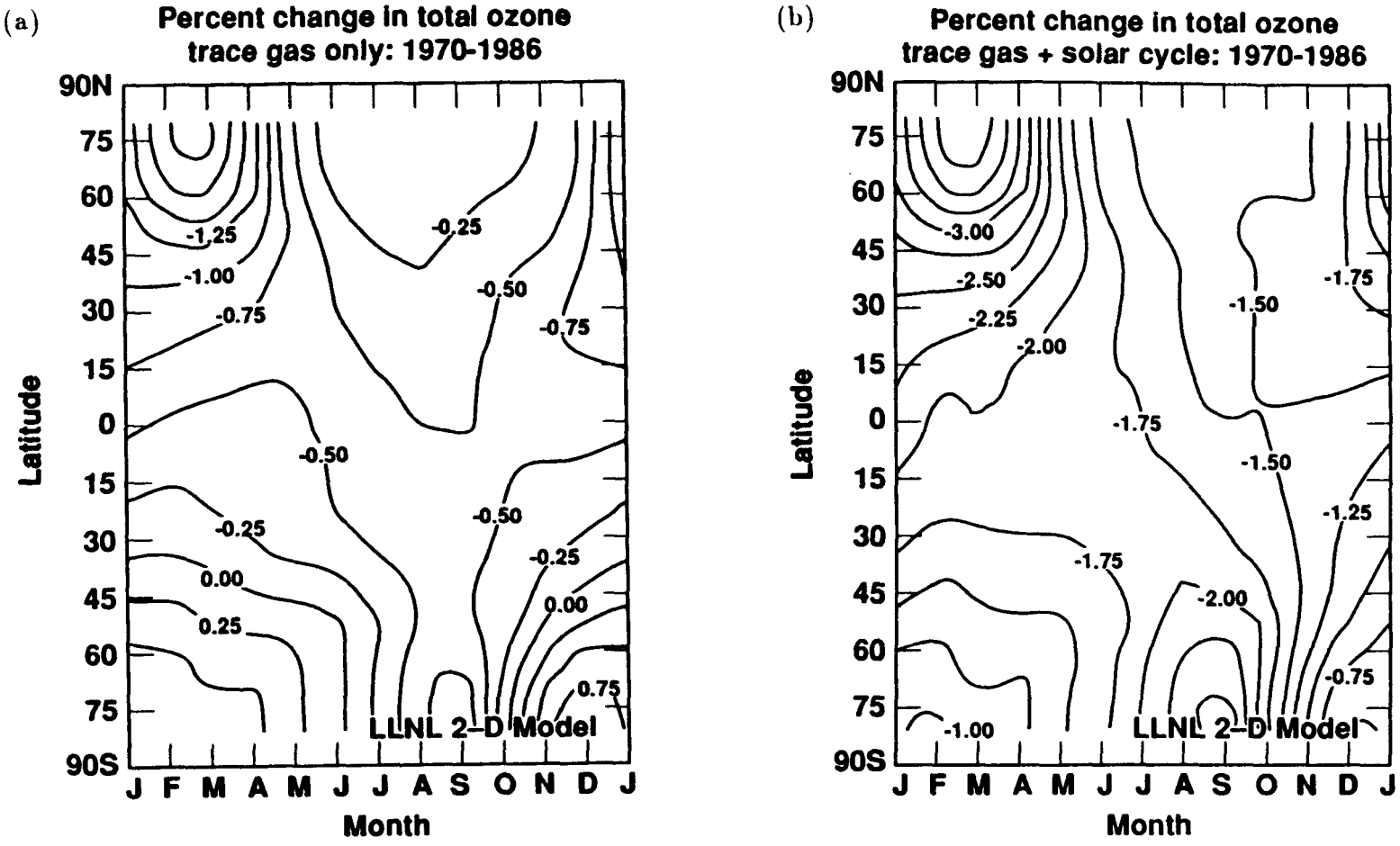

Figure 5.31. Percent change in total O_3, between 1970-1986, for scenarios, (a) trace gas only, and (b) trace gas plus solar variability.

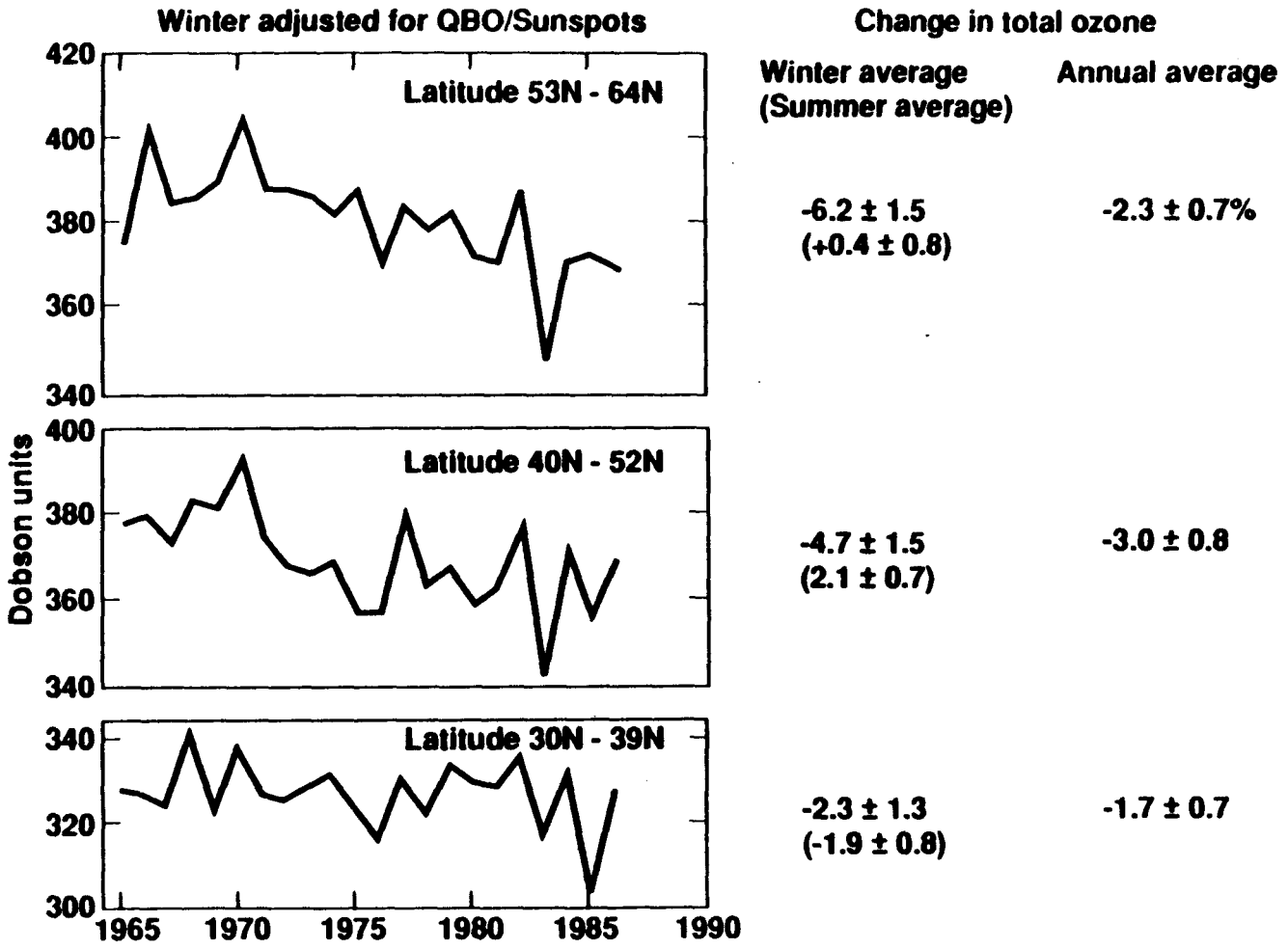

Figure 5.32. Winter-Spring O_3 concentrations for three latitude bands in the northern hemisphere (December, January, February, March). The calculated statistical contribution from the QBO and the solar sunspot cycle have been removed from the data. Plot taken from NASA-WMO [1988].

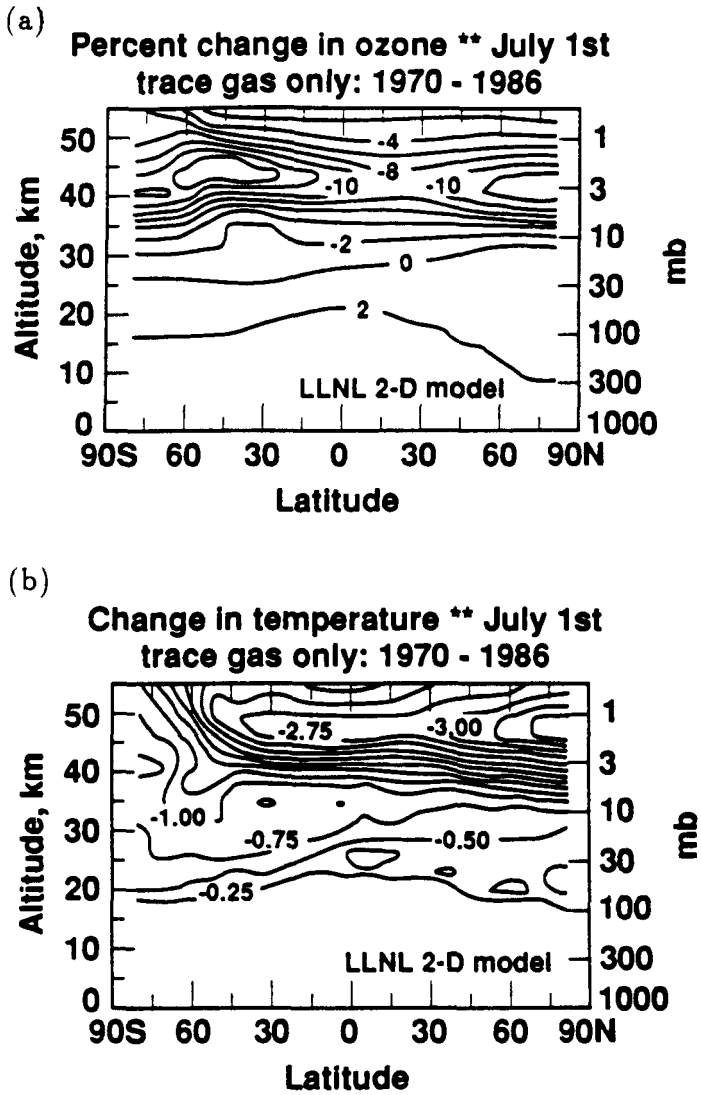

Figure 5.33. Trace gas only scenario, between 1970–1986, on July 1st, for, (a) percent change in O_3, and (b) change in temperature (K).

5.4.4 Trends between 1979–1986

In Figure 5.35, percent change in total O_3 for the time period 1979–1986 is shown. Here, the effect of solar variability is very apparent. The trace gas effect on O_3 between 1979–1986 is comparable to the period 1970–1980 (Figure 5.28-a). This trend can also be seen in Figure 5.18, where the global averaged "trace gas only" trend is decreasing more rapidly than in the 1970's. Reinsel et al. [1987].

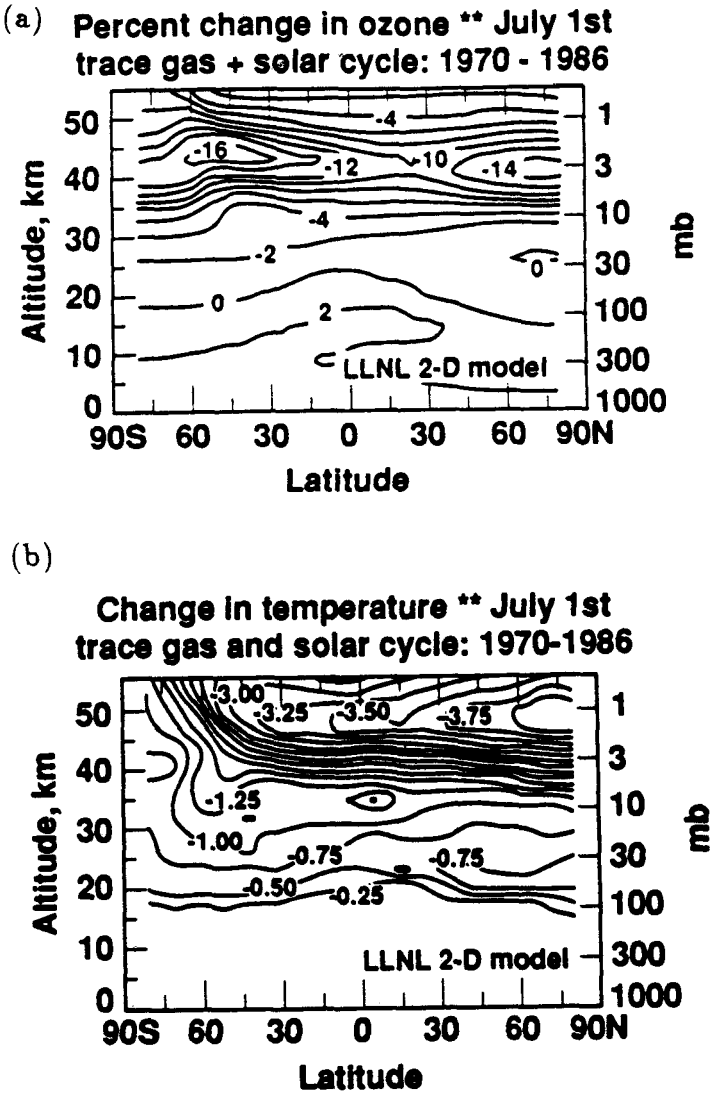

Figure 5.34. Trace gas only plus solar variability scenario, between 1970–1986, on July 1st, for, (a) percent change in O_3, and (b) change in temperature (K).

anaylzed 35 Dobson stations and estimated a global trend between November 1978 through December 1985, of -0.34 ± 0.28 percent per year (-2.4 percent per seven years). In Table 5.5, the LLNL two-dimensional model calculates a northern hemispherical average decrease of 2.0 percent during this same time period. In 1985, data were released from instruments on the Nimbus 7 (Solar Backscatter Ultraviolet (SBUV) and Total Ozone Mapping Spectrometer (TOMS)) satellite that

depicted large decreases in O_3. Due to instrument degradation of the diffuser plate which is used to calibrate the detectors, the data cannot be used alone to derive trends in O_3. Therefore, the TOMS satellite data were normalized by comparison with coincident ground-based Dobson measurements in the northern hemisphere. For a complete description of the uncertainties in spacecraft instrument calibration and stability, see NASA-WMO '1989'. In Figure 5.36 and Table 5.6, percent change in total O_3 is shown for the TOMS data set, normalized to the Dobson network. The percent change in O_3 averaged between 53° S and 53° N latitudes, show a decrease of about 2 to 3 percent from October 1978 to October 1985. The model calculates in the same latitude zone a 2 percent decrease over this time period (Figure 5.35-b). Since the two-dimensional model study presented here did not include calculations predicting the loss in O_3 due to the Antarctic Hole, comparison with observation are not very meaningful at high southern latitudes.

In Figures 5.37 and 5.38, the percent change in O_3 and the temperature change in the 1979 to 1986 time period are shown. The change of -8 percent by the model at 40 km can be compared to both Satellite and Umkehr measurements. In 1985, SBUV data was released and showed a 20 to 24 percent decrease (45 km) between 1979 and 1986. This is three times the magnitude predicted by the model. With indepth reanalysis [NASA-WMO, 1989], it was concluded that a trend determined from these data is unreliable. In Figure 5.39, the percent change in O_3 calculated by the LLNL two-dimensional model (at 42.5° N), is shown along with recent reanalysis of the Umkehr data by DeLuisi et al. [1988] (northern mid-latitudes). The percent change in O_3 measured by the Umkehr technique is -9 percent at 40 km. The change in O_3 calculated by the two-dimensional model at 40 km is between -8 and -9 percent. This data was corrected for aerosol contamination from the El Chichon eruption by ozonesonde observations

Table 5.6 Percent change in total column O_3. Measured by TOMS on Nimbus 7 satellite. Data was calibrated by comparison with ground-based measurements. Taken from NASA-WMO [1989].

Latitude Band	Total Change 11/1978 to 10/1985	(1969–1986)	Total Change 11/1978 to 11/1987
Global, except high latitudes			
53° S–53° N	-2.6 ± 0.5		-2.5 ± 0.6
Hemispheric			
0–53° S	-2.6 ± 0.9		-2.9 ± 0.9
0–53° N	-2.1 ± 1.5		-1.8 ± 1.4
Bands			
53° S–65° S	-9.0 ± 1.8		-10.6 ± 1.6
39° S–53° S	-5.0 ± 1.8		-4.9 ± 1.8
29° S–39° S	-3.2 ± 2.4		-2.7 ± 2.1
19° S–29° S	-2.5 ± 1.9		-2.6 ± 1.5
0–19° S	-1.1 ± 0.8		-2.1 ± 0.8
0–19° N	-1.1 ± 1.5		-1.6 ± 1.3
19° N–29° N	-3.5 ± 2.2		-3.1 ± 1.9
29° N–39° N	-3.7 ± 2.0	-1.7 ± 0.7	-2.5 ± 1.7
39° N–53° N	-2.7 ± 1.7	-3.0 ± 0.8	-1.2 ± 1.5
53° N–65° N	-2.4 ± 1.6	-2.3 ± 0.7	-1.4 ± 1.4

(Linear trends with an autoregressive model through TOMS data, with uncertainties at the one sigma level of significance.)

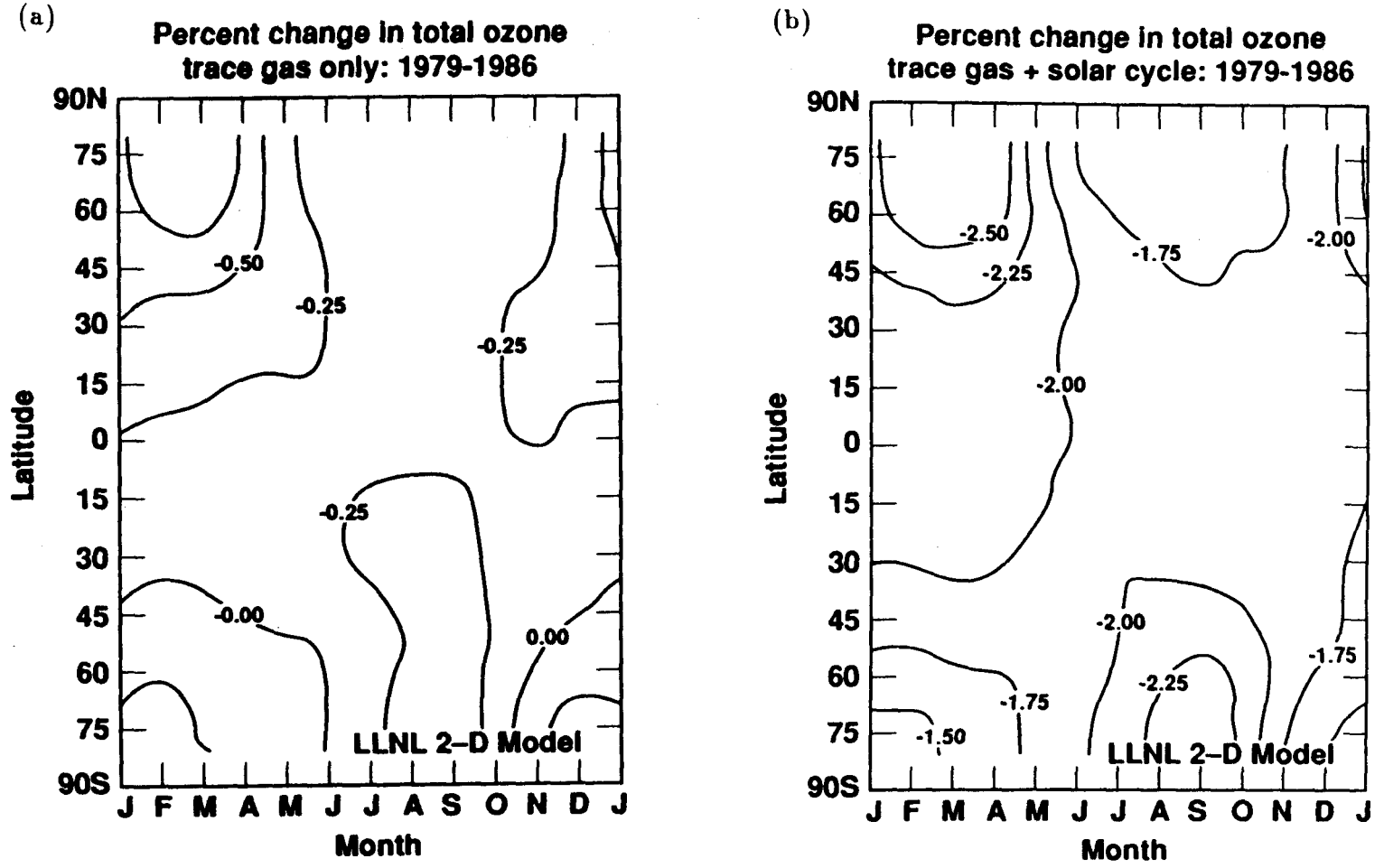

Figure 5.35. Percent change in total O_3, between 1979-1986, for scenarios, (a) trace gas only, and (b) trace gas plus solar variability.

and observations provided by five lidar stations in the northern hemsphere middle-latitudes. In Figure 5.40, the Stratospheric Aerosol and Gas Experiment (SAGE) I and II visible spectrometers are used to obtain a trend in local O_3 during this time period. SAGE I collected data between February 1979 and December 1981, and SAGE II collected data between November 1984 and September 1987. By use of careful statistical sampling techniques, the measured decrease in O_3 between 1979 and 1985, is 3 percent at 40 km. An interesting feature of the SAGE data set, is the 3 to 4 percent decrease in O_3 at low altitudes (25 km). The model does not reproduce this feature. It is possible that there exists an addition mechanism at this altitude not represented in current LLNL two-dimensional models.

In Figure 5.41, temperature change measurements are displayed for satellite, radiosonde, and rocketsonde between 1979 and 1986. The trend between 45 and 55 km, deduced from the intercomparison of the data in Figure 5.40 [see NASA-WMO, 1989] is -1.75 K, which would be consistent with a change in O_3 of less than 10 percent. This corresponds with the maximum temperature change of -2.75 K calculated by the LLNL two-dimensional model (Figure 5.38-b). The change in local temperature at 40 km is due to three processes in the model: solar variability, the ClC reduction of O_3, and CO_2 infrared cooling. The solar variability contribution can be obtained by subtracting Figure 5.38-b from Figure 5.37-b, which is about 1.25° K at northern latitudes for July 1st. This leaves 1.25° K due the summation of both ClC's and CO_2 effect. It would be interesting in the future to run a scenario with CO_2 fixed, in order to obtain all three contributions to the calculated cooling.

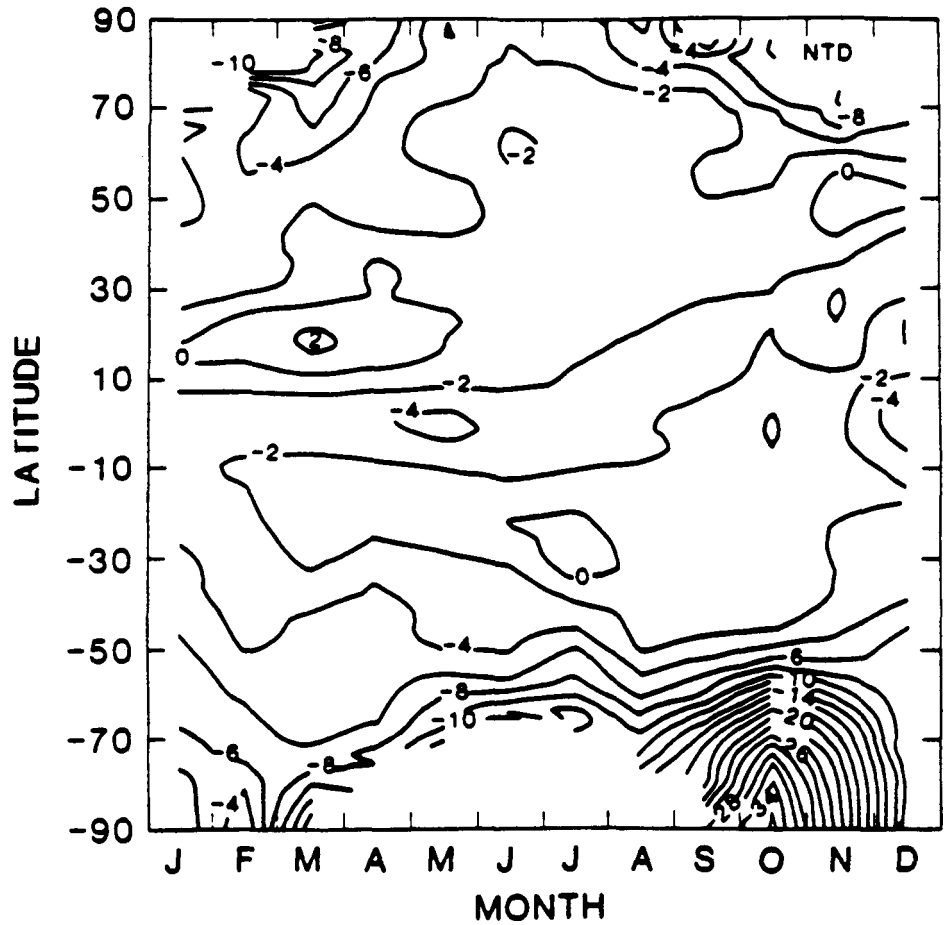

Figure 5.36. Change in total O_3, between 1979/1980 and 1986/1987 as measured with TOMS on the Nimbus 7 satellite. The TOMS data have been normalized to the Dobson (NTD) ground-based network. The TOMS instrument operates with sunlight scattered from the atmosphere and therefore provides no data from the areas in the polar night. Taken from NASA-WMO [1989].

5.4.5 Trends between 1986–1990

For the period of 1986–1990, the LLNL two-dimensional model calculates a increase in total O_3 of 1.5 to 2.0 percent (Figure 5.42). This corresponds to a local O_3 change of −2.0 percent between 20 and 30 km (Figure 5.43). At higher altitudes the effect due to Cl_y chemistry reduces O_3 by 1 percent. Column O_3 increases because the solar sunspot cycle is starting in a minimum (1986) and proceeding to a maximum (1990) during this time period. This is partially seen in

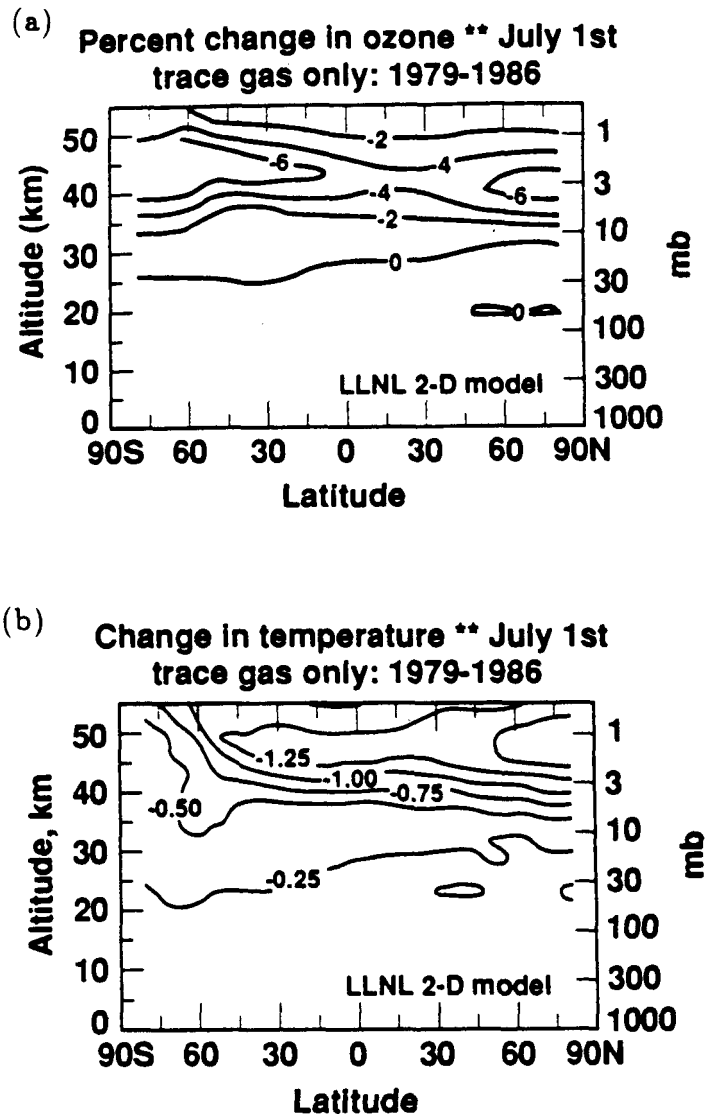

Figure 5.37. Trace gas only scenario, between 1979–1986, on July 1st, for, (a) percent change in O_3, and (b) change in temperature (K).

the analysis of Harris et al. [NASA-WMO, 1989], Table 5.6, for data collected up to November 1987. For example, the 53–65° N band shows a -2.4 ± 1.6 percent change in O_3 between 1979 and 1986, and the same band shows a -1.4 ± 1.4 change between 1979–1988.

Solar variability based on the 10.7 cm radio flux, has been analyzed for 4 cycles, dating back to 1946 [Lean, 1987]. In general the solar variability follows a sine function, however, deviations do occur. For example, the rise from solar

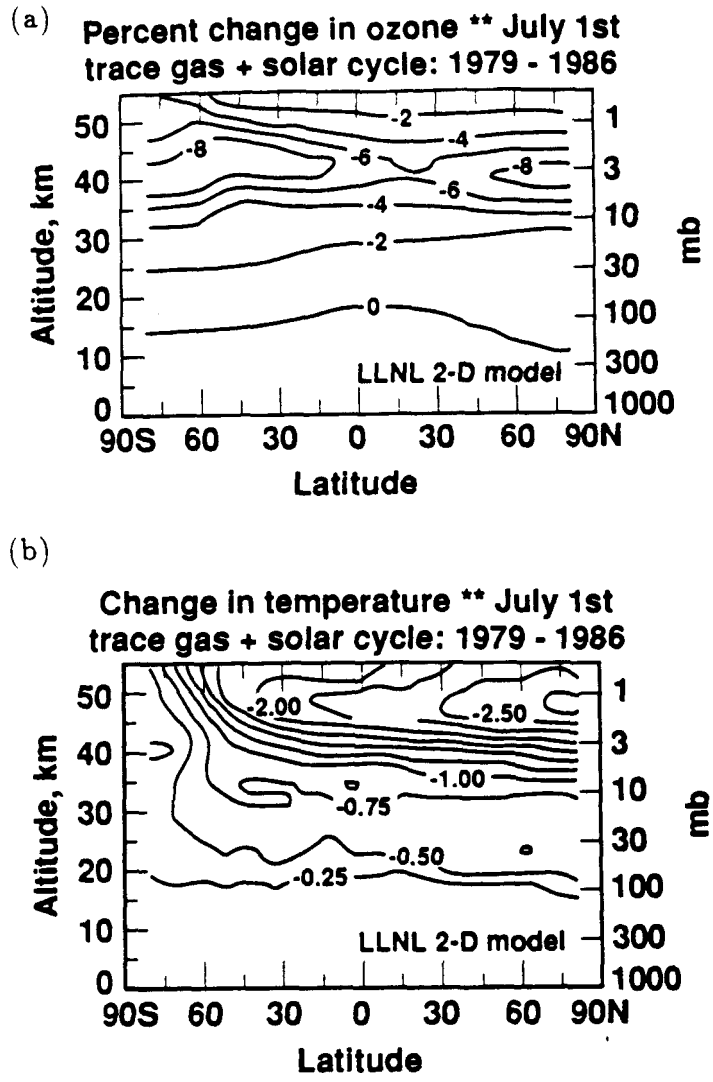

Figure 5.38. Trace gas plus solar variability scenario, between 1979–1986, on July 1st, for, (a) percent change in O_3, and (b) change in temperature (K).

minimum to solar maximum is sharper in the observed data than that given by a sine function. This will have two effects on comparisons made between that calculated by the LLNL two-dimensional model and observational measurements. First, the total column O_3 will increase faster for observational measurements relative to the model derived ozone-column amounts. Second, the change in local O_3 between 40–50 km calculated by the model will show a larger decrease, since the model will underestimate the production of O_3 due to the solar cycle.

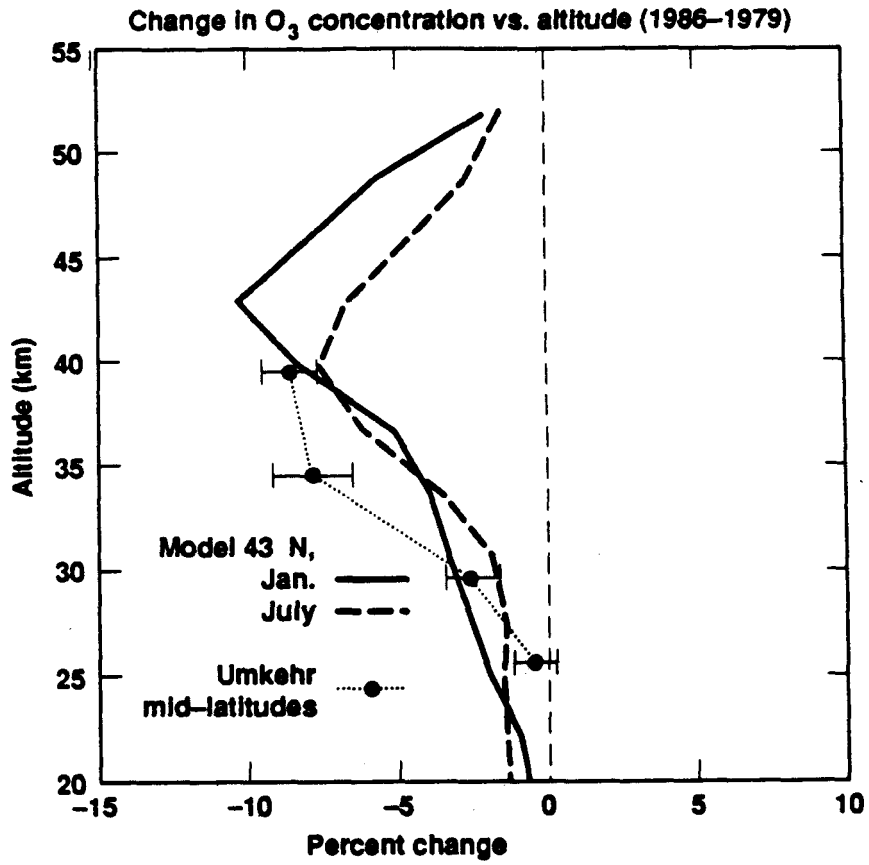

Figure 5.39. Change in the mid-latitude O_3 profiles from 1979 to 1986, for Umkehr data, taken from DiLuisi et al. [1988], and the LLNL two-dimensional model for January and July 1st at 42.5° N.

5.5 Summary and Conclusion

In modeling past or future trends, it is important to consider how well the model represents the present atmosphere. The following atmospheric constituents were compared to observational data: O_3, N_2O, CH_4, NO_y, HNO_3, Cl_y, and HCl. A summary of some of the comparisons are:

1) Column ozone calculated by the model does not show the maximum between 50° S and 60° S in the southern hemisphere spring season. The northern hemisphere maximum calculated by the model is 400 Dobson

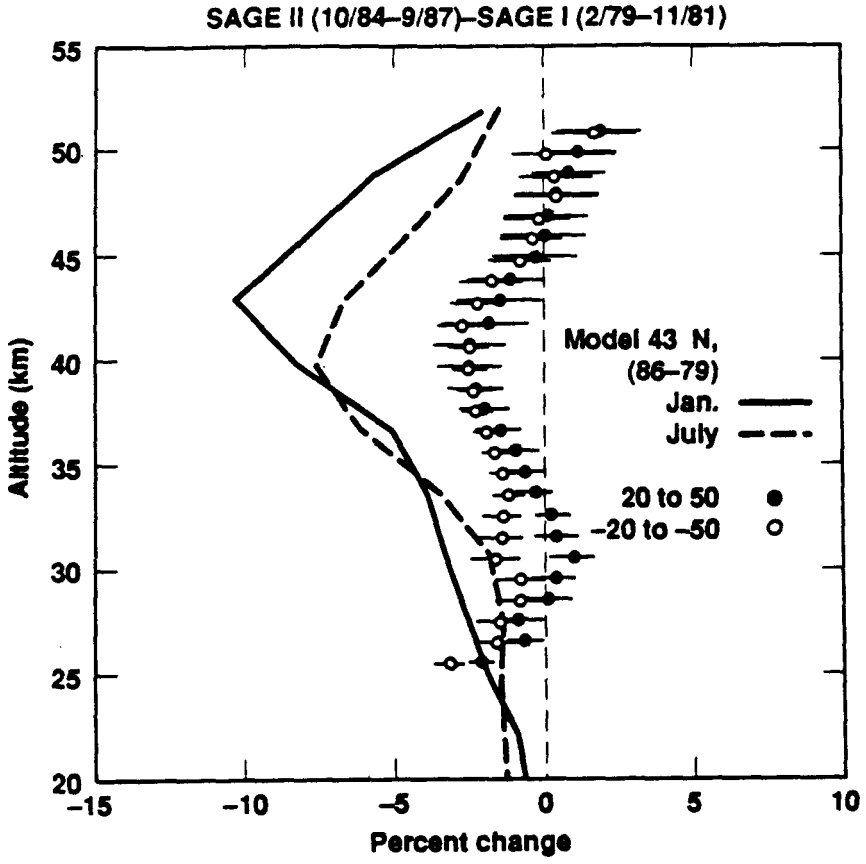

Figure 5.40. Mean percentage difference between SAGE II and SAGE I (SAGE I is the reference). All intersections occuring between 20° N and 50° N (or 20° S to 50° S) were combined into one sample (Taken from NASA-WMO [1989]). The horizontal bars are the standard errors of the sample of percentage differences. The LLNL two-dimensional model is also shown for January and July 1st at 42.5° N.

units (using case A eddy diffusion representation, Chapter 6). Observed (Dobson network and SAMS) measurements show 440 Dobson Units for the northern hemispherical maximum.

2) Local ozone mixing ratio calculated by the model at mid-latitudes (January) peaks at the same altitude as observed measurement taken by SBUV (4 year average). The magnitudes of the local ozone mixing ratio are 11 and 10 ppmv for SBUV and that calculated by the model, respectively.

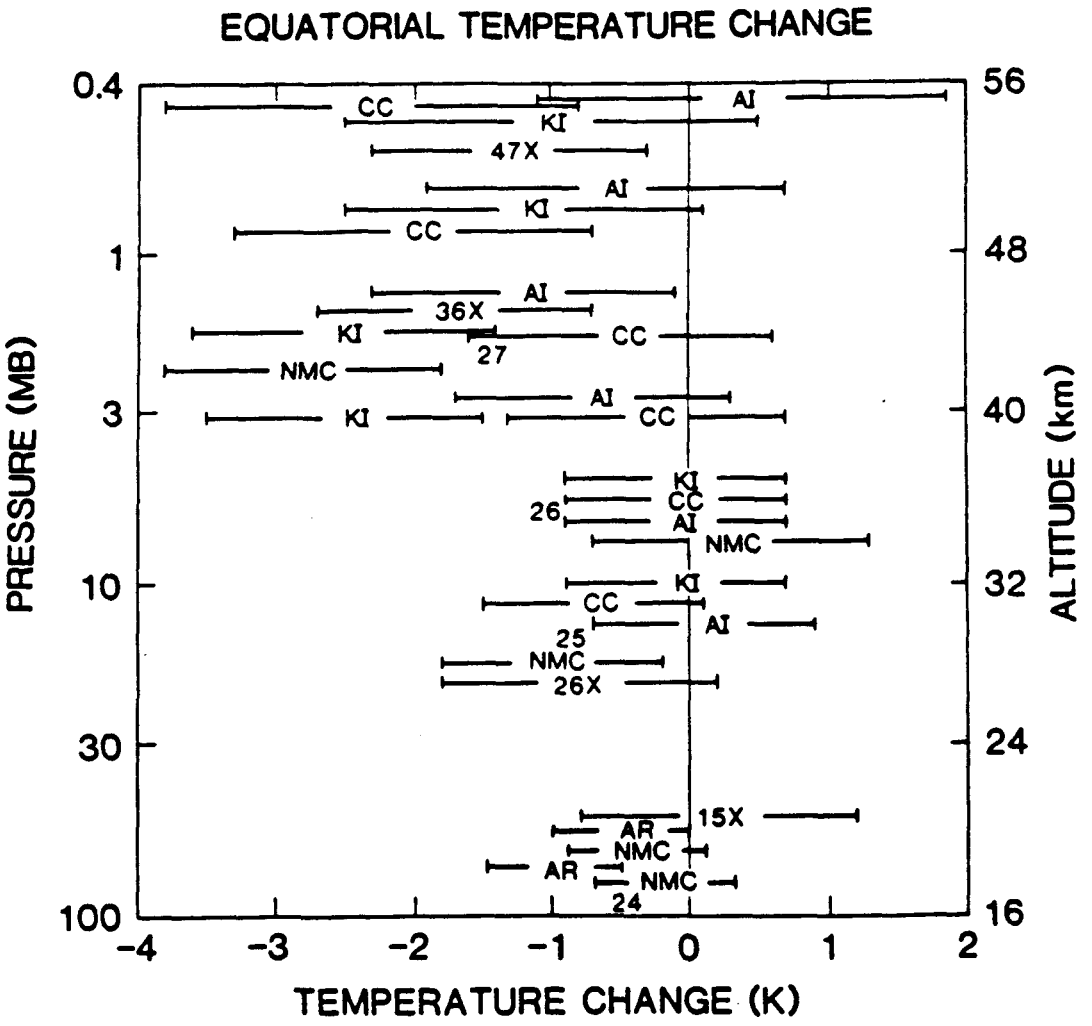

Figure 5.41. Temperature differences between 1979/1980 and 1985/1986 from 30° N to 30° S, where: NMC indicates National Meteorological Center data; AR is Angell and Korshover's radiosonde analysis; AI is Ascension Island rocket data; CC is Cape Canaveral; KI is Kwajelein. Taken from NASA-WMO [1989].

3) Measurement of N_2O by SAMS at 30 km are higher (300 ppbv) than that calculated by the model (200 ppbv). Between 45 and 50 km, observed measurements of N_2O and that calculated by the model are 20 ppbv.

4) The difference between observed CH_4 mixing ratios (SAMS) and that calculated by the model, differ no more than 0.1–0.2 ppmv between 30–55 km in the equatorial region. The transition region between the troposphere and stratosphere at mid-latitudes show large differences between observed

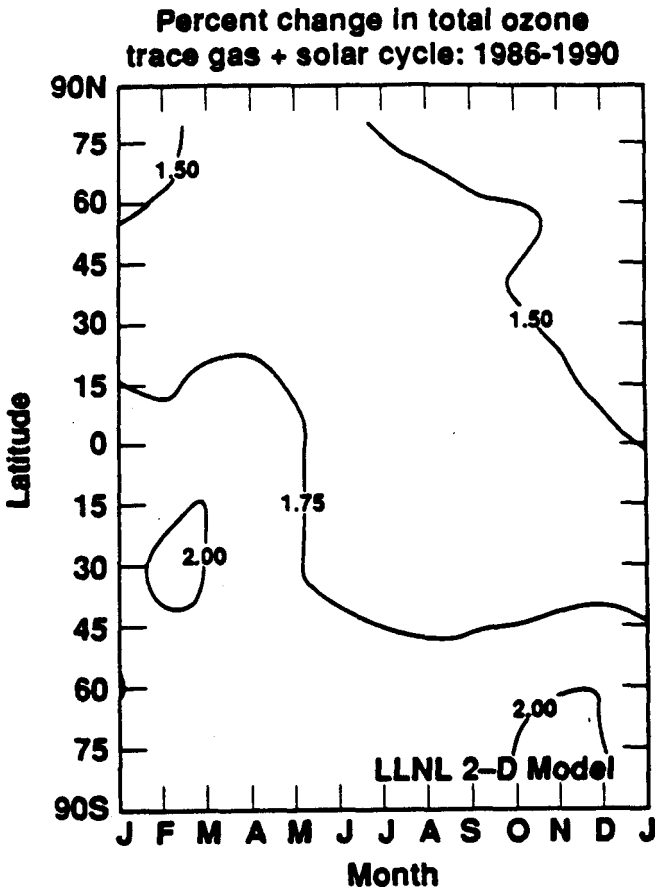

Figure 5.42. Percent change in total O_3, between 1986–1990, for trace gas plus solar variability scenario.

and calculated CH_4 values. *In situ* measurements at mid-latitudes observe a smaller mixing ratio than that calculated by the model above 23 km (maximum difference is .3–.4 ppmv).

5) NO_y observed measurements (LIMS) for 3 pressure regions, 3 (40 km), 16 (29 km), and 30 (24 km) mb were compared to the LLNL two-dimensional model. At 3 mb, NO_y calculated by the model is larger than observed data (about 3 ppbv). At 16 mb, the NO_y mixing ratio calculated by the model is lower than that observed by LIMS (1–5 ppbv). At 30 mb, there is good agreement between the model and LIMS (approximately 1 ppbv average difference across latitude zones).

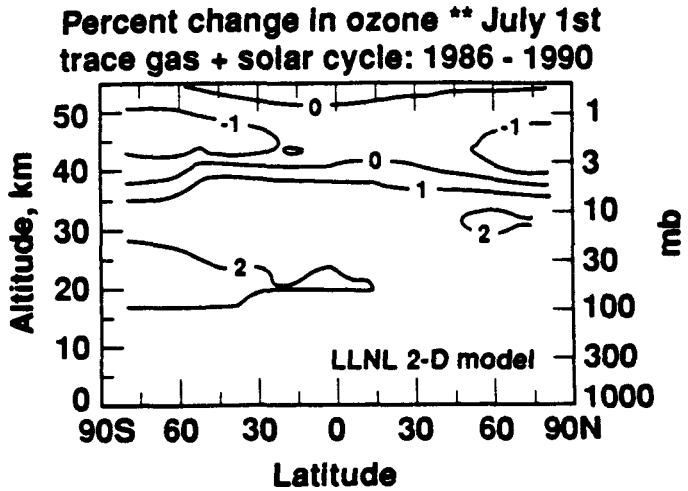

Figure 5.43. Percent change in O_3, between 1986–1990, for trace gas plus solar variability scenario.

6) The model calculated HNO_3 at northern mid-latitudes and that observed by LIMS and in situ measurements are in agreement between 10 and 35 km. Above 35 km, LIMS observes a lower mixing ratio of HNO_3 than that calculated by the model.

7) Cl_y calculated by the model at the top of the atmosphere is between 2.5 and 2.6 ppbv for July 1, 1985. Observed measurements of Cly from *in situ* data analyzed by Berg et al. [1980], at 20 km, range between 2.7 $\pm$ 0.9 and 3.2 $\pm$ 0.7 ppbv. Gallagher et al. [1985], from *in situ* measurements, observed the total chlorine mixing ratio to be 2.6 ppbv at 15 km, decreasing to 2.2–2.5 ppbv for higher altitudes.

8) HCl calculated by the model for July 1985 at 30° N is within the range of in situ data (between 20–50 km). The trend in column HCl is 2–3 percent per year. Recent, but not conclusive ground based measurements suggest a 10 percent increase annually.

The nuclear test series of the late 1950's and early 1960's was reinvestigated using the LLNL two-dimensional model. The northern hemispheric average real time value of 4.3 and 3.5 percent decrease for Peterson [1970] and Seitz [1968] bomb stabilization cloud heights compare reasonably well to Reinsel's [1981] value of a 2–4.5 percent decrease based on analysis of ozone measurements. For the band analysis of Harris et al. [NASA-WMO, 1989], the model overestimates the effect due the nuclear test series. If individual stations are considered (instead of the band approach), the model compares more closely, especially at higher latitude stations (northern hemisphere).

The percent decrease in local O_3 peaked in November of 1962 due to the nuclear test series. There was a secondary maximum local O_3 observed in 1963, a few months after the last test. The NO_x at high latitudes during the winter was converted to HNO_3 and N_2O_5 (which have long lifetimes due to low ultraviolet solar flux during this season at high latitudes), later (spring of 1963) releasing NO and NO_2, which catalytically reduced ozone.

The trends in total O_3 during the 1970's, from ground based Dobson stations (using time series analysis), agree well with the model calculated trend. The temperature profile during this period is measured to be higher (depending on altitude) than model calculations would suggest. Local O_3 was measured to have changed between 3–5 percent (depending on study) at 40 km; the model gives for the same altitude a 3–8 percent change depending on latitude.

The model calculates a much larger change in both local and column ozone between 1970 and 1986 than between 1970 and 1980. This is due primarily to the solar sunspot cycle going from maximum in 1979 to minimum value in 1986. Comparison of model trends to that of Harris et al. [NASA-WMO, 1989], show surprising seasonal differences. Analysis of the Dobson network indicate a 6.2 $\pm$

1.5 winter average percent decrease in total O_3, with a 0.4 ± 0.8 percent increase for a summer averaged trend. The model does not show as large or pronounced seasonal effect.

The trend between 1979 and 1986 for local O_3 compares best with the reanalyzed Umkehr data Deluisi et al. [1988]. The trend derived from the SAGE data is smaller at 40 km than the model and larger at 20–25 km than the model. It is possible that the decrease observed between 20–25 km may be a signature of missing processes in the model. The differences at 40 km are unresolved. Column O_3 trends calculated by the model is -2 percent during this time period. Reinsel [1987], using the Dobson network data calculated a -2.4 percent decrease during the same period.

Future prediction by the model suggest an increase from 1986 to 1990 in total ozone, with a decrease of -1.0 percent at 40 km and and increase of approximately 2 percent below 30 km. The decrease is due to odd chlorine, released from ClC photolysis, and the increase is attributed specifically to the solar sunspot cycle, going from a minimum in 1986 to a maximum in 1990.

Chapter 6: Tracer Study

6.1 Introduction

In modeling the global atmosphere, the distribution of species can in a few limiting cases, be compared to tracers from observational analysis. A tracer is typically a atom or molecule that has a relatively long atmospheric lifetime and preferably does not interact chemically or photochemically in the region of interest (e.g., the stratosphere). Observing the distribution of tracers at given latitudes, altitudes, and times helps clarify the understanding of transport process in the global atmosphere. Tracers are also useful in two-dimensional models for verifying existing transport representation and/or provided means for making improvements.

Atmospheric nuclear explosions create tracers, like carbon-14 and strontium-90, that are useful because they are chemically and photochemically inert in the stratosphere and can be monitored relatively easily by aircraft and balloon sondes. In addition, the background concentration of these nuclear tracers are low, allowing easy detection over long periods of time [Johnston et al., 1976]. The primary purpose of this study is to help clarify the understanding of transport in the LLNL two-dimensional chemical-radiative-transport model using recently reanalyzed carbon-14 and strontium-90 data from the nuclear test series in the late 1950's and early 1960's. A secondary purpose is to clarify understanding of the nuclear tests and their production of those tracers spacially.

The objectives in this study, are four-fold. First, to compare the LLNL two-dimensional models transport with tracer transport information from recent reanalysis of carbon-14 and strontium-90 data [Johnston, 1989, in press]. These data are from the nuclear test series of the late 1950's and early 1960's. Here various

K_{yy} and K_{zz} values, as a function of latitude and altitude, were used to see what values best represented or corresponded with short and long term transport of the above two tracers. Second, the model was used to help verify which of the two available estimates for bomb stabilization cloud height, Seitz [1968] or Peterson [1970], bests represents the available data. Third, the effect of varying the eddy transport based on the first objective is examined in terms of the effects on the model-calculated change in the eddy transport O_3 column distribution. Fourth, the effect of K_{zz} on the sensitivity of aircraft injections at 20 km is examined. In a sense these studies provide verification and refinement of the treatment of transport processes in the two-dimensional model. At the same time, this study improves our understanding of nuclear explosions in the global atmosphere.

6.2 Tracer Transport in Two-Dimensional Models

Currently there is no fully satisfactory way to have a fully self-consistent interactive two-dimensional model, largely because adequate evaluation of the eddy terms have not been sufficiently developed [WMO, 1985]. The current approach in modeling eddies is to assume that they are diffusive in nature. Physically this process may not be correct for all transient occurences, but mechanistically it generates species distributions that are consistent with observational data [Harwood and Pyle, 1980; Holton, 1981; Ko et al., 1985].

In the LLNL two-dimensional model the horizontal and vertical eddies are represented by the diffusion coefficients K_{yy} and K_{zz} respectively (see Chapter 2, Equation (7)). There have been several studies attempting to estimate the diffusion coefficients, K_{yy} and K_{zz}, both from satellite data and general circulation models. Kida [1983] derived global averaged K_{yy} and K_{zz} values from tracer dispersion studies using a General Circulation Model (GCM). His values were 3×10^9 cm^2 s^{-1} and 1×10^3 cm^2 s^{-1} in the stratosphere for K_{yy} and K_{zz} respectively.

Guthrie et al. [1984], used values of 2×10^9 cm^2 s^{-1} for K_{yy} and 2.0×10^4 cm^2 s^{-1} for K_{zz}, in their study of the distribution of trace gases N_2O, $CFCl_3$, and CF_2Cl_2. Ko et al. [1985], used the value of 3×10^9 cm^2 s^{-1} for K_{yy}, and found good results for many tracers. They found for HNO_3 specifically, that low latitude values are best fit with values close to 3×10^9 cm^2 s^{-1}. Plumb and Mahlman [1987], using a general circulation/tracer model, concluded for K_{yy}, that strong quasi-horizontal mixing in the middle lower troposphere should have a magnitude of 1×10^{10} cm^2 s^{-1}, and 2×10^{10} cm^2 s^{-1} across the tropical upper troposphere and the subtropical winter stratosphere. With values as high as 5×10^9 cm^2 s^{-1} outside the extra-tropical "surf zone" [McIntyre and Palmer, 1983] where primary wave breaking occurs in the stratosphere. For the vertical mixing, K_{zz}, they calculated values of 1×10^5 cm^2 s^{-1} in the troposphere at or near latitudes of the intertropical convergence zone, with mixing of 0.5×10^5 cm^2 s^{-1} through most of the troposphere. Newman et al. [1988], calculated horizontal diffusion coefficients using quasi-geostrophic potential vorticity data from the National Meteorological Center. Potential vorticity is a horizontally quasi-conserved quantity, which provides a good measure of the mixing associatied with eddies. They found that large-scale nongeostrophic winds yielded values for K_{yy} that were mostly positive, typically in excess of 1×10^{10} cm^2 s^{-1} in the middle to upper stratosphere during winter in the northern hemisphere. They also noted large K_{yy} values for the middle to upper stratosphere during spring in the southern hemisphere (however, weaker than the northern hemisphere by a factor of two). Smith et al. [1988], derived the K_{yy} component of the transport matrices for several months for O_3, HNO_3, and quasi-geostrophic potential vorticity. They compared the parameterized transports for these three species with the exact transport also computed from the Limb Interferometer Monitor of the Stratosphere (LIMS) data. They concluded that eddies can account for most of the observed ozone transport in early winter. The value

of the K_{yy} diffusion coefficient for O_3 is larger in mid-latitudes and smaller in the subtropics than the K_{yy} values of Plumb and Mahlman [1987] for mid-winter.

6.3 Method of Analysis

Carbon-14 was measured by balloon, U-2 aircraft, and ordinary aircraft during and after the nuclear test series of the late 1950's and early 1960's. The observed "excess" carbon-14 was measured from 1955 to 1967, approximately every three months, with more sporadic sampling between 1967 and 1971 [Telegadas, 1971; Telegadas et al., 1972]. These data were published in Health and Safety Laboratory (HASL) reports, for example volumns 243 [1971] and 246 [1972]. In these reports, the data were displayed in altitude versus latitude [e.g., see Figure 6.1, taken from Johnston, 1976], in units of 10^5 atoms of excess carbon-14 per gram of air (relative mixing ratio units). These units are proportional to mixing ratio. When multiplied by 4.82×10^{-18} they are mixing ratio by volume. There were typically four latitudes (70° N, 31° N, 9° N and 42° S) where carbon-14 measurements were taken. For November 1970, data was taken at five latitudes (65° N, 42° N, 30° N, 9° N, and 34° S).

Strontium-90 measurements were also published in HASL, for example volume 184 [1967], by Telegadas. The measurements were taken in the same manner as carbon-14. In Figure 6.2, the altitude versus latitude contour plot for strontium-90 is shown [also taken from Johnston et al., 1976]. The units (disintegrations per minute per 1000 ft^3 of standard air), are proportional to mixing ratio. In this study, the data for strontium-90 that will be used starts in October 1964 and ends in January 1967. The sample period was approximately every three months for four latitudes (64° N, 31° N, 9° N, and 34° S).

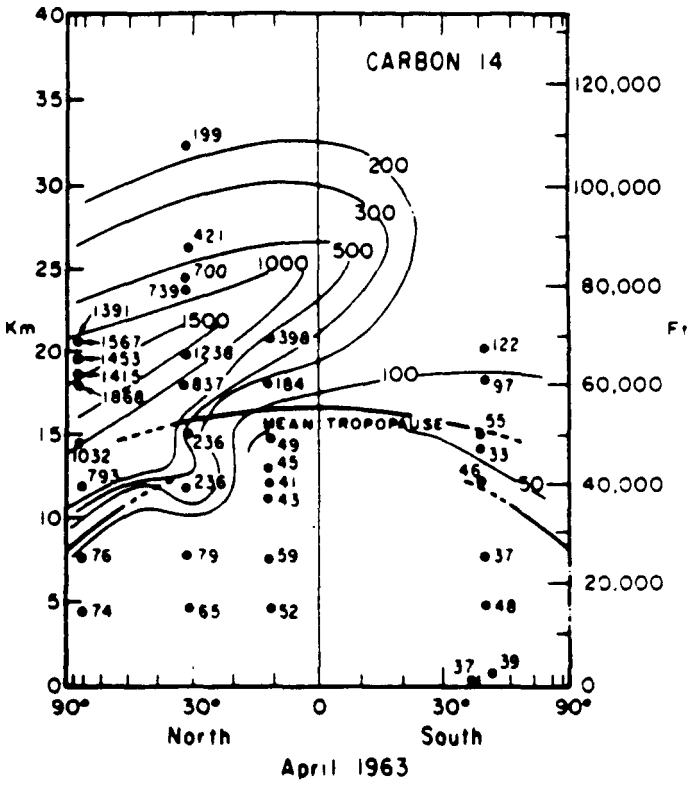

Figure 6.1. Relative mixing ratios of carbon-14 (10^5 atoms of excess carbon-14 per gram of air). The data were taken during the period March-May 1963 and are referred to as April 1963. Taken from Johnston et al. [1976].

The bulk residence time of carbon-14 in the stratosphere between 1963 and 1965 was shown by Johnston et al. [1973], to be twice as long for for carbon-14 compared to strontium-90. Johnston [1989], comments on the relative differences of carbon-14 and strontium-90. First, they are produced by two different mechanisms: strontium-90 by fission bombs only; and carbon-14 by neutrons colliding with nitrogen, which is produce by fission and fusion. The majority of the nuclear tests were of low megatonage, primarily fission nuclear devices, which had cloud tops that were less than 25 km on average [see Bauer, 1979]. The bomb cloud stabilization heights were based on analysis of both Peterson [1970] and Seitz [1968]

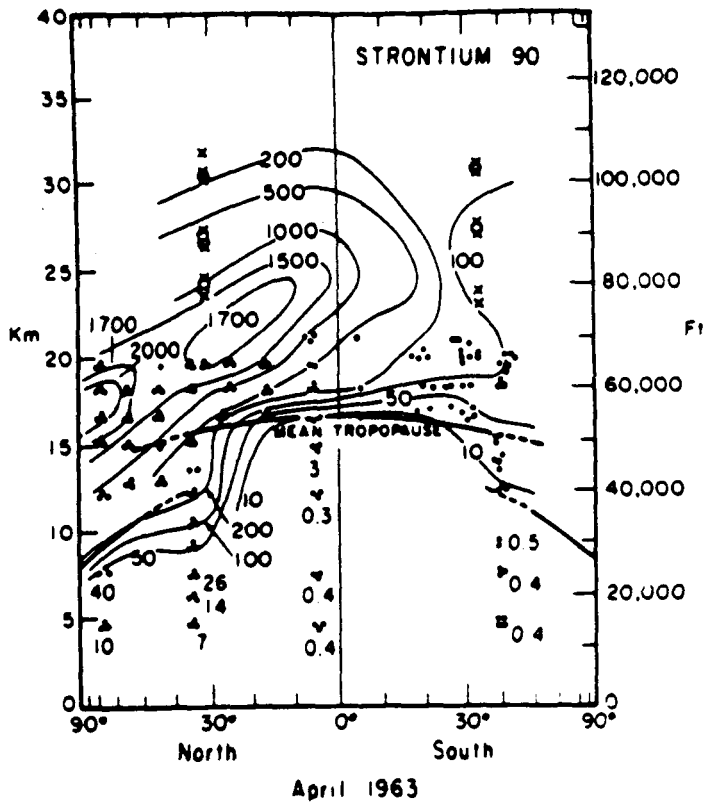

Figure 6.2. Relative mixing ratios of strontium-90 for April 1963 (disintegrations per minute per 1000 ft^3 of standard air). Taken from Johnston et al. [1976].

(see Chapter 5. and Appendix A). Bomb cloud stabilization profiles from Peterson [1970] were derived from U.S. tests, only at equatorial latitudes; all U.S. nuclear bomb tests had yields below 15 Mt. Thus Peterson's polar tests and all nuclear explosion above 15 Mt are estimates. In contrast, Seitz [1968], estimated the cloud base and top from the collection of polar observations. Bauer [1979] provides cloud base and top altitude for each nuclear test based on his reformulation of the Seitz [1968] data.

Johnston [1989] lists "Target" data for both carbon-14 and strontium-90 between October 1963 and November 1971, and October 1964 and January 1967 respectively. Target data is defined as "the numerical values of carbon-14 and

Strontium-90 observations at known times, altitudes, and latitudes." The carbon-14 data for 70° N, 9° N, and 42° S have vertical profiles measured up to 20 km based on aircraft data while at 31° N, there are aircraft and balloon-borne observation up to approximately 32 ± 2 km. Comparing results from the two-dimensional model to "Target" data, taking October 1963 as the initial time, provides a good means for comparing the model with data. Such comparisons particularly provide a useful test of the models treatment of transport processes in the lower stratosphere and tropospause regions. For long term "Target" data (July 1966 or later), the models net downward transport from the middle stratosphere can be compared.

Johnston [1989] also establishes the initial conditions assumed in the model calculations based on the data for October 1963 (carbon-14) and October 1964 (strontium-90) [Appendix B]. Both times were well after the nuclear test moratorium in late 1962. Due to the lack of latitudinal and vertical resolution in sampling sites (e.g., only one sampling site was available for the southern hemisphere), there were assumptions and extrapolation made in order to obtain these initial distributions. For a description of the method of obtaining these initial profiles, see Johnston [1989].

The data described above were used in conjunction with the LLNL two-dimensional model of the troposphere and stratosphere. Initial conditions were interpolated onto the models grid (Appendix B). The lower boundary value for both carbon-14 and strontium-90 were established from observation at the surface and a spline fit though this data in time was used in the LLNL two-dimensional model. There was no removal rate assumed for either carbon-14 or strontium-90 (e.g., deposition velocity or rainout). For a special case, the profile of carbon-14 was set up (Johnston, private communication, 1989) for October 1960, in order

to inject the carbon-14 into the atmosphere from the known nuclear tests. The amount of carbon-14 per megaton was assumed to be 2×10^{26} atoms [Telegadas and List, page 1341, 1969]. There is remaining uncertainty regarding the validity of this assumption.

It is generally felt that the diabatic circulation in the model, being based on observed temperatures, was being well determined. However, there are greater uncertainties about the model's values for K_{yy} and K_{zz}. Based on initial results from the carbon-14 analysis, as well as the derivation of chemical trace constituents, there was particularly concern about the treatment of K_{yy} and K_{zz} in the tropopause region [Wuebbles, private communication, 1989].

The eddy coefficients in the LLNL two-dimensional model were varied for each study that used the "initial Johnston, October 1960" and "initial Johnston, October 1963, 1964" conditions in order to improve the comparison. The change made to the values for K_{yy} and K_{zz} are listed in Appendix B. The differences between the 12 cases are listed in Table 6.1.

6.4 Results

This study is separated into four sections. In sections 6.4.1 through 6.4.3, both carbon-14 and strontium-90 data, taken from Johnston [1989], are used as tracers in the LLNL two-dimensional model. In section 6.4.1, observed carbon-14 profiles are compared with model calculations at sequential times in order to investigate the sensitivity of eddy terms (K_{yy} and K_{zz}) and their influence on net atmospheric transport of tracers. Here each scenario, is started on October 1, 1963, and terminate either on January 1, 1967 (cases G, H, I, and J) or January 1, 1971 (cases A and B). The initial carbon-14 distribution for October 1963 in this section are based on Johnston [1989]. Between 1967 and November 1970

Table 6.1 Description of the scenarios used in the carbon-14 and strontium-90 tracer studies.

Case	Description
A	K_{yy} in the troposphere, 1×10^{11} cm^2 s^{-1} K_{yy} in the stratosphere, 2×10^9 cm^2 s^{-1} No seasonal distribution No latitudinal distribution K_{zz} in the troposphere. 1×10^5 cm^2 s^{-1} K_{zz} in lower and middle stratosphere, 1×10^3 K_{yy} and K_{zz} have gradual transition near tropopause Johnston initial condition scenario Started in October 1963 for ^{14}C Started in October 1964 for ^{90}Sr Model run from initial time to 1970
B	K_{yy} in the troposphere, 5×10^{10} cm^2 s^{-1} K_{yy} in the stratosphere, 2×10^9 cm^2 s^{-1} K_{yy} at the tropopause has a sharper transtion than case A No seasonal distribution No latitudinal distribution K_{zz} in the troposphere, 5×10^4 cm^2 s^{-1} K_{zz} at the tropopause has a sharper transition than case A K_{zz} in lower and middle stratosphere, 1×10^3 Johnston initial condition scenario Started in October 1963 for ^{14}C Started in October 1964 for ^{90}Sr Model run from initial time to 1970
C	K_{yy} and K_{zz} same as case A Peterson bomb cloud stabilization heights Started in October 1960 Derived carbon-14 distributions for each individual nuclear test Model run from initial time to 1970
D	K_{yy} and K_{zz} same as case A Seitz bomb cloud stabilization heights Started in October 1960 Derived carbon-14 distributions for each individual nuclear test Model run from initial time to 1970
E	K_{yy} and K_{zz} same as case B Peterson bomb cloud stabilization heights Started in October 1960 Derived carbon-14 distributions for each individual nuclear test Model run from initial time to 1970

Table 6.1 Continued

Case	Description
F	K_{yy} and K_{zz} same as case B Seitz bomb cloud stabilization heights Started in October 1960 Derived carbon-14 distributions for each individual nuclear test Model run from initial time to 1970
G	K_{zz} same as case B K_{yy} based on Schneider et al., 1989 K_{yy} in the troposphere 5.0×10^{10} cm^2 s^{-1} K_{yy} in the stratosphere is variable with latitude and season Maximum winter value 1.3×10^{10} cm^2 s^{-1} Maximum summer value 5×10^{9} cm^2 s^{-1} Maximum equinox value 9×10^{9} cm^2 s^{-1} Johnston initial condition scenario Started in October 1963 Model run from initial time to 1970
H	K_{zz} same as case B K_{yy} based on Schneider et al., 1989 K_{yy} in the troposphere 5×10^{10} cm^2 s^{-1} K_{yy} in the stratosphere is variable with latitude and season Maximum winter value 5×10^{9} cm^2 s^{-1} Maximum summer value 1.5×10^{9} cm^2 s^{-1} Maximum equinox value 3.5×10^{9} cm^2 s^{-1} Johnston initial condition scenario Started in October 1963 Model run from initial time to 1970
I	K_{zz} same as case B K_{yy} based on Schneider et al., 1989 No seasonal distribution No latitudinal distribution Constant low diffusion of 2×10^{8} cm^2 s^{-1} in the stratosphere Both North and South Hemispheres Johnston initial condition scenario Started in October 1963 Model run from initial time to 1970

Table 6.1 Continued

Case	Description
J	K_{zz} same as case B K_{yy} based on Schneider et al., 1989 No seasonal distribution No latitudinal distribution Northern hemisphere. 2×10^9 cm^2 s^{-1} Southern hemisphere. 2×10^8 cm^2 s^{-1} Johnston initial condition scenario Started in October 1963 Model run from initial time to 1970

(last Target data) there were 5 nuclear explosions detonated by the Chinese and French. The contribution from these tests were found to be negligible (all the tests were less than or equal to 3 Mt) and not considered in cases A and B. In section 6.4.2, the initial conditions started on October 1, 1960, and terminated on January 1, 1970 (cases C, D, E, and F). The initial conditions represented the background amount of carbon-14 at that time. In this section, carbon-14 is produced by assuming an amount of carbon-14 per Mt distributed within the nuclear bomb cloud. The distribution at long-times is highly dependent on the base and top of the nuclear bomb cloud. Therefore, two different estimates for bomb cloud stabilization heights are considered. All nuclear tests, as described by Bauer [1979], were considered between 1960 and November 1971 (last Target data). In section 6.4.3, the initial condition for Strontium-90, is started on October 1, 1964 (using the Johnston initial condition profile). There were two eddy diffusion cases, A and B, examined using the strontium-90 tracer data set. These two cases represent the original K_{yy}'s and K_{zz}'s as compared to those that best compared with carbon-14. In this section, the scenarios, cases A and B, were terminated in January 1967 (last Target data). The last two sections, 6.4.4 and 6.4.5, examine the sensitivity of the diffusion representation (cases A and B, plus several others) in the LLNL two-dimensional model for several different perturbed atmospheres.

Section 6.4.4, assumes lower boundary values for the source trace species (ClCs, CH_4, N_2O, etc.) in the model that correspond to a present atmosphere (1985). By selecting a eddy diffusion representation, and calculating a steady state solution, the total O_3 column can be obtained for cases A, B, G, H, I, and J. In section 6.4.5, the effects of vertical diffusion on the results of a aircraft perturbation (19.5 km injection of NO_x) is studied (also discussed in Chapter 4).

6.4.1 Johnston Initial Conditions, ^{14}C

In Appendix B, both the initial carbon-14 conditions as presented by Johnston, 1989 (for every 10° in latitude and 1 km in altitude), and those actually used in the LLNL two-dimensional model based on the model's spatial grid (approximately every 10° in latitude and 3 km in altitude) are given. Using this initial distribution for carbon-14, two different K_{yy} and K_{zz} distributions where examined and labeled case A and case B (others were examined towards getting to the best fit of model results with the data; these other cases are not presented here). In the troposphere case A has larger K_{yy} values (1×10^{11} cm^2 s^{-1}) than case B (5×10^{10} cm^2 s^{-1}) [see Table 6.1]. Although somewhat arbitrary because of a lack of data for defining tropospheric K_{yy} values, the latter value seems more appropriate based on other studies. In the stratosphere, both cases assumed the same K_{yy} value at all latitudes and altitudes, with no seasonal variation (2×10^9 cm^2 s^{-1}). Near the tropopause, K_{yy} for case B shows a sharper transition than case A. In the troposphere, case A has larger K_{zz} values (1×10^5 cm^2 s^{-1}) than case B (5×10^4 cm^2 s^{-1}). Both cases A and B have the same lower to middle stratospheric value of K_{zz} (1×10^3 cm^2 s^{-1}), but they are not identical in the tropopause region, where case B shows a sharper transition and a lower tropopause height at high latitudes. The above changes in effect lowered the tropopause for case B relative to case A, and as will be shown, provide a better fit to the carbon-14 and strontium-90 data.

In Figures 6.3-a through 6.3-g, there are two latitude profiles displayed for excess carbon-14 (70° N and 31° N), where case A is the dotted line and case B is the slash dot slash line. The other two latitude zones where carbon-14 is available (9° N and 42° S) are not shown due to limited space, but also because they are generally less insignificant. Since the eddy diffusion representation for case A is more diffusive, particularly in the tropopause transition region, both horizontally and vertically than case B, the residence time in the global atmosphere is shorter for case A than case B. This can be seen more clearly when comparing the model profiles of both cases with each other sequentially through time. In Figure 6.3-a, the difference between cases A and B are negligible at both 31° N and 70° N. After one year (Figure 6.3-b), October 1964, the mixing ratio of case A is decreasing more rapidly than case B at both 31° N and 70° N (between 10 and 30 km). Also, at this time, the carbon-14 profile at 31° N as calculated by the two-dimensional model is unfolding (at altitudes greater than 25 km) faster for both cases A and B than that observed. By October 1965, there is a distinct difference between cases A and B. By November 1970 (Figure 6.3-g), there is a difference of 50 mixing ratio units between case A and case B. In general and especially at longer times (July 1966 or longer), case B better represents the observed carbon-14 profile. Case A in general, underestimates the mixing ratio at a given altitude during the complete time series when comparing to the observed carbon-14 data. For November 1970 case A is clearly not representing the correct magnitude, while case B is comparing well, at all five latitudes, to the observed carbon-14 profile. In Figure 6.3-g, at 34° S, transport into the southern hemisphere from northern hemispherical sources can be compared. At this latitude, case B indicates that both the diabatic circulation plus the eddy diffusion contribution models the global transport correctly.

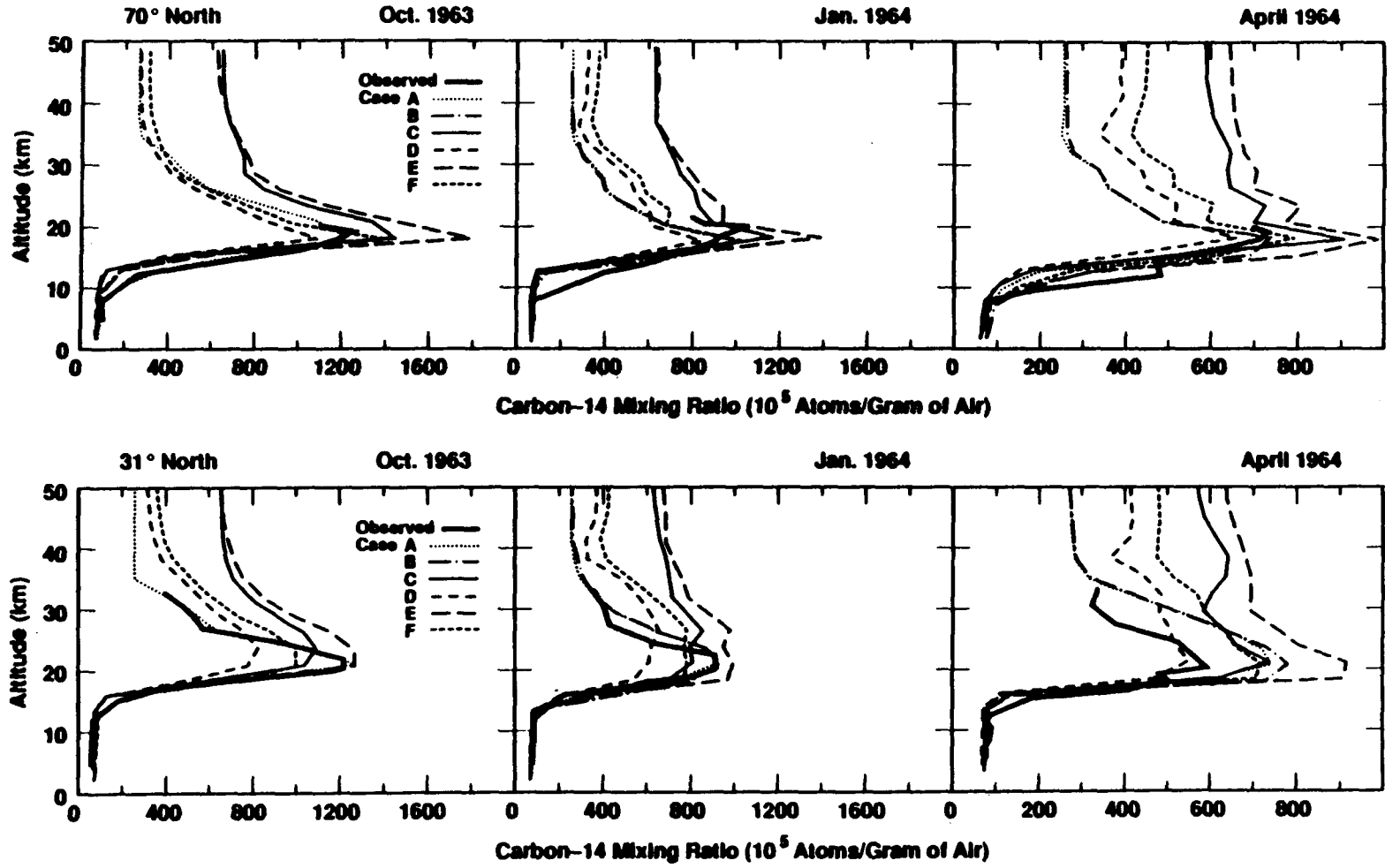

Figure 6.3a. Excess carbon-14 mixing ratio units (10^5 atoms of excess carbon-14 per gram of air). Carbon-14 profiles for the observed data taken from Johnston [1989]. Cases A and B, start from Johnston October 1963 initial conditions. Cases C, D, E, and F start from Johnston October 1960 initial conditions.

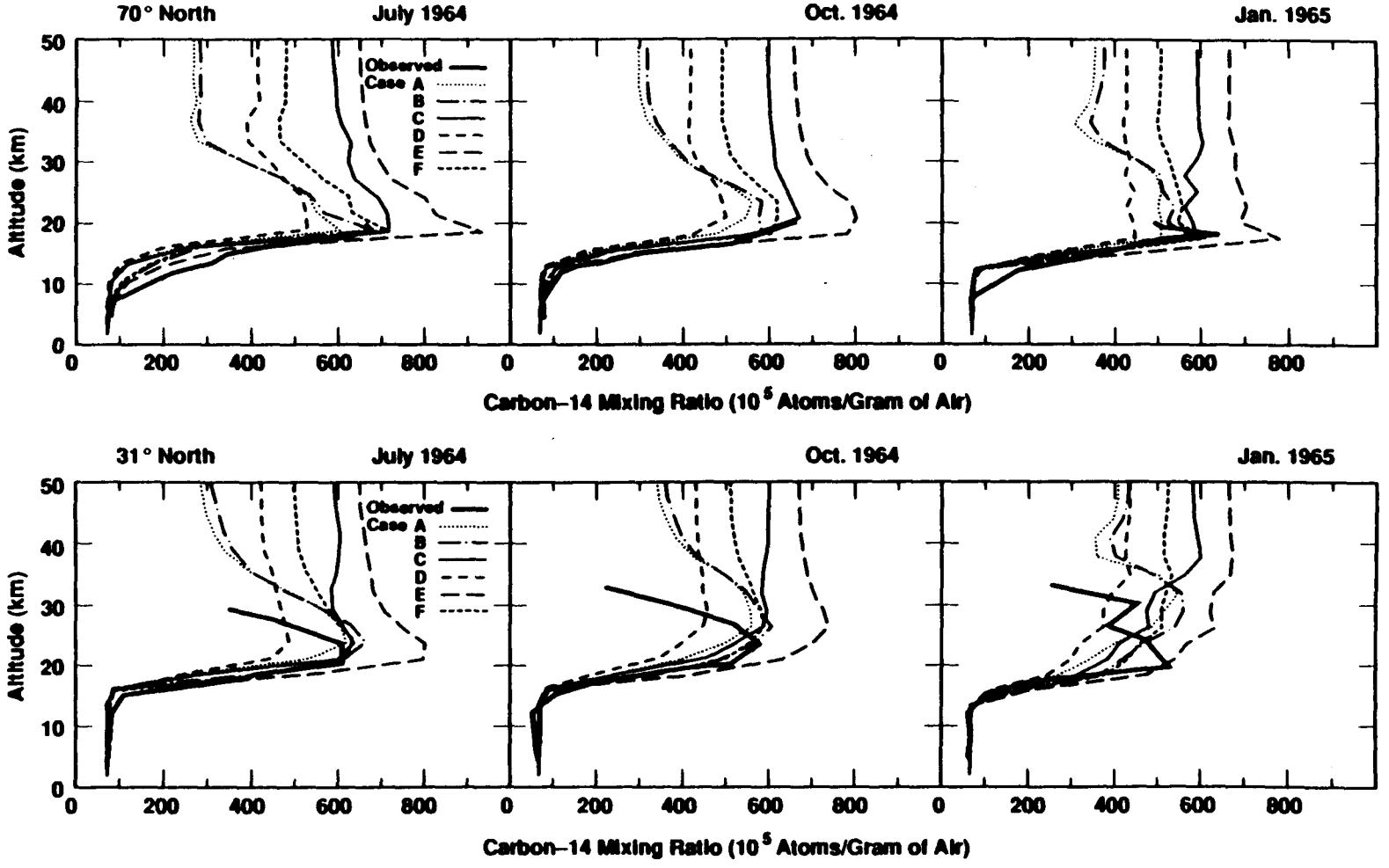

Figure 6.3b. Excess carbon-14 mixing ratio units (10^5 atoms of excess carbon-14 per gram of air). Carbon-14 profiles for the observed data taken from Johnston [1989]. Cases A and B, start from Johnston October 1963 initial conditions. Cases C, D, E, and F start from Johnston October 1960 initial conditions.

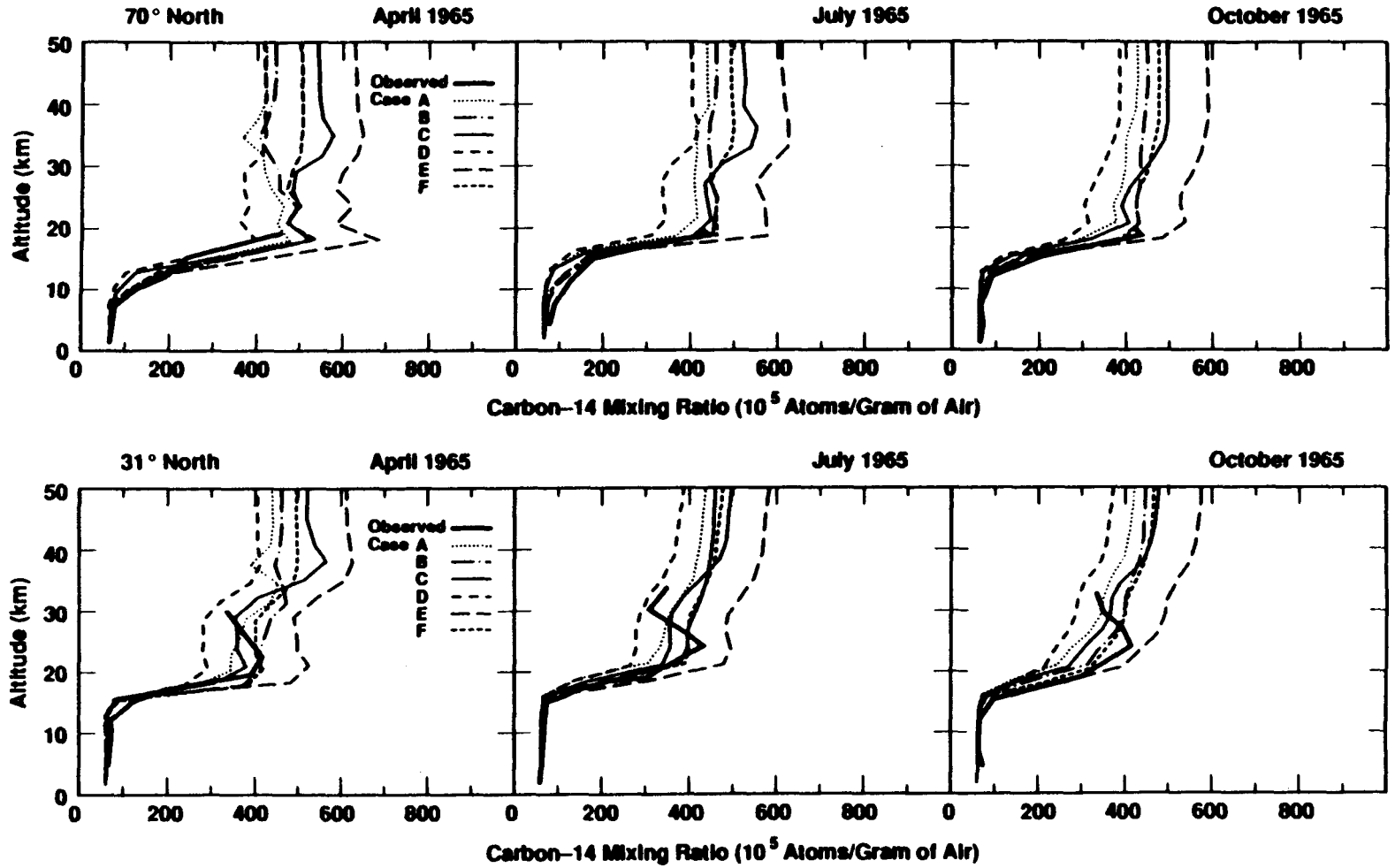

Figure 6.3c. Excess carbon-14 mixing ratio units (10^5 atoms of excess carbon-14 per gram of air). Carbon-14 profiles for the observed data taken from Johnston [1989]. Cases A and B, start from Johnston October 1963 initial conditions. Cases C, D, E, and F start from Johnston October 1960 initial conditions.

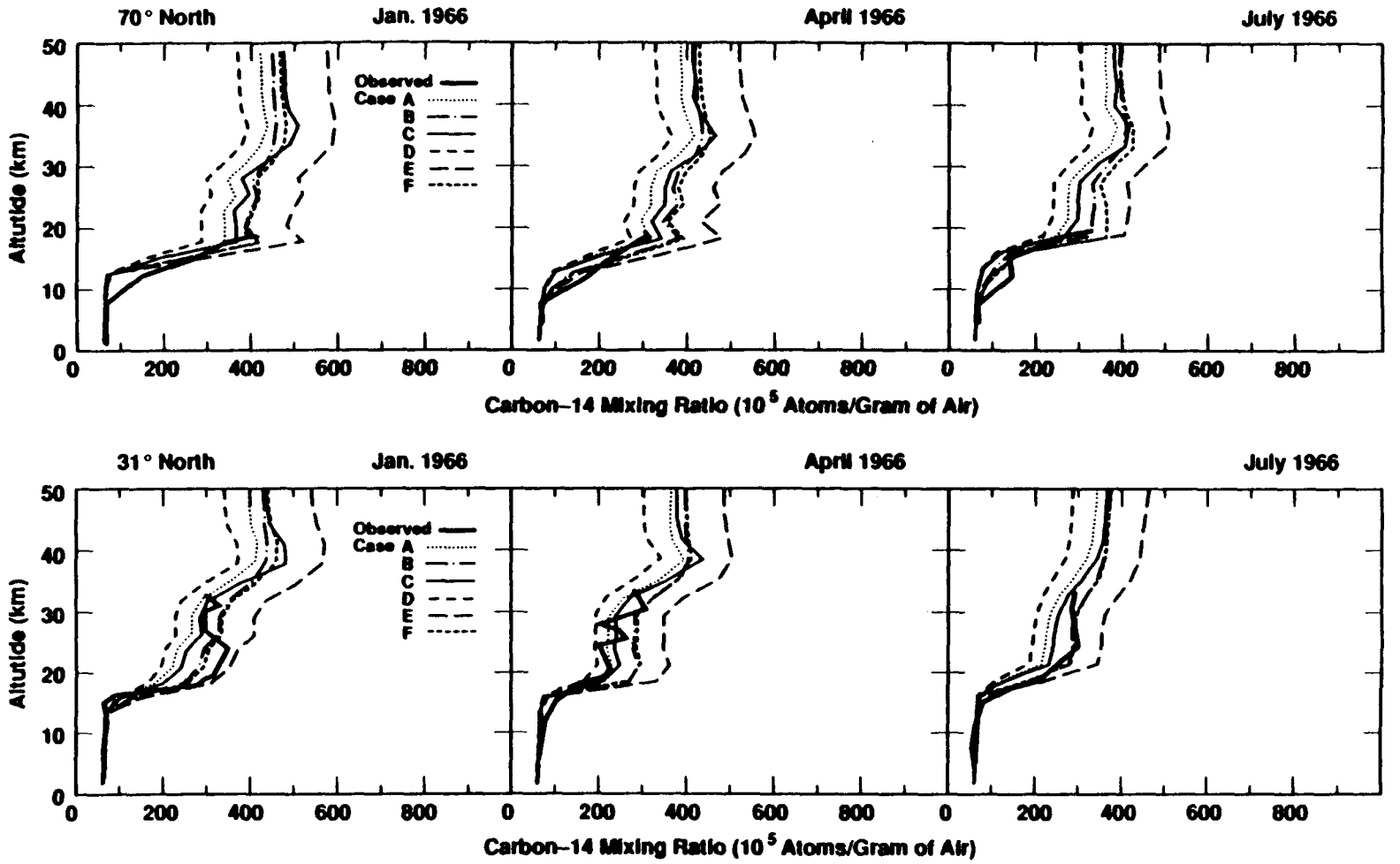

Figure 6.3d. Excess carbon-14 mixing ratio units (10^5 atoms of excess carbon-14 per gram of air). Carbon-14 profiles for the observed data taken from Johnston [1989]. Cases A and B, start from Johnston October 1963 initial conditions. Cases C, D, E, and F start from Johnston October 1960 initial conditions.

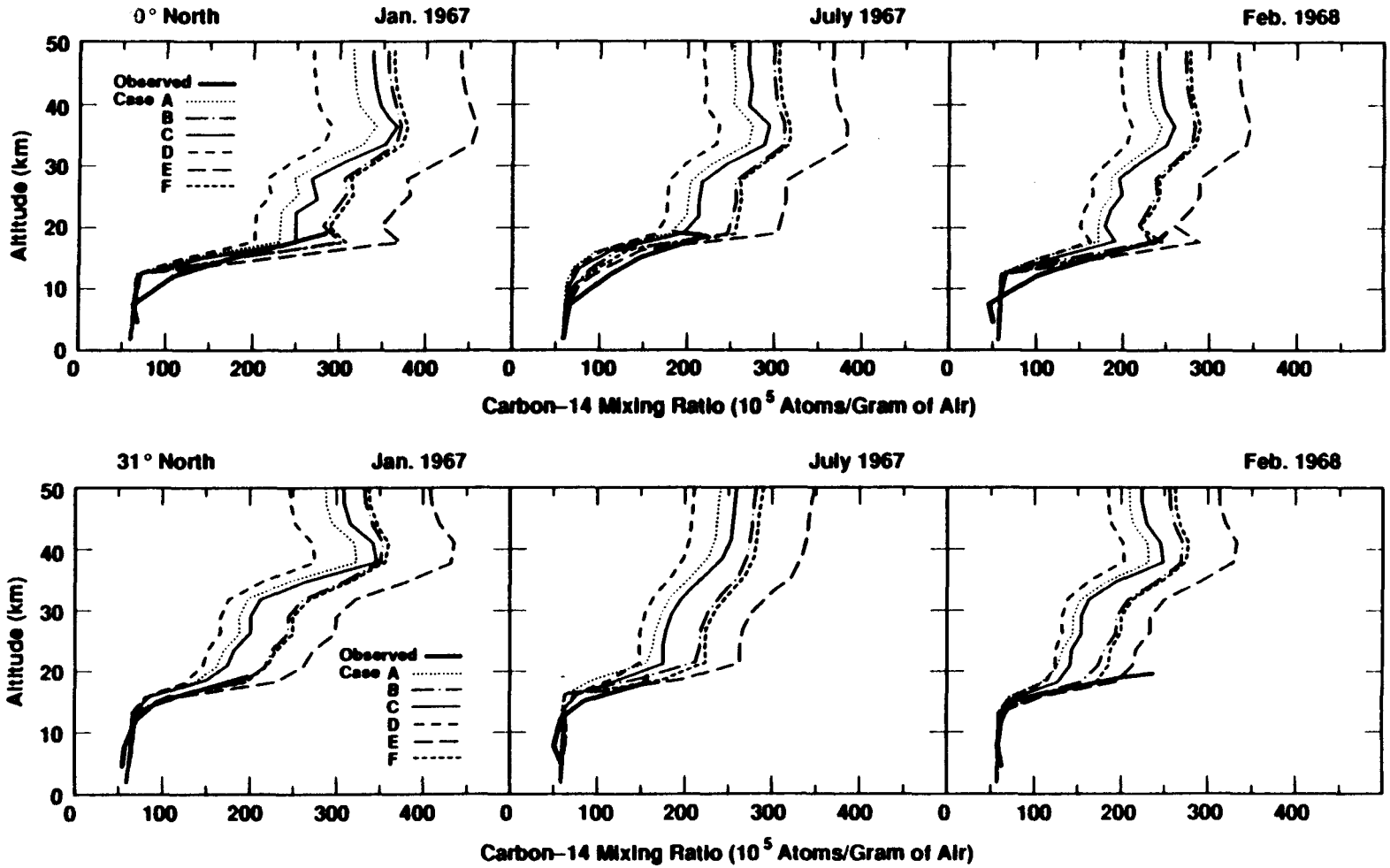

Figure 6.3e. Excess carbon-14 mixing ratio units (10^5 atoms of excess carbon-14 per gram of air). Carbon-14 profiles for the observed data taken from Johnston [1989]. Cases A and B, start from Johnston October 1963 initial conditions. Cases C, D, E, and F start from Johnston October 1960 initial conditions.

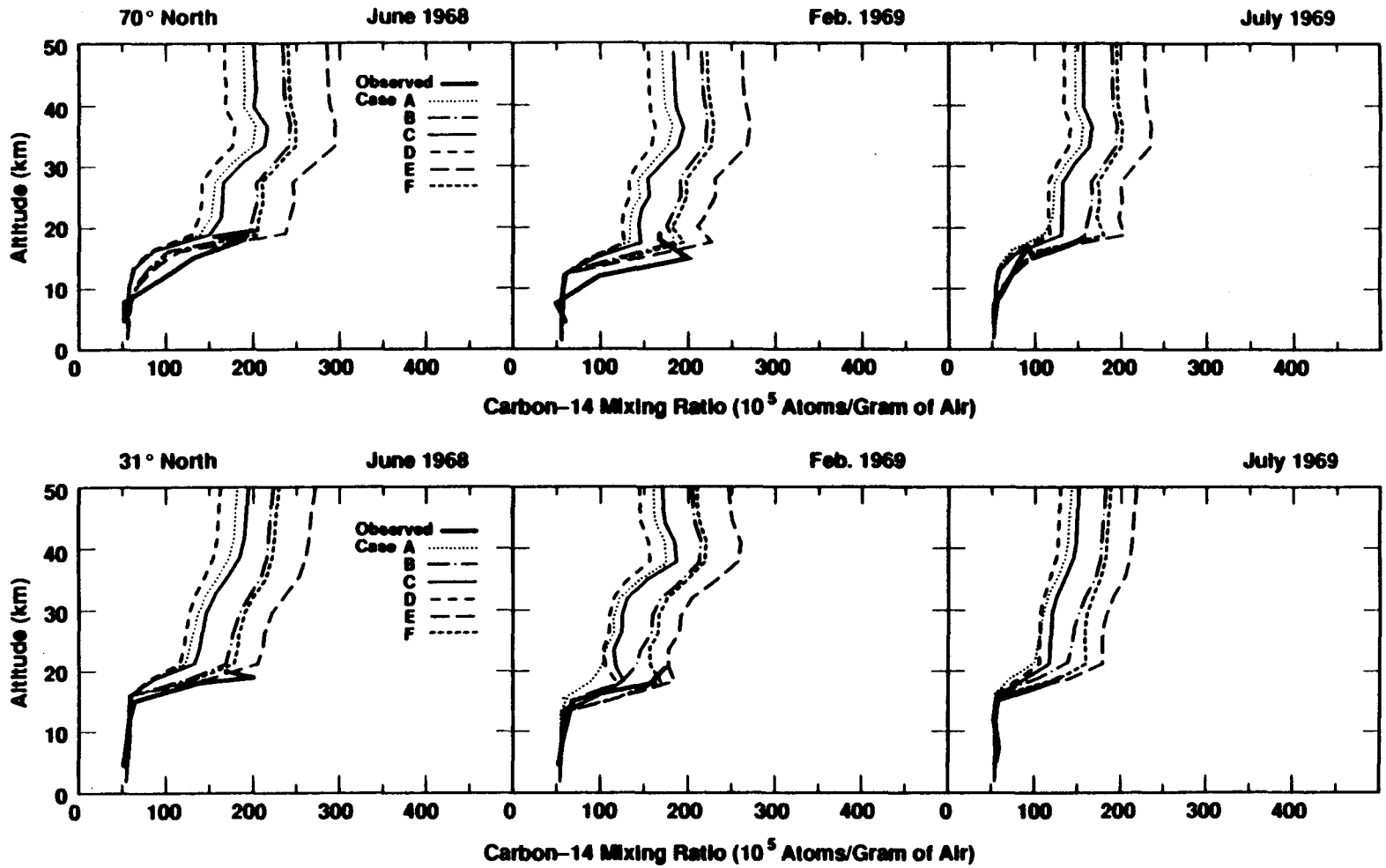

Figure 6.3f. Excess carbon-14 mixing ratio units (10^5 atoms of excess carbon-14 per gram of air). Carbon-14 profiles for the observed data taken from Johnston [1989]. Cases A and B, start from Johnston October 1963 initial conditions. Cases C, D, E, and F start from Johnston October 1960 initial conditions.

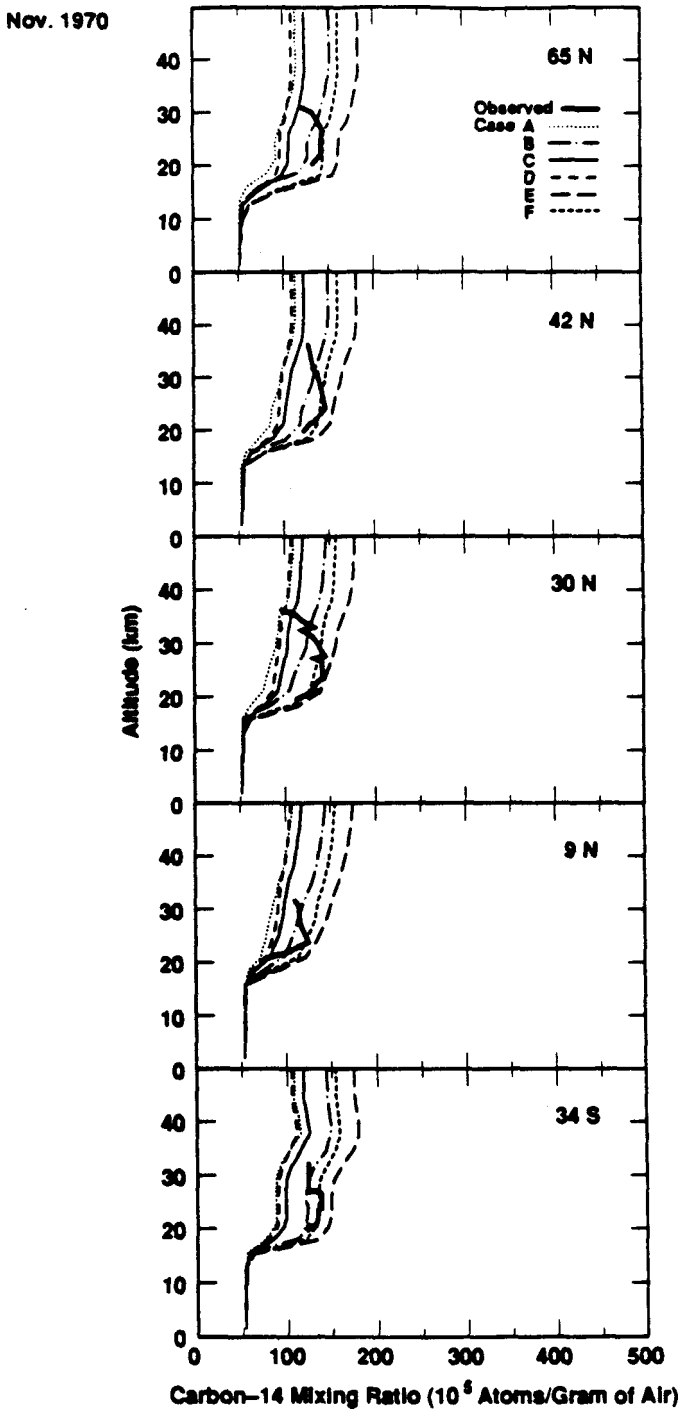

Figure 6.3g. Excess carbon-14 mixing ratio units (10^5 atoms of excess carbon-14 per gram of air). Carbon-14 profiles for the observed data taken from Johnston [1989]. Cases A and B, start from Johnston October 1963 initial conditions. Cases C. D. E. and F start from Johnston October 1960 initial conditions.

In general, at all four latitudes the LLNL two-dimensional model represents the tropopause height correctly relative to the carbon-14 Target data. However, exceptions occur consistently in the winter season, northern hemisphere (January) between 1963 and 1970. The tropopause height at high latitudes in January (e.g., January 1964) is at a higher altitude for the two-dimensional model than the Target data. The carbon-14 transported using the two-dimensional model from the October 1963 initial condition, shows a mixing ratio magnitude that is smaller than the observed data. Case B shows a slightly higher carbon-14 mixing ratio than case A in this region. This is due to the difference in tropopause heights at high latitudes, with case B exhibits a lower tropopause due to the sharper transition in K_{yy} and K_{zz}, therefore increasing the mixing ratio at a lower altitude (see Appendix B). This adjustment of the tropopause height at high latitudes between cases A and B did not make a large difference in the model calculated carbon-14 profile. The discrepency between the tropopause height at high latitudes calculated by the model (either cases A or B) and observed by *in situ* measurements is unresolved at this time. (It may be related to the magnitude of the diabatic circulation, which is based on observed temperature data from Barnett and Corney 1984.)

In summary, in the LLNL two-dimensional model, case B, which has smaller eddy diffusion values in the troposphere and a sharper transition at the tropopause, compares better than case A to the observed carbon-14 profiles of Johnston [1989]. This is not to imply that these are definitive choices for K_{yy} and K_{zz}, but does imply that a sharp transition in eddy coefficients at the tropopause are necessary to achieve a reasonable fit with the data.

Using the same initial conditions described above, four different cases of K_{yy} and K_{zz} were selected. These choices of K_{yy} and K_{zz} were based on a study

by Schneider et al. (1989). In each of the cases G, H, I, and J, the same K_{zz}, case B, was selected because it showed the best fit to the carbon-14 tracer profile at long times (Table 6.1). For the two cases, G and H, the K_{yy} coefficient in the stratosphere varied with latitude and season, with case G being over 3 times larger than case H at most latitudes (see Appendix B). In January (winter season, northern hemisphere), both cases G ($K_{yy} = 1.3 \times 10^{10}$ cm^2 s^{-1}) and H ($K_{yy} = 3.4 \times 10^{10}$ cm^2 s^{-1}) have larger maximum K_{yy} values than the "best" constant stratospheric latitudinal K_{yy} representation (case B, $K_{yy} = 2 \times 10^9$ cm^2 s^{-1} used in section 6.4.1. In July (summer season, northern hemisphere), case G is still larger (5.3×10^9 cm^2 s^{-1}) than case B, and case H (1.4×10^9 cm^2 s^{-1}) is slightly less than case B. The variation of K_{yy} with latitude and season is an attempt to model the different wave properties of wave-driven transport that are known to occur between hemispheres and at different times during the year. Case I has small diffusion everywhere in the stratosphere, for both the northern and southern hemispheres (2×10^8 cm^2 s^{-1}). Case J, in the stratosphere, has medium diffusion in the northern hemisphere (2×10^9 cm^2 s^{-1}) and small diffusion in the southern hemisphere (2×10^8 cm^2 s^{-1}). In the equatorial zone, between 20° N and 20° S, the K_{yy} value was held fixed at 2×10^8 cm^2 s^{-1} in the stratosphere for all four cases, implying small horizontal mixing due to the eddies.

In Figures 6.4-a and 6.4-b, three plots for each latitude (70° N, 31° N, 9° N, and 42° S) are shown at various times on July 1st. At 70° N, on July 1, 1964, case I (small horizontal diffusion) is the only scenario that deviates drastically by underestimating the magnitude of carbon-14 compared to the observed tracer profile. At 31° N, case I also deviates from the carbon-14 tracer profile, however; this time it overestimate the magnitude rather than underestimating it. Therefore, in the LLNL two-dimensional model, small values everywhere for horizontal diffusion

(K_{yy}) in the stratosphere represented in case I, do not reproduce everywhere adequately the carbon-14 tracer data. For case G (large horizontal diffusion), at 31° N, the carbon-14 distributions calculated by the model overestimates the observed carbon-14 tracer profile at long times, suggesting that the eddy diffusion representation with large K_{yy} values may not adequately reproduce the C-14 data. For all cases, at 9° N and 42° S, there is not a significant difference between the carbon-14 tracer profile for the four scenarios. At 42° S, for all four cases, the model overestimates the amount of carbon-14 at 20 km compared to observations. In general after examining both figures 6.4-a and 6.4-b, plus examining the complete set of carbon-14 tracer "Target" data supplied by Johnston [1989], the comparison between the observed carbon-14 tracer profiles and each of the four cases, suggest that cases J and H are the best fits. This is not surprising, since the seasonally varying K_{yy} function that best fits the observed data have average values about the same as the best fitting non-seasonally varying function. This comparison implies that the seasonal deviation about the mean are almost linear.

In a later section, 6.4.4, all six of the above eddy coefficient cases (A, B, G, H, I, and J) will be used in the LLNL two-dimensional model, and a ambient "1985" atmosphere will be calculated. From this a total column O_3 plot is generated for each case.

6.4.2 Injection from Nuclear Test Series, ^{14}C

During the late 1950's and early 1960's, numerous nuclear test were detonated in the troposphere. These tests are calculated to have produced large amounts of NO_x, which was lifted by convective motion and deposited in the stratosphere. In the stratosphere, the excess NO_x could catalytically react and reduce the concentration of O_3. The distribution of NO_x from the nuclear bomb clouds, is a subject of debate. In this section, the LLNL two-dimensional model, injects the

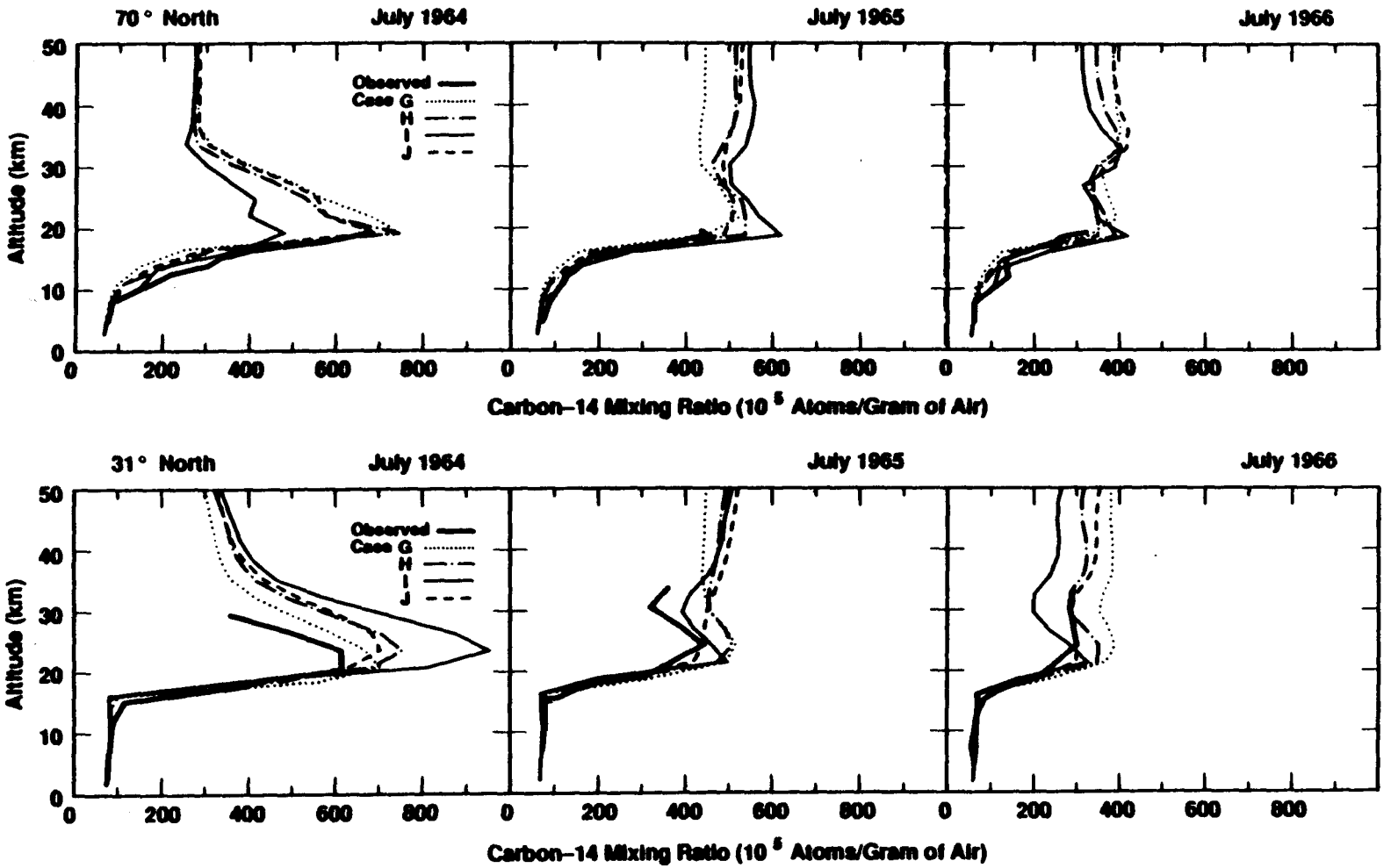

Figure 6.4a. Excess carbon-14 mixing ratio units (10^5 atoms of excess carbon-14 per gram of air). Carbon-14 profiles for the observed data taken from Johnston [1989]. Cases G, H, I, and J started from Johnston October 1963 initial conditions.

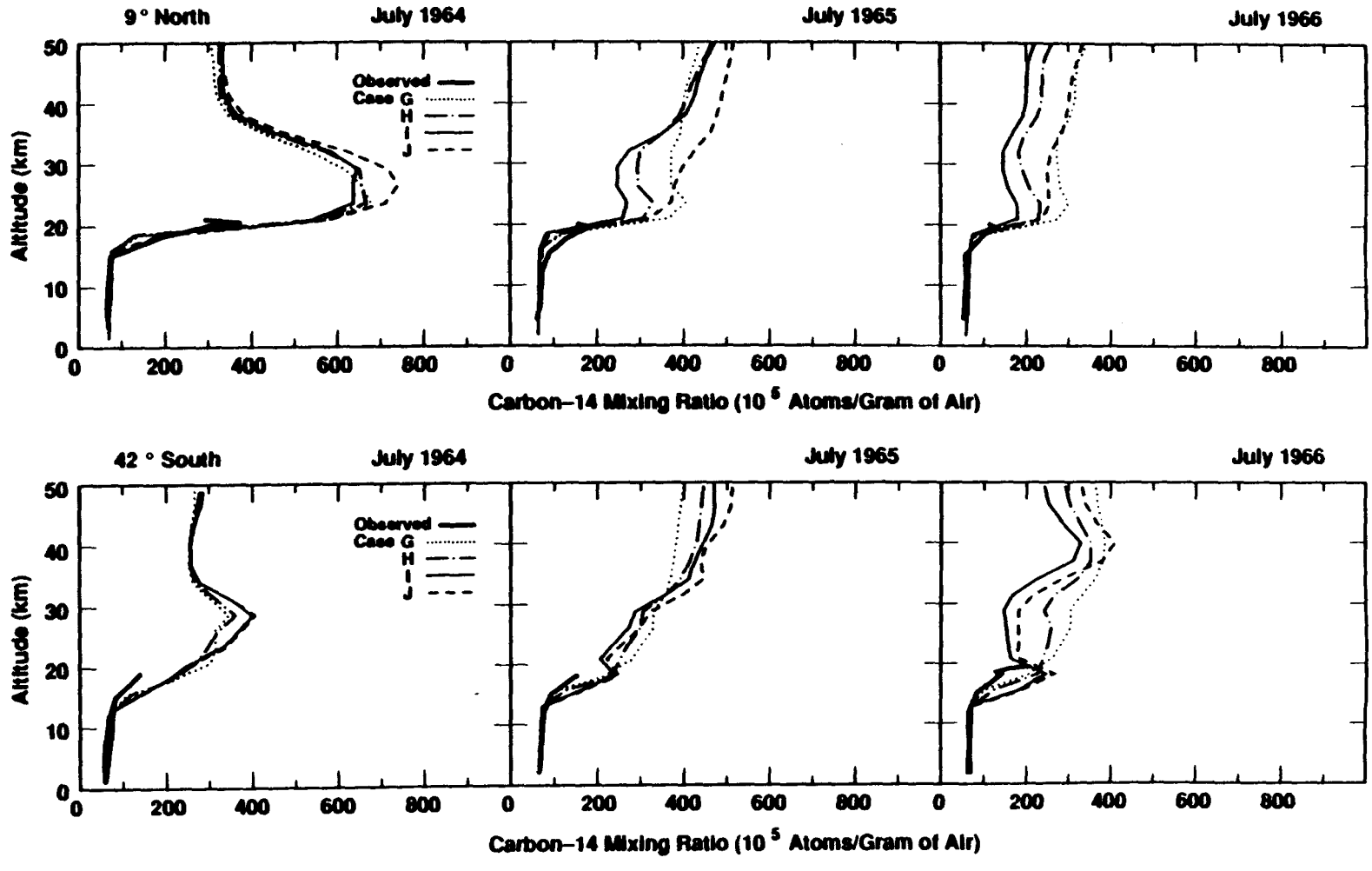

Figure 6.4b. Excess carbon-14 mixing ratio units (10^5 atoms of excess carbon-14 per gram of air). Carbon-14 profiles for the observed data taken from Johnston [1989]. Cases G, H, I, and J started from Johnston October 1963 initial conditions.

NO_x using two different bomb cloud stabilization heights. The first is based on Peterson [1970], who examined the U.S. nuclear tests at equatorial latitudes and extrapolated these results to higher latitudes. The second study used the analysis of Seitz [1968] (based on eyewitness observations), for the tests at high latitudes, in the northern hemisphere. Both studies predict approximately the same bomb cloud stabilization heights in the tropics (where smaller megaton bombs were detonated), but differ greatly at high latitudes (see Appendix A). In this study, the amount of carbon-14 atoms per megaton is assumed to be 2×10^{26} [Telegadas and List, 1969]. The distributions of carbon-14 for each known nuclear test were calculated within the two-dimensional model, and the results compared with the available observations.

In Figure 6.3, cases C, D, E, and F are shown along with cases A and B which were discussed in section 6.4.1. Cases C and D use the same diffusion coefficients, K_{yy} and K_{zz}, as case A [see Table 6.1 and Appendix B]. Cases E and F use the same diffusion coefficients as case B. Cases C and E use Peterson [1970], while cases D and F use Seitz [1968] bomb cloud stabilization heights. Both sets of diffusion coefficients (cases A and B) were examined for the sake of completeness, even though section 6.4.1 conclude that case B was the better set. In examining Figure 6.3 at 31° N, for July 1966 or longer, case F compares best with the carbon-14 tracer data. Again, this case is for the K_{yy} and K_{zz} diffusion coefficients of case B, section 6.4.1, with the bomb stabilization height for case F being based on Seitz [1968]. Case E, which has the same diffusion coefficients as case F, but uses Peterson's [1970] bomb stabilization heights, overestimates the mixing ratio of carbon-14 compared to the observed carbon-14 profiles. For cases C (Peterson) and D (Seitz), which use the same diffusion coefficients as that of case A, both cases underestimate the mixing ratio of carbon-14 compared to the observed values

for July 1966 (31° N). In Figure 6.5-a, the excess mixing ratio of carbon-14, based on the Johnston [1989] analysis of available observations is shown (altitude versus latitude) for October 1, 1963. Figures 6.5-b and 6.5-c show cases C and D, and cases E and F respectively.

In Table 6.2, the column carbon-14, for October 1963, is shown for the five cases, i.e., Johnston for the initial condition, and for cases C, D, E, and F where the C-14 is derived from the known nuclear explosion information (location, time). The observed excess carbon-14 column sums were constructed from contour plots (e.g., Figure 1). The Johnston analysis and case F global column carbon-14 agree well but are 13.5 percent high compared to an estimate by Telegadas [1971]. When comparing the total number of carbon atoms from Telagadis [1971] to that calculated by the model, one should recognize that they had limited spatial resolution in constructing their global inventory. Case C, which showed poor agreement with "Target" data, compares best with Telegadas and List [1969]. Case E, overestimates the column carbon-14 by 25 percent relative to Telegadas [1971].

Table 6.2. Total inventory of carbon-14 atoms for October 1, 1963.

October 1963	^{14}C Atoms ($\times 10^{28}$)		
Case	Global Avg.	N.H. Avg.	S.H. Avg.
Johnston Initial*	5.9	4.0	1.9
C	5.8	3.6	2.2
D	5.2	3.2	2.0
E	6.5	4.2	2.3
F	5.9	3.6	2.3
Telagadas**	5.2	3.6	1.6

* Johnston [1989]

** Telagadas [1971]

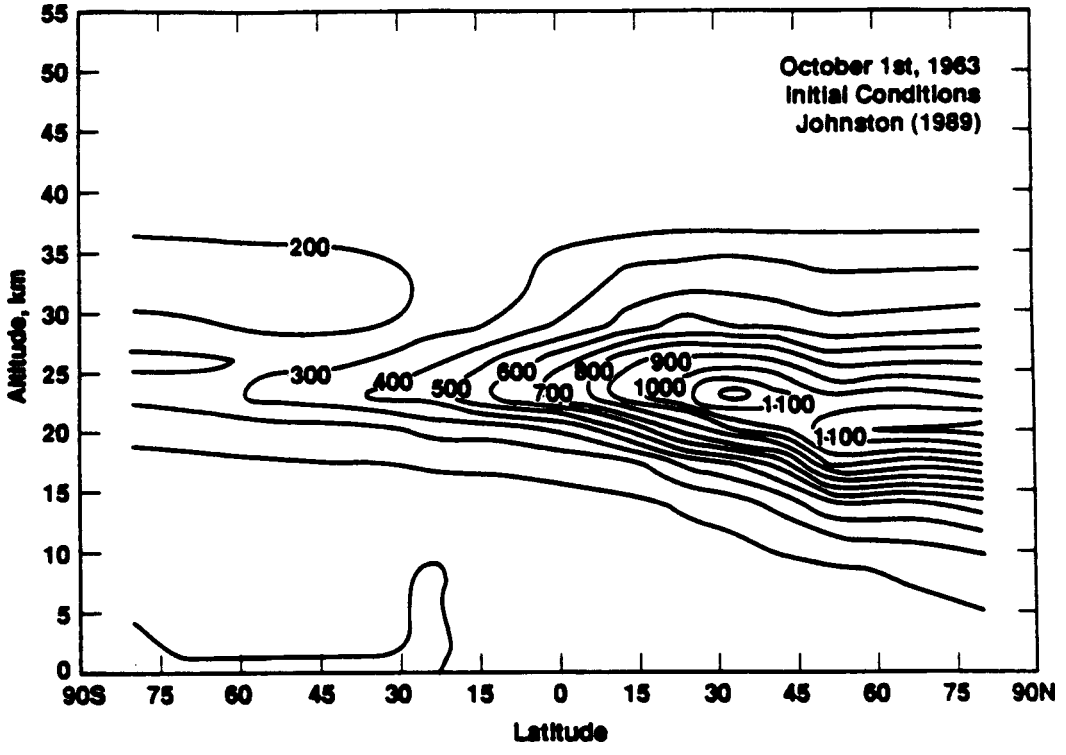

Figure 6.5a. Excess carbon-14 mixing ratio units (10^5 atoms of excess carbon-14 per gram of air) for October 1, 1963.

6.4.3 Johnston Initial Conditions, ^{90}Sr

In Figures 6.6 and 6.7, strontium-90 is used as the tracer, and the results of the LLNL two-dimensional model are compared at four latitudes (64° N, 31° N, 9° N, and 34° S) for various "Target" times between October 1964 and April 1966. In this study, no removal rate was assumed for the process of strontium-90 coalescing and forming a particulate, and eventually washing out of the atmosphere (the lower boundary value was zero at the the ground surface). It is evident from the figures that the mixing ratio of strontium-90 from the observed data set, decreases at a faster rate than the model. This conforms well with the theory that part of the removal process of strontium-90 is to coalesce with other stratospheric aerosols and precipate out of the atmosphere. However, we believe that using strontium-90

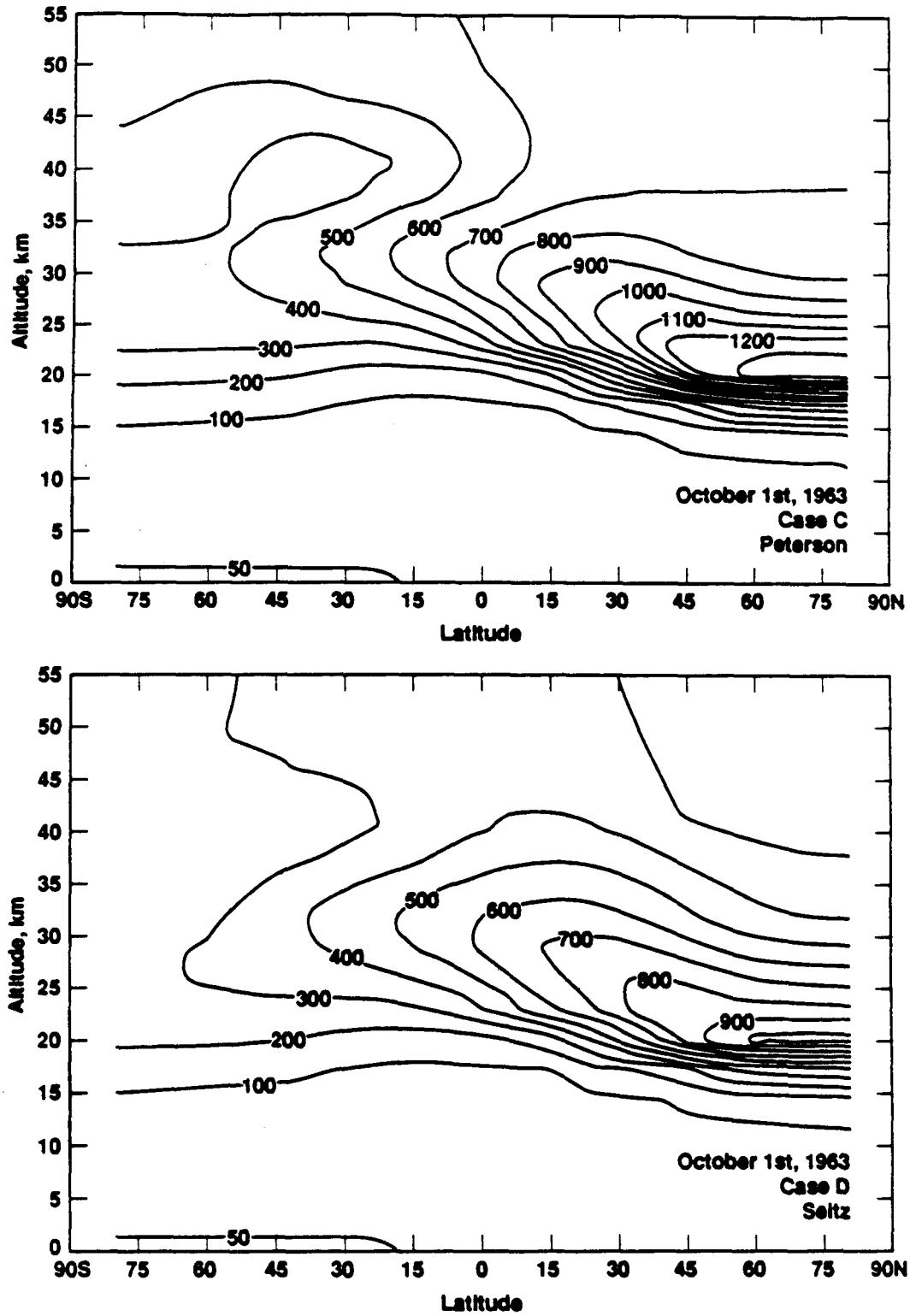

Figure 6.5b. Excess carbon-14 mixing ratio units (10^5 atoms of excess carbon-14 per gram of air) for October 1, 1963.

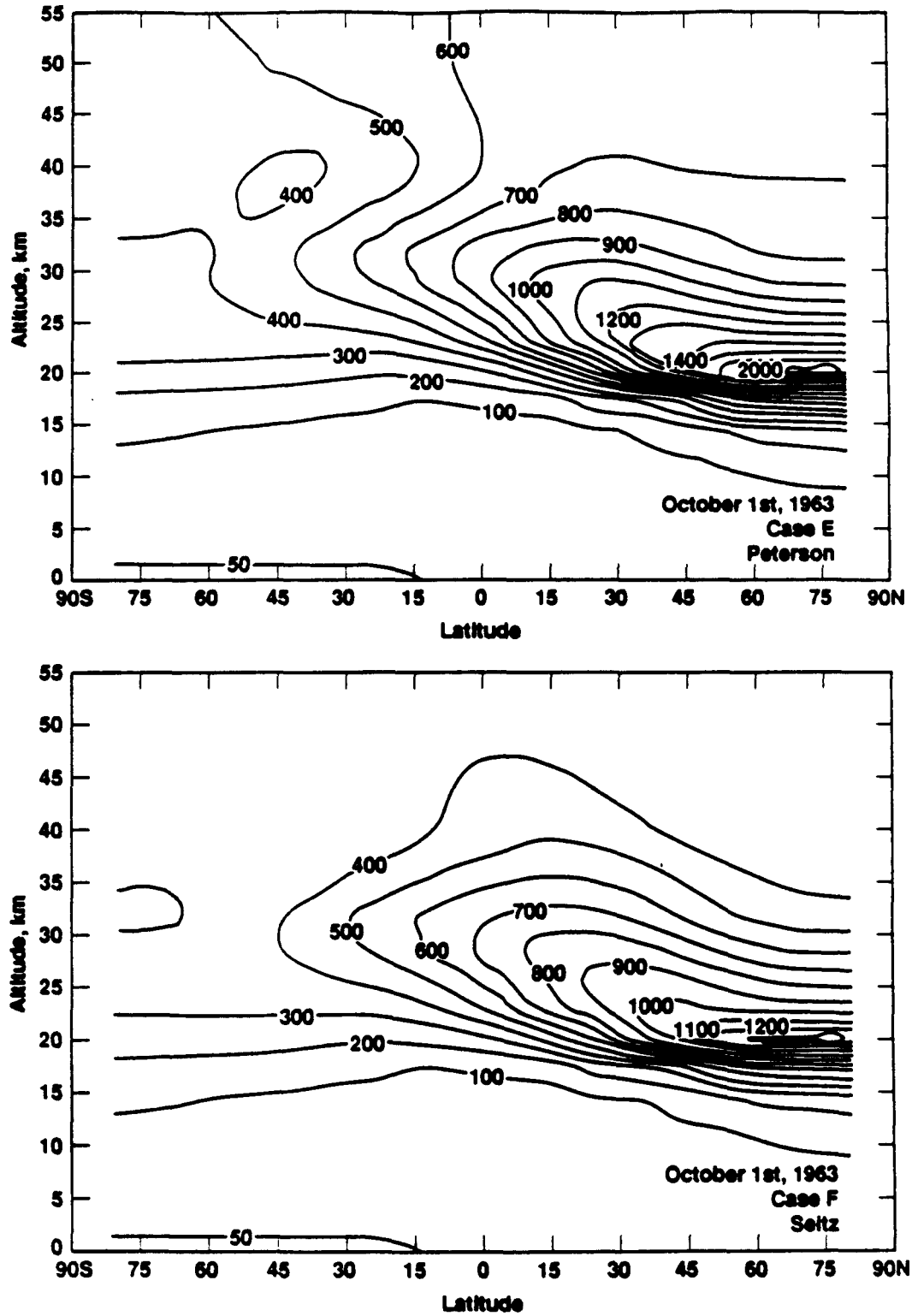

Figure 6.5c. Excess carbon-14 mixing ratio units (10^5 atoms of excess carbon-14 per gram of air) for October 1, 1963.

measurements near the tropopause should still be reliably resolved by the model if transport processes are being adequately represented.

For 31° N, 9° N, and 34° S, strontium-90 derived near the model tropopause compares well with that suggested from observations. At higher latitudes, the same discrepancy exists that was noticed in the carbon-14 tracer study, where the mixing ratio for the calculated distribution is less than that observed near or below the high latitude tropopause. In this case, the observed mixing ratio for strontium-90 is larger for any given altitude between 8 and 15 km. This suggests that K_{yy} and K_{zz} values at high latitudes may need to be revised further to effectively lower the model tropopause in order to fit this data.

6.4.4 Total Ozone Variation

In Figure 6.8-a through 6.8-f, total column O_3 is shown for an ambient "1985" atmosphere with different assumptions for K_{yy} and K_{zz} coefficients. Observational data from the Dobson network and TOMS are displayed in Figures 5.1-b and 5.1-c. In Figures 6.8-a and 6.8-b, cases A and B are shown respectively. Again, the major difference between cases A and B, are the magnitudes of the eddy diffusion coefficients at the tropopause and in the troposphere. Both cases compare adequately to the column O_3 derived from the Dobson network in the equatorial region. Case B represents the northern hemisphere winter maximum better than case A. The southern hemisphere observed column O_3 maximum is off the pole, which is not evident in either cases A or B.

Schneider et al. [1989], investigated the effects of varying the magnitude of K_{yy} in the stratosphere, seasonally and latitudinally. Their scenarios are followed in cases G, H, I, and J. In their study, O_3 was computed using a relatively simple scheme. They considered only an oxygen-hydrogen atmosphere, with O_3 being the

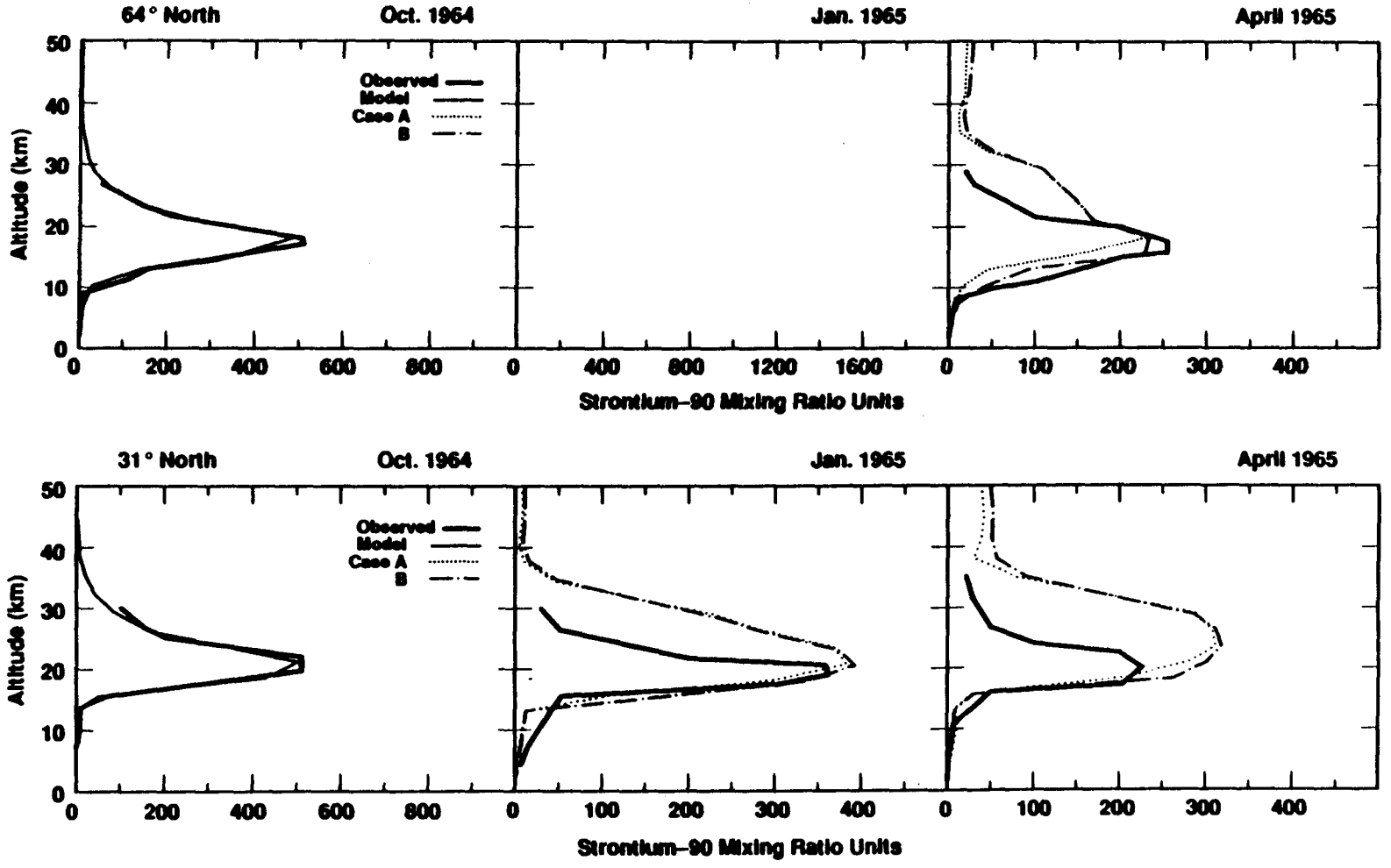

Figure 6.6a. Strontium-90 relative mixing ratio units (disintegrations per minute per 1000 ft^3 of standard air) for 64° N and 31° N. The observed data taken from Johnston [1989]. Cases A and B start from Johnston October 1964 initial conditions.

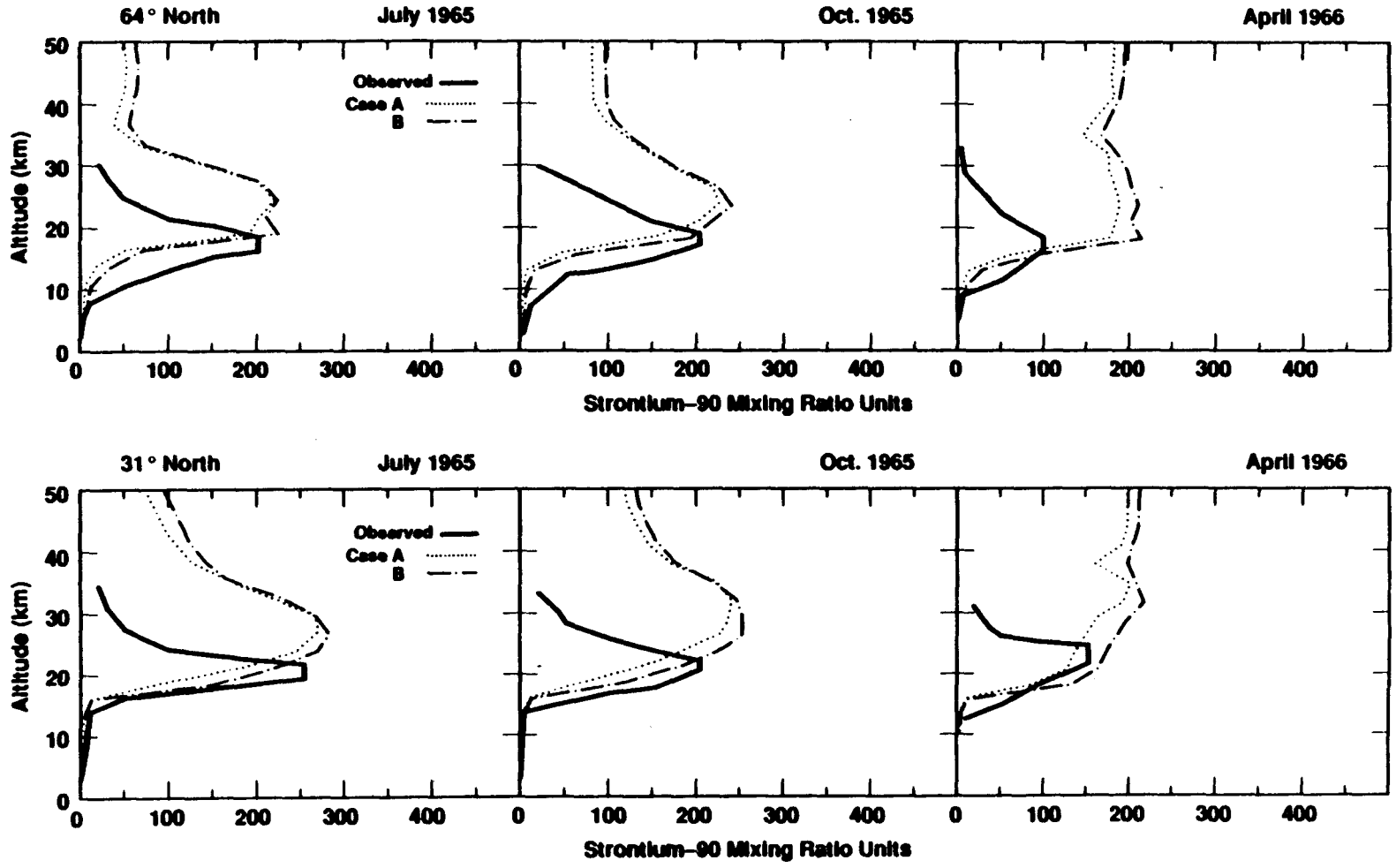

Figure 6.6b. Strontium-90 relative mixing ratio units (disintegrations per minute per 1000 ft^3 of standard air) for 64° N and 31° N. The observed data taken from Johnston [1989]. Cases A and B start from Johnston October 1964 initial conditions.

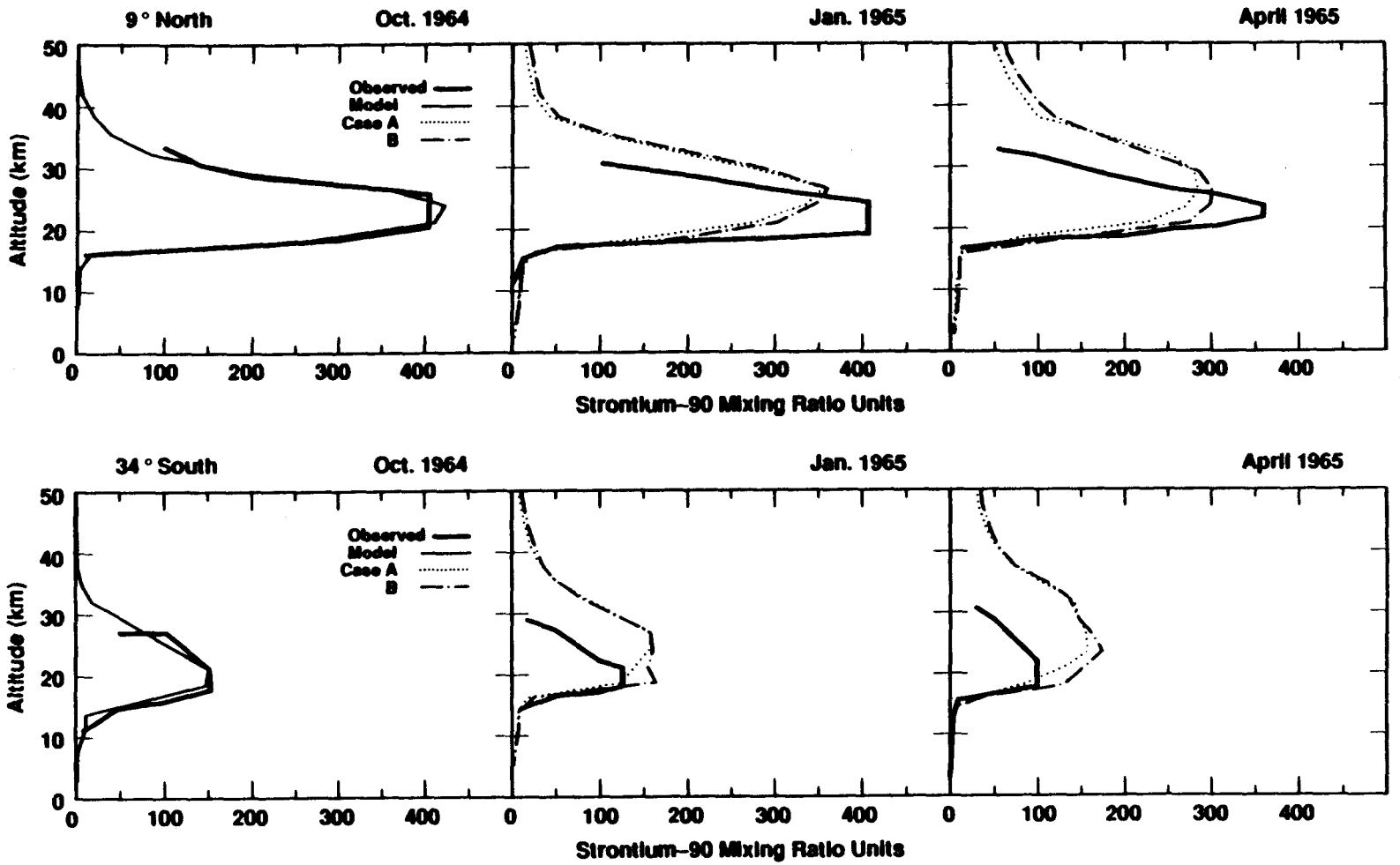

Figure 6.7a. Strontium-90 relative mixing ratio units (disintegrations per minute per 1000 ft^3 of standard air) for 9° N and 34° S. The observed data taken from Johnston [1989]. Cases A and B start from Johnston October 1964 initial conditions.

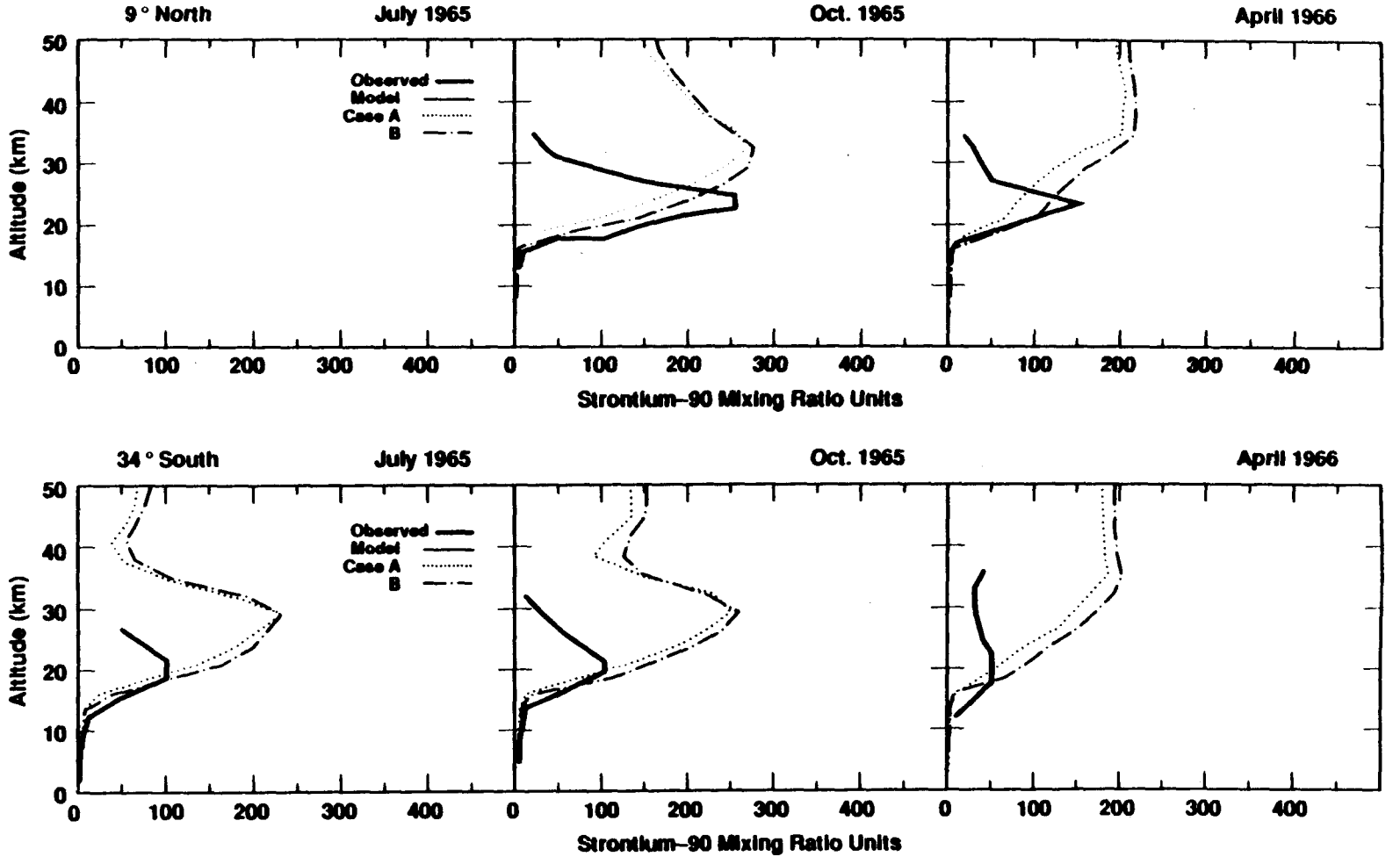

Figure 6.7b. Strontium-90 relative mixing ratio units (disintegrations per minute per 1000 ft^3 of standard air) for 9° N and 34° S. The observed data taken from Johnston [1989]. Cases A and B start from Johnston October 1964 initial conditions.

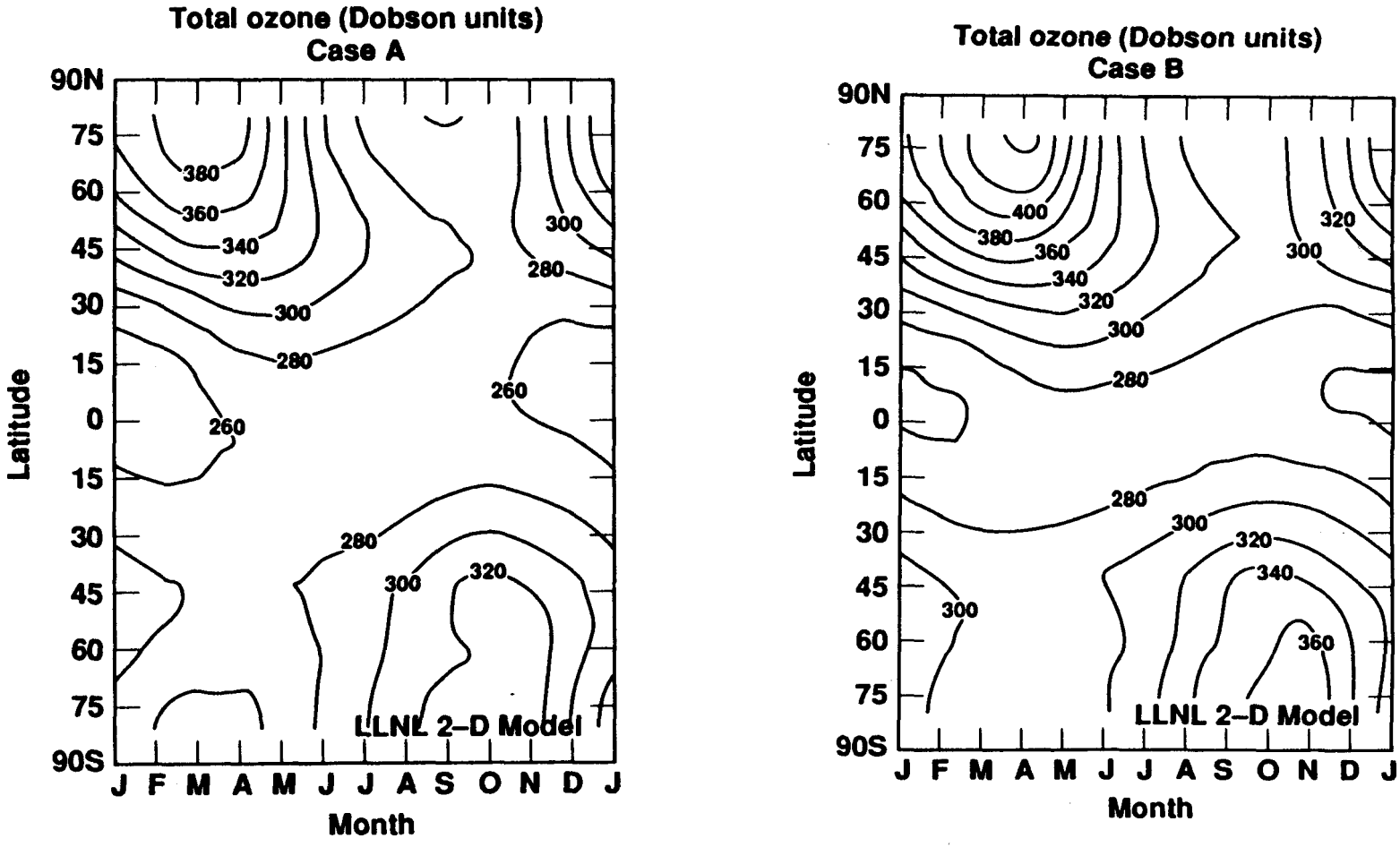

Figure 6.8a,b. Column ozone (Dobson units) as a function of latitude and time of the year. Calculated by the LLNL two-dimensional model (1985 reference atmosphere), where: (a) eddy diffusion case A and (b) eddy diffusion case B.

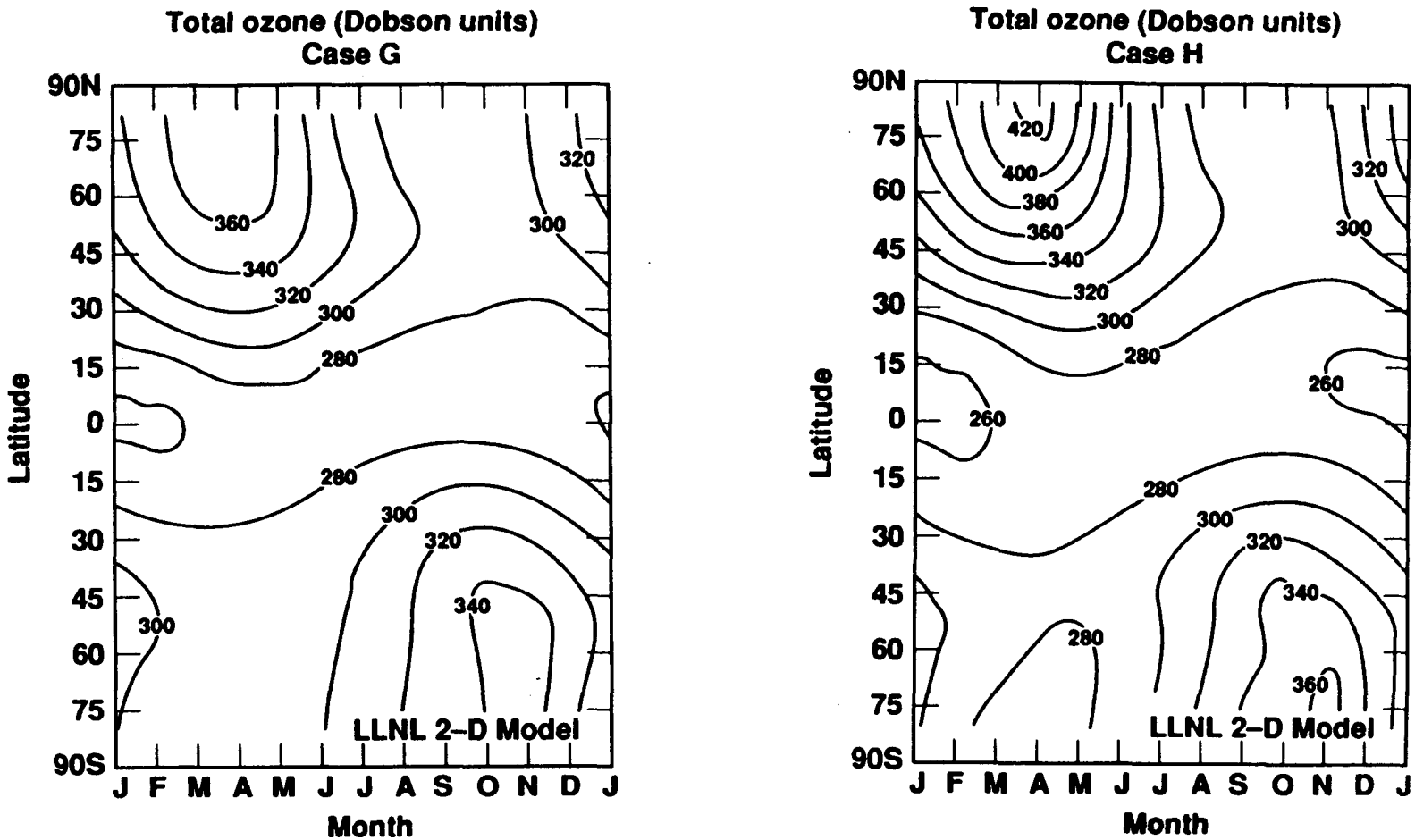

Figure 6.8c,d. Column ozone (Dobson units) as a function of latitude and time of the year. Calculated by the LLNL two-dimensional model (1985 reference atmosphere), where: (c) eddy diffusion case G and (d) eddy diffusion case H.

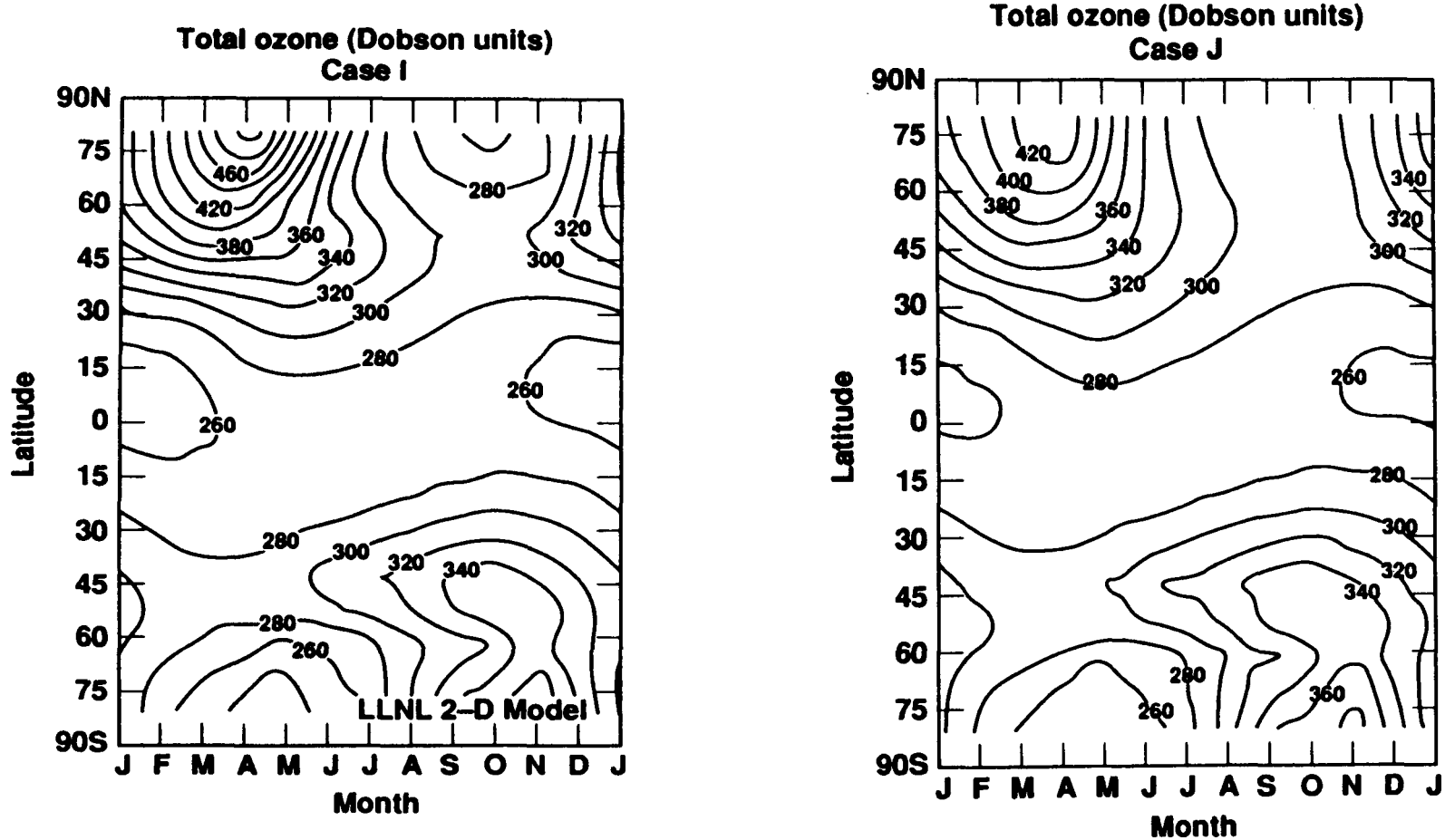

Figure 6.8e,f. Column ozone (Dobson units) as a function of latitude and time of the year. Calculated by the LLNL two-dimensional model (1985 reference atmosphere), where: (e) eddy diffusion case I and (f) eddy diffusion case J.

only transported species in the model. In the LLNL two-dimensional model, the complete set of reactions from the oxygen, hydrogen, nitrogen and chlorine families are considered. In Figure 6.8-c, case G, the effects of large horizontal diffusion show the tendency to spread the O_3 contours out, reducing the winter O_3 maximum, and increasing the equatorial minimum. This effect on O_3 was also observed by Schneider et al. 1989 . For case H (medium horizontal diffusion), Figure 6.8-d, the diffusion is reduced by approximately a factor of three. This corresponds approximately to case B, Figure 6.8-b. Like case B, the magnitude of the northern hemispherical maximum compares well to the observed value. In the southern hemisphere, for case H, even with seasonal and latitudinal variability prescribed in the horizontal diffusion coefficient (K_{yy}), the maximum column O_3 did not form off the pole. For case I, where the diffusion in the stratosphere is 2×10^8 cm^2 s^{-1} in both hemispheres, two interesting features are present. First, the magnitude of column O_3 (500 Dobson Units maximum) in the northern hemisphere increases dramatically, due to less O_3 diffusing into the southern hemisphere. Second, the O_3 maximum in the southern hemisphere is forming at lower latitudes, away from the pole. If Antarctic O_3 chemistry were included in the model, the O_3 column contours possibly would close completely, forming the observed effect. In section 6.4.1, it was shown that case I (small horizontal diffusion) was not a good choice for eddy diffusion in the LLNL two-dimesional model, however case J, adequately represented the observed profiles of carbon-14 at long times. Case J, had values for K_{yy} in the northern and southern hemispheres of 2×10^9 cm^2 s^{-1} and 2×10^8 cm^2 s^{-1} respectively. This increased diffusion in the northern hemisphere reduced the magnitude of column O_3 from 500 Dobson units to 420 Dobson Units, while still representing the distribution in the southern hemispheres (Figure 6.8-f).

6.4.5 Perturbation Study: Aircraft Injection at 20 km

When using models to predict future effects on O_3 or climate, the sensitivity of uncertainties in the eddy diffusion coefficients should be considered. In chapter 4, numerous scenarios were conducted to better understand the effects of NO_x from aircrafts using the LLNL one- and two-dimensional models. When comparing the results of both models, it was noticed that the lifetime for NO_x in the atmosphere for an injection at 19.5 km (see Table 4.4), was over twice as long in the one-dimensional model compared to the two-dimensional model. In Figures 6.9-a and 6.9-b, the eddy diffusion representation of cases A and B were considered respectively. The scenario in each case corresponded to a global injection (1.8×10^{12} g yr^{-1} as NO_2) of NO_x at 19.5 km. In comparing the results of the two scenarios, case B, which has a smaller K_{zz} values in the troposphere and a sharper transition region at the tropopause, increased the NO_x lifetime. As mentioned in section 6.4.1, this has the effect of lowering the tropopause for case B relative to case C. Specifically for case B relative to case A, the NO_x that is omitted is in a region where the K_{zz} coefficient is smaller (e.g., 1×10^3 cm^2 s^{-1}) instead of the transition region where the magnitude increases by a larger factor. Increasing the NO_x lifetime increases the magnitude of the ozone reduction in the global atmosphere. In Table 4.5, the lifetime for NO_y and the percent change in global-averaged column ozone is shown. The NO_y lifetime increased from 1.0 to 1.9 years for cases A and B respectively. At the same time the percent change in global-averaged column ozone decrease from -2.6 to -7.2 for cases A and B respectively.

In summary, for perturbation scenarios it is important to consider the uncertainties in the diffusion representation, especially for the upper troposphere and lower stratosphere, where the magnitudes of the K_{zz} coefficients change rapidly with altitude.

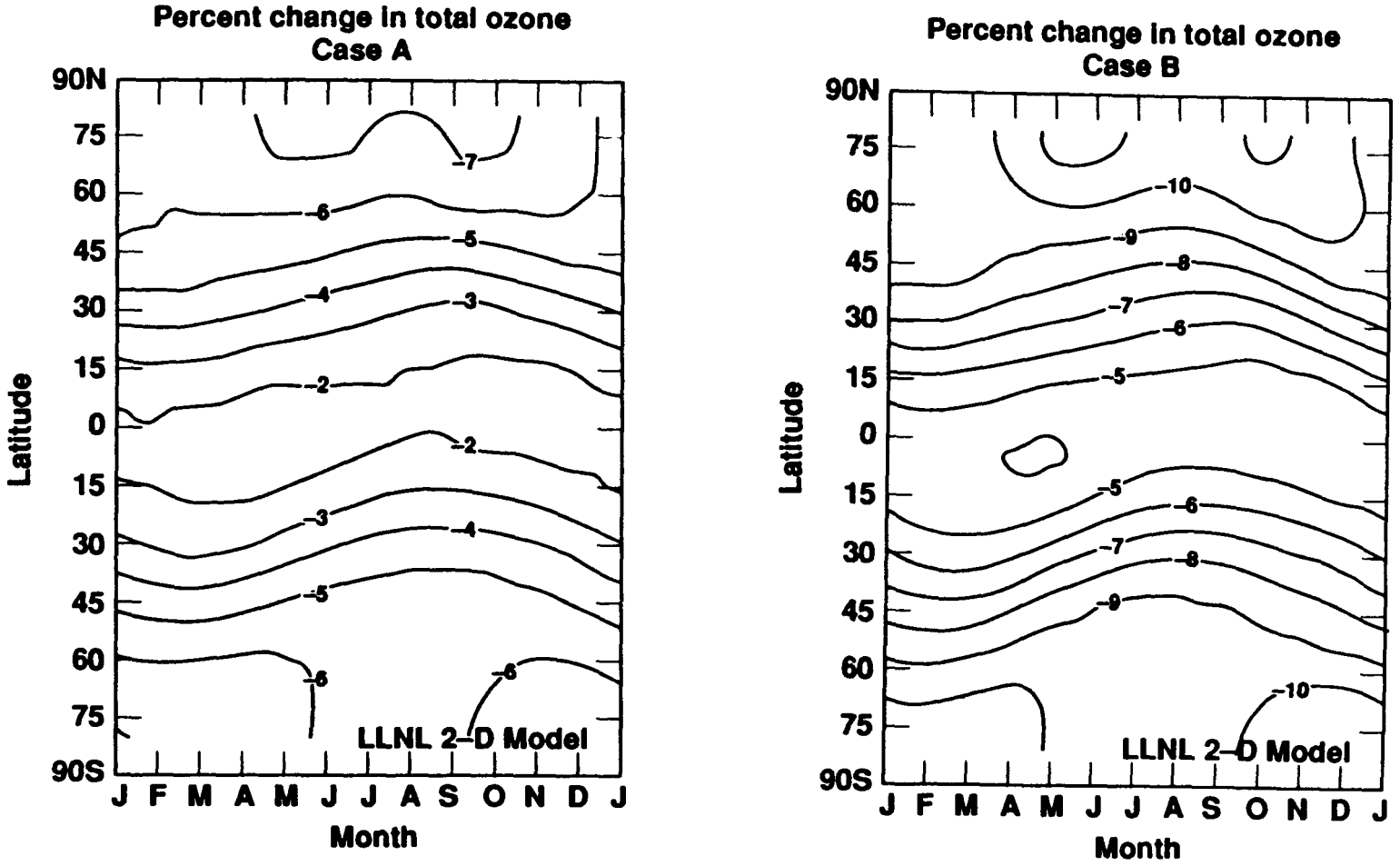

Figure 6.9a,b. Percent change in column ozone for a global injection of 1.8 MT yr^{-1} of NO_2 at 19.5 km, where: (a) eddy diffusion case A and (b) eddy diffusion case B.

6.5 Conclusion

(1) The better fit to the carbon-14 tracer was case B (relative to case A), which had a sharp transition for both K_{yy} and K_{zz} at the tropopause and smaller diffusion in the troposphere. This has the effect of lowering the tropopause height for case B relative to case A.

(2) The LLNL two-dimensional model tropopause height and the strontium-90 tracer show good agreement at 31° N, 9° N, and 31° S. At 64° N, the tropopause height of the observed profile is lower than that calculated by the model.

(3) Seitz [1968] bomb cloud stabilization heights with case B eddy diffusion representation, compared the best to the observed carbon-14 October 1963 initial condition supplied by Johnston [1989].

(4) The column-ozone distribution compares best to observations with medium horizontal diffusion (e.g., $K_{yy} = 2 \times 10^9$ cm^2 s^{-1}).

(5) In one scenario (case J), varing the horizontal diffusion between hemispheres (2×10^9 cm^2 s^{-1}, tended to pull the maximum column-ozone off the pole in the southern hemisphere, which corresponds to similiar observations by ground based and satellite data.

(6) A perturbation study, which injected NO_x globally at 19.5 km, increased the NO_y lifetime for the eddy diffusion representation of case B (1.9 years) relative to case A (1.0 years). In the same scenario, column-ozone decreased 2.6 and 7.2 percent for cases A and B respectively.

Chapter 7: Summary and Conclusion

In this study, the naturally-occurring and anthropogenic trace gases emitted into the troposphere and stratosphere have been examined for their effects on global atmospheric chemical and physical processes. The LLNL one- and two-dimensional models were used to study the interaction between the individual species from the four major chemical families (O_x, HO_x, NO_x, and Cl_x). The outcome was an improved understanding of these mechanisms and their importance in global atmospheric chemistry. The model was also applied to specific scenarios, where observational data could be compared with the model-derived concentrations of relevant gases, and the performance of the model and the accuracy of the data could be scrutinized. The combination of detailed sensitivity calculations coupled with realistic scenarios strengthens the credibility of the model and its uses in future perturbations. There are many findings in the studies presented here that contribute to the understanding of atmospheric processes. In the discussion below, I will try to elucidate some of these findings.

In Chapter 3, the purpose was to broadly reinvestigate NO_x-Cl_x interactions relative to O_3 control in the stratosphere, using the long-established LLNL one-dimensional model. To obtain perspective on reasonably expected atmospheric perturbations, this study includes unrealistic conditions in the calculations, and several interesting and/or unexpected features were found: (i) By varying both NO_x and Cl_x over wide ranges, regions were found where ozone-column reduction is linear and non-linear in added chlorine or in added nitrogen oxides. (ii) If the stratosphere had much less NO_x than the natural amount, small chlorine increases would cause large reductions of O_3. (iii) At high Cl_x, a region of NO_x-Cl_x space is found where added NO_x (at constant Cl_x) increases the O_3 column,

but no region was found where added chlorine (at constant nitrous oxide boundary condition) increases the O_3 column. (iv) The solar self-healing effect in response to O_3 reduction by increasing Clx is much greater than that associated with O_3 reduction by increasing nitrous oxide. (v) For any fixed amount of Cl_x, the amount of chlorine nitrate in the stratosphere is decreased by added NO_x; this unsuspected result is explainable in terms of NO_x and Cl_x chemical interactions. (vi) Any increase of stratospheric Cl_x shrinks the rate profile of O_3 destruction by NO_x, and any increase of nitrous oxide shrinks the rate profile of O_3 destruction by Cl_x. (vii) Total O_3 decreases linearly with increasing Cl_x until the rate of ClO + O exceeds that of NO_2 + O below about 30 km, and then it becomes non-linear with downward curvature. (viii) Removal of all Cl_x and all HO_x from the stratosphere has only a slight effect on the magnitude and shape of the altitude profile of the rate of O_3 destruction by NO_x. (ix) The NO_x and HO_x families almost completely suppress the effect of 1 ppb chlorine on O_3; but in the absence of NO_x and HO_x, even 1 ppb chlorine is a powerful ozone-destroying catalyst from the bottom to the top of the stratosphere. (x) In its altitude flexibility, Cl_x destruction of O_3 is qualitatively different from NO_x and HO_x destruction of O_3.

In Chapter 4, a sensitivity study was carried out using the LLNL one-dimensional and two-dimensional chemical-radiative-transport models of the global atmosphere to examine possible effects of future aircraft NO_x emissions on stratospheric O_3. A broad range in magnitude, altitude, and latitude of the assumed NO_x emissions were examined. Major findings of this initial study are: (i) Significant decreases in the total O_3 column and in local stratospheric O_3 can result from stratospheric NO_x emissions. (ii) Larger reductions of total O_3 are found as the altitude of emission increases, until a maximum effect is calculated near an injection altitude of about 25 $\pm$ 2 kilometers. Above this injection altitude, effects

on O_3 decrease slowly with altitude. (iii) For very large Cl_x concentrations, the NO_x emissions can partially counteract the effects of the large Cl_x concentration on O_3, but this relationship only occurs in a highly Cl_x perturbed stratosphere where O_3 is already greatly depleted. (iv) Effects of water vapor emissions at a factor of 90 greater than the NO_x emissions is negligible compared to the effects of the assumed NO_x emissions. (v) Doubling methane weakly diminishes the effect of injected NO_x on O_3. (vi) In the two-dimensional model, maximum effects on total O_3 due to NO_x emitted at mid-latitudes occur at the poles, with the season of the maximum effect depending on the altitude of the NO_x emissions. (vii) Global reduction of O_3 due to NO_x emissions are smaller in the two-dimensional model than in the one-dimensional model. (viii) According to case A eddy diffusion in the two-dimensional model, the extra stratospheric NO_x from an injection of NO_x at 1.8 Mt yr^{-1} at 19.5 km has a 1.0 year stratospheric residence time and reduces global ozone by 2.6 percent. According to case B, NO_x from this injection rate has a 1.9 year stratospheric residence time and reduces ozone by 7.2 percent. The one-dimensional model using the same injection rate at 20 km calculates a 10 percent decrease in ozone with an NO_y lifetime of 2.7 years.

In Chapter 5, the LLNL one- and two-dimensional models were used to investigate past trends in O_3 and temperature. The following atmospheric constituents were compared to observational data (ground based, airplane, balloon, and satellite): O_3, N_2O, CH_4, NO_y, HNO_3, Cl_y, and HCl. There were many comparisons, too numerous to recapitulate them all, between the observed data and that calculated by the LLNL two-dimensional model. In general, the model and the observed data compare well; however, there were several notable exceptions, including: (i) Like other two-dimensional models the calculated O_3 mixing ratio in the upper

stratosphere is too low compared to observed data. (ii) The ozone-column calculated by the model does not show the spring time maximum in the southern hemisphere forming off the pole. The northern hemisphere winter maximum is 40 Dobson units too low. In the equatorial region, the model overestimates the ozone-column by as much as 20 Dobson units. (iii) There is a large discrepency between the model calculated mixing ratio of N_2O and that derived from SAMS at 30 km (model is low). Above 30 km the agreement is satisfactory. (iv) CH_4 derived from *in situ* data is lower than that calculated by the model (mid-latitudes, northern hemisphere). (v) NO_y calculated by the model is greater than that determined from available LIMS data at 40 km. At 29 km the model underestimates the mixing ratio of NO_y. (vi) The winter local HNO_3 mixing ratio maximum is not modeled correctly due to the heterogeneous processes not considered in the chemical reaction set.

The trends in O_3 and temperature due to varying the trace gases, 11 year solar sunspot cycle, and injections of NO_x from the nuclear test series showed many interesting features. Some of the main finding are: (i) Large decreases in O_3 were calculated (up to 12 percent at high latitudes using Peterson bomb stabilization cloud heights and case A eddy diffusion representation) from NO_x injected by nuclear explosion on or above the surface from the nuclear test series. (ii) Comparisons with statistical analysis of the Dobson network showed good agreement between model and observed data. The northern hemispheric yearly averaged decrease calculated by the model was -3.5 and -2.6 for Peterson [1970] and Seitz [1968]. Reinsel [1981], using time series analysis, concluded that a 2–4.5 percent northern hemispheric decrease due to the nuclear tests would not be inconsistent with the Dobson network record. (iii) The decrease in ozone-column calculated by the model at three latitudinal bands was compared to Dobson

network data analyzed by Harris et al. [NASA-WMO, 1989]. The model calculated decrease was higher in all three bands than the observed data would suggest, but compared well in terms of relative decrease with latitude. Individual stations gave a better comparison with the observed Dobson record. (iv) A local O_3 maximum was calculated to have occurred in spring of 1963, well after the nuclear tests were concluded. This was attributed to the excess NO_x being converted to HNO_3 and N_2O_5 at high latitudes during the winter season, and being released due to photolysis at later times. Measurements were not sufficiently accurate to determine these differences. (v) The trend in ozone-column between 1970 and 1980 was within the statistical limits of the analyzed trend from the Dobson network. (vi) Between 1970 and 1980, local O_3 was measured to have changed between 3–5 percent (depending on study) at 40 km; the model gives for the same altitude a 3–8 percent change depending on latitude. (vii) The temperature change calculated by the model between 1970 and 1980 is less than observations interpreted by Angell [1982] (e.g., the model calculates a temperature change of -1.75 K between 45–50 km, and the observed temperature change at the same altitude was between -1.5 and -3.0 K). (viii) The trend between 1970 and 1986 shows a seasonal inconsistency between that calculated by the model and the analysis of Harris et al. [NASA-WMO, 1989]. In the northern hemisphere, between 53–63° N, the observed data showed a large percent change in O_3 for the winter season (-6.2 ± 1.5) compared to the summer season (0.4 ± 0.8). The model did not reproduce this result in the above latitude band (approximately -3.5 and -1.5 reduction in O_3 for winter and summer respectively). (ix) In contrast, the model compared well with trends in ozone for the period from 1979–1986. The trend in ozone-column between 1979–1986, with both trace gas and solar variability included, was calculated to have a maximum decrease of 2.5 percent at high latitudes in the winter season northern hemisphere (1.0 percent due to the trace gases and 1.5

percent due to the effect of solar variability). Reinsel et al. [1987] using the data from the Dobson network calculated a northern hemispherical reduction in O_3 of -2.4 percent between 1979 and 1986. (x) The change in local O_3 between 1979 and 1986 compares best with Umkehr data analyzed by DeLuisi et al. [1988]. The model does not calculate the decrease in local O_3 at 25 km that the difference between SAGE I and II analysis observed. The model also overestimates the reduction of O_3 that the difference between SAGE I and II observes at 40 km. Discrepancies between the Umkehr data and analysis of SAGE I and II satellite data are yet unexplained. (xi) The model calculated temperature change between 1979 and 1986 is consistent with the observed decrease in O_3 and the observed temperature measurements over this period. (xii) In the following period, into the near future (1986–1990), the ozone-column is predicted to increase due to the 11 year solar sunspot cycle, and local O_3 is calculated to decrease between 35 and 50 km due to emissions of ClC's.

In Chapter 6, measurements of carbon-14 and strontium-90 tracers, based on the recent analysis by Johnston [1989], were used to help clarify the understanding of transport in the LLNL two-dimensional model. In addition, the model was used to clarifly the bomb cloud stabilization heights of the nuclear test series. The major finding of this study are: (i) In the LLNL two-dimensional model, the best fit to the carbon-14 tracer was for a eddy diffusion representation (K_{yy} and K_{zz}) that showed a sharp transiton at the tropopause (case B, in Appendix B). This had the same effect as lowering the tropopause height. (ii) Strontium-90 and carbon-14 results suggest that the tropopause height in the LLNL two-dimensional model is being represented correctly. Exceptions were at high latitudes (January only for carbon-14), where the tropopause heights observed from the tracer data were lower than that calculate by the two-dimensional model. (iii) Using the eddy

diffusion representation of case B (which compared the best to data supplied by Johnston 1989), it was concluded that Seitz 1968 better represented the bomb cloud stabilization heights produced from the nuclear test series compared to the Peterson 1970 analysis. (iv) The best representation of eddy transport from the carbon-14 studies also gave the best comparison of the ozone-column distributions with TOMS satellite and the ground-based Dobson network data. Results with smaller horizontal diffusion in the southern hemisphere, tended to further improve the comparison with the O_3 data. Cases with either large or small horizontal diffusion showed a bad comparison with the carbon-14 tracer at long-time, while also not giving column-ozone distributions that compare well with observations. (v) A case which had medium horizontal diffusion in the northern hemisphere and small horizontal diffusion in the southern hemisphere, showed the beginnings of forming a column-ozone maximum off the pole. (vi) A perturbation study, which injected NO_x globally at 19.5 km, increased the NO_y lifetime for the best eddy transport representation (1.9 years) relative to using the original diffusion coefficients (1.0 years).

In conclusion, based on calculations using the LLNL two-dimensional chemical-radiative-transport models of the troposphere and stratosphere, the increase in trace gases from natural and anthropogenic sources, will have an impact on the chemical and physical processes that control ozone distribution and temperature structure in the global atmosphere.

Chapter 8. References

Alyea, F. N., D. M. Cunnold, and R. G. Prinn, "Stratospheric ozone destruction by aircraft-induced nitrogen oxides," *Science, 188*, 117–121, 1975.

Andrews, D. G. and M. E. McIntyre, "Planetary waves in horizontal and vertical shear: The generalized Eliassen-Palm relation and the mean zonal acceleration, *J. Atmos. Sci., 33*, 2031–2048, 1976.

Andrews, D. G. and M. E. McIntyre, "Generalized Eliassen-Palm and Charney-Drazin theorems for waves on axisymmetric mean flows in compressible atmospheres, *J. Atmos. Sci., 35*, 175–185, 1978a.

Andrews, D. G. and M. E. McIntyre, "An exact theory of nonlinear waves on a Lagragian mean flow, *J. Atmos. Sci., 89*, 609–646, 1978b.

Angell, J. K. and J. Korshover, "Global analysis of recent total ozone fluctuations," *Mon. Weather Rev., 104*, 63–75, 1976.

Angell, J. K., "Trends in surface and upper air temperatures," in *Interpretation of Climate and Photochemical Models, Ozone and Temperature Measurements*, R. A. Reck and J. R. Hummel (eds.), American Institute of Physics, New York, 241–245, 1982.

Angell, J. K. and J. Korshover, "Global variation in total ozone and layer-mean ozone: An update through 1981," *J. Clim. Appl. Meteor., 22*, 1611–1627, 1983.

Austin, J., E. E. Remsberg, R. L. Jones, and A. F. Tuck, "Polar stratospheric clouds inferred from satellite data," *Geophys. Res. Lett., 13*, 1256, 1986a.

Austin, J., R. R. Garcia, J. M. Russell III, S. Solomon, and A. F. Tuck, "On the atmospheric photochemistry of nitric acid," *J. Geophys. Res., 91*, 5477–5485,

1986b.

Barnett, J. J. and M. Corney, "A middle atmosphere temperature reference model from satellite measurements," *Adv. Space Res., 5,* 125–134, 1984.

Bates, D. R. and M. Nicolet, "The photochemistry of atmospheric water vapor," *J. Geophys. Res., 55,* 301–327, 1950.

Bates, D. R. and P. B. Hays, "Atmospheric nitrous oxide," *Planet. Space. Sci., 15,* 189–197, 1967.

Bauer, E., "A catalog of perturbing influences on stratospheric ozone, 1955-1975," *J. Geophys. Res., 84,* 6929–6940, 1979.

Berg, W. W., P. J. Crutzen, F. E. Grahek, S. N. Gitlen, and W. A. Sedlacek, "First measurements of total chlorine and bromine in the lower stratosphere," *Geophys. Res. Lett., 7,* 937–940, 1980.

Birrer, W. M., "Some critcal remarks on trend analysis of total ozone data," *Pure Appl. Geophys., 112,* 523–532, 1974.

Blake D. R., E. W. Mayer, S. C. Tyler, Y. Makide, D. C. Montague, and F. S. Rowland, "Global increase in atmospheric methane concentrations between 1978 and 1980," *Geophys. Res. Lett., 9,* 477–480, 1982.

Blake, D. R. and F. S. Rowland, "World-wide increases in tropospheric methane, 1978-1983," *J. Atmos. Chem.*, 4, 43–62, 1986.

Blake, D. R. and F. S. Rowland, "Continuing world-wide increase in tropospheric methane, 1978 to 1987," *Science, 239,* 1129–1131, 1988.

Bloomfield, P., G. Oehlert, M. L. Thompson, and S. Zeger, "A frequency domain analysis of trends in Dobson total ozone records," *J. Geophys. Res., 88,* 8512–8522, 1983.

Brasseur G. and S. Solomon, "Aeronomy of the Middle Atmosphere," *Atmospheric Science Library,* D. Reidel Publishing Co., Dordrecht, Holland, 1984.

Brasseur, G., A. De Redder, and C. Tricot, "Stratospheric response to chemical perturbations," *J. Atmos. Chem., 3,* 261–288, 1985.

Brewer, A. W., "Evidence for a world circulation provided by the measurements of helium and water vapour distribution in the stratosphere," *Quart. J. Roy. Meteorol. Soc., 75,* 351–363, 1949.

Callis, L. B., M. Natarajan, and R. E. Boughner, "On the relationship between the greenhouse effect, atmospheric photochemistry, and species distribution," *J. Geophys. Res., 88,* 1401–1426, 1983.

Callis, L. B. and M. Natarajan, "The Antarctic ozone minimum: Relationship to odd nitrogen, odd chlorine, the final warming, and the 11-year solar cycle," *J. Geophys. Res., 91:10,* 771, 1986.

Chang, J. S. and W. H. Duewer, "On the possible effect of NO_x injection in the stratosphere due to past atmospheric nuclear weapons test," paper presented at the AIAA/AMS Meeting, Amer. Inst. of Aeronaut. and Astronaut., Denver, Colo., June 1973. (Also Rep. UCRL-74480, Lawrence Livermore Lab., Livermore, 1973)

Chang, J. S., A. C. Hindmarsh, and N. K. Madsen, "Simulation of chemical kinetics transport in the stratosphere," in *Stiff Differential Systems,* R. A. Willoughby (ed.), Plenum, New York, 51–65, 1974.

Chang, J. S. and Duewer, W. H., "Modeling chemical processes in the stratosphere," *Ann. Rev. Phys. Chem., 30,* 443–469, 1979.

Chang, J. S., W. H. Duewer, and D. J. Wuebbles, "The atmospheric nuclear tests of the 1950s and 1960s: A possible test of ozone depletion theories," *J. Geophys. Res.*, *94*, 1755–1765, 1979.

Chapman, S., "A theory of upper-atmospheric ozone," *Mem. Roy. Soc.*, *3*, 103-125, 1930a.

Chapman, S., "On the annual variations of upper-atmospheric ozone," *Phil. Mag. S.*, *7*, 10, 345–352, 1930b.

Chapman, S., "On ozone and atomic oxygen in the upper-atmosphere," *Phil. Mag. S.*, *7*, *10*, 369–383, 1930c.

Charney, J., *Carbon Dioxide and Climate: A Scientific Assessment*, 33 pp., National Academy Press, Washington, D.C., 1979.

CIAP Monograph 2, "Propulsion effluent in the stratosphere;" Monograph 3, "The stratosphere perturbed by propulsion effluent." U.S. Department of Transportation, Washington, D.C., 1975.

Cicerone, R. J. and J. D. Shetter, "Sources of atmospheric methane: Measurements in rice paddies and a discussion," *J. Geophys. Res.*, *86*, 7203–7209, 1981.

Cicerone, R. J., S. Walters, and S. C. Liu, "Non-linear response of stratospheric ozone column to chlorine injections," *J. Geophys. Res.*, *88*, 3647–3661, 1983.

Connell P. S. and D. J. Wuebbles, "Ozone perturbations in the LLNL one-dimensional model. Calculated effects of projected trends in CFC, CH_4, CO_2, N_2O, and Halons over 90 years," Rep. UCRL-95548, Lawrence Livermore Natl. Lab., Livermore, Calif., 1986.

Connell, P. S., K. E. Grant, and D. J. Wuebbles," Aspects of CFC relative ozone destruction efficiencies determined in the LLNL two-dimensional model," In-

ternational Quadrennial Ozone Symposium, Gottingen, Fed. Rep. of Germany. in press, 1988.

Craig, H. and C. C. Chou, "Methane: The record in polar ice cores," *Geophys. Res. Lett.*, *9*, 1221–1224, 1982.

Crutzen, P. J., "Determination of parameters appearing in the dry and wet photochemical theories for ozone in the stratosphere." *Tellus*, *21*. 368–388, 1969.

Crutzen, P. J., "The influence of nitrogen oxides on the atmospheric ozone content," *Quart. J. Roy. Met. Soc., 96,* 320–325, 1970.

Crutzen, P. J., "Ozone production rates in an oxygen, hydrogen, nitrogen-oxide atmosphere," *J. Geophys. Res., 76,* 7311–7327, 1971.

Crutzen, P. J. and U. Schmailzl, "Chemical budgets of the stratosphere," *Planet. Space Sci., 31,* 1009–1032, 1983.

Crutzen, P. J. and F. Arnold, "Nitric acid cloud formation in the cold Antarctic stratosphere: A major cause for the springtime 'ozone hole'," *Nature, 324,* 651, 1986.

Cunnold, D. M., F. N. Alyea, N. A. Phillips, and R. G. Prinn. "Relative effects on atmospheric ozone of latitude and altitude of supersonic flight," *AIAA Journal, 15,* 337–345, 1977.

DeLuisi, J. J., D. U. Longenecker, C. L. Mateer, and D. J. Wuebbles, "An analysis of northern middle-latitude Umkehr measurements corrected for stratospheric aerosols for 1979–1986," in press, 1988. (Also see Rep. UCRL-100713, Lawrence Livermore Natl. Lab., Livermore, 1988.)

Demore, W. B., J. J. Margitan, M. J. Molina, R. T. Watson, D. M. Golden, R. F. Hampson, M. J. Kurylo, C. J. Howard, and A. R. Ravishankara, "Chem-

ical kinetics and photochemical data for use in stratospheric modeling, Evaluation Number 7," *JPL Publication 85-37,* 226 pp., Jet Propulsion Lab., Pasadena, CA, 1985.

Demore, W. B., J. J. Margitan, M. J. Kurylo, C. J. Howard, and A. R. Ravishankara, "Chemical kinetics and photochemical data for use in stratospheric modeling, Evaluation Number 8" *JPL Publication* 87-41, 196 pp., Jet Propulsion Lab., Pasadena, CA, 1987.

Dobson, G. M. B. and D. N. Harrison, "Measurements of the amount ozone in the earth's atmosphere and its relation to other geo-physical conditions," *Proc. Roy. Soc., 110,* 660-693, 1926.

Drummond, J. R., J. T. Houghton, G. D. Peskett, C. D. Rogers, M. J. Wale, J. Whitney, and E. J. Williamson, "The stratospheric and mesospheric sounder on Nimbus 7," *Phil. Trans. Roy. Soc. London, A296,* 219-241, 1980.

Duewer, W. H., D. J. Wuebbles, H. W. Ellsaesser, J. S. Chang, NO_x catalytic ozone destruction: Sensitivity to rate coefficients, *J. Geophys. Res., 82,* 935-942, 1977.

Dunkerton, T., "On the mean meridional mass motions of the stratosphere and mesosphere, *J. Atmos. Sci., 35,* 2325-2333, 1978.

Ehhalt, D. H., "Methane in the global atmosphere," *Environment, 27 (10):6-12,* 30-33, 1985.

Environmental Protection Agency, "Assessing the risks of trace gases that can modify the stratosphere," Rep. 400/1-871001A, Vol 1, 1987.

Environmental Protection Agency, "Future concentrations of stratospheric chlorine and bromine," Rep. 400/1-88/005, 1988.

Fabian, P., R. Borchers, G. Flentje, W. A. Matthews, W. Seiler, H. Giehl, K. Bunse, F. Muller, U. Schmidt, A. Volz, A. Khedim, and F. J. Johnen, "The vertical distribution of stable trace gases at mid-latitudes," *J. Geophys. Res.*, *86*, 5179–5184, 1981.

Fabry, C. and Buisson, M., "L' absorption de l'ultraviolet par l'ozone et la limite du spectre solaire," *F. Phys. Rad.*, *5*, 196–206, 1913.

Fabry, C., "Etudede l'extremite ultraudetle du spectre solaire," *F. Phys. Rad.* *6*, 197–226, 1921.

Farman, J. C., B. G. Gardiner, and J. D. Shanklin, "Large losses of total ozone in Antarctica reveal seasonal ClO_x/NO_x interaction," *Nature*, *315*, 207–210, 1985.

Foley, H. M., and M. A. Ruderman, "Stratospheric NO production from past nuclear explosions," *J. Geophys. Res.*, *78*, 4441–4450, 1973.

Fraser, P. J., J. A. K. Khalil, R. A. Rasmussen, and A. J. Crawford, "Trends of atmosphereic methane in the southern hemisphere," *Geophys. Res. Lett.*, *9*, 461–464, 1982.

Frederick, J. E. and R. J. Cicerone, "Dissociation of metastable O_2 as a potential source of atmospheric odd oxygen," *J. Geophys. Res.*, *90*, 10733–10738, 1985.

Froidevaux, L., M. Allen, S. Berman, and A. Daughton, "Analysis of LIMS observations in the upper stratosphere and lower mesosphere, I. The mean O_3 profile and its temperature sensitivity at mid-latitudes in May, 1979," 1985.

Gallagher, C. C., C. A. Forsberg, A. S. Mason, B. W. Gandrud, and M. Janghorbani, "Total chlorine content in the lower stratosphere," *J. Geophys. Res.*, *90*, 10747–10752, 1985.

Garcia, R. R., and S. Solomon, "A numerical model of the zonally averaged dynamical and chemical structure of the middle atmosphere," *J. Geophys. Res.*, *88*, 1379–1400, 1983.

Garcia, R. R., and S. Solomon, "The effect of breaking gravity waves on the dynamics and chemical composition of the mesosphere and lower thermosphere," *J. Geophys. Res.*, *90*, 3850–3868, 1985.

Gear, C. W., "The Automatic Integration of Stiff Ordinary Differential Equations," *Proc. Int. Fed. Inform. Proc. Congr.*, New York, Humanities Press, P. A–81, 1968.

Gille, J. C., J. M. Russell III, P. L. Bailey, E. E. Remsberg, L. L. Gordley, W. F. J. Evans, H. Fischer, B. W. Gandrud, A. Girard, J. E. Harries, and S. A. Beck, "Accuracy and precision of the nitric acid concentrations determined by the Limb Infrared Monitor of the Stratosphere experiment on NIMBUS 7," *J. Geophys. Res.*, *89*, 5179–5190, 1984.

Gilmore, F. R., "The production of nitrogen oxides by low-altitude nuclear explosions," *J. Geophys. Res.*, *82*, 674–681, 1977.

Goldsmith, P., A. F. Tuck, J. S. Foot, E. L. Simmons, and R. L. Newson, "Nitrogen oxides, nuclear weapon testing, Concorde and stratospheric ozone," *Nature*, *244*, 545–551, 1973.

Gotz, F., P. W. Meetham, A. R., and Dobson, G. M. B., "The vertical distribution of ozone in the atmosphere," *Proc. Roy. Soc.*, *a145*, 416–446, 1934.

Grant K. E. and D. J. Wuebbles, "Production of NO by galactic rays and lightning," Rep. UCID-21145, Lawrence Livermore Natl. Lab., Livermore, Calif., 1987.

Grant, K. E., K. E. Taylor, J. S. Ellis, and D. J. Wuebbles, "Status of solar and infrared radiation submodels in the LLNL one and two-dimensional chemical-transport models," Rep. UCID-21146, Lawrence Livermore Natl. Lab., Livermore, Calif., 1987.

Grant, K. E. and D. J. Wuebbles, "A two-dimensional modeling study of the sensitivity of ozone to radiative flux uncertainties," International Quadrennial Ozone Symposium, Gottingen, Fed. Rep. of Germany, in press, 1988.

Guthrie, P. D., C. H. Jackman, J. R. Herman, and C. J. McQuillan, "A diabatic circulation experiment in a two-dimensional photochemical model," *J. Geophys. Res.*, *89*, 9589-9602, 1984.

Haight, J. D. and J. A. Pyle, "Ozone perturbation experiments in a two-dimensional circulation model," *Quart. J. Roy. Meteorol. Soc.*, *110*, 167–185, 1984.

Hampson, J., "Photochemical behavior of the ozone layer," *Can. Armament Res. and Development Establishment,* TN1627/64, 1964.

Harwood, R. S., and J. A. Pyle, "A two-dimensional mean circulation model for the atmosphere below 80 km," *Quart. J. Roy. Meteorol. Soc., 101,"* 723–747, 1975.

Heath, D. F. and B. M. Schlesinger, "Temporal variability of uv solar spectral irradiance form 160–400 nm over periods of the evolution and rotation of active regions from maximum to minimum phases of the sunspot cycle," In IRS 1984: *Current Problems in Atmospheric Radiation*, edited by G. Fiocco, A. Deepak Publishing, Hampton, VA, 1984.

Heath, D. F. and B. M. Schlesinger, "The Mg 280-nm doublet as a monitor of changes in solar ultraviolet irradiance," *J. Geophys. Res., 91,* 8672–8628, 1986.

Herman, J. R. and C. J. McQuillan, "Atmospheric chlorine and stratospheric ozone nonlinearities and trend detection," *J. Geophys. Res.*, *90*, 5721–5732, 1985.

Hindmarsh, A. C., "Linear multistep methods for ordinary differential equations: Method formulations, stability, and the methods of Nordsieck and Gear," Rep. UCRL-51186, Lawrence Livermore Natl. Lab., Livermore, Calif., 1972.

Hindmarsh, A. C., "Preliminary documentation of GEARBI: Solution of ODE systems with block-iterative treatment of the jacobian," Rep. UCID-30149, Lawrence Livermore Natl. Lab., Livermore, Calif., 1976.

Holton, J. R., "An advective model for two-dimensional transport of stratospheric trace species," *J. Geophys. Res.*, *86*, 11989–11994, 1981.

Houghton, J. T., F. W. Taylor, and C. D. Rodgers, "Remote Sounding of Atmospheres," *Cambridge Planetary Science Series 5*, Cambridge University Press, Cambridge, New York, 1984.

Hunt B. G., "Photochemistry of ozone in a moist atmosphere," *J. Geophys. Res. 71, 5*, 1385–1398, 1966.

Isaksen, I. S. A. and F. Stordal, "Ozone perturbations by enhanced levels of CFCs, N_2O, and CH_4: A two-dimensional diabatic circulation study including uncertainty estimates," *J. Geophys. Res.*, *91*, 5249–5263, 1986.

Jackman, C. H., P. D. Guthrie, and J. A. Kaye, "An intercomparison of nitrogen-containing species in Nimbus 7 LIMS and SAMS data," *J. Geophys. Res.*, *92*, 995–1008, 1987.

Jackman, C. H., P. A. Newman, P. D. Guthrie, and M. R. Schoeberl, "Effect of computed horizontal diffusion coefficients on two-dimensional N_2O model distributions, *J. Geophys. Res.*, *93*, 5213–5219, 1988.

Johnston, H. S.. "Reduction of stratospheric ozone by nitrogen oxide catalysts from supersonic transport exhaust, *Science, 173*, 517–522, 1971.

Johnston, H. S., G. Whitten, and J. Birks, "Effect of nuclear explosions on stratospheric nitric oxide and ozone." *J. Geophys. Res.*, *78*, 6107–6135, 1973.

Johnston, H. S. "Global ozone balance in the natural stratosphere," *Rev. of Geophys. and S. Phys.*, *13*, 5, 637–649, 1975.

Johnston, H. S., D. Kattenhorn, and G. Whitten, "Use of excess carbon 14 data to calibrate models of stratospheric ozone depletion by supersonic transports," *J. Geophys. Res.*, *81*, 368–380, 1976.

Johnston, H. S., "Expected short-term local effect of nuclear bombs on stratospheric ozone," *J. Geophys. Res.*, *82*, 3119–3124, 1977.

Johnston, H. S. and J. Podolske, "Interpretations of stratospheric photochemistry," *Rev. of Geophy. and S. Phys.*, *16*, *4*, 491–519, 1978.

Johnston, H. S., "Odd nitrogen processes," *Stratospheric Ozone and Man, Vol I*, CRC Press, Inc, Boca Raton, Florida, Chapter 4, 87–140, 1982.

Johnston, H. S., "Proposed use of excess carbon-14 data to test two-dimensional stratospheric models," in press, 1989.

Johnston, H. S., D. E. Kinnison, and D. J. Wuebbles, "Nitrogen oxides from high altitude aircraft: An update of potential effects on ozone, in press, 1989.

Jones, R. L. and J. A. Pyle, "Observations of CH_4 and N_2O by the Nimbus 7 SAMS: A comparison with in-situ data and two-dimensional numerical model calculations," *J. Geophys. Res.*, *89*, 5263–5279, 1984.

Keeling, C. D., R. B. Bacastow, and T. P. Whorf, "Measurements of the concentration of carbon dioxide at Mauna Loa Observatory, Hawaii," in *Carbon*

Dioxide Review: 1982, W. C. Clark (ed.), Oxford University Press, New York, 377–385, 1982.

Khalil, M. A. K. and R. A. Rasmussen, "Secular trends of atmospheric methane," *Chemosphere*, *11*, 877–883, 1982.

Khalil, M. A. K. and R. A. Rasmussen, "Increases and seasonal cycles in the atmospheric concentration of nitrous oxide." *Tellus*, *35B*, 1961–1969, 1983.

Kida, H., "General circulation of air parcels and transport characteristics from a hemispheric GCM, Part 1. A determination of advective mass flow in the lower stratosphere," *J. Meteorol. Soc. Japan*, *61*, 171–188, 1983.

Kiehl, J. T. and S. Solomon, "On the radiative balance of the stratosphere," *J. Atmos. Sci.*, *43*, 1525–1534, 1986.

Kinnison, D. E., H. S. Johnston, and D. J. Wuebbles, "Ozone calculations with large nitrous oxide and chlorine changes," *J. Geophy. Res.*, *93*, 14165–14175, 1988a.

Kinnison, D. E., D. J. Wuebbles, and H. S. Johnston, "A study of the sensitivity of stratospheric ozone to hypersonic aircraft emissions." First International Conference on Hypersonics Flight in the 21st Century, Grand Forks, North Dakota, 1988b.

Kinnison, D. E., H. S. Johnston, and D. J. Wuebbles, "Sensitivity study of global ozone to NO_x emission from aircraft," International Quadrennial Ozone Symposium, Gottingen, Fed. Rep. of Germany, in press, 1988c.

Ko, M. K. W., K. K. Tung, D. K. Weinstein, and N. D. Sze, "A zonal-mean model of stratospheric tracer transport in isentropic coordinates: Numerical simulations for nitrous oxide and nitric acid," *J. Geophys. Res.*, *90*, 2313–2329, 1985.

Komhyr, W. D., E. W. Barrett, G. Slocum, and H. K. Weickmann, "Atmospheric total ozone increase during the 1960's," *Nature, 233*, 390–391, 1971.

Kondratyev, K. Y. and G. A. Nikolsky, "Possible climatic impacts of a nuclear war." *Climate Shocks: Natural and Anthropogenic*, Wiley Series in Climate and the Biosphere, edited by M. H. Glantz and R. E. Dickerson, 173–221, New York, 1988.

Lean, J., "Solar ultraviolet irradiance variations: A review," *J. Geophys. Res., 92*, 839–868, 1987.

Luther, F. M., D. J. Wuebbles, W. H. Duewer, and J. S. Chang, "Effect of multiple scattering on species concentrations and model sensitivity," *J. Geophys. Res., 83*, 3563–3570, 1978.

Luther, F. M., Chang, J. S., Duewer, W. H., Penner, J. E., Tarp, R. L., and Wuebbles, D. J., "Potential environmental effects of aircraft emissions," Rep. UCRL-52861, Lawrence Livermore Natl. Lab., Livermore, Calif., 1979.

Mahlman, J. D. and S. B. Fels, "Antarctic ozone decreases: A dynamical cause," *Geophys. Res. Lett., 13,* 1316, 1986.

Matthews, E. and I. Fung, "Methane emissions from natural wetlands: Global distribution, area, and environmental characteristics of sources," *Global Biogeochemical Cycles, 1:* 61–86, 1987.

Matthews, W. A., P. V. Johnston, D. G. Murcray, F. J. Murcray, and R. D. Blatherwick, "Column abundance of hydrogen chloride above Lauder, New Zealand," in press, 1989.

McElroy, M. B., R. J. Salawitch, S. C. Wofsy, and J. A. Logan, "Reductions of Antarctic ozone due to synergistic interactions of chlorine and bromine," *Nature, 321*, 759–762, 1986.

McElroy, M. B. and S. C. Wofsy, "Tropical Forests: Interactions with the atmosphere," in *Symposium Volumn, Tropical Forests and World Atmosphere*, G. T. Prance, Westview Press, 1987.

McGrath, W. D. and R. G. W. Norrish, "Studies of the reactions of excited atoms and molecules produced in the flash photolysis of ozone," *Proc. Roy. Soc. London A. 254*, 317, 1960.

McIntyre, M. E. and T. N. Palmer, "Breaking planetary waves in the stratosphere," *Nature, 305,* 593–600, 1983.

Molina, M. J. and Rowland, F. S., "Stratospheric sink for chloro-fluoromethanes: chlorine atom-catalysed destruction of ozone," *Nature, 249,* 810–812, 1974.

Molina, L. T. and M. J. Molina, "Production of Cl_2O_2 by the self reaction of the ClO radical," *J. Phys. Chem., 91,* 433, 1986.

Montreal Protocal, Substances that deplete the ozone layer, *United Nations Environment Programme*, Montreal, 1987.

Murcray, D. G., T. G. Kyle, F. H. Murcray, and W. J. Williams, "Nitric acid and nitric oxide in the lower stratospheric concentrations of HNO_3, *Nature, 218,* 78–79, 1968.

Murcray, F. J., F. H. Murcray, A. Goldman, D. G. Murcray, and C. P. Rinsland, "Infrared measurements of several nitrogen species above the South Pole in December 1980 and November–December 1986," *J. Geophys. Res., 92,* 13373–13376, 1987.

NASA-WMO *Ozone Trends Panel Report,* in press, 1989.

National Reseach Council, "Environmental impact of stratospheric flight: Biological and climate effects of aircraft emissions in the stratosphere," National

Academy Press, Washington, D.C., 1975.

National Reseach Council, "Causes and Effects of Stratospheric Ozone reduction: An update 1981," National Academy Press, Washington, D.C., 1982.

National Research Council, "Causes and Effects of Changes in Stratospheric Ozone: Update 1983," National Academy Press, Washington, D.C., 1984.

Newman, P. A., M. R. Schoeberl, R. A. Plumb, and J. E. Rosenfield, "Mixing rates calculated from potential vorticity," *J. Geophy. Res., 93,* 5221–5240, 1988.

Nicolet, M., "Nitrogen oxides in the chemosphere," *J. Geophys. Res., 70, 3,* 679–689, 1965.

Oehlert, G. W., "Trends in Dobson total ozone: an update through 1983," *J. Geophys. Res., 91,* 2675–2679, 1986.

Owens, A. J., C. H. Hales, D. L. Filkin, C. Miller, J. M. Steed, and J. P. Jesson, "A coupled one-dimensional radiative-convective chemistry-transport model for the atmosphere 1. Model structure and steady-state perturbation calculations," *J. Geophys. Res., 90,* 2283–2311, 1985.

Peterson, K. R., "An empirical model for estimating world-wide deposition from atmospheric nuclear detonations," *Health Physics, 18,* 357–378, 1970.

Plumb, R. A. and J. D. Mahlman, "The zonally averaged transport characteristics of the GFDL general circulation/transport model," *J. Atm. Sci., 44,* 298–327, 1987.

Prabhakara, C., "Effects of non-photochemical processes on the meridional distribution ant total amount of ozone in the atmosphere," *Mon. Weather Rev., 91,* 411–431, 1963.

Prather, M. J., M. B. McElroy, and S. C. Wofsy, "Reductions in ozone at high concentrations of stratospheric halogens," *Nature, 312*, 227–231, 1984.

Prather, M. J., "Continental sources of halocarbons and nitrous oxide," *Nature, 317*, 221–225, 1985.

Pyle, J. A., "A calculation of the possible depletion of ozone by chlorofluorocarbons using a two-dimensional model," *Pure Appl. Geophys., 118*, 355–377, 1980.

Quinn, T. H., Wolf, K. A., Mooz, W. E., Hammitt, J. K., Chesnutt, T. W., and Sarma, S., "Projected use, emissions, and banks of potential ozone depleting substances," N-2282-EPA, Rand Corp., Santa Monica, CA, 1985.

Ramanathan, V., R. J. Cicerone, H. B. Singh, and J. T. Kiehl, "Trace gas trends and their potential role in climate change," *J. Geophys. Res., 90*, 5547–5566, 1985.

Ramanathan, V., L. Callis, R. Cess, J. Hansen, I. Isaksen, W. Kuhn, A. Lacis, F. Luther, J. Mahlman, R. Reck, and M. Schlesinger, "Climate-chemical interactions and effects of changing atmospheric trace gases," *Rev. Geophys., 25*, 1441–1482, 1987.

Rasmussen, R. A. and M. A. K. Khalil, "Atmospheric trace gases: Trends and seasonal cycles," *J. Geophys. Res., 86*, 9826–9832, 1981.

Reinsel, G. C., "Analysis of total ozone data for the detection of recent trends and the effects of nuclear testing during the 1960's," *Geophys. Res. Lett., 8*, 1227–1230, 1981.

Reinsel, G. C., G. C. Tiao, J. L. DeLuisi, C. L. Mateer, A.J. Miller, and J. E. Frederick, "Analysis of upper stratospheric Umkehr ozone profile data for trends and the effects of stratospheric aerosols," *J. Geophys. Res., 89*, 4833–4840, 1984.

Reinsel, G. C., G. C. Tiao, A. J. Miller, D. J. Wuebbles, P. S. Connell, C. L. Mateer, and J. J. DeLuisi, "Statistical analysis of total ozone and stratospheric Umkehr data for trends and solar cycle relationship," *J. Geophys. Res.*, *92*, 2201–2209, 1987.

Reinsel, G. C., G. C. Tiao, S. K. Ahn, M. Pugh, S. Basu, J. J. DeLuisi, C. L. Mateer, A. J. Miller, P. S. Connell, and D. J. Wuebbles, "An analysis of the 7-year record of SBUV satellite ozone data: Global profile features and trends in total ozone," *J. Geophys. Res.*, *93*, 1689–1703, 1988.

Rhine, P. E., L. D. Tubbs, and D. Williams, "Nitric acid vapour above 19 km in the earth's atmosphere," *App. Optics*, *8*, 1500–1501, 1969.

Rinsland, C. P., J. S. Levine, and T. Miles, "Concentration of methane in the troposphere deduced from 1951 solar spectrum," *Nature*, *318*, 245–249, 1985.

Rinsland, C. P., A. Goldman, F. J. Murcray, R. D. Blatherwick, F. H. Murcray, and D. G. Murcray, "Infrared measurements of atmopheric gases above Mauna Loa, Hawaii, in February 1987," in press, *JGR*, 1989.

Robbins, R. C., L. A. Cavanaugh, L. J. Salos, and E. Robinson, "Analysis of ancient atmospheres," *J. Geophys. Res.*, *78*, 5341–5344, 1973.

Rosenfield, J. E., M. R. Schoeberl, and M. A. Geller, "A computation of the stratospheric diabatic circulation using and accurate radiative transfer model," *J. Atmos. Sci.*, *44*, 859–876, 1987.

Rowland, F. S., Spencer, J. E., and Molina, M. J., "Stratospheric formation and photolysis of chlorine nitrate," *J. Phys. Chem.*, *80*, *24*, 2711–2713, 1976.

Schmidt, U., A. Khedim, D. Knapska, G. Kulessa, and F. J. Johnen, "Stratospheric trace gas distributions observed in different seasons," *Adv. Space Res.*, *4*, 131–134, 1984.

Schneider, H. R., M. K. W. Ko, N. D. Sze, G. S. Shi, and W. Wang, "The effects of eddy diffusion, drag, and nonlinear terms on the meridional circulation and ozone distributions in an interactive 2-D Model," submitted to *J. Atm. Sci.*, 1988.

Seitz, H., et al., "Final Report on Project Streak: Numerical Models of transport, diffusion and fallout of stratospheric radioactive material," report nyo-3654-4, Isotopes, Inc., prepared for AEC/DBER, 31 May 1968.

Shimazaki, T. and D. J. Wuebbles, "Time-dependent two-dimensional parameterized model," *Proceedings of the Second Conference on the Climatic Impact Assessment Program,* U.S. Department of Transportation, Washington, D.C., 1972.

Slanger, T. G., L. E. Jusinski, G. B. Black, and G. E. Gadd, "A new laboratory source of ozone and its potential atmospheric implications," *Science, 241,* 945–950, 1988.

Smagorinsky, J., *Carbon Dioxide and Climate: A Second Assessment,* 92 pp., National Academy Press, Washington, D.C., 1982.

Smith, A. K., L. V. Lyjak, and J. C. Gille, "The eddy transport of nonconserved trace species derived from satellite data," *J. Geophys. Res., 93,* 11103–11122, 1988.

Smolarkiewicz, P. K., "A fully multidimensional positive definitive advection transport algorithm with small implicit diffusion," *J. Comp. Phys., 54,* 325–362, 1984.

Solomon, S., J. M. Russell III, M. P. McCormick, D. W. Rusch, and J. M. Zawodny, "Intercomparison of satellite datasets for NO_2 and odd nitrogen photochemistry," 1985.

Solomon, S., R. R. Garcia, F. S. Rowland, and D. J. Wuebbles, "On the depletion of Antarctic ozone," *Nature, 321,* 755–758, 1986a.

Solomon, S., J. T. Kiehl, R. R. Garcia, and W. Grose, "Tracer transport by the diabatic circulation deduced from satellite observations," *J. Atmos. Sci., 43,* 1604–1617, 1986b.

Solomon, S., "The mystery of the Antarctic ozone hole," *Rev. Geophys.*, in press, 1988.

St. John, D., W. H. Bailey, W. H. Fellner, J. M. Minor, and R. D. Sull, "Time series analysis of stratospheric ozone," *Commun. Statist. Theory Methods, 11,* 1293–1333, 1982.

Stolarski, R. S. and R. J. Cicerone, "Stratospheric chlorine: A possible sink for ozone," *Can. J. Chem., 52,* 1610, 1974.

Stolarski, R. S. and A. R. Douglass, "Sensitivity of an atmospheric photochemistry model to chlorine perturbations including considerations of uncertainty propagation," *J. Geophys. Res., 91,* 7853–7864, 1986.

Stolarski, R. S., A. J. Krueger, M. R. Schoeberl, R. D. McPeters, P. A. Newman, and J. C. Alpert, "Nimbus 7 satellite measurements of the springtime Antarctic ozone decrease," *Nature, 322,* 808–811, 1986.

Telegadas, K., "The seasonal stratospheric distribution of cadmium-109, plutonium-238, and strontium-90," *Rep. 184,* pp. 53-118, Health and Safety Lab., U.S. Atomic Energy Comm., Washington, D. C., 1967.

Telegadas, K., "The seasonal stratospheric distribution and inventories of excess carbon-14 from March 1955 to July 1969," *Rep. 243,* pp. 3–86, Health and Safety Lab., U.S. Atomic Energy Comm., Washington, D.C., 1971.

Telegadas, K., J. Gray, Jr., R. E. Sowl, and T. E. Ashenfelter, Carbon-14 measurements in the stratosphere from a balloon-borne molecular sieve sampler," *Rep. 246*, pp. 69–106, Health and Safety Lab., U.S. Atomic Energy Comm., Washington, D.C., 1972.

Telegadas, K., and R. J. List, "Are particulate radioactive tracers indicative of stratospheric motions?," *J. Geophys. Res.*, *74*, 1339–1350, 1969.

Tung, K. K., M. K. W. Ko, J. M. Rodriguez, and N. D. Sze, "Are Antarctic variations a manifestation of dynamics or chemistry?," *Nature*, *333*, 811–813, 1986.

U.S. Standard Atmosphere, 1976, NOAA-S/T76-1562, Supt. of Documents, U.S. Government Printing Office, Washington, D.C., 1976.

Wang W.-C., D. J. Wuebbles, W. M. Washington, R. G. Isaacs, and G. Molnar, "Trace gases and other potential perturbations to global climate," *Rev. Geophys.*, *24*, 110–140, 1986.

Watson, R., and Ozone Trends Panel, M. J. Prather and AD Hoc Theory Panel, and M. J. Kurylo and NASA Panel for Data Evaluation, "Present state of knowledge of the upper atmosphere 1988: An assessment report," NASA Reference Publication 1208, August 1988.

Weiss, R. F., "The temporal and spatial distribution of tropospheric nitrous oxide," *J. Geophys. Res.*,*86*, 7185–7196, 1981.

Widhopf, G. F., L. G. Glatt, and R. S. Kramer, "Potential ozone column increase resulting from subsonic and supersonic aircraft emissions," *Journal of AAIA*, *15*, 1322–1330, 1977.

Widhopf, G. F. and L. G. Glatt, "Two-dimensional description of the natural atmosphere including active water vapor modeling and potential perturbations

due to NO_x and HO_x aircraft emissions." High Altitude Pollution Program. U.S. Department of Transportation, Report No. FAA-E-79-07, Washington, D.C., April 15, 1979.

WMO (World Meteorological Organization), "The Stratosphere 1981. Theory and measurements." Global ozone research and monitoring project. Report No. 11. 1981.

WMO (World Meteorological Organization), Atmospheric ozone: Assessment of out understanding of the processes controlling its present distribution and change." Global ozone research and monitoring project. Report No. 16, 1985.

Wofsy, S. C., McElroy, M. B., and Yung, Y. L., "The chemistry of atmospheric bromine," *Geophys. Res. Lett., 2,* 215–218, 1975.

Wuebbles, D. J., and J. C. Chang, "Sensitivity of time-varying parameters in stratospheric modeling," *J. Geophys. Res., 80,* 2637–2642, 1975.

Wuebbles, D. J., "The LLNL one-dimensional transport kinetic model of the troposphere and stratosphere: 1981," Rep. UCID-19185, Lawrence Livermore Natl. Lab., Livermore, Calif., 1981.

Wuebbles, D. J., "A theoretical analysis of the past variations in global atmospheric composition and temperature," Rep. UCRL-53423, Lawrence Livermore Natl. Lab., Livermore, Calif., 1983.

Wuebbles, D. J., F. M. Luther, and J. E. Penner, "Effect of coupled anthropogenic perturbations on stratospheric ozone," *J. Geophys. Res., 88,* 1444–1456, 1983.

Wuebbles, D. J., M. C. MacCracken and F. M. Luther, "A proposed reference set of scenarios for radiatively active atmospheric constituents," U.S. Department of Energy, Carbon Dioxide Research Division, Technical Report 015, 1984.

Wuebbles, D. J., "Trends in ozone and temperature structure: comparison of theory and measurements," In *Atmospheric Ozone*, edited by C. S. Zerefos and A. Ghazi. D. Reidel Publishing, Dordrecht, Holland, 1984.

Wuebbles, D. J., "Natural and anthropogenic perturbations to the stratosphere," *Rev. Geophys., 25*, 487-493, 1987.

Wuebbles, D. J., P. S. Connell, K. E. Grant, R. Tarp, and K. E. Taylor, "Initial results with the LLNL two-dimensional chemical-radiative-transport model of the troposphere and stratosphere," Lawrence Livermore National Laboratory, UCID-21178, 1987.

Wuebbles, D. J. and J. Edmonds, A primer on greenhouse gases," Carbon Dioxide Research Division, DOE/NBB-83, 1988.

Wuebbles, D. J. and D. E. Kinnison, "A two-dimensional model study of past trends in global ozone," International Quadrennial Ozone Symposium, Gottingen, Fed. Rep. of Germany, in press, 1988.

Wuebbles, D. J., D. E. Grant, P. S. Connell, and J. E. Penner, "The role of atmospheric chemistry in climate change," *APCA Journal, 39*, 1, 22-28, 1989.

Wulf, O. R. and L. S. Deming, "The theoretical calculation of the distribution of photochemically-formed ozone in the atmosphere," *Terr. Mag., 41*, 299-310, 1936.

Appendix A: Supplement to Chapter 5
Trends in Stratospheric Ozone

A.1-a Taken from Bauer 1979.

Nuclear Test Series: 1958–1968

Date	*Country*	*Latitude (North)*	*Yield (Mt)*	*Altitude Range Peterson (km)*	*Altitude Range Seitz (km)*
23 Feb 58	USSR	75	3	15.0–24.0	10.0–20.7
27 Feb 58	USSR	75	3	15.0–24.0	10.0–20.7
28 Apr 58	UK	2	1	12.0–18.0	—
12 May 58	USA	11	1.4^{SB}	13.2–20.4	—
28 July 58	USA	11	8.9^{SB}	18.0–29.0	—
2 Sept 58	UK	2	1	12.0–18.0	—
11 Sept 58	UK	2	1	12.0–18.0	—
10 Oct 58	USSR	75	1	7.5–17.0	7.9–16.0
12 Oct 58	USSR	75	3	11.0–22.0	10.0–20.7
15 Oct 58	USSR	75	3	11.0–22.0	10.0–20.7
18 Oct 58	USSR	75	3	11.0–22.0	10.0–20.7
20 Oct 58	USSR	75	3	11.0–22.0	10.0–20.7
24 Oct 58	USSR	75	3	11.0–22.0	10.0–20.7
25 Oct 58	USSR	75	1	7.5–17.0	7.9–16.0
10 Sept 61	USSR	75	3	11.0–22.0	10.0–20.7
12 Sept 61	USSR	75	3	11.0–22.0	10.0–20.7
14 Sept 61	USSR	75	3	11.0–22.0	10.0–20.7
16 Sept 61	USSR	75	1	7.5–17.0	7.0–16.0
18 Sept 61	USSR	75	1	7.5–17.0	7.9–16.0
20 Sept 61	USSR	75	1	7.5–17.0	7.9–16.0
22 Sept 61	USSR	75	1	7.5–17.0	7.9–16.0

A.1-b Taken from Bauer 1979.

Date	*Country*	*Latitude (North)*	*Yield (Mt)*	*Altitude Range Peterson (km)*	*Altitude Range Seitz (km)*
2 Oct 61	USSR	75	1	7.5–17.0	7.9–16.0
4 Oct 61	USSR	75	3	11.0–22.0	10.0–20.7
6 Oct 61	USSR	75	3	11.0–22.0	10.0–20.7
20 Oct 61	USSR	75	3	11.0–22.0	10.0–20.7
23 Oct 61	USSR	75	25	19.0–37.0	14.5–29.7
30 Oct 61	USSR	75	58	20.0–42.0	16.2–33.1
31 Oct 61	USSR	75	3	11.0–22.0	10.0–20.7
4 Nov 61	USSR	75	3	11.0–22.0	10.0–20.7
2 May 62	USA	2	3	15.0–24.0	—
10 June 62	USA	2	3	15.0–24.0	—
27 June 62	USA	2	11	18.0–31.0	—
30 June 62	USA	2	3	15.0–24.0	—
11 July 62	USA	2	3	15.0–24.0	—
5 Aug 62	USSR	75	38	20.0–41.0	14.7–30.2
20 Aug 62	USSR	75	7	14.0–27.0	11.8–24.3
22 Aug 62	USSR	75	3	11.0–22.0	10.0–20.7
25 Aug 62	USSR	75	7	14.0–27.0	11.8–24.3
27 Aug 62	USSR	75	7	14.0–27.0	11.8–24.3
8 Sept 62	USSR	75	1	7.5–17.0	7.5–17.0
15 Sept 62	USSR	75	7	14.0–27.0	11.8–24.3
16 Sept 62	USSR	75	7	14.0–27.0	11.8–24.3
18 Sept 62	USSR	75	3	11.0–22.0	10.0–20.7

A.1-c Taken from Bauer 1979.

Date	*Country*	*Latitude (North)*	*Yield (Mt)*	*Altitude Range Peterson (km)*	*Altitude Range Seitz (km)*
19 Sept 62	USSR	75	24	18.0–36.0	14.4–29.4
21 Sept 62	USSR	75	3	11.0–22.0	10.0–20.7
25 Sept 62	USSR	75	27	18.0–36.0	14.9–30.1
27 Sept 62	USSR	75	24	18.0–36.0	14.4–29.4
18 Oct 62	USA	17	3	15.0–24.0	—
22 Oct 62	USSR	75	7	14.0–27.0	11.8–24.3
30 Oct 62	USA	17	10	18.0–30.0	—
23 Dec 62	USSR	75	20	19.0–35.0	13.9–28.4
25 Dec 62	USSR	75	3	11.0–22.0	10.0–20.7
17 June 67	China	40	3	12.0–22.0	—
24 Aug 68	France	21 S	2.5	11.0–21.0	—
8 Sept 68	France	21 S	1	10.0–17.0	—
27 Dec 68	China	40	3	12.0–22.0	—

SB = Surface Burst

From Bauer (1979)

A.2-a Percent change in ozone due to the nuclear test series. (case A, eddy diffusion representation)

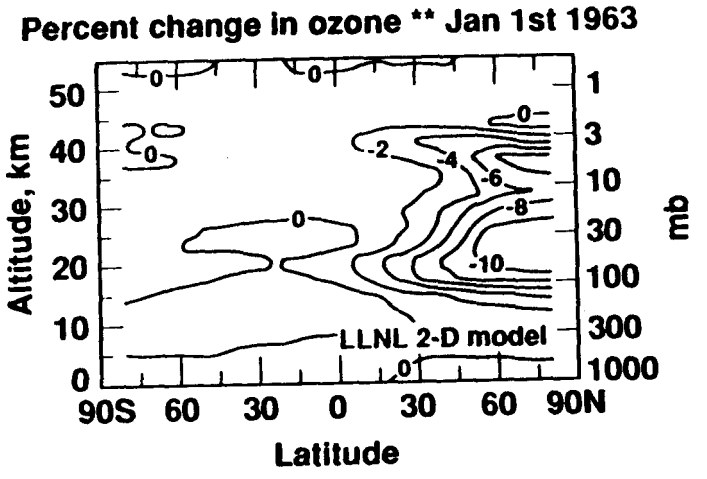

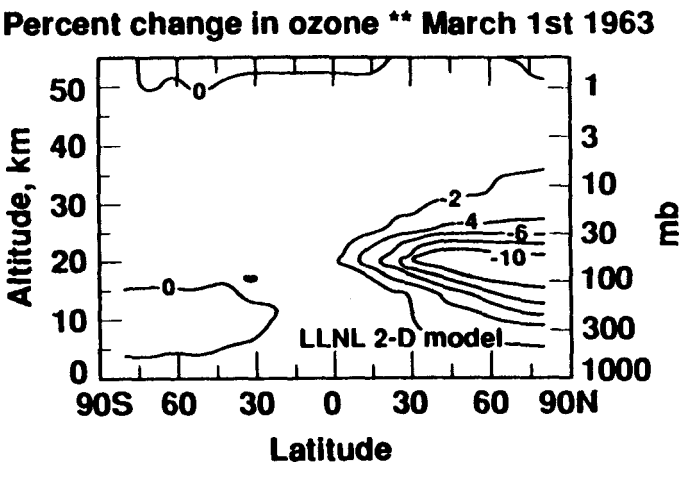

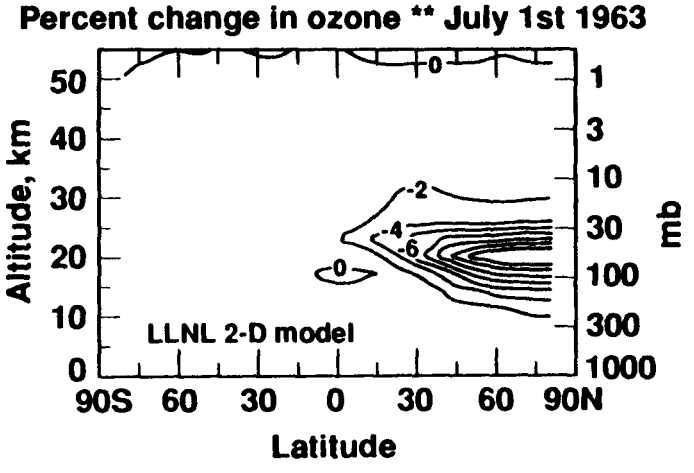

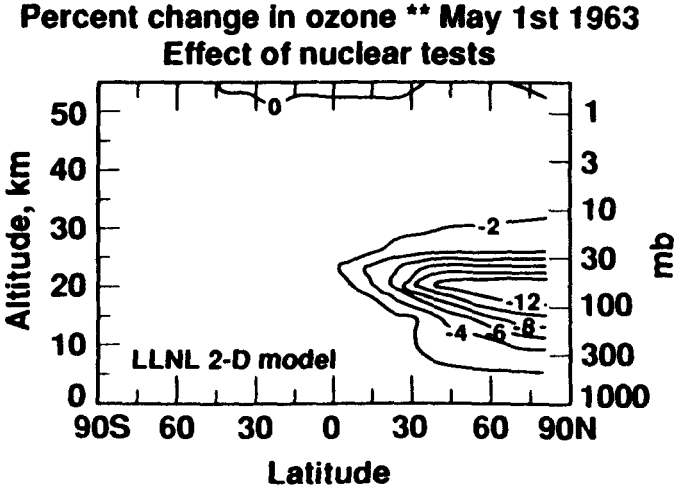

A.2-b Percent change in ozone due to the nuclear test series. (case A, eddy diffusion representation)

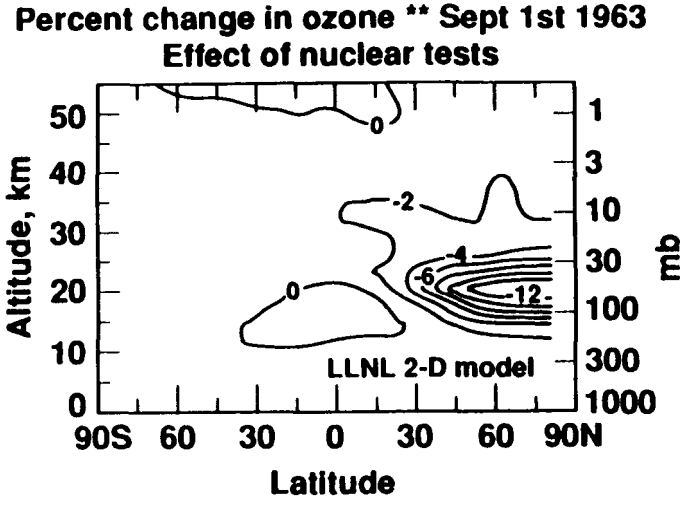

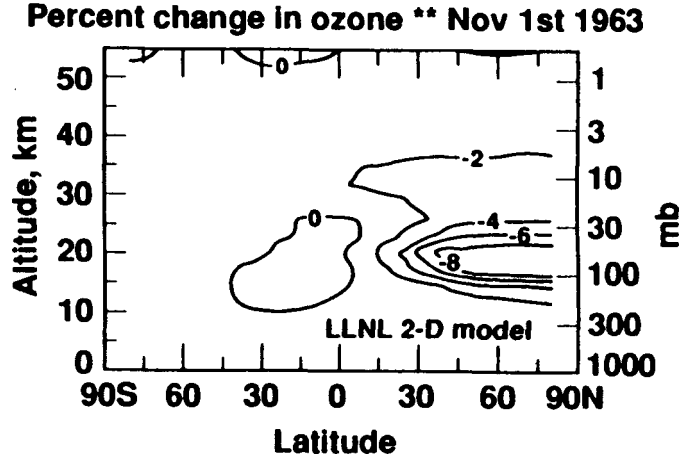

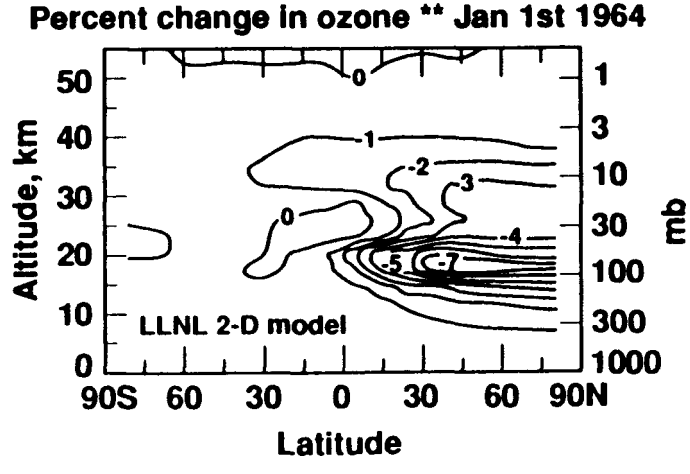

Appendix B: Supplement to Chapter 6
Tracer Study

B.1-a Original data taken from Johnston [1989]. Initial distribution of carbon-14 for October 1963. Relative mixing ratios (10^5 atoms of excess carbon 14 per gram of air). Latitude zones are expressed in units of sine latitude. Altitude zones are expressed in units of km.

c14

	x	-0.985	-0.940	-0.866	-0.766	-0.643	-0.500	-0.342	-0.174	0.000	0.174
1	1.0	5.000e+01	5.000e+01	5.000e+01	5.000e+01	5.000e+01	5.000e+01	5.000e+01	5.000e+01	6.100e+01	7.300e+01
2	2.0	5.000e+01	5.000e+01	5.000e+01	5.000e+01	5.000e+01	5.000e+01	5.000e+01	5.000e+01	6.100e+01	7.300e+01
3	3.0	5.000e+01	5.000e+01	5.000e+01	5.000e+01	5.000e+01	5.000e+01	5.000e+01	5.000e+01	6.100e+01	7.300e+01
4	4.0	5.000e+01	5.000e+01	5.000e+01	5.000e+01	5.000e+01	5.000e+01	5.000e+01	5.000e+01	6.100e+01	7.300e+01
5	5.0	5.000e+01	5.000e+01	5.000e+01	5.000e+01	5.000e+01	5.000e+01	5.000e+01	5.000e+01	6.100e+01	7.300e+01
6	6.0	5.000e+01	5.000e+01	5.000e+01	5.000e+01	5.000e+01	5.000e+01	5.000e+01	5.000e+01	6.100e+01	7.300e+01
7	7.0	5.000e+01	5.000e+01	5.000e+01	5.000e+01	5.000e+01	5.000e+01	5.000e+01	5.000e+01	6.100e+01	7.300e+01
8	8.0	5.100e+01	5.100e+01	5.100e+01	5.100e+01	5.100e+01	5.000e+01	5.000e+01	5.000e+01	6.100e+01	7.300e+01
9	9.0	5.200e+01	5.200e+01	5.200e+01	5.200e+01	5.200e+01	5.000e+01	5.000e+01	5.000e+01	6.100e+01	7.300e+01
10	10.0	5.400e+01	5.400e+01	5.400e+01	5.400e+01	5.400e+01	5.000e+01	5.000e+01	5.000e+01	6.100e+01	7.300e+01
11	11.0	5.500e+01	5.500e+01	5.500e+01	5.500e+01	5.500e+01	5.200e+01	5.000e+01	5.000e+01	6.100e+01	7.300e+01
12	12.0	6.100e+01	6.100e+01	6.100e+01	6.100e+01	6.100e+01	5.400e+01	5.000e+01	5.000e+01	6.100e+01	7.300e+01
13	13.0	6.000e+01	6.000e+01	6.000e+01	6.000e+01	6.000e+01	5.600e+01	5.100e+01	5.000e+01	6.100e+01	7.300e+01
14	14.0	6.500e+01	6.500e+01	6.500e+01	6.500e+01	6.500e+01	6.600e+01	6.600e+01	7.600e+01	7.500e+01	7.500e+01
15	15.0	7.200e+01	7.200e+01	7.200e+01	7.200e+01	7.200e+01	7.200e+01	7.300e+01	8.000e+01	7.700e+01	7.700e+01
16	16.0	8.200e+01	8.200e+01	8.200e+01	8.200e+01	8.200e+01	8.600e+01	8.900e+01	1.000e+02	9.000e+01	1.000e+02
17	17.0	9.300e+01	9.300e+01	9.300e+01	9.300e+01	9.300e+01	1.010e+02	1.090e+02	1.250e+02	1.500e+02	1.750e+02
18	18.0	1.160e+02	1.160e+02	1.160e+02	1.160e+02	1.160e+02	1.220e+02	1.330e+02	1.550e+02	1.750e+02	2.060e+02
19	19.0	1.530e+02	1.530e+02	1.530e+02	1.530e+02	1.530e+02	1.480e+02	1.630e+02	2.000e+02	2.800e+02	4.500e+02
20	20.0	2.350e+02	2.350e+02	2.350e+02	2.350e+02	2.350e+02	2.780e+02	3.300e+02	3.910e+02	4.640e+02	5.500e+02
21	21.0	3.600e+02	3.600e+02	3.600e+02	3.600e+02	3.600e+02	4.300e+02	5.140e+02	6.140e+02	7.330e+02	8.760e+02
22	22.0	3.450e+02	3.450e+02	3.450e+02	3.450e+02	3.450e+02	4.240e+02	5.220e+02	6.430e+02	7.920e+02	9.750e+02
23	23.0	3.200e+02	3.200e+02	3.200e+02	3.200e+02	3.200e+02	3.930e+02	4.840e+02	5.960e+02	7.330e+02	9.020e+02
24	24.0	2.880e+02	2.880e+02	2.880e+02	2.880e+02	2.880e+02	3.540e+02	4.360e+02	5.370e+02	6.600e+02	8.130e+02
25	25.0	2.480e+02	2.480e+02	2.480e+02	2.480e+02	2.480e+02	3.050e+02	3.730e+02	4.620e+02	5.680e+02	6.990e+02
26	26.0	1.960e+02	1.960e+02	1.960e+02	1.960e+02	1.960e+02	2.410e+02	2.960e+02	3.630e+02	4.490e+02	5.530e+02
27	27.0	1.600e+02	1.600e+02	1.600e+02	1.600e+02	1.600e+02	1.970e+02	2.420e+02	2.980e+02	3.680e+02	4.520e+02
28	28.0	1.530e+02	1.530e+02	1.530e+02	1.530e+02	1.530e+02	1.880e+02	2.320e+02	2.830e+02	3.500e+02	4.310e+02
29	29.0	1.470e+02	1.470e+02	1.470e+02	1.470e+02	1.470e+02	1.810e+02	2.230e+02	2.740e+02	3.370e+02	4.150e+02
30	30.0	1.430e+02	1.430e+02	1.430e+02	1.430e+02	1.430e+02	1.760e+02	2.170e+02	2.660e+02	3.280e+02	4.030e+02
31	31.0	1.500e+02	1.500e+02	1.500e+02	1.500e+02	1.500e+02	1.810e+02	2.190e+02	2.640e+02	3.190e+02	3.850e+02
32	32.0	1.700e+02	1.700e+02	1.700e+02	1.700e+02	1.700e+02	1.980e+02	2.300e+02	2.670e+02	3.110e+02	3.610e+02
33	33.0	2.000e+02	2.000e+02	2.000e+02	2.000e+02	2.000e+02	2.230e+02	2.490e+02	2.780e+02	3.100e+02	3.460e+02
34	34.0	2.350e+02	2.350e+02	2.350e+02	2.350e+02	2.350e+02	2.420e+02	2.490e+02	2.570e+02	2.640e+02	2.720e+02
35	35.0	2.500e+02	2.500e+02	2.500e+02	2.500e+02	2.500e+02	2.500e+02	2.500e+02	2.500e+02	2.500e+02	2.500e+02
36	36.0	2.500e+02	2.500e+02	2.500e+02	2.500e+02	2.500e+02	2.500e+02	2.500e+02	2.500e+02	2.500e+02	2.500e+02
37	37.0	2.500e+02	2.500e+02	2.500e+02	2.500e+02	2.500e+02	2.500e+02	2.500e+02	2.500e+02	2.500e+02	2.500e+02
38	38.0	2.500e+02	2.500e+02	2.500e+02	2.500e+02	2.500e+02	2.500e+02	2.500e+02	2.500e+02	2.500e+02	2.500e+02
39	39.0	2.500e+02	2.500e+02	2.500e+02	2.500e+02	2.500e+02	2.500e+02	2.500e+02	2.500e+02	2.500e+02	2.500e+02
40	40.0	2.500e+02	2.500e+02	2.500e+02	2.500e+02	2.500e+02	2.500e+02	2.500e+02	2.500e+02	2.500e+02	2.500e+02
41	41.0	2.500e+02	2.500e+02	2.500e+02	2.500e+02	2.500e+02	2.500e+02	2.500e+02	2.500e+02	2.500e+02	2.500e+02
42	42.0	2.500e+02	2.500e+02	2.500e+02	2.500e+02	2.500e+02	2.500e+02	2.500e+02	2.500e+02	2.500e+02	2.500e+02
43	43.0	2.500e+02	2.500e+02	2.500e+02	2.500e+02	2.500e+02	2.500e+02	2.500e+02	2.500e+02	2.500e+02	2.500e+02
44	44.0	2.500e+02	2.500e+02	2.500e+02	2.500e+02	2.500e+02	2.500e+02	2.500e+02	2.500e+02	2.500e+02	2.500e+02
45	45.0	2.500e+02	2.500e+02	2.500e+02	2.500e+02	2.500e+02	2.500e+02	2.500e+02	2.500e+02	2.500e+02	2.500e+02
46	46.0	2.500e+02	2.500e+02	2.500e+02	2.500e+02	2.500e+02	2.500e+02	2.500e+02	2.500e+02	2.500e+02	2.500e+02
47	47.0	2.500e+02	2.500e+02	2.500e+02	2.500e+02	2.500e+02	2.500e+02	2.500e+02	2.500e+02	2.500e+02	2.500e+02
48	48.0	2.500e+02	2.500e+02	2.500e+02	2.500e+02	2.500e+02	2.500e+02	2.500e+02	2.500e+02	2.500e+02	2.500e+02
49	49.0	2.500e+02	2.500e+02	2.500e+02	2.500e+02	2.500e+02	2.500e+02	2.500e+02	2.500e+02	2.500e+02	2.500e+02
50	50.0	2.500e+02	2.500e+02	2.500e+02	2.500e+02	2.500e+02	2.500e+02	2.500e+02	2.500e+02	2.500e+02	2.500e+02

B.1-b Original data taken from Johnston [1989]. Initial distribution of carbon-14 for October 1963. Relative mixing ratios (10^5 atoms of excess carbon-14 per gram of air). Latitude zones are expressed in units of sine latitude. Altitude zones are expressed in units of km.

c14

	x	0.342	0.500	0.643	0.766	0.866	0.940	0.985
1	1.0	7.300e+01	7.300e+01	7.300e+01	7.300e+01	7.300e+01	7.300e+01	7.300e+01
2	2.0	7.300e+01	7.300e+01	7.300e+01	7.300e+01	7.300e+01	7.300e+01	7.300e+01
3	3.0	7.300e+01	7.300e+01	7.300e+01	7.300e+01	7.300e+01	7.300e+01	7.300e+01
4	4.0	7.300e+01	7.300e+01	7.300e+01	7.300e+01	7.300e+01	7.300e+01	9.500e+01
5	5.0	7.300e+01	7.300e+01	7.300e+01	7.300e+01	7.300e+01	9.100e+01	9.500e+01
6	6.0	7.300e+01	7.300e+01	7.300e+01	7.300e+01	7.300e+01	9.100e+01	9.500e+01
7	7.0	7.300e+01	7.300e+01	7.300e+01	7.300e+01	7.300e+01	9.100e+01	9.500e+01
8	8.0	7.300e+01	7.300e+01	7.300e+01	7.300e+01	7.300e+01	9.600e+01	1.150e+02
9	9.0	7.300e+01	7.300e+01	7.300e+01	7.500e+01	1.000e+02	1.150e+02	1.650e+02
10	10.0	7.300e+01	7.300e+01	7.300e+01	1.300e+02	1.500e+02	1.800e+02	2.200e+02
11	11.0	7.300e+01	7.300e+01	7.300e+01	1.800e+02	2.000e+02	2.500e+02	2.800e+02
12	12.0	7.300e+01	7.300e+01	1.100e+02	2.300e+02	2.500e+02	3.150e+02	3.600e+02
13	13.0	7.300e+01	9.200e+01	1.600e+02	3.500e+02	3.200e+02	3.750e+02	4.500e+02
14	14.0	8.000e+01	1.250e+02	2.000e+02	6.800e+02	4.000e+02	5.000e+02	6.300e+02
15	15.0	8.500e+01	1.760e+02	2.500e+02	8.500e+02	7.000e+02	7.000e+02	8.000e+02
16	16.0	1.600e+02	2.500e+02	3.200e+02	9.600e+02	9.400e+02	9.400e+02	1.050e+03
17	17.0	3.000e+02	3.600e+02	4.000e+02	1.100e+03	1.100e+03	1.100e+03	1.250e+03
18	18.0	4.800e+02	6.440e+02	8.000e+02	1.200e+03	1.210e+03	1.200e+03	1.300e+03
19	19.0	6.400e+02	9.500e+02	1.100e+03	1.200e+03	1.210e+03	1.200e+03	1.150e+03
20	20.0	8.810e+02	1.148e+03	1.200e+03	1.100e+03	1.200e+03	1.120e+03	1.050e+03
21	21.0	1.050e+03	1.250e+03	1.220e+03	1.010e+03	1.100e+03	1.050e+03	9.600e+02
22	22.0	1.200e+03	1.200e+03	1.200e+03	9.200e+02	1.000e+03	9.400e+02	9.000e+02
23	23.0	1.100e+03	1.110e+03	1.100e+03	8.300e+02	9.000e+02	8.500e+02	8.300e+02
24	24.0	1.000e+03	1.000e+03	9.500e+02	7.200e+02	7.800e+02	7.500e+02	7.500e+02
25	25.0	8.600e+02	8.600e+02	8.000e+02	6.000e+02	6.600e+02	6.500e+02	6.500e+02
26	26.0	6.800e+02	6.800e+02	6.500e+02	5.500e+02	5.700e+02	5.600e+02	5.600e+02
27	27.0	5.570e+02	5.570e+02	5.800e+02	5.000e+02	5.100e+02	5.100e+02	5.000e+02
28	28.0	5.300e+02	5.300e+02	5.300e+02	4.600e+02	4.700e+02	4.700e+02	4.700e+02
29	29.0	5.100e+02	5.100e+02	4.900e+02	4.300e+02	4.500e+02	4.500e+02	4.400e+02
30	30.0	4.960e+02	4.960e+02	4.500e+02	4.400e+02	4.300e+02	4.300e+02	4.100e+02
31	31.0	4.650e+02	4.650e+02	4.350e+02	4.200e+02	4.100e+02	4.000e+02	3.700e+02
32	32.0	4.200e+02	4.200e+02	4.100e+02	3.700e+02	3.500e+02	3.400e+02	3.000e+02
33	33.0	3.860e+02	3.860e+02	3.600e+02	3.200e+02	2.800e+02	2.800e+02	2.720e+02
34	34.0	2.800e+02	2.800e+02	3.000e+02	2.700e+02	2.600e+02	2.600e+02	2.600e+02
35	35.0	2.500e+02	2.500e+02	2.500e+02	2.500e+02	2.500e+02	2.500e+02	2.500e+02
36	36.0	2.500e+02	2.500e+02	2.500e+02	2.500e+02	2.500e+02	2.500e+02	2.500e+02
37	37.0	2.500e+02	2.500e+02	2.500e+02	2.500e+02	2.500e+02	2.500e+02	2.500e+02
38	38.0	2.500e+02	2.500e+02	2.500e+02	2.500e+02	2.500e+02	2.500e+02	2.500e+02
39	39.0	2.500e+02	2.500e+02	2.500e+02	2.500e+02	2.500e+02	2.500e+02	2.500e+02
40	40.0	2.500e+02	2.500e+02	2.500e+02	2.500e+02	2.500e+02	2.500e+02	2.500e+02
41	41.0	2.500e+02	2.500e+02	2.500e+02	2.500e+02	2.500e+02	2.500e+02	2.500e+02
42	42.0	2.500e+02	2.500e+02	2.500e+02	2.500e+02	2.500e+02	2.500e+02	2.500e+02
43	43.0	2.500e+02	2.500e+02	2.500e+02	2.500e+02	2.500e+02	2.500e+02	2.500e+02
44	44.0	2.500e+02	2.500e+02	2.500e+02	2.500e+02	2.500e+02	2.500e+02	2.500e+02
45	45.0	2.500e+02	2.500e+02	2.500e+02	2.500e+02	2.500e+02	2.500e+02	2.500e+02
46	46.0	2.500e+02	2.500e+02	2.500e+02	2.500e+02	2.500e+02	2.500e+02	2.500e+02
47	47.0	2.500e+02	2.500e+02	2.500e+02	2.500e+02	2.500e+02	2.500e+02	2.500e+02
48	48.0	2.500e+02	2.500e+02	2.500e+02	2.500e+02	2.500e+02	2.500e+02	2.500e+02
49	49.0	2.500e+02	2.500e+02	2.500e+02	2.500e+02	2.500e+02	2.500e+02	2.500e+02
50	50.0	2.500e+02	2.500e+02	2.500e+02	2.500e+02	2.500e+02	2.500e+02	2.500e+02

B.1-c Taken from Johnston [1989] and regridded for the LLNL two-dimensional model. Initial distribution of carbon-14 for October 1963. Relative mixing ratios (10^5 atoms of excess carbon-14 per gram of air). Latitude zones are expressed in units of sine latitude. Altitude zones are expressed in units of km.

c14

	x	-0.985	-0.945	-0.885	-0.800	-0.675	-0.500	-0.300	-0.100	0.100	0.300
1	1.6	5.000e+01	5.000e+01	5.000e+01	5.000e+01	5.000e+01	5.000e+01	5.000e+01	5.467e+01	6.791e+01	7.300e+01
2	4.5	5.000e+01	5.000e+01	5.000e+01	5.000e+01	5.000e+01	5.000e+01	5.000e+01	5.467e+01	6.791e+01	7.300e+01
3	7.2	5.005e+01	5.011e+01	5.027e+01	5.045e+01	5.066e+01	5.000e+01	5.000e+01	5.467e+01	6.791e+01	7.300e+01
4	9.9	5.313e+01	5.332e+01	5.374e+01	5.408e+01	5.436e+01	5.128e+01	5.000e+01	5.467e+01	6.791e+01	7.300e+01
5	12.6	6.095e+01	6.082e+01	6.055e+01	6.027e+01	6.030e+01	5.850e+01	5.754e+01	6.365e+01	7.111e+01	7.547e+01
6	15.3	6.864e+01	6.995e+01	7.254e+01	7.568e+01	7.852e+01	8.320e+01	8.896e+01	9.319e+01	9.320e+01	1.370e+02
7	18.0	9.346e+01	9.868e+01	1.075e+02	1.176e+02	1.272e+02	1.321e+02	1.506e+02	1.881e+02	2.606e+02	4.813e+02
8	20.6	1.997e+02	2.216e+02	2.706e+02	3.221e+02	3.545e+02	4.298e+02	5.322e+02	6.495e+02	7.994e+02	1.001e+03
9	23.2	3.408e+02	3.330e+02	3.197e+02	3.064e+02	2.974e+02	3.649e+02	4.801e+02	6.158e+02	7.810e+02	9.883e+02
10	25.7	2.556e+02	2.385e+02	2.101e+02	1.901e+02	1.801e+02	2.208e+02	2.920e+02	3.765e+02	4.789e+02	6.050e+02
11	28.3	1.558e+02	1.531e+02	1.498e+02	1.474e+02	1.462e+02	1.797e+02	2.346e+02	2.996e+02	3.805e+02	4.840e+02
12	30.9	1.473e+02	1.499e+02	1.592e+02	1.665e+02	1.714e+02	2.010e+02	2.406e+02	2.860e+02	3.393e+02	4.033e+02
13	33.5	2.287e+02	2.363e+02	2.428e+02	2.470e+02	2.495e+02	2.500e+02	2.500e+02	2.500e+02	2.500e+02	2.500e+02
14	36.1	2.500e+02	2.500e+02	2.500e+02	2.500e+02	2.500e+02	2.500e+02	2.500e+02	2.500e+02	2.500e+02	2.500e+02
15	38.9	2.500e+02	2.500e+02	2.500e+02	2.500e+02	2.500e+02	2.500e+02	2.500e+02	2.500e+02	2.500e+02	2.500e+02
16	41.7	2.500e+02	2.500e+02	2.500e+02	2.500e+02	2.500e+02	2.500e+02	2.500e+02	2.500e+02	2.500e+02	2.500e+02
17	44.8	2.500e+02	2.500e+02	2.500e+02	2.500e+02	2.500e+02	2.500e+02	2.500e+02	2.500e+02	2.500e+02	2.500e+02
18	47.9	2.500e+02	2.500e+02	2.500e+02	2.500e+02	2.500e+02	2.500e+02	2.500e+02	2.500e+02	2.500e+02	2.500e+02

c14

	x	0.500	0.675	0.800	0.885	0.945	0.985
1	1.6	7.300e+01	7.300e+01	7.300e+01	7.300e+01	7.300e+01	7.300e+01
2	4.5	7.300e+01	7.300e+01	7.300e+01	7.574e+01	8.496e+01	9.505e+01
3	7.2	7.300e+01	7.300e+01	7.300e+01	7.810e+01	9.362e+01	9.986e+01
4	9.9	7.300e+01	9.253e+01	1.519e+02	1.660e+02	1.875e+02	2.165e+02
5	12.6	1.032e+02	2.153e+02	3.394e+02	3.243e+02	3.667e+02	4.170e+02
6	15.3	2.382e+02	4.640e+02	8.922e+02	8.270e+02	8.143e+02	8.805e+^2
7	18.0	7.664e+02	9.823e+02	1.203e+03	1.207e+03	1.212e+03	1.298e+03
8	20.6	1.250e+03	1.166e+03	1.047e+03	1.100e+03	1.060e+03	9.974e+02
9	23.2	1.034e+03	9.390e+02	7.876e+02	8.308e+02	8.147e+02	8.163e+02
10	25.7	6.296e+02	6.019e+02	5.441e+02	5.608e+02	5.655e+02	5.843e+02
11	28.3	5.075e+02	4.718e+02	4.383e+02	4.547e+02	4.587e+02	4.610e+02
12	30.9	4.190e+02	4.050e+02	3.816e+02	3.805e+02	3.851e+02	3.747e+02
13	33.5	2.509e+02	2.607e+02	2.583e+02	2.585e+02	2.628e+02	2.665e+02
14	36.1	2.500e+02	2.500e+02	2.500e+02	2.500e+02	2.500e+02	2.500e+02
15	38.9	2.500e+02	2.500e+02	2.500e+02	2.500e+02	2.500e+02	2.500e+02
16	41.7	2.500e+02	2.500e+02	2.500e+02	2.500e+02	2.500e+02	2.500e+02
17	44.8	2.500e+02	2.500e+02	2.500e+02	2.500e+02	2.500e+02	2.500e+02
18	47.9	2.500e+02	2.500e+02	2.500e+02	2.500e+02	2.500e+02	2.500e+02

B.2-a Original data taken from Johnston [1989]. Initial distribution of strontium-90 for October 1964. Relative mixing ratios (disintegrations per minute per 1000 ft^3 of standard air). Latitude zones are expressed in units of sine latitude. Altitude zones are expressed in units of km.

	x	-0.985	-0.940	-0.866	-0.766	-0.643	-0.500	-0.342	-0.174	0.000	0.174
1	1.0	1.000e+00	1.000e+00	1.000e+00	1.000e+00	1.000e+00	1.000e+00	1.000e+00	1.000e+00	1.000e+00	1.000e+00
2	2.0	1.000e+00	1.000e+00	1.000e+00	1.000e+00	1.000e+00	1.000e+00	1.000e+00	1.000e+00	1.000e+00	1.000e+00
3	3.0	1.000e+00	1.000e+00	1.000e+00	1.000e+00	1.000e+00	1.000e+00	1.000e+00	1.000e+00	1.000e+00	1.000e+00
4	4.0	1.000e+00	1.000e+00	1.000e+00	1.000e+00	1.000e+00	1.000e+00	1.000e+00	1.000e+00	1.000e+00	1.000e+00
5	5.0	1.000e+00	1.000e+00	1.000e+00	1.000e+00	1.000e+00	1.000e+00	1.000e+00	1.000e+00	1.000e+00	1.000e+00
6	6.0	1.000e+00	1.000e+00	1.000e+00	1.000e+00	1.000e+00	1.000e+00	1.000e+00	1.000e+00	1.000e+00	1.000e+00
7	7.0	2.000e+00	2.000e+00	2.000e+00	2.000e+00	2.000e+00	1.000e+00	1.000e+00	1.000e+00	1.000e+00	1.000e+00
8	8.0	4.000e+00	4.000e+00	4.000e+00	4.000e+00	3.000e+00	1.000e+00	1.000e+00	1.000e+00	1.000e+00	1.000e+00
9	9.0	1.000e+01	1.000e+01	1.000e+01	1.000e+01	6.000e+00	2.000e+00	1.000e+00	1.000e+00	1.000e+00	1.000e+00
10	10.0	2.000e+01	2.000e+01	2.000e+01	2.000e+01	1.000e+01	3.000e+00	1.000e+00	1.000e+00	1.000e+00	1.000e+00
11	11.0	4.200e+01	4.200e+01	4.200e+01	4.200e+01	2.000e+01	5.000e+00	1.000e+00	1.000e+00	1.000e+00	1.000e+00
12	12.0	7.000e+01	7.000e+01	7.000e+01	7.000e+01	3.700e+01	8.000e+00	1.000e+00	1.000e+00	1.000e+00	1.000e+00
13	13.0	1.050e+02	1.050e+02	1.050e+02	1.050e+02	6.500e+01	1.300e+01	1.000e+00	1.000e+00	1.000e+00	1.000e+00
14	14.0	1.300e+02	1.300e+02	1.300e+02	1.300e+02	1.000e+02	2.300e+01	2.000e+00	1.000e+00	1.000e+00	1.000e+00
15	15.0	1.480e+02	1.480e+02	1.480e+02	1.480e+02	1.250e+02	4.000e+01	9.000e+00	2.000e+00	1.000e+00	2.000e+00
16	16.0	1.600e+02	1.600e+02	1.600e+02	1.600e+02	1.500e+02	1.000e+02	5.000e+01	1.500e+01	1.000e+01	2.200e+01
17	17.0	1.620e+02	1.620e+02	1.620e+02	1.620e+02	1.600e+02	1.250e+02	1.200e+02	1.000e+02	1.000e+02	1.500e+02
18	18.0	1.570e+02	1.570e+02	1.570e+02	1.570e+02	1.650e+02	1.400e+02	1.600e+02	1.900e+02	2.300e+02	2.300e+02
19	19.0	1.400e+02	1.400e+02	1.400e+02	1.400e+02	1.650e+02	1.500e+02	1.700e+02	2.500e+02	3.000e+02	3.500e+02
20	20.0	1.170e+02	1.170e+02	1.170e+02	1.170e+02	1.350e+02	1.520e+02	1.750e+02	3.200e+02	3.600e+02	4.000e+02
21	21.0	1.000e+02	1.000e+02	1.000e+02	1.000e+02	1.300e+02	1.500e+02	1.780e+02	3.700e+02	4.000e+02	4.150e+02
22	22.0	8.100e+01	8.100e+01	8.100e+01	8.100e+01	1.100e+02	1.400e+02	1.750e+02	3.850e+02	4.200e+02	4.200e+02
23	23.0	7.000e+01	7.000e+01	7.000e+01	7.000e+01	9.500e+01	1.240e+02	1.680e+02	3.900e+02	4.250e+02	4.200e+02
24	24.0	6.000e+01	6.000e+01	6.000e+01	6.000e+01	8.200e+01	1.100e+02	1.550e+02	3.800e+02	4.200e+02	4.150e+02
25	25.0	5.000e+01	5.000e+01	5.000e+01	5.000e+01	7.000e+01	9.600e+01	1.300e+02	3.500e+02	4.000e+02	4.000e+02
26	26.0	4.000e+01	4.000e+01	4.000e+01	4.000e+01	5.500e+01	8.200e+01	1.150e+02	3.000e+02	3.700e+02	3.700e+02
27	27.0	3.000e+01	3.000e+01	3.000e+01	3.000e+01	4.100e+01	7.000e+01	9.700e+01	2.150e+02	3.200e+02	3.000e+02
28	28.0	2.400e+01	2.400e+01	2.400e+01	2.400e+01	3.100e+01	5.800e+01	8.200e+01	1.600e+02	2.500e+02	2.050e+02
29	29.0	1.800e+01	1.800e+01	1.800e+01	1.800e+01	2.300e+01	4.600e+01	6.500e+01	1.250e+02	1.850e+02	1.750e+02
30	30.0	1.400e+01	1.400e+01	1.400e+01	1.400e+01	1.700e+01	3.300e+01	5.200e+01	9.000e+01	1.450e+02	1.350e+02
31	31.0	1.100e+01	1.100e+01	1.100e+01	1.100e+01	1.300e+01	2.300e+01	4.000e+01	6.500e+01	1.060e+02	1.080e+02
32	32.0	8.000e+00	8.000e+00	8.000e+00	8.000e+00	1.000e+01	1.600e+01	3.000e+01	4.800e+01	8.100e+01	8.400e+01
33	33.0	6.000e+00	6.000e+00	6.000e+00	6.000e+00	7.000e+00	1.100e+01	2.100e+01	3.500e+01	6.200e+01	6.700e+01
34	34.0	5.000e+00	5.000e+00	5.000e+00	5.000e+00	6.000e+00	8.000e+00	1.500e+01	2.500e+01	5.000e+01	5.100e+01
35	35.0	4.000e+00	4.000e+00	4.000e+00	4.000e+00	4.000e+00	6.000e+00	1.000e+01	1.800e+01	3.800e+01	4.000e+01
36	36.0	3.000e+00	3.000e+00	3.000e+00	3.000e+00	3.000e+00	4.000e+00	7.000e+00	1.300e+01	2.900e+01	3.100e+01
37	37.0	2.000e+00	2.000e+00	2.000e+00	2.000e+00	2.000e+00	3.000e+00	5.000e+00	1.000e+01	2.200e+01	2.500e+01
38	38.0	1.000e+00	1.000e+00	1.000e+00	1.000e+00	1.000e+00	2.000e+00	4.000e+00	7.000e+00	1.700e+01	1.900e+01
39	39.0	1.000e+00	1.000e+00	1.000e+00	1.000e+00	1.000e+00	1.000e+00	3.000e+00	5.000e+00	1.300e+01	1.500e+01
40	40.0	1.000e+00	1.000e+00	1.000e+00	1.000e+00	1.000e+00	1.000e+00	2.000e+00	4.000e+00	1.000e+01	1.200e+01
41	41.0	1.000e+00	1.000e+00	1.000e+00	1.000e+00	1.000e+00	1.000e+00	1.000e+00	3.000e+00	1.000e+00	1.000e+01
42	42.0	1.000e+00	1.000e+00	1.000e+00	1.000e+00	1.000e+00	1.000e+00	1.000e+00	2.000e+00	1.000e+00	8.000e+00
43	43.0	1.000e+00	1.000e+00	1.000e+00	1.000e+00	1.000e+00	1.000e+00	1.000e+00	1.000e+00	1.000e+00	6.000e+00
44	44.0	1.000e+00	1.000e+00	1.000e+00	1.000e+00	1.000e+00	1.000e+00	1.000e+00	1.000e+00	1.000e+00	5.000e+00
45	45.0	1.000e+00	1.000e+00	1.000e+00	1.000e+00	1.000e+00	1.000e+00	1.000e+00	1.000e+00	1.000e+00	4.000e+00
46	46.0	1.000e+00	1.000e+00	1.000e+00	1.000e+00	1.000e+00	1.000e+00	1.000e+00	1.000e+00	1.000e+00	3.000e+00
47	47.0	1.000e+00	1.000e+00	1.000e+00	1.000e+00	1.000e+00	1.000e+00	1.000e+00	1.000e+00	1.000e+00	2.000e+00
48	48.0	1.000e+00	1.000e+00	1.000e+00	1.000e+00	1.000e+00	1.000e+00	1.000e+00	1.000e+00	1.000e+00	1.000e+00
49	49.0	1.000e+00	1.000e+00	1.000e+00	1.000e+00	1.000e+00	1.000e+00	1.000e+00	1.000e+00	1.000e+00	1.000e+00
50	50.0	1.000e+00	1.000e+00	1.000e+00	1.000e+00	1.000e+00	1.000e+00	1.000e+00	1.000e+00	1.000e+00	1.000e+00

B.2-b Original data taken from Johnston [1989]. Initial distribution of strontium-90 for October 1964. Relative mixing ratios (disintegrations per minute per 1000 ft^3 of standard air). Latitude zones are expressed in units of sine latitude. Altitude zones are expressed in units of km.

	x	0.342	0.500	0.643	0.766	0.866	0.940	0.985
1	1.0	1.000e+00	1.000e+00	1.000e+00	1.000e+00	1.000e+00	1.000e+00	1.000e+00
2	2.0	1.000e+00	1.000e+00	1.000e+00	1.000e+00	1.000e+00	1.000e+00	1.000e+00
3	3.0	1.000e+00	1.000e+00	1.000e+00	1.000e+00	1.000e+00	1.000e+00	1.000e+00
4	4.0	1.000e+00	1.000e+00	1.000e+00	1.000e+00	1.000e+00	1.000e+00	1.000e+00
5	5.0	1.000e+00	1.000e+00	1.000e+00	1.000e+00	1.000e+00	1.000e+00	1.000e+00
6	6.0	1.000e+00	1.000e+00	1.000e+00	1.000e+00	1.000e+00	1.000e+00	1.000e+00
7	7.0	1.000e+00	1.000e+00	1.000e+00	1.000e+00	2.000e+00	3.000e+00	3.000e+00
8	8.0	1.000e+00	1.000e+00	1.000e+00	1.000e+00	4.000e+00	5.000e+00	5.000e+00
9	9.0	1.000e+00	1.000e+00	1.000e+00	2.000e+00	1.000e+01	1.700e+01	1.700e+01
10	10.0	1.000e+00	2.000e+00	3.000e+00	7.000e+00	3.000e+01	7.000e+01	7.000e+01
11	11.0	1.000e+00	3.000e+00	6.000e+00	2.000e+01	1.000e+02	1.200e+02	1.200e+02
12	12.0	1.000e+00	7.000e+00	1.500e+01	6.000e+01	1.200e+02	1.750e+02	1.750e+02
13	13.0	1.000e+00	8.000e+00	3.500e+01	8.500e+01	1.400e+02	2.400e+02	2.400e+02
14	14.0	1.000e+00	2.000e+01	6.500e+01	1.250e+02	2.200e+02	3.000e+02	3.000e+02
15	15.0	4.000e+00	5.000e+01	1.000e+02	2.000e+02	3.000e+02	3.800e+02	3.800e+02
16	16.0	5.000e+01	1.000e+02	2.000e+02	3.000e+02	4.000e+02	4.600e+02	4.600e+02
17	17.0	1.500e+02	2.000e+02	3.500e+02	4.000e+02	4.900e+02	5.200e+02	5.200e+02
18	18.0	3.000e+02	3.800e+02	4.300e+02	4.800e+02	5.000e+02	5.000e+02	5.000e+02
19	19.0	4.100e+02	4.800e+02	4.500e+02	4.800e+02	4.600e+02	4.000e+02	4.000e+02
20	20.0	4.700e+02	5.000e+02	4.500e+02	4.200e+02	3.600e+02	3.000e+02	3.000e+02
21	21.0	5.000e+02	4.950e+02	4.300e+02	3.300e+02	2.500e+02	2.300e+02	2.300e+02
22	22.0	5.000e+02	4.500e+02	3.500e+02	2.250e+02	1.800e+02	1.700e+02	1.700e+02
23	23.0	4.700e+02	4.000e+02	2.400e+02	1.700e+02	1.500e+02	1.300e+02	1.300e+02
24	24.0	4.300e+02	3.000e+02	1.800e+02	1.470e+02	1.240e+02	1.000e+02	1.000e+02
25	25.0	3.500e+02	2.150e+02	1.500e+02	1.220e+02	1.070e+02	7.400e+01	7.400e+01
26	26.0	2.700e+02	1.700e+02	1.270e+02	1.020e+02	7.000e+01	5.600e+01	5.600e+01
27	27.0	2.000e+02	1.300e+02	1.100e+02	7.000e+01	5.000e+01	4.100e+01	4.100e+01
28	28.0	1.700e+02	1.020e+02	8.800e+01	5.000e+01	3.500e+01	3.100e+01	3.100e+01
29	29.0	1.300e+02	8.200e+01	6.800e+01	3.500e+01	2.600e+01	2.400e+01	2.400e+01
30	30.0	9.700e+01	6.600e+01	5.300e+01	2.500e+01	2.000e+01	1.800e+01	1.800e+01
31	31.0	7.500e+01	5.100e+01	4.100e+01	1.900e+01	1.500e+01	1.400e+01	1.400e+01
32	32.0	6.000e+01	4.000e+01	3.200e+01	1.400e+01	1.100e+01	1.000e+01	1.000e+01
33	33.0	4.500e+01	3.300e+01	2.500e+01	1.000e+01	8.000e+00	8.000e+00	8.000e+00
34	34.0	3.500e+01	2.600e+01	2.000e+01	7.000e+00	6.000e+00	6.000e+00	6.000e+00
35	35.0	2.600e+01	2.000e+01	1.500e+01	5.000e+00	4.000e+00	4.000e+00	4.000e+00
36	36.0	1.900e+01	1.500e+01	1.100e+01	4.000e+00	3.000e+00	3.000e+00	3.000e+00
37	37.0	1.400e+01	1.200e+01	8.000e+00	3.000e+00	2.000e+00	2.000e+00	2.000e+00
38	38.0	1.100e+01	9.000e+00	6.000e+00	2.000e+00	1.000e+00	1.000e+00	1.000e+00
39	39.0	8.000e+00	7.000e+00	5.000e+00	1.000e+00	1.000e+00	1.000e+00	1.000e+00
40	40.0	6.000e+00	5.000e+00	4.000e+00	1.000e+00	1.000e+00	1.000e+00	1.000e+00
41	41.0	4.000e+00	4.000e+00	3.000e+00	1.000e+00	1.000e+00	1.000e+00	1.000e+00
42	42.0	3.000e+00	3.000e+00	2.000e+00	1.000e+00	1.000e+00	1.000e+00	1.000e+00
43	43.0	2.000e+00	2.000e+00	1.000e+00	1.000e+00	1.000e+00	1.000e+00	1.000e+00
44	44.0	2.000e+00	2.000e+00	1.000e+00	1.000e+00	1.000e+00	1.000e+00	1.000e+00
45	45.0	1.000e+00	1.000e+00	1.000e+00	1.000e+00	1.000e+00	1.000e+00	1.000e+00
46	46.0	1.000e+00	1.000e+00	1.000e+00	1.000e+00	1.000e+00	1.000e+00	1.000e+00
47	47.0	1.000e+00	1.000e+00	1.000e+00	1.000e+00	1.000e+00	1.000e+00	1.000e+00
48	48.0	1.000e+00	1.000e+00	1.000e+00	1.000e+00	1.000e+00	1.000e+00	1.000e+00
49	49.0	1.000e+00	1.000e+00	1.000e+00	1.000e+00	1.000e+00	1.000e+00	1.000e+00
50	50.0	1.000e+00	1.000e+00	1.000e+00	1.000e+00	1.000e+00	1.000e+00	1.000e+00

B.2-c Taken from Johnston [1989] and regridded for the LLNL two-dimensional model. Initial distribution of strontium-90 for October 1964. Relative mixing ratios (disintegrations per minute per 1000 ft^3 of standard air). Latitude zones are expressed in units of sine latitude. Altitude zones are expressed in units of km.

	x	-0.985	-0.945	-0.885	-0.800	-0.675	-0.500	-0.300	-0.100	0.100	0.300
1	1.6	1.000e+00	1.000e+00	1.000e+00	1.000e+00	1.000e+00	1.000e+00	1.000e+00	1.000e+00	1.000e+00	1.000e+00
2	4.5	1.000e+00	1.000e+00	1.000e+00	1.000e+00	1.000e+00	1.000e+00	1.000e+00	1.000e+00	1.000e+00	1.000e+00
3	7.2	2.092e+00	2.216e+00	2.548e+00	2.902e+00	2.790e+00	1.000e+00	1.000e+00	1.000e+00	1.000e+00	1.000e+00
4	9.9	1.567e+01	1.659e+01	1.870e+01	2.241e+01	1.675e+01	4.280e+00	1.000e+00	1.000e+00	1.000e+00	1.000e+00
5	12.6	7.175e+01	7.628e+01	8.567e+01	9.562e+01	7.575e+01	1.550e+01	1.271e+00	1.000e+00	1.000e+00	1.000e+00
6	15.3	1.394e+02	1.427e+02	1.480e+02	1.524e+02	1.457e+02	8.800e+01	3.559e+01	1.118e+01	1.483e+01	3.792e+01
7	18.0	1.619e+02	1.608e+02	1.589e+02	1.558e+02	1.623e+02	1.439e+02	1.754e+02	2.294e+02	2.660e+02	3.260e+02
8	20.6	1.269e+02	1.207e+02	1.125e+02	1.051e+02	1.223e+02	1.497e+02	2.251e+02	3.799e+02	4.071e+02	4.783e+02
9	23.2	7.913e+01	7.573e+01	7.030e+01	6.575e+01	7.975e+01	1.139e+02	2.157e+02	4.002e+02	4.191e+02	4.372e+02
10	25.7	5.190e+01	4.823e+01	4.272e+01	3.820e+01	4.523e+01	7.648e+01	1.491e+02	3.070e+02	3.500e+02	2.693e+02
11	28.3	2.640e+01	2.409e+01	2.077e+01	1.835e+01	2.049e+01	4.275e+01	7.694e+01	1.456e+02	1.739e+02	1.354e+02
12	30.9	1.217e+01	1.111e+01	9.619e+00	8.527e+00	9.355e+00	1.540e+01	3.372e+01	6.126e+01	8.187e+01	6.498e+01
13	33.5	5.180e+00	4.886e+00	4.481e+00	4.197e+00	4.018e+00	5.820e+00	1.167e+01	2.594e+01	3.850e+01	2.908e+01
14	36.1	1.810e+00	1.597e+00	1.306e+00	1.107e+00	1.014e+00	1.840e+00	4.486e+00	1.065e+01	1.737e+01	1.251e+01
15	38.9	1.000e+00	1.000e+00	1.000e+00	1.000e+00	1.000e+00	1.000e+00	1.390e+00	1.900e+00	5.725e+00	5.065e+00
16	41.7	1.000e+00	1.000e+00	1.000e+00	1.000e+00	1.000e+00	1.000e+00	1.000e+00	1.000e+00	2.919e+00	2.167e+00
17	44.8	1.000e+00	1.000e+00	1.000e+00	1.000e+00	1.000e+00	1.000e+00	1.000e+00	1.000e+00	1.029e+00	1.013e+00
18	47.9	1.000e+00	1.000e+00	1.000e+00	1.000e+00	1.000e+00	1.000e+00	1.000e+00	1.000e+00	1.000e+00	1.000e+00

	x	0.500	0.675	0.800	0.885	0.945	0.985
1	1.6	1.000e+00	1.000e+00	1.000e+00	1.000e+00	1.000e+00	1.000e+00
2	4.5	1.000e+00	1.000e+00	1.000e+00	1.000e+00	1.000e+00	1.000e+00
3	7.2	1.000e+00	1.000e+00	1.677e+00	3.180e+00	3.690e+00	3.482e+00
4	9.9	2.770e+00	6.467e+00	2.258e+01	5.131e+01	7.186e+01	6.650e+01
5	12.6	1.208e+01	5.174e+01	1.032e+02	1.599e+02	2.229e+02	2.160e+02
6	15.3	9.200e+01	1.981e+02	2.962e+02	3.712e+02	4.141e+02	4.056e+02
7	18.0	4.200e+02	4.483e+02	4.837e+02	4.906e+02	4.912e+02	5.008e+02
8	20.6	4.946e+02	4.052e+02	3.100e+02	2.588e+02	2.494e+02	2.594e+02
9	23.2	3.310e+02	1.889e+02	1.492e+02	1.319e+02	1.200e+02	1.249e+02
10	25.7	1.536e+02	1.137e+02	8.405e+01	6.407e+01	5.710e+01	6.086e+01
11	28.3	7.912e+01	5.844e+01	3.265e+01	2.741e+01	2.717e+01	2.890e+01
12	30.9	3.979e+01	2.836e+01	1.449e+01	1.295e+01	1.326e+01	1.448e+01
13	33.5	2.018e+01	1.345e+01	5.737e+00	5.644e+00	6.334e+00	7.080e+00
14	36.1	9.000e+00	5.454e+00	2.310e+00	2.018e+00	2.449e+00	2.900e+00
15	38.9	3.870e+00	2.598e+00	1.000e+00	1.000e+00	1.000e+00	1.000e+00
16	41.7	1.660e+00	1.000e+00	1.000e+00	1.000e+00	1.000e+00	1.000e+00
17	44.8	1.000e+00	1.000e+00	1.000e+00	1.000e+00	1.000e+00	1.000e+00
18	47.9	1.000e+00	1.000e+00	1.000e+00	1.000e+00	1.000e+00	1.000e+00

B.3-a Case A horizontal eddy diffusion representation (K_{yy}, $cm^2\ s^{-1}$). Latitude zones are expressed in units of sine latitude. Altitude zones are expressed in units of km.

kyy

	x	-1.000	-0.970	-0.920	-0.850	-0.750	-0.600	-0.400	-0.200	0.000	0.200
1	1.5	0.	1.000e+11	1.000e+11	1.000e+11	1.000e+11	1.000e+11	1.000e+11	1.000e+11	1.000e+11	1.000e+11
2	4.5	0.	1.000e+11	1.000e+11	1.000e+11	1.000e+11	1.000e+11	1.000e+11	1.000e+11	1.000e+11	1.000e+11
3	7.5	0.	1.000e+11	1.000e+11	1.000e+11	1.000e+11	1.000e+11	1.000e+11	1.000e+11	1.000e+11	1.000e+11
4	10.5	0.	5.000e+09	5.000e+09	1.000e+11	1.000e+11	1.000e+11	1.000e+11	1.000e+11	1.000e+11	1.000e+11
5	13.5	0.	2.000e+09	2.000e+09	3.000e+09	2.500e+10	5.000e+09	1.000e+11	1.000e+11	1.000e+11	1.000e+11
6	16.5	0.	2.000e+09	2.000e+09	2.000e+09	2.500e+09	3.000e+09	5.000e+09	5.000e+09	5.000e+09	5.000e+09
7	19.5	0.	2.000e+09	2.000e+09	2.000e+09	2.000e+09	2.000e+09	2.000e+09	3.000e+09	3.000e+09	3.000e+09
8	22.5	0.	2.000e+09	2.000e+09	2.000e+09	2.000e+09	2.000e+09	2.000e+09	2.000e+09	2.000e+09	2.000e+09
9	25.5	0.	2.000e+09	2.000e+09	2.000e+09	2.000e+09	2.000e+09	2.000e+09	2.000e+09	2.000e+09	2.000e+09
10	28.5	0.	2.000e+09	2.000e+09	2.000e+09	2.000e+09	2.000e+09	2.000e+09	2.000e+09	2.000e+09	2.000e+09
11	31.5	0.	2.000e+09	2.000e+09	2.000e+09	2.000e+09	2.000e+09	2.000e+09	2.000e+09	2.000e+09	2.000e+09
12	34.5	0.	2.000e+09	2.000e+09	2.000e+09	2.000e+09	2.000e+09	2.000e+09	2.000e+09	2.000e+09	2.000e+09
13	37.5	0.	2.000e+09	2.000e+09	2.000e+09	2.000e+09	2.000e+09	2.000e+09	2.000e+09	2.000e+09	2.000e+09
14	40.5	0.	2.000e+09	2.000e+09	2.000e+09	2.000e+09	2.000e+09	2.000e+09	2.000e+09	2.000e+09	2.000e+09
15	43.5	0.	2.000e+09	2.000e+09	2.000e+09	2.000e+09	2.000e+09	2.000e+09	2.000e+09	2.000e+09	2.000e+09
16	46.5	0.	2.000e+09	2.000e+09	2.000e+09	2.000e+09	2.000e+09	2.000e+09	2.000e+09	2.000e+09	2.000e+09
17	49.5	0.	2.000e+09	2.000e+09	2.000e+09	2.000e+09	2.000e+09	2.000e+09	2.000e+09	2.000e+09	2.000e+09
18	52.5	0.	2.000e+09	2.000e+09	2.000e+09	2.000e+09	2.000e+09	2.000e+09	2.000e+09	2.000e+09	2.000e+09

kyy

	x	0.400	0.600	0.750	0.850	0.920	0.970	1.000
1	1.5	1.000e+11	1.000e+11	1.000e+11	1.000e+11	1.000e+11	1.000e+11	0.
2	4.5	1.000e+11	1.000e+11	1.000e+11	1.000e+11	1.000e+11	1.000e+11	0.
3	7.5	1.000e+11	1.000e+11	1.000e+11	1.000e+11	1.000e+11	1.000e+11	0.
4	10.5	1.000e+11	1.000e+11	1.000e+11	1.000e+11	5.000e+09	5.000e+09	0.
5	13.5	1.000e+11	5.000e+09	2.500e+10	3.000e+09	2.000e+09	2.000e+09	0.
6	16.5	5.000e+09	3.000e+09	2.500e+09	2.000e+09	2.000e+09	2.000e+09	0.
7	19.5	2.000e+09	2.000e+09	2.000e+09	2.000e+09	2.000e+09	2.000e+09	0.
8	22.5	2.000e+09	2.000e+09	2.000e+09	2.000e+09	2.000e+09	2.000e+09	0.
9	25.5	2.000e+09	2.000e+09	2.000e+09	2.000e+09	2.000e+09	2.000e+09	0.
10	28.5	2.000e+09	2.000e+09	2.000e+09	2.000e+09	2.000e+09	2.000e+09	0.
11	31.5	2.000e+09	2.000e+09	2.000e+09	2.000e+09	2.000e+09	2.000e+09	0.
12	34.5	2.000e+09	2.000e+09	2.000e+09	2.000e+09	2.000e+09	2.000e+09	0.
13	37.5	2.000e+09	2.000e+09	2.000e+09	2.000e+09	2.000e+09	2.000e+09	0.
14	40.5	2.000e+09	2.000e+09	2.000e+09	2.000e+09	2.000e+09	2.000e+09	0.
15	43.5	2.000e+09	2.000e+09	2.000e+09	2.000e+09	2.000e+09	2.000e+09	0.
16	46.5	2.000e+09	2.000e+09	2.000e+09	2.000e+09	2.000e+09	2.000e+09	0.
17	49.5	2.000e+09	2.000e+09	2.000e+09	2.000e+09	2.000e+09	2.000e+09	0.
18	52.5	2.000e+09	2.000e+09	2.000e+09	2.000e+09	2.000e+09	2.000e+09	0.

B.3-b Case A vertical eddy diffusion representation (K_{zz}, $cm^2\ s^{-1}$). Latitude zones are expressed in units of sine latitude. Altitude zones are expressed in units of km.

kzz :

	x	-0.985	-0.945	-0.885	-0.800	-0.675	-0.500	-0.300	-0.100	0.100	0.300
1	0.0	0.	0.	0.	0.	0.	0.	0.	0.	0.	0.
2	3.0	1.000e+05	1.000e+05	1.000e+05	1.000e+05	1.000e+05	1.000e+05	1.000e+05	1.000e+05	1.000e+05	1.000e+05
3	6.0	1.000e+05	1.000e+05	1.000e+05	1.000e+05	1.000e+05	1.000e+05	1.000e+05	1.000e+05	1.000e+05	1.000e+05
4	9.0	1.000e+05	1.000e+05	1.000e+05	1.000e+05	1.000e+05	1.000e+05	1.000e+05	1.000e+05	1.000e+05	1.000e+05
5	12.0	3.500e+04	3.500e+04	3.500e+04	5.000e+04	1.000e+05	1.000e+05	1.000e+05	1.000e+05	1.000e+05	1.000e+05
6	15.0	3.500e+03	3.500e+03	3.500e+03	5.000e+03	6.500e+03	6.500e+03	3.300e+04	3.300e+04	3.300e+04	3.300e+04
7	18.0	1.700e+03	1.700e+03	1.700e+03	1.800e+03	2.000e+03	2.000e+03	6.600e+03	6.600e+03	6.600e+03	6.600e+03
8	21.0	1.000e+03	1.000e+03	1.000e+03	1.000e+03	1.000e+03	1.000e+03	1.000e+03	1.000e+03	1.000e+03	1.000e+03
9	24.0	1.000e+03	1.000e+03	1.000e+03	1.000e+03	1.000e+03	1.000e+03	1.000e+03	1.000e+03	1.000e+03	1.000e+03
10	27.0	1.000e+03	1.000e+03	1.000e+03	1.000e+03	1.000e+03	1.000e+03	1.000e+03	1.000e+03	1.000e+03	1.000e+03
11	30.0	1.000e+03	1.000e+03	1.000e+03	1.000e+03	1.000e+03	1.000e+03	1.000e+03	1.000e+03	1.000e+03	1.000e+03
12	33.0	1.000e+03	1.000e+03	1.000e+03	1.000e+03	1.000e+03	1.000e+03	1.000e+03	1.000e+03	1.000e+03	1.000e+03
13	36.0	1.000e+03	1.000e+03	1.000e+03	1.000e+03	1.000e+03	1.000e+03	1.000e+03	1.000e+03	1.000e+03	1.000e+03
14	39.0	1.000e+03	1.000e+03	1.000e+03	1.000e+03	1.000e+03	1.000e+03	1.000e+03	1.000e+03	1.000e+03	1.000e+03
15	42.0	5.000e+03	5.000e+03	5.000e+03	5.000e+03	5.000e+03	5.000e+03	5.000e+03	5.000e+03	5.000e+03	5.000e+03
16	45.0	1.000e+04	1.000e+04	1.000e+04	1.000e+04	1.000e+04	1.000e+04	1.000e+04	1.000e+04	1.000e+04	1.000e+04
17	48.0	2.500e+04	2.500e+04	2.500e+04	2.500e+04	2.500e+04	2.500e+04	2.500e+04	2.500e+04	2.500e+04	2.500e+04
18	51.0	5.475e+04	5.475e+04	5.475e+04	5.475e+04	5.475e+04	5.475e+04	5.475e+04	5.475e+04	5.475e+04	5.475e+04
19	54.0	8.580e+04	8.580e+04	8.580e+04	8.580e+04	8.580e+04	8.580e+04	8.580e+04	8.580e+04	8.580e+04	8.580e+04

kzz

	x	0.500	0.675	0.800	0.885	0.945	0.985
1	0.0	0.	0.	0.	0.	0.	0.
2	3.0	1.000e+05	1.000e+05	1.000e+05	1.000e+05	1.000e+05	1.000e+05
3	6.0	1.000e+05	1.000e+05	1.000e+05	1.000e+05	1.000e+05	1.000e+05
4	9.0	1.000e+05	1.000e+05	1.000e+05	1.000e+05	1.000e+05	1.000e+05
5	12.0	1.000e+05	1.000e+05	5.000e+04	3.500e+04	3.500e+04	3.500e+04
6	15.0	6.500e+03	6.500e+03	5.000e+03	3.500e+03	3.500e+03	3.500e+03
7	18.0	2.000e+03	2.000e+03	1.800e+03	1.700e+03	1.700e+03	1.700e+03
8	21.0	1.000e+03	1.000e+03	1.000e+03	1.000e+03	1.000e+03	1.000e+03
9	24.0	1.000e+03	1.000e+03	1.000e+03	1.000e+03	1.000e+03	1.000e+03
10	27.0	1.000e+03	1.000e+03	1.000e+03	1.000e+03	1.000e+03	1.000e+03
11	30.0	1.000e+03	1.000e+03	1.000e+03	1.000e+03	1.000e+03	1.000e+03
12	33.0	1.000e+03	1.000e+03	1.000e+03	1.000e+03	1.000e+03	1.000e+03
13	36.0	1.000e+03	1.000e+03	1.000e+03	1.000e+03	1.000e+03	1.000e+03
14	39.0	1.000e+03	1.000e+03	1.000e+03	1.000e+03	1.000e+03	1.000e+03
15	42.0	5.000e+03	5.000e+03	5.000e+03	5.000e+03	5.000e+03	5.000e+03
16	45.0	1.000e+04	1.000e+04	1.000e+04	1.000e+04	1.000e+04	1.000e+04
17	48.0	2.500e+04	2.500e+04	2.500e+04	2.500e+04	2.500e+04	2.500e+04
18	51.0	5.475e+04	5.475e+04	5.475e+04	5.475e+04	5.475e+04	5.475e+04
19	54.0	8.580e+04	8.580e+04	8.580e+04	8.580e+04	8.580e+04	8.580e+04

B.4-a Case B horizontal eddy diffusion representation (K_{yy}, $cm^2\ s^{-1}$). Latitude zones are expressed in units of sine latitude. Altitude zones are expressed in units of km.

kyy

	x	-1.000	-0.970	-0.920	-0.850	-0.750	-0.600	-0.400	-0.200	0.000	0.200
1	1.5	0.	5.000e+10	5.000e+10	5.000e+10	5.000e+10	5.000e+10	5.000e+10	5.000e+10	5.000e+10	5.000e+10
2	4.5	0.	5.000e+10	5.000e+10	5.000e+10	5.000e+10	5.000e+10	5.000e+10	5.000e+10	5.000e+10	5.000e+10
3	7.5	0.	5.000e+10	5.000e+10	5.000e+10	5.000e+10	5.000e+10	5.000e+10	5.000e+10	5.000e+10	5.000e+10
4	10.5	0.	2.000e+09	2.000e+09	5.000e+10	5.000e+10	5.000e+10	5.000e+10	5.000e+10	5.000e+10	5.000e+10
5	13.5	0.	2.000e+09	2.000e+09	2.000e+09	2.000e+09	2.000e+09	5.000e+10	5.000e+10	5.000e+10	5.000e+10
6	16.5	0.	2.000e+09	2.000e+09	2.000e+09	2.000e+09	2.000e+09	2.000e+09	2.000e+09	2.000e+09	2.000e+09
7	19.5	0.	2.000e+09	2.000e+09	2.000e+09	2.000e+09	2.000e+09	2.000e+09	2.000e+09	2.000e+09	2.000e+09
8	22.5	0.	2.000e+09	2.000e+09	2.000e+09	2.000e+09	2.000e+09	2.000e+09	2.000e+09	2.000e+09	2.000e+09
9	25.5	0.	2.000e+09	2.000e+09	2.000e+09	2.000e+09	2.000e+09	2.000e+09	2.000e+09	2.000e+09	2.000e+09
10	28.5	0.	2.000e+09	2.000e+09	2.000e+09	2.000e+09	2.000e+09	2.000e+09	2.000e+09	2.000e+09	2.000e+09
11	31.5	0.	2.000e+09	2.000e+09	2.000e+09	2.000e+09	2.000e+09	2.000e+09	2.000e+09	2.000e+09	2.000e+09
12	34.5	0.	2.000e+09	2.000e+09	2.000e+09	2.000e+09	2.000e+09	2.000e+09	2.000e+09	2.000e+09	2.000e+09
13	37.5	0.	2.000e+09	2.000e+09	2.000e+09	2.000e+09	2.000e+09	2.000e+09	2.000e+09	2.000e+09	2.000e+09
14	40.5	0.	2.000e+09	2.000e+09	2.000e+09	2.000e+09	2.000e+09	2.000e+09	2.000e+09	2.000e+09	2.000e+09
15	43.5	0.	2.000e+09	2.000e+09	2.000e+09	2.000e+09	2.000e+09	2.000e+09	2.000e+09	2.000e+09	2.000e+09
16	46.5	0.	2.000e+09	2.000e+09	2.000e+09	2.000e+09	2.000e+09	2.000e+09	2.000e+09	2.000e+09	2.000e+09
17	49.5	0.	2.000e+09	2.000e+09	2.000e+09	2.000e+09	2.000e+09	2.000e+09	2.000e+09	2.000e+09	2.000e+09
18	52.5	0.	2.000e+09	2.000e+09	2.000e+09	2.000e+09	2.000e+09	2.000e+09	2.000e+09	2.000e+09	2.000e+09

kyy

	x	0.400	0.600	0.750	0.850	0.920	0.970	1.000
1	1.5	5.000e+10	5.000e+10	5.000e+10	5.000e+10	5.000e+10	5.000e+10	0.
2	4.5	5.000e+10	5.000e+10	5.000e+10	5.000e+10	5.000e+10	5.000e+10	0.
3	7.5	5.000e+10	5.000e+10	5.000e+10	5.000e+10	5.000e+10	5.000e+10	0.
4	10.5	5.000e+10	5.000e+10	5.000e+10	5.000e+10	2.000e+09	2.000e+09	0.
5	13.5	5.000e+10	2.000e+09	2.000e+09	2.000e+09	2.000e+09	2.000e+09	0.
6	16.5	2.000e+09	2.000e+09	2.000e+09	2.000e+09	2.000e+09	2.000e+09	0.
7	19.5	2.000e+09	2.000e+09	2.000e+09	2.000e+09	2.000e+09	2.000e+09	0.
8	22.5	2.000e+09	2.000e+09	2.000e+09	2.000e+09	2.000e+09	2.000e+09	0.
9	25.5	2.000e+09	2.000e+09	2.000e+09	2.000e+09	2.000e+09	2.000e+09	0.
10	28.5	2.000e+09	2.000e+09	2.000e+09	2.000e+09	2.000e+09	2.000e+09	0.
11	31.5	2.000e+09	2.000e+09	2.000e+09	2.000e+09	2.000e+09	2.000e+09	0.
12	34.5	2.000e+09	2.000e+09	2.000e+09	2.000e+09	2.000e+09	2.000e+09	0.
13	37.5	2.000e+09	2.000e+09	2.000e+09	2.000e+09	2.000e+09	2.000e+09	0.
14	40.5	2.000e+09	2.000e+09	2.000e+09	2.000e+09	2.000e+09	2.000e+09	0.
15	43.5	2.000e+09	2.000e+09	2.000e+09	2.000e+09	2.000e+09	2.000e+09	0.
16	46.5	2.000e+09	2.000e+09	2.000e+09	2.000e+09	2.000e+09	2.000e+09	0.
17	49.5	2.000e+09	2.000e+09	2.000e+09	2.000e+09	2.000e+09	2.000e+09	0.
18	52.5	2.000e+09	2.000e+09	2.000e+09	2.000e+09	2.000e+09	2.000e+09	0.

B.4-b Case B vertical eddy diffusion representation (K_{zz}, $cm^2\ s^{-1}$). Latitude zones are expressed in units of sine latitude. Altitude zones are expressed in units of km.

kzz

	x	-0.985	-0.945	-0.885	-0.800	-0.675	-0.500	-0.300	-0.100	0.100	0.300
1	0.0	0.	0.	0.	0.	0.	0.	0.	0.	0.	0.
2	3.0	5.000e+04	5.000e+04	5.000e+04	5.000e+04	5.000e+04	5.000e+04	5.000e+04	5.000e+04	5.000e+04	5.000e+04
3	6.0	5.000e+04	5.000e+04	5.000e+04	5.000e+04	5.000e+04	5.000e+04	5.000e+04	5.000e+04	5.000e+04	5.000e+04
4	9.0	2.500e+04	2.500e+04	5.000e+04	5.000e+04	5.000e+04	5.000e+04	5.000e+04	5.000e+04	5.000e+04	5.000e+04
5	12.0	1.000e+03	1.000e+03	1.000e+03	1.000e+03	5.000e+04	5.000e+04	5.000e+04	5.000e+04	5.000e+04	5.000e+04
6	15.0	1.000e+03	1.000e+03	1.000e+03	1.000e+03	1.000e+03	1.000e+03	1.000e+03	1.000e+03	1.000e+03	1.000e+03
7	18.0	1.000e+03	1.000e+03	1.000e+03	1.000e+03	1.000e+03	1.000e+03	1.000e+03	1.000e+03	1.000e+03	1.000e+03
8	21.0	1.000e+03	1.000e+03	1.000e+03	1.000e+03	1.000e+03	1.000e+03	1.000e+03	1.000e+03	1.000e+03	1.000e+03
9	24.0	1.000e+03	1.000e+03	1.000e+03	1.000e+03	1.000e+03	1.000e+03	1.000e+03	1.000e+03	1.000e+03	1.000e+03
10	27.0	1.000e+03	1.000e+03	1.000e+03	1.000e+03	1.000e+03	1.000e+03	1.000e+03	1.000e+03	1.000e+03	1.000e+03
11	30.0	1.000e+03	1.000e+03	1.000e+03	1.000e+03	1.000e+03	1.000e+03	1.000e+03	1.000e+03	1.000e+03	1.000e+03
12	33.0	2.045e+03	2.045e+03	2.045e+03	2.045e+03	2.045e+03	2.045e+03	2.045e+03	2.045e+03	2.045e+03	2.045e+03
13	36.0	3.980e+03	3.980e+03	3.980e+03	3.980e+03	3.980e+03	3.980e+03	3.980e+03	3.980e+03	3.980e+03	3.980e+03
14	39.0	8.155e+03	8.155e+03	8.155e+03	8.155e+03	8.155e+03	8.155e+03	8.155e+03	8.155e+03	8.155e+03	8.155e+03
15	42.0	1.360e+04	1.360e+04	1.360e+04	1.360e+04	1.360e+04	1.360e+04	1.360e+04	1.360e+04	1.360e+04	1.360e+04
16	45.0	2.180e+04	2.180e+04	2.180e+04	2.180e+04	2.180e+04	2.180e+04	2.180e+04	2.180e+04	2.180e+04	2.180e+04
17	48.0	3.420e+04	3.420e+04	3.420e+04	3.420e+04	3.420e+04	3.420e+04	3.420e+04	3.420e+04	3.420e+04	3.420e+04
18	51.0	5.475e+04	5.475e+04	5.475e+04	5.475e+04	5.475e+04	5.475e+04	5.475e+04	5.475e+04	5.475e+04	5.475e+04
19	54.0	8.580e+04	8.580e+04	8.580e+04	8.580e+04	8.580e+04	8.580e+04	8.580e+04	8.580e+04	8.580e+04	8.580e+04

kzz

	x	0.500	0.675	0.800	0.885	0.945	0.985
1	0.0	0.	0.	0.	0.	0.	0.
2	3.0	5.000e+04	5.000e+04	5.000e+04	5.000e+04	5.000e+04	5.000e+04
3	6.0	5.000e+04	5.000e+04	5.000e+04	5.000e+04	5.000e+04	5.000e+04
4	9.0	5.000e+04	5.000e+04	5.000e+04	5.000e+04	2.500e+04	2.500e+04
5	12.0	5.000e+04	5.000e+04	1.000e+03	1.000e+03	1.000e+03	1.000e+03
6	15.0	1.000e+03	1.000e+03	1.000e+03	1.000e+03	1.000e+03	1.000e+03
7	18.0	1.000e+03	1.000e+03	1.000e+03	1.000e+03	1.000e+03	1.000e+03
8	21.0	1.000e+03	1.000e+03	1.000e+03	1.000e+03	1.000e+03	1.000e+03
9	24.0	1.000e+03	1.000e+03	1.000e+03	1.000e+03	1.000e+03	1.000e+03
10	27.0	1.000e+03	1.000e+03	1.000e+03	1.000e+03	1.000e+03	1.000e+03
11	30.0	1.000e+03	1.000e+03	1.000e+03	1.000e+03	1.000e+03	1.000e+03
12	33.0	2.045e+03	2.045e+03	2.045e+03	2.045e+03	2.045e+03	2.045e+03
13	36.0	3.980e+03	3.980e+03	3.980e+03	3.980e+03	3.980e+03	3.980e+03
14	39.0	8.155e+03	8.155e+03	8.155e+03	8.155e+03	8.155e+03	8.155e+03
15	42.0	1.360e+04	1.360e+04	1.360e+04	1.360e+04	1.360e+04	1.360e+04
16	45.0	2.180e+04	2.180e+04	2.180e+04	2.180e+04	2.180e+04	2.180e+04
17	48.0	3.420e+04	3.420e+04	3.420e+04	3.420e+04	3.420e+04	3.420e+04
18	51.0	5.475e+04	5.475e+04	5.475e+04	5.475e+04	5.475e+04	5.475e+04
19	54.0	8.580e+04	8.580e+04	8.580e+04	8.580e+04	8.580e+04	8.580e+04

B.5-a Case G vertical eddy diffusion representation (K_{yy}, $cm^2\ s^{-1}$). Latitude zones are expressed in units of sine latitude. Altitude zones are expressed in units of km.

edit january 1

kyy

	x	-1.000	-0.970	-0.920	-0.850	-0.750	-0.600	-0.400	-0.200	0.000	0.200
1	1.5	0.	5.000e+10	5.000e+10	5.000e+10	5.000e+10	5.000e+10	5.000e+10	5.000e+10	5.000e+10	5.000e+10
2	4.5	0.	5.000e+10	5.000e+10	5.000e+10	5.000e+10	5.000e+10	5.000e+10	5.000e+10	5.000e+10	5.000e+10
3	7.5	0.	5.000e+10	5.000e+10	5.000e+10	5.000e+10	5.000e+10	5.000e+10	5.000e+10	5.000e+10	5.000e+10
4	10.5	0.	4.499e+09	5.343e+09	5.000e+10	5.000e+10	5.000e+10	5.000e+10	5.000e+10	5.000e+10	5.000e+10
5	13.5	0.	4.499e+09	5.343e+09	5.351e+09	4.670e+09	3.582e+09	5.000e+10	5.000e+10	5.000e+10	5.000e+10
6	16.5	0.	4.499e+09	5.343e+09	5.351e+09	4.670e+09	3.582e+09	1.315e+09	2.000e+08	2.000e+08	2.000e+08
7	19.5	0.	4.499e+09	5.343e+09	5.351e+09	4.670e+09	3.582e+09	1.315e+09	2.000e+08	2.000e+08	2.000e+08
8	22.5	0.	4.499e+09	5.343e+09	5.351e+09	4.670e+09	3.582e+09	1.315e+09	2.000e+08	2.000e+08	2.000e+08
9	25.5	0.	4.499e+09	5.343e+09	5.351e+09	4.670e+09	3.582e+09	1.315e+09	2.000e+08	2.000e+08	2.000e+08
10	28.5	0.	4.499e+09	5.343e+09	5.351e+09	4.670e+09	3.582e+09	1.315e+09	2.000e+08	2.000e+08	2.000e+08
11	31.5	0.	4.499e+09	5.343e+09	5.351e+09	4.670e+09	3.582e+09	1.315e+09	2.000e+08	2.000e+08	2.000e+08
12	34.5	0.	4.499e+09	5.343e+09	5.351e+09	4.670e+09	3.582e+09	1.315e+09	2.000e+08	2.000e+08	2.000e+08
13	37.5	0.	4.499e+09	5.343e+09	5.351e+09	4.670e+09	3.582e+09	1.315e+09	2.000e+08	2.000e+08	2.000e+08
14	40.5	0.	4.499e+09	5.343e+09	5.351e+09	4.670e+09	3.582e+09	1.315e+09	2.000e+08	2.000e+08	2.000e+08
15	43.5	0.	4.499e+09	5.343e+09	5.351e+09	4.670e+09	3.582e+09	1.315e+09	2.000e+08	2.000e+08	2.000e+08
16	46.5	0.	4.499e+09	5.343e+09	5.351e+09	4.670e+09	3.582e+09	1.315e+09	2.000e+08	2.000e+08	2.000e+08
17	49.5	0.	4.499e+09	5.343e+09	5.351e+09	4.670e+09	3.582e+09	1.315e+09	2.000e+08	2.000e+08	2.000e+08
18	52.5	0.	4.499e+09	5.343e+09	5.351e+09	4.670e+09	3.582e+09	1.315e+09	2.000e+08	2.000e+08	2.000e+08

kyy

	x	0.400	0.600	0.750	0.850	0.920	0.970	1.000
1	1.5	5.000e+10	5.000e+10	5.000e+10	5.000e+10	5.000e+10	5.000e+10	0.
2	4.5	5.000e+10	5.000e+10	5.000e+10	5.000e+10	5.000e+10	5.000e+10	0.
3	7.5	5.000e+10	5.000e+10	5.000e+10	5.000e+10	5.000e+10	5.000e+10	0.
4	10.5	5.000e+10	5.000e+10	5.000e+10	5.000e+10	1.242e+10	1.049e+10	0.
5	13.5	5.000e+10	9.207e+09	1.256e+10	1.279e+10	1.242e+10	1.049e+10	0.
6	16.5	2.951e+09	9.207e+09	1.256e+10	1.279e+10	1.242e+10	1.049e+10	0.
7	19.5	2.951e+09	9.207e+09	1.256e+10	1.279e+10	1.242e+10	1.049e+10	0.
8	22.5	2.951e+09	9.207e+09	1.256e+10	1.279e+10	1.242e+10	1.049e+10	0.
9	25.5	2.951e+09	9.207e+09	1.256e+10	1.279e+10	1.242e+10	1.049e+10	0.
10	28.5	2.951e+09	9.207e+09	1.256e+10	1.279e+10	1.242e+10	1.049e+10	0.
11	31.5	2.951e+09	9.207e+09	1.256e+10	1.279e+10	1.242e+10	1.049e+10	0.
12	34.5	2.951e+09	9.207e+09	1.256e+10	1.279e+10	1.242e+10	1.049e+10	0.
13	37.5	2.951e+09	9.207e+09	1.256e+10	1.279e+10	1.242e+10	1.049e+10	0.
14	40.5	2.951e+09	9.207e+09	1.256e+10	1.279e+10	1.242e+10	1.049e+10	0.
15	43.5	2.951e+09	9.207e+09	1.256e+10	1.279e+10	1.242e+10	1.049e+10	0.
16	46.5	2.951e+09	9.207e+09	1.256e+10	1.279e+10	1.242e+10	1.049e+10	0.
17	49.5	2.951e+09	9.207e+09	1.256e+10	1.279e+10	1.242e+10	1.049e+10	0.
18	52.5	2.951e+09	9.207e+09	1.256e+10	1.279e+10	1.242e+10	1.049e+10	0.

B.5-b Case G vertical eddy diffusion representation (K_{yy}, $cm^2\ s^{-1}$) for April. Latitude zones are expressed in units of sine latitude. Altitude zones are expressed in units of km.

edit april 1

kyy

	x	-1.000	-0.970	-0.920	-0.850	-0.750	-0.600	-0.400	-0.200	0.000	0.200
1	1.5	0.	5.000e+10	5.000e+10	5.000e+10	5.000e+10	5.000e+10	5.000e+10	5.000e+10	5.000e+10	5.000e+10
2	4.5	0.	5.000e+10	5.000e+10	5.000e+10	5.000e+10	5.000e+10	5.000e+10	5.000e+10	5.000e+10	5.000e+10
3	7.5	0.	5.000e+10	5.000e+10	5.000e+10	5.000e+10	5.000e+10	5.000e+10	5.000e+10	5.000e+10	5.000e+10
4	10.5	0.	7.991e+09	9.377e+09	5.000e+10	5.000e+10	5.000e+10	5.000e+10	5.000e+10	5.000e+10	5.000e+10
5	13.5	0.	7.991e+09	9.377e+09	9.514e+09	9.050e+09	6.867e+09	5.000e+10	5.000e+10	5.000e+10	5.000e+10
6	16.5	0.	7.991e+09	9.377e+09	9.514e+09	9.050e+09	6.867e+09	2.561e+09	2.000e+08	2.000e+08	2.000e+08
7	19.5	0.	7.991e+09	9.377e+09	9.514e+09	9.050e+09	6.867e+09	2.561e+09	2.000e+08	2.000e+08	2.000e+08
8	22.5	0.	7.991e+09	9.377e+09	9.514e+09	9.050e+09	6.867e+09	2.561e+09	2.000e+08	2.000e+08	2.000e+08
9	25.5	0.	7.991e+09	9.377e+09	9.514e+09	9.050e+09	6.867e+09	2.561e+09	2.000e+08	2.000e+08	2.000e+08
10	28.5	0.	7.991e+09	9.377e+09	9.514e+09	9.050e+09	6.867e+09	2.561e+09	2.000e+08	2.000e+08	2.000e+08
11	31.5	0.	7.991e+09	9.377e+09	9.514e+09	9.050e+09	6.867e+09	2.561e+09	2.000e+08	2.000e+08	2.000e+08
12	34.5	0.	7.991e+09	9.377e+09	9.514e+09	9.050e+09	6.867e+09	2.561e+09	2.000e+08	2.000e+08	2.000e+08
13	37.5	0.	7.991e+09	9.377e+09	9.514e+09	9.050e+09	6.867e+09	2.561e+09	2.000e+08	2.000e+08	2.000e+08
14	40.5	0.	7.991e+09	9.377e+09	9.514e+09	9.050e+09	6.867e+09	2.561e+09	2.000e+08	2.000e+08	2.000e+08
15	43.5	0.	7.991e+09	9.377e+09	9.514e+09	9.050e+09	6.867e+09	2.561e+09	2.000e+08	2.000e+08	2.000e+08
16	46.5	0.	7.991e+09	9.377e+09	9.514e+09	9.050e+09	6.867e+09	2.561e+09	2.000e+08	2.000e+08	2.000e+08
17	49.5	0.	7.991e+09	9.377e+09	9.514e+09	9.050e+09	6.867e+09	2.561e+09	2.000e+08	2.000e+08	2.000e+08
18	52.5	0.	7.991e+09	9.377e+09	9.514e+09	9.050e+09	6.867e+09	2.561e+09	2.000e+08	2.000e+08	2.000e+08

kyy

	x	0.400	0.600	0.750	0.850	0.920	0.970	1.000
1	1.5	5.000e+10	5.000e+10	5.000e+10	5.000e+10	5.000e+10	5.000e+10	0.
2	4.5	5.000e+10	5.000e+10	5.000e+10	5.000e+10	5.000e+10	5.000e+10	0.
3	7.5	5.000e+10	5.000e+10	5.000e+10	5.000e+10	5.000e+10	5.000e+10	0.
4	10.5	5.000e+10	5.000e+10	5.000e+10	5.000e+10	8.418e+09	7.180e+09	0.
5	13.5	5.000e+10	6.104e+09	7.981e+09	8.505e+09	8.418e+09	7.180e+09	0.
6	16.5	2.339e+09	6.104e+09	7.981e+09	8.505e+09	8.418e+09	7.180e+09	0.
7	19.5	2.339e+09	6.104e+09	7.981e+09	8.505e+09	8.418e+09	7.180e+09	0.
8	22.5	2.339e+09	6.104e+09	7.981e+09	8.505e+09	8.418e+09	7.180e+09	0.
9	25.5	2.339e+09	6.104e+09	7.981e+09	8.505e+09	8.418e+09	7.180e+09	0.
10	28.5	2.339e+09	6.104e+09	7.981e+09	8.505e+09	8.418e+09	7.180e+09	0.
11	31.5	2.339e+09	6.104e+09	7.981e+09	8.505e+09	8.418e+09	7.180e+09	0.
12	34.5	2.339e+09	6.104e+09	7.981e+09	8.505e+09	8.418e+09	7.180e+09	0.
13	37.5	2.339e+09	6.104e+09	7.981e+09	8.505e+09	8.418e+09	7.180e+09	0.
14	40.5	2.339e+09	6.104e+09	7.981e+09	8.505e+09	8.418e+09	7.180e+09	0.
15	43.5	2.339e+09	6.104e+09	7.981e+09	8.505e+09	8.418e+09	7.180e+09	0.
16	46.5	2.339e+09	6.104e+09	7.981e+09	8.505e+09	8.418e+09	7.180e+09	0.
17	49.5	2.339e+09	6.104e+09	7.981e+09	8.505e+09	8.418e+09	7.180e+09	0.
18	52.5	2.339e+09	6.104e+09	7.981e+09	8.505e+09	8.418e+09	7.180e+09	0.

B.5-c Case G vertical eddy diffusion representation (K_{yy}, $cm^2\ s^{-1}$) for July. Latitude zones are expressed in units of sine latitude. Altitude zones are expressed in units of km.

edit july 1

kyy

	x	-1.000	-0.970	-0.920	-0.850	-0.750	-0.600	-0.400	-0.200	0.000	0.200
1	1.5	0.	5.000e+10	5.000e+10	5.000e+10	5.000e+10	5.000e+10	5.000e+10	5.000e+10	5.000e+10	5.000e+10
2	4.5	0.	5.000e+10	5.000e+10	5.000e+10	5.000e+10	5.000e+10	5.000e+10	5.000e+10	5.000e+10	5.000e+10
3	7.5	0.	5.000e+10	5.000e+10	5.000e+10	5.000e+10	5.000e+10	5.000e+10	5.000e+10	5.000e+10	5.000e+10
4	10.5	0.	1.050e+10	1.244e+10	5.000e+10	5.000e+10	5.000e+10	5.000e+10	5.000e+10	5.000e+10	5.000e+10
5	13.5	0.	1.050e+10	1.244e+10	1.281e+10	1.258e+10	9.223e+09	5.000e+10	5.000e+10	5.000e+10	5.000e+10
6	16.5	0.	1.050e+10	1.244e+10	1.281e+10	1.258e+10	9.223e+09	2.954e+09	2.000e+08	2.000e+08	2.000e+08
7	19.5	0.	1.050e+10	1.244e+10	1.281e+10	1.258e+10	9.223e+09	2.954e+09	2.000e+08	2.000e+08	2.000e+08
8	22.5	0.	1.050e+10	1.244e+10	1.281e+10	1.258e+10	9.223e+09	2.954e+09	2.000e+08	2.000e+08	2.000e+08
9	25.5	0.	1.050e+10	1.244e+10	1.281e+10	1.258e+10	9.223e+09	2.954e+09	2.000e+08	2.000e+08	2.000e+08
10	28.5	0.	1.050e+10	1.244e+10	1.281e+10	1.258e+10	9.223e+09	2.954e+09	2.000e+08	2.000e+08	2.000e+08
11	31.5	0.	1.050e+10	1.244e+10	1.281e+10	1.258e+10	9.223e+09	2.954e+09	2.000e+08	2.000e+08	2.000e+08
12	34.5	0.	1.050e+10	1.244e+10	1.281e+10	1.258e+10	9.223e+09	2.954e+09	2.000e+08	2.000e+08	2.000e+08
13	37.5	0.	1.050e+10	1.244e+10	1.281e+10	1.258e+10	9.223e+09	2.954e+09	2.000e+08	2.000e+08	2.000e+08
14	40.5	0.	1.050e+10	1.244e+10	1.281e+10	1.258e+10	9.223e+09	2.954e+09	2.000e+08	2.000e+08	2.000e+08
15	43.5	0.	1.050e+10	1.244e+10	1.281e+10	1.258e+10	9.223e+09	2.954e+09	2.000e+08	2.000e+08	2.000e+08
16	46.5	0.	1.050e+10	1.244e+10	1.281e+10	1.258e+10	9.223e+09	2.954e+09	2.000e+08	2.000e+08	2.000e+08
17	49.5	0.	1.050e+10	1.244e+10	1.281e+10	1.258e+10	9.223e+09	2.954e+09	2.000e+08	2.000e+08	2.000e+08
18	52.5	0.	1.050e+10	1.244e+10	1.281e+10	1.258e+10	9.223e+09	2.954e+09	2.000e+08	2.000e+08	2.000e+08

kyy

	x	0.400	0.600	0.750	0.850	0.920	0.970	1.000
1	1.5	5.000e+10	5.000e+10	5.000e+10	5.000e+10	5.000e+10	5.000e+10	0.
2	4.5	5.000e+10	5.000e+10	5.000e+10	5.000e+10	5.000e+10	5.000e+10	0.
3	7.5	5.000e+10	5.000e+10	5.000e+10	5.000e+10	5.000e+10	5.000e+10	0.
4	10.5	5.000e+10	5.000e+10	5.000e+10	5.000e+10	5.321e+09	4.480e+09	0.
5	13.5	5.000e+10	3.564e+09	4.646e+09	5.329e+09	5.321e+09	4.480e+09	0.
6	16.5	1.308e+09	3.564e+09	4.646e+09	5.329e+09	5.321e+09	4.480e+09	0.
7	19.5	1.308e+09	3.564e+09	4.646e+09	5.329e+09	5.321e+09	4.480e+09	0.
8	22.5	1.308e+09	3.564e+09	4.646e+09	5.329e+09	5.321e+09	4.480e+09	0.
9	25.5	1.308e+09	3.564e+09	4.646e+09	5.329e+09	5.321e+09	4.480e+09	0.
10	28.5	1.308e+09	3.564e+09	4.646e+09	5.329e+09	5.321e+09	4.480e+09	0.
11	31.5	1.308e+09	3.564e+09	4.646e+09	5.329e+09	5.321e+09	4.480e+09	0.
12	34.5	1.308e+09	3.564e+09	4.646e+09	5.329e+09	5.321e+09	4.480e+09	0.
13	37.5	1.308e+09	3.564e+09	4.646e+09	5.329e+09	5.321e+09	4.480e+09	0.
14	40.5	1.308e+09	3.564e+09	4.646e+09	5.329e+09	5.321e+09	4.480e+09	0.
15	43.5	1.308e+09	3.564e+09	4.646e+09	5.329e+09	5.321e+09	4.480e+09	0.
16	46.5	1.308e+09	3.564e+09	4.646e+09	5.329e+09	5.321e+09	4.480e+09	0.
17	49.5	1.308e+09	3.564e+09	4.646e+09	5.329e+09	5.321e+09	4.480e+09	0.
18	52.5	1.308e+09	3.564e+09	4.646e+09	5.329e+09	5.321e+09	4.480e+09	0.

B.5-d Case G vertical eddy diffusion representation (K_{yy}, $cm^2\ s^{-1}$) for October. Latitude zones are expressed in units of sine latitude. Altitude zones are expressed in units of km.

edit october 1

kyy

	x	-1.000	-0.970	-0.920	-0.850	-0.750	-0.600	-0.400	-0.200	0.000	0.200
1	1.5	0.	5.000e+10	5.000e+10	5.000e+10	5.000e+10	5.000e+10	5.000e+10	5.000e+10	5.000e+10	5.000e+10
2	4.5	0.	5.000e+10	5.000e+10	5.000e+10	5.000e+10	5.000e+10	5.000e+10	5.000e+10	5.000e+10	5.000e+10
3	7.5	0.	5.000e+10	5.000e+10	5.000e+10	5.000e+10	5.000e+10	5.000e+10	5.000e+10	5.000e+10	5.000e+10
4	10.5	0.	7.236e+09	8.482e+09	5.000e+10	5.000e+10	5.000e+10	5.000e+10	5.000e+10	5.000e+10	5.000e+10
5	13.5	0.	7.236e+09	8.482e+09	8.571e+09	8.050e+09	6.157e+09	5.000e+10	5.000e+10	5.000e+10	5.000e+10
6	16.5	0.	7.236e+09	8.482e+09	8.571e+09	8.050e+09	6.157e+09	2.361e+09	2.000e+08	2.000e+08	2.000e+08
7	19.5	0.	7.236e+09	8.482e+09	8.571e+09	8.050e+09	6.157e+09	2.361e+09	2.000e+08	2.000e+08	2.000e+08
8	22.5	0.	7.236e+09	8.482e+09	8.571e+09	8.050e+09	6.157e+09	2.361e+09	2.000e+08	2.000e+08	2.000e+08
9	25.5	0.	7.236e+09	8.482e+09	8.571e+09	8.050e+09	6.157e+09	2.361e+09	2.000e+08	2.000e+08	2.000e+08
10	28.5	0.	7.236e+09	8.482e+09	8.571e+09	8.050e+09	6.157e+09	2.361e+09	2.000e+08	2.000e+08	2.000e+08
11	31.5	0.	7.236e+09	8.482e+09	8.571e+09	8.050e+09	6.157e+09	2.361e+09	2.000e+08	2.000e+08	2.000e+08
12	34.5	0.	7.236e+09	8.482e+09	8.571e+09	8.050e+09	6.157e+09	2.361e+09	2.000e+08	2.000e+08	2.000e+08
13	37.5	0.	7.236e+09	8.482e+09	8.571e+09	8.050e+09	6.157e+09	2.361e+09	2.000e+08	2.000e+08	2.000e+08
14	40.5	0.	7.236e+09	8.482e+09	8.571e+09	8.050e+09	6.157e+09	2.361e+09	2.000e+08	2.000e+08	2.000e+08
15	43.5	0.	7.236e+09	8.482e+09	8.571e+09	8.050e+09	6.157e+09	2.361e+09	2.000e+08	2.000e+08	2.000e+08
16	46.5	0.	7.236e+09	8.482e+09	8.571e+09	8.050e+09	6.157e+09	2.361e+09	2.000e+08	2.000e+08	2.000e+08
17	49.5	0.	7.236e+09	8.482e+09	8.571e+09	8.050e+09	6.157e+09	2.361e+09	2.000e+08	2.000e+08	2.000e+08
18	52.5	0.	7.236e+09	8.482e+09	8.571e+09	8.050e+09	6.157e+09	2.361e+09	2.000e+08	2.000e+08	2.000e+08

kyy

	x	0.400	0.600	0.750	0.850	0.920	0.970	1.000
1	1.5	5.000e+10	5.000e+10	5.000e+10	5.000e+10	5.000e+10	5.000e+10	0.
2	4.5	5.000e+10	5.000e+10	5.000e+10	5.000e+10	5.000e+10	5.000e+10	0.
3	7.5	5.000e+10	5.000e+10	5.000e+10	5.000e+10	5.000e+10	5.000e+10	0.
4	10.5	5.000e+10	5.000e+10	5.000e+10	5.000e+10	9.313e+09	7.939e+09	0.
5	13.5	5.000e+10	6.818e+09	8.977e+09	9.445e+09	9.313e+09	7.939e+09	0.
6	16.5	2.553e+09	6.818e+09	8.977e+09	9.445e+09	9.313e+09	7.939e+09	0.
7	19.5	2.553e+09	6.818e+09	8.977e+09	9.445e+09	9.313e+09	7.939e+09	0.
8	22.5	2.553e+09	6.818e+09	8.977e+09	9.445e+09	9.313e+09	7.939e+09	0.
9	25.5	2.553e+09	6.818e+09	8.977e+09	9.445e+09	9.313e+09	7.939e+09	0.
10	28.5	2.553e+09	6.818e+09	8.977e+09	9.445e+09	9.313e+09	7.939e+09	0.
11	31.5	2.553e+09	6.818e+09	8.977e+09	9.445e+09	9.313e+09	7.939e+09	0.
12	34.5	2.553e+09	6.818e+09	8.977e+09	9.445e+09	9.313e+09	7.939e+09	0.
13	37.5	2.553e+09	6.818e+09	8.977e+09	9.445e+09	9.313e+09	7.939e+09	0.
14	40.5	2.553e+09	6.818e+09	8.977e+09	9.445e+09	9.313e+09	7.939e+09	0.
15	43.5	2.553e+09	6.818e+09	8.977e+09	9.445e+09	9.313e+09	7.939e+09	0.
16	46.5	2.553e+09	6.818e+09	8.977e+09	9.445e+09	9.313e+09	7.939e+09	0.
17	49.5	2.553e+09	6.818e+09	8.977e+09	9.445e+09	9.313e+09	7.939e+09	0.
18	52.5	2.553e+09	6.818e+09	8.977e+09	9.445e+09	9.313e+09	7.939e+09	0.

B.6-a Case H vertical eddy diffusion representation (K_{yy}, $cm^2\ s^{-1}$) for January. Latitude zones are expressed in units of sine latitude. Altitude zones are expressed in units of km.

edit january 1

kyy

	x	-1.000	-0.970	-0.920	-0.850	-0.750	-0.600	-0.400	-0.200	0.000	0.200
1	1.5	0.	5.000e+10	5.000e+10	5.000e+10	5.000e+10	5.000e+10	5.000e+10	5.000e+10	5.000e+10	5.000e+10
2	4.5	0.	5.000e+10	5.000e+10	5.000e+10	5.000e+10	5.000e+10	5.000e+10	5.000e+10	5.000e+10	5.000e+10
3	7.5	0.	5.000e+10	5.000e+10	5.000e+10	5.000e+10	5.000e+10	5.000e+10	5.000e+10	5.000e+10	5.000e+10
4	10.5	0.	1.211e+09	1.439e+09	5.000e+10	5.000e+10	5.000e+10	5.000e+10	5.000e+10	5.000e+10	5.000e+10
5	13.5	0.	1.211e+09	1.439e+09	1.441e+09	1.257e+09	9.644e+08	5.000e+10	5.000e+10	5.000e+10	5.000e+10
6	16.5	0.	1.211e+09	1.439e+09	1.441e+09	1.257e+09	9.644e+08	3.540e+08	5.385e+07	5.385e+07	5.385e+07
7	19.5	0.	1.211e+09	1.439e+09	1.441e+09	1.257e+09	9.644e+08	3.540e+08	5.385e+07	5.385e+07	5.385e+07
8	22.5	0.	1.211e+09	1.439e+09	1.441e+09	1.257e+09	9.644e+08	3.540e+08	5.385e+07	5.385e+07	5.385e+07
9	25.5	0.	1.211e+09	1.439e+09	1.441e+09	1.257e+09	9.644e+08	3.540e+08	5.385e+07	5.385e+07	5.385e+07
10	28.5	0.	1.211e+09	1.439e+09	1.441e+09	1.257e+09	9.644e+08	3.540e+08	5.385e+07	5.385e+07	5.385e+07
11	31.5	0.	1.211e+09	1.439e+09	1.441e+09	1.257e+09	9.644e+08	3.540e+08	5.385e+07	5.385e+07	5.385e+07
12	34.5	0.	1.211e+09	1.439e+09	1.441e+09	1.257e+09	9.644e+08	3.540e+08	5.385e+07	5.385e+07	5.385e+07
13	37.5	0.	1.211e+09	1.439e+09	1.441e+09	1.257e+09	9.644e+08	3.540e+08	5.385e+07	5.385e+07	5.385e+07
14	40.5	0.	1.211e+09	1.439e+09	1.441e+09	1.257e+09	9.644e+08	3.540e+08	5.385e+07	5.385e+07	5.385e+07
15	43.5	0.	1.211e+09	1.439e+09	1.441e+09	1.257e+09	9.644e+08	3.540e+08	5.385e+07	5.385e+07	5.385e+07
16	46.5	0.	1.211e+09	1.439e+09	1.441e+09	1.257e+09	9.644e+08	3.540e+08	5.385e+07	5.385e+07	5.385e+07
17	49.5	0.	1.211e+09	1.439e+09	1.441e+09	1.257e+09	9.644e+08	3.540e+08	5.385e+07	5.385e+07	5.385e+07
18	52.5	0.	1.211e+09	1.439e+09	1.441e+09	1.257e+09	9.644e+08	3.540e+08	5.385e+07	5.385e+07	5.385e+07

kyy

	x	0.400	0.600	0.750	0.850	0.920	0.970	1.000
1	1.5	5.000e+10	5.000e+10	5.000e+10	5.000e+10	5.000e+10	5.000e+10	0.
2	4.5	5.000e+10	5.000e+10	5.000e+10	5.000e+10	5.000e+10	5.000e+10	0.
3	7.5	5.000e+10	5.000e+10	5.000e+10	5.000e+10	5.000e+10	5.000e+10	0.
4	10.5	5.000e+10	5.000e+10	5.000e+10	5.000e+10	3.344e+09	2.824e+09	0.
5	13.5	5.000e+10	2.479e+09	3.382e+09	3.443e+09	3.344e+09	2.824e+09	0.
6	16.5	7.946e+08	2.479e+09	3.382e+09	3.443e+09	3.344e+09	2.824e+09	0.
7	19.5	7.946e+08	2.479e+09	3.382e+09	3.443e+09	3.344e+09	2.824e+09	0.
8	22.5	7.946e+08	2.479e+09	3.382e+09	3.443e+09	3.344e+09	2.824e+09	0.
9	25.5	7.946e+08	2.479e+09	3.382e+09	3.443e+09	3.344e+09	2.824e+09	0.
10	28.5	7.946e+08	2.479e+09	3.382e+09	3.443e+09	3.344e+09	2.824e+09	0.
11	31.5	7.946e+08	2.479e+09	3.382e+09	3.443e+09	3.344e+09	2.824e+09	0.
12	34.5	7.946e+08	2.479e+09	3.382e+09	3.443e+09	3.344e+09	2.824e+09	0.
13	37.5	7.946e+08	2.479e+09	3.382e+09	3.443e+09	3.344e+09	2.824e+09	0.
14	40.5	7.946e+08	2.479e+09	3.382e+09	3.443e+09	3.344e+09	2.824e+09	0.
15	43.5	7.946e+08	2.479e+09	3.382e+09	3.443e+09	3.344e+09	2.824e+09	0.
16	46.5	7.946e+08	2.479e+09	3.382e+09	3.443e+09	3.344e+09	2.824e+09	0.
17	49.5	7.946e+08	2.479e+09	3.382e+09	3.443e+09	3.344e+09	2.824e+09	0.
18	52.5	7.946e+08	2.479e+09	3.382e+09	3.443e+09	3.344e+09	2.824e+09	0.

B.6-b Case H vertical eddy diffusion representation (K_{yy}, $cm^2\ s^{-1}$) for April. Latitude zones are expressed in units of sine latitude. Altitude zones are expressed in units of km.

edit april 1

kyy

	x	-1.000	-0.970	-0.920	-0.850	-0.750	-0.600	-0.400	-0.200	0.000	0.200
1	1.5	0.	5.000e+10	5.000e+10	5.000e+10	5.000e+10	5.000e+10	5.000e+10	5.000e+10	5.000e+10	5.000e+10
2	4.5	0.	5.000e+10	5.000e+10	5.000e+10	5.000e+10	5.000e+10	5.000e+10	5.000e+10	5.000e+10	5.000e+10
3	7.5	0.	5.000e+10	5.000e+10	5.000e+10	5.000e+10	5.000e+10	5.000e+10	5.000e+10	5.000e+10	5.000e+10
4	10.5	0.	2.152e+09	2.525e+09	5.000e+10	5.000e+10	5.000e+10	5.000e+10	5.000e+10	5.000e+10	5.000e+10
5	13.5	0.	2.152e+09	2.525e+09	2.562e+09	2.437e+09	1.849e+09	5.000e+10	5.000e+10	5.000e+10	5.000e+10
6	16.5	0.	2.152e+09	2.525e+09	2.562e+09	2.437e+09	1.849e+09	6.896e+08	5.385e+07	5.385e+07	5.385e+07
7	19.5	0.	2.152e+09	2.525e+09	2.562e+09	2.437e+09	1.849e+09	6.896e+08	5.385e+07	5.385e+07	5.385e+07
8	22.5	0.	2.152e+09	2.525e+09	2.562e+09	2.437e+09	1.849e+09	6.896e+08	5.385e+07	5.385e+07	5.385e+07
9	25.5	0.	2.152e+09	2.525e+09	2.562e+09	2.437e+09	1.849e+09	6.896e+08	5.385e+07	5.385e+07	5.385e+07
10	28.5	0.	2.152e+09	2.525e+09	2.562e+09	2.437e+09	1.849e+09	6.896e+08	5.385e+07	5.385e+07	5.385e+07
11	31.5	0.	2.152e+09	2.525e+09	2.562e+09	2.437e+09	1.849e+09	6.896e+08	5.385e+07	5.385e+07	5.385e+07
12	34.5	0.	2.152e+09	2.525e+09	2.562e+09	2.437e+09	1.849e+09	6.896e+08	5.385e+07	5.385e+07	5.385e+07
13	37.5	0.	2.152e+09	2.525e+09	2.562e+09	2.437e+09	1.849e+09	6.896e+08	5.385e+07	5.385e+07	5.385e+07
14	40.5	0.	2.152e+09	2.525e+09	2.562e+09	2.437e+09	1.849e+09	6.896e+08	5.385e+07	5.385e+07	5.385e+07
15	43.5	0.	2.152e+09	2.525e+09	2.562e+09	2.437e+09	1.849e+09	6.896e+08	5.385e+07	5.385e+07	5.385e+07
16	46.5	0.	2.152e+09	2.525e+09	2.562e+09	2.437e+09	1.849e+09	6.896e+08	5.385e+07	5.385e+07	5.385e+07
17	49.5	0.	2.152e+09	2.525e+09	2.562e+09	2.437e+09	1.849e+09	6.896e+08	5.385e+07	5.385e+07	5.385e+07
18	52.5	0.	2.152e+09	2.525e+09	2.562e+09	2.437e+09	1.849e+09	6.896e+08	5.385e+07	5.385e+07	5.385e+07

kyy

	x	0.400	0.600	0.750	0.850	0.920	0.970	1.000
1	1.5	5.000e+10	5.000e+10	5.000e+10	5.000e+10	5.000e+10	5.000e+10	0.
2	4.5	5.000e+10	5.000e+10	5.000e+10	5.000e+10	5.000e+10	5.000e+10	0.
3	7.5	5.000e+10	5.000e+10	5.000e+10	5.000e+10	5.000e+10	5.000e+10	0.
4	10.5	5.000e+10	5.000e+10	5.000e+10	5.000e+10	2.267e+09	1.933e+09	0.
5	13.5	5.000e+10	1.644e+09	2.149e+09	2.290e+09	2.267e+09	1.933e+09	0.
6	16.5	6.299e+08	1.644e+09	2.149e+09	2.290e+09	2.267e+09	1.933e+09	0.
7	19.5	6.299e+08	1.644e+09	2.149e+09	2.290e+09	2.267e+09	1.933e+09	0.
8	22.5	6.299e+08	1.644e+09	2.149e+09	2.290e+09	2.267e+09	1.933e+09	0.
9	25.5	6.299e+08	1.644e+09	2.149e+09	2.290e+09	2.267e+09	1.933e+09	0.
10	28.5	6.299e+08	1.644e+09	2.149e+09	2.290e+09	2.267e+09	1.933e+09	0.
11	31.5	6.299e+08	1.644e+09	2.149e+09	2.290e+09	2.267e+09	1.933e+09	0.
12	34.5	6.299e+08	1.644e+09	2.149e+09	2.290e+09	2.267e+09	1.933e+09	0.
13	37.5	6.299e+08	1.644e+09	2.149e+09	2.290e+09	2.267e+09	1.933e+09	0.
14	40.5	6.299e+08	1.644e+09	2.149e+09	2.290e+09	2.267e+09	1.933e+09	0.
15	43.5	6.299e+08	1.644e+09	2.149e+09	2.290e+09	2.267e+09	1.933e+09	0.
16	46.5	6.299e+08	1.644e+09	2.149e+09	2.290e+09	2.267e+09	1.933e+09	0.
17	49.5	6.299e+08	1.644e+09	2.149e+09	2.290e+09	2.267e+09	1.933e+09	0.
18	52.5	6.299e+08	1.644e+09	2.149e+09	2.290e+09	2.267e+09	1.933e+09	0.

B.6-c Case H vertical eddy diffusion representation (K_{yy}, $cm^2\ s^{-1}$)for July. Latitude zones are expressed in units of sine latitude. Altitude zones are expressed in units of km.

edit july 1

kyy

	x	-1.000	-0.970	-0.920	-0.850	-0.750	-0.600	-0.400	-0.200	0.000	0.200
1	1.5	0.	5.000e+10	5.000e+10	5.000e+10	5.000e+10	5.000e+10	5.000e+10	5.000e+10	5.000e+10	5.000e+10
2	4.5	0.	5.000e+10	5.000e+10	5.000e+10	5.000e+10	5.000e+10	5.000e+10	5.000e+10	5.000e+10	5.000e+10
3	7.5	0.	5.000e+10	5.000e+10	5.000e+10	5.000e+10	5.000e+10	5.000e+10	5.000e+10	5.000e+10	5.000e+10
4	10.5	0.	2.828e+09	3.349e+09	5.000e+10	5.000e+10	5.000e+10	5.000e+10	5.000e+10	5.000e+10	5.000e+10
5	13.5	0.	2.828e+09	3.349e+09	3.450e+09	3.388e+09	2.483e+09	5.000e+10	5.000e+10	5.000e+10	5.000e+10
6	16.5	0.	2.828e+09	3.349e+09	3.450e+09	3.388e+09	2.483e+09	7.953e+08	5.385e+07	5.385e+07	5.385e+07
7	19.5	0.	2.828e+09	3.349e+09	3.450e+09	3.388e+09	2.483e+09	7.953e+08	5.385e+07	5.385e+07	5.385e+07
8	22.5	0.	2.828e+09	3.349e+09	3.450e+09	3.388e+09	2.483e+09	7.953e+08	5.385e+07	5.385e+07	5.385e+07
9	25.5	0.	2.828e+09	3.349e+09	3.450e+09	3.388e+09	2.483e+09	7.953e+08	5.385e+07	5.385e+07	5.385e+07
10	28.5	0.	2.828e+09	3.349e+09	3.450e+09	3.388e+09	2.483e+09	7.953e+08	5.385e+07	5.385e+07	5.385e+07
11	31.5	0.	2.828e+09	3.349e+09	3.450e+09	3.388e+09	2.483e+09	7.953e+08	5.385e+07	5.385e+07	5.385e+07
12	34.5	0.	2.828e+09	3.349e+09	3.450e+09	3.388e+09	2.483e+09	7.953e+08	5.385e+07	5.385e+07	5.385e+07
13	37.5	0.	2.828e+09	3.349e+09	3.450e+09	3.388e+09	2.483e+09	7.953e+08	5.385e+07	5.385e+07	5.385e+07
14	40.5	0.	2.828e+09	3.349e+09	3.450e+09	3.388e+09	2.483e+09	7.953e+08	5.385e+07	5.385e+07	5.385e+07
15	43.5	0.	2.828e+09	3.349e+09	3.450e+09	3.388e+09	2.483e+09	7.953e+08	5.385e+07	5.385e+07	5.385e+07
16	46.5	0.	2.828e+09	3.349e+09	3.450e+09	3.388e+09	2.483e+09	7.953e+08	5.385e+07	5.385e+07	5.385e+07
17	49.5	0.	2.828e+09	3.349e+09	3.450e+09	3.388e+09	2.483e+09	7.953e+08	5.385e+07	5.385e+07	5.385e+07
18	52.5	0.	2.828e+09	3.349e+09	3.450e+09	3.388e+09	2.483e+09	7.953e+08	5.385e+07	5.385e+07	5.385e+07

kyy

	x	0.400	0.600	0.750	0.850	0.920	0.970	1.000
1	1.5	5.000e+10	5.000e+10	5.000e+10	5.000e+10	5.000e+10	5.000e+10	0.
2	4.5	5.000e+10	5.000e+10	5.000e+10	5.000e+10	5.000e+10	5.000e+10	0.
3	7.5	5.000e+10	5.000e+10	5.000e+10	5.000e+10	5.000e+10	5.000e+10	0.
4	10.5	5.000e+10	5.000e+10	5.000e+10	5.000e+10	1.433e+09	1.206e+09	0.
5	13.5	5.000e+10	9.596e+08	1.251e+09	1.435e+09	1.433e+09	1.206e+09	0.
6	16.5	3.521e+08	9.596e+08	1.251e+09	1.435e+09	1.433e+09	1.206e+09	0.
7	19.5	3.521e+08	9.596e+08	1.251e+09	1.435e+09	1.433e+09	1.206e+09	0.
8	22.5	3.521e+08	9.596e+08	1.251e+09	1.435e+09	1.433e+09	1.206e+09	0.
9	25.5	3.521e+08	9.596e+08	1.251e+09	1.435e+09	1.433e+09	1.206e+09	0.
10	28.5	3.521e+08	9.596e+08	1.251e+09	1.435e+09	1.433e+09	1.206e+09	0.
11	31.5	3.521e+08	9.596e+08	1.251e+09	1.435e+09	1.433e+09	1.206e+09	0.
12	34.5	3.521e+08	9.596e+08	1.251e+09	1.435e+09	1.433e+09	1.206e+09	0.
13	37.5	3.521e+08	9.596e+08	1.251e+09	1.435e+09	1.433e+09	1.206e+09	0.
14	40.5	3.521e+08	9.596e+08	1.251e+09	1.435e+09	1.433e+09	1.206e+09	0.
15	43.5	3.521e+08	9.596e+08	1.251e+09	1.435e+09	1.433e+09	1.206e+09	0.
16	46.5	3.521e+08	9.596e+08	1.251e+09	1.435e+09	1.433e+09	1.206e+09	0.
17	49.5	3.521e+08	9.596e+08	1.251e+09	1.435e+09	1.433e+09	1.206e+09	0.
18	52.5	3.521e+08	9.596e+08	1.251e+09	1.435e+09	1.433e+09	1.206e+09	0.

B.6-d Case H vertical eddy diffusion representation (K_{yy}, $cm^2\ s^{-1}$) for October. Latitude zones are expressed in units of sine latitude. Altitude zones are expressed in units of km.

edit october 1

kyy

	x	-1.000	-0.970	-0.920	-0.850	-0.750	-0.600	-0.400	-0.200	0.000	0.200
1	1.5	0.	5.000e+10	5.000e+10	5.000e+10	5.000e+10	5.000e+10	5.000e+10	5.000e+10	5.000e+10	5.000e+10
2	4.5	0.	5.000e+10	5.000e+10	5.000e+10	5.000e+10	5.000e+10	5.000e+10	5.000e+10	5.000e+10	5.000e+10
3	7.5	0.	5.000e+10	5.000e+10	5.000e+10	5.000e+10	5.000e+10	5.000e+10	5.000e+10	5.000e+10	5.000e+10
4	10.5	0.	1.948e+09	2.284e+09	5.000e+10	5.000e+10	5.000e+10	5.000e+10	5.000e+10	5.000e+10	5.000e+10
5	13.5	0.	1.948e+09	2.284e+09	2.308e+09	2.167e+09	1.658e+09	5.000e+10	5.000e+10	5.000e+10	5.000e+10
6	16.5	0.	1.948e+09	2.284e+09	2.308e+09	2.167e+09	1.658e+09	6.356e+08	5.385e+07	5.385e+07	5.385e+07
7	19.5	0.	1.948e+09	2.284e+09	2.308e+09	2.167e+09	1.658e+09	6.356e+08	5.385e+07	5.385e+07	5.385e+07
8	22.5	0.	1.948e+09	2.284e+09	2.308e+09	2.167e+09	1.658e+09	6.356e+08	5.385e+07	5.385e+07	5.385e+07
9	25.5	0.	1.948e+09	2.284e+09	2.308e+09	2.167e+09	1.658e+09	6.356e+08	5.385e+07	5.385e+07	5.385e+07
10	28.5	0.	1.948e+09	2.284e+09	2.308e+09	2.167e+09	1.658e+09	6.356e+08	5.385e+07	5.385e+07	5.385e+07
11	31.5	0.	1.948e+09	2.284e+09	2.308e+09	2.167e+09	1.658e+09	6.356e+08	5.385e+07	5.385e+07	5.385e+07
12	34.5	0.	1.948e+09	2.284e+09	2.308e+09	2.167e+09	1.658e+09	6.356e+08	5.385e+07	5.385e+07	5.385e+07
13	37.5	0.	1.948e+09	2.284e+09	2.308e+09	2.167e+09	1.658e+09	6.356e+08	5.385e+07	5.385e+07	5.385e+07
14	40.5	0.	1.948e+09	2.284e+09	2.308e+09	2.167e+09	1.658e+09	6.356e+08	5.385e+07	5.385e+07	5.385e+07
15	43.5	0.	1.948e+09	2.284e+09	2.308e+09	2.167e+09	1.658e+09	6.356e+08	5.385e+07	5.385e+07	5.385e+07
16	46.5	0.	1.948e+09	2.284e+09	2.308e+09	2.167e+09	1.658e+09	6.356e+08	5.385e+07	5.385e+07	5.385e+07
17	49.5	0.	1.948e+09	2.284e+09	2.308e+09	2.167e+09	1.658e+09	6.356e+08	5.385e+07	5.385e+07	5.385e+07
18	52.5	0.	1.948e+09	2.284e+09	2.308e+09	2.167e+09	1.658e+09	6.356e+08	5.385e+07	5.385e+07	5.385e+07

kyy

	x	0.400	0.600	0.750	0.850	0.920	0.970	1.000
1	1.5	5.000e+10	5.000e+10	5.000e+10	5.000e+10	5.000e+10	5.000e+10	0.
2	4.5	5.000e+10	5.000e+10	5.000e+10	5.000e+10	5.000e+10	5.000e+10	0.
3	7.5	5.000e+10	5.000e+10	5.000e+10	5.000e+10	5.000e+10	5.000e+10	0.
4	10.5	5.000e+10	5.000e+10	5.000e+10	5.000e+10	2.508e+09	2.138e+09	0.
5	13.5	5.000e+10	1.836e+09	2.417e+09	2.543e+09	2.508e+09	2.138e+09	0.
6	16.5	6.874e+08	1.836e+09	2.417e+09	2.543e+09	2.508e+09	2.138e+09	0.
7	19.5	6.874e+08	1.836e+09	2.417e+09	2.543e+09	2.508e+09	2.138e+09	0.
8	22.5	6.874e+08	1.836e+09	2.417e+09	2.543e+09	2.508e+09	2.138e+09	0.
9	25.5	6.874e+08	1.836e+09	2.417e+09	2.543e+09	2.508e+09	2.138e+09	0.
10	28.5	6.874e+08	1.836e+09	2.417e+09	2.543e+09	2.508e+09	2.138e+09	0.
11	31.5	6.874e+08	1.836e+09	2.417e+09	2.543e+09	2.508e+09	2.138e+09	0.
12	34.5	6.874e+08	1.836e+09	2.417e+09	2.543e+09	2.508e+09	2.138e+09	0.
13	37.5	6.874e+08	1.836e+09	2.417e+09	2.543e+09	2.508e+09	2.138e+09	0.
14	40.5	6.874e+08	1.836e+09	2.417e+09	2.543e+09	2.508e+09	2.138e+09	0.
15	43.5	6.874e+08	1.836e+09	2.417e+09	2.543e+09	2.508e+09	2.138e+09	0.
16	46.5	6.874e+08	1.836e+09	2.417e+09	2.543e+09	2.508e+09	2.138e+09	0.
17	49.5	6.874e+08	1.836e+09	2.417e+09	2.543e+09	2.508e+09	2.138e+09	0.
18	52.5	6.874e+08	1.836e+09	2.417e+09	2.543e+09	2.508e+09	2.138e+09	0.

B.7 Case I vertical eddy diffusion representation (K_{yy}, cm^2 s^{-1}). Latitude zones are expressed in units of sine latitude. Altitude zones are expressed in units of km.

kyy

	x	-1.000	-0.970	-0.920	-0.850	-0.750	-0.600	-0.400	-0.200	0.000	0.200
1	1.5	0.	5.000e+10	5.000e+10	5.000e+10	5.000e+10	5.000e+10	5.000e+10	5.000e+10	5.000e+10	5.000e+10
2	4.5	0.	5.000e+10	5.000e+10	5.000e+10	5.000e+10	5.000e+10	5.000e+10	5.000e+10	5.000e+10	5.000e+10
3	7.5	0.	5.000e+10	5.000e+10	5.000e+10	5.000e+10	5.000e+10	5.000e+10	5.000e+10	5.000e+10	5.000e+10
4	10.5	0.	2.000e+08	2.000e+08	5.000e+10	5.000e+10	5.000e+10	5.000e+10	5.000e+10	5.000e+10	5.000e+10
5	13.5	0.	2.000e+08	2.000e+08	2.000e+08	2.000e+08	2.000e+08	5.000e+10	5.000e+10	5.000e+10	5.000e+10
6	16.5	0.	2.000e+08	2.000e+08	2.000e+08	2.000e+08	2.000e+08	2.000e+08	2.000e+08	2.000e+08	2.000e+08
7	19.5	0.	2.000e+08	2.000e+08	2.000e+08	2.000e+08	2.000e+08	2.000e+08	2.000e+08	2.000e+08	2.000e+08
8	22.5	0.	2.000e+08	2.000e+08	2.000e+08	2.000e+08	2.000e+08	2.000e+08	2.000e+08	2.000e+08	2.000e+08
9	25.5	0.	2.000e+08	2.000e+08	2.000e+08	2.000e+08	2.000e+08	2.000e+08	2.000e+08	2.000e+08	2.000e+08
10	28.5	0.	2.000e+08	2.000e+08	2.000e+08	2.000e+08	2.000e+08	2.000e+08	2.000e+08	2.000e+08	2.000e+08
11	31.5	0.	2.000e+08	2.000e+08	2.000e+08	2.000e+08	2.000e+08	2.000e+08	2.000e+08	2.000e+08	2.000e+08
12	34.5	0.	2.000e+08	2.000e+08	2.000e+08	2.000e+08	2.000e+08	2.000e+08	2.000e+08	2.000e+08	2.000e+08
13	37.5	0.	2.000e+08	2.000e+08	2.000e+08	2.000e+08	2.000e+08	2.000e+08	2.000e+08	2.000e+08	2.000e+08
14	40.5	0.	2.000e+08	2.000e+08	2.000e+08	2.000e+08	2.000e+08	2.000e+08	2.000e+08	2.000e+08	2.000e+08
15	43.5	0.	2.000e+08	2.000e+08	2.000e+08	2.000e+08	2.000e+08	2.000e+08	2.000e+08	2.000e+08	2.000e+08
16	46.5	0.	2.000e+08	2.000e+08	2.000e+08	2.000e+08	2.000e+08	2.000e+08	2.000e+08	2.000e+08	2.000e+08
17	49.5	0.	2.000e+08	2.000e+08	2.000e+08	2.000e+08	2.000e+08	2.000e+08	2.000e+08	2.000e+08	2.000e+08
18	52.5	0.	2.000e+08	2.000e+08	2.000e+08	2.000e+08	2.000e+08	2.000e+08	2.000e+08	2.000e+08	2.000e+08

kyy

	x	0.400	0.600	0.750	0.850	0.920	0.970	1.000
1	1.5	5.000e+10	5.000e+10	5.000e+10	5.000e+10	5.000e+10	5.000e+10	0.
2	4.5	5.000e+10	5.000e+10	5.000e+10	5.000e+10	5.000e+10	5.000e+10	0.
3	7.5	5.000e+10	5.000e+10	5.000e+10	5.000e+10	5.000e+10	5.000e+10	0.
4	10.5	5.000e+10	5.000e+10	5.000e+10	5.000e+10	2.000e+08	2.000e+08	0.
5	13.5	5.000e+10	2.000e+08	2.000e+08	2.000e+08	2.000e+08	2.000e+08	0.
6	16.5	2.000e+08	2.000e+08	2.000e+08	2.000e+08	2.000e+08	2.000e+08	0.
7	19.5	2.000e+08	2.000e+08	2.000e+08	2.000e+08	2.000e+08	2.000e+08	0.
8	22.5	2.000e+08	2.000e+08	2.000e+08	2.000e+08	2.000e+08	2.000e+08	0.
9	25.5	2.000e+08	2.000e+08	2.000e+08	2.000e+08	2.000e+08	2.000e+08	0.
10	28.5	2.000e+08	2.000e+08	2.000e+08	2.000e+08	2.000e+08	2.000e+08	0.
11	31.5	2.000e+08	2.000e+08	2.000e+08	2.000e+08	2.000e+08	2.000e+08	0.
12	34.5	2.000e+08	2.000e+08	2.000e+08	2.000e+08	2.000e+08	2.000e+08	0.
13	37.5	2.000e+08	2.000e+08	2.000e+08	2.000e+08	2.000e+08	2.000e+08	0.
14	40.5	2.000e+08	2.000e+08	2.000e+08	2.000e+08	2.000e+08	2.000e+08	0.
15	43.5	2.000e+08	2.000e+08	2.000e+08	2.000e+08	2.000e+08	2.000e+08	0.
16	46.5	2.000e+08	2.000e+08	2.000e+08	2.000e+08	2.000e+08	2.000e+08	0.
17	49.5	2.000e+08	2.000e+08	2.000e+08	2.000e+08	2.000e+08	2.000e+08	0.
18	52.5	2.000e+08	2.000e+08	2.000e+08	2.000e+08	2.000e+08	2.000e+08	0.

B.8 Case J vertical eddy diffusion representation (K_{yy}, $cm^2\ s^{-1}$). Latitude zones are expressed in units of sine latitude. Altitude zones are expressed in units of km.

kyy

	x	-1.000	-0.970	-0.920	-0.850	-0.750	-0.600	-0.400	-0.200	0.000	0.200
1	1.5	0.	5.000e+10	5.000e+10	5.000e+10	5.000e+10	5.000e+10	5.000e+10	5.000e+10	5.000e+10	5.000e+10
2	4.5	0.	5.000e+10	5.000e+10	5.000e+10	5.000e+10	5.000e+10	5.000e+10	5.000e+10	5.000e+10	5.000e+10
3	7.5	0.	5.000e+10	5.000e+10	5.000e+10	5.000e+10	5.000e+10	5.000e+10	5.000e+10	5.000e+10	5.000e+10
4	10.5	0.	2.000e+08	2.000e+08	5.000e+10	5.000e+10	5.000e+10	5.000e+10	5.000e+10	5.000e+10	5.000e+10
5	13.5	0.	2.000e+08	2.000e+08	2.000e+08	2.000e+08	2.000e+08	5.000e+10	5.000e+10	5.000e+10	5.000e+10
6	16.5	0.	2.000e+08	2.000e+08	2.000e+08	2.000e+08	2.000e+08	2.000e+08	2.000e+08	2.000e+08	2.000e+09
7	19.5	0.	2.000e+08	2.000e+08	2.000e+08	2.000e+08	2.000e+08	2.000e+08	2.000e+08	2.000e+08	2.000e+09
8	22.5	0.	2.000e+08	2.000e+08	2.000e+08	2.000e+08	2.000e+08	2.000e+08	2.000e+08	2.000e+08	2.000e+09
9	25.5	0.	2.000e+08	2.000e+08	2.000e+08	2.000e+08	2.000e+08	2.000e+08	2.000e+08	2.000e+08	2.000e+09
10	28.5	0.	2.000e+08	2.000e+08	2.000e+08	2.000e+08	2.000e+08	2.000e+08	2.000e+08	2.000e+08	2.000e+09
11	31.5	0.	2.000e+08	2.000e+08	2.000e+08	2.000e+08	2.000e+08	2.000e+08	2.000e+08	2.000e+08	2.000e+09
12	34.5	0.	2.000e+08	2.000e+08	2.000e+08	2.000e+08	2.000e+08	2.000e+08	2.000e+08	2.000e+08	2.000e+09
13	37.5	0.	2.000e+08	2.000e+08	2.000e+08	2.000e+08	2.000e+08	2.000e+08	2.000e+08	2.000e+08	2.000e+09
14	40.5	0.	2.000e+08	2.000e+08	2.000e+08	2.000e+08	2.000e+08	2.000e+08	2.000e+08	2.000e+08	2.000e+09
15	43.5	0.	2.000e+08	2.000e+08	2.000e+08	2.000e+08	2.000e+08	2.000e+08	2.000e+08	2.000e+08	2.000e+09
16	46.5	0.	2.000e+08	2.000e+08	2.000e+08	2.000e+08	2.000e+08	2.000e+08	2.000e+08	2.000e+08	2.000e+09
17	49.5	0.	2.000e+08	2.000e+08	2.000e+08	2.000e+08	2.000e+08	2.000e+08	2.000e+08	2.000e+08	2.000e+09
18	52.5	0.	2.000e+08	2.000e+08	2.000e+08	2.000e+08	2.000e+08	2.000e+08	2.000e+08	2.000e+08	2.000e+09

kyy

	x	0.400	0.600	0.750	0.850	0.920	0.970	1.000
1	1.5	5.000e+10	5.000e+10	5.000e+10	5.000e+10	5.000e+10	5.000e+10	0.
2	4.5	5.000e+10	5.000e+10	5.000e+10	5.000e+10	5.000e+10	5.000e+10	0.
3	7.5	5.000e+10	5.000e+10	5.000e+10	5.000e+10	5.000e+10	5.000e+10	0.
4	10.5	5.000e+10	5.000e+10	5.000e+10	5.000e+10	2.000e+09	2.000e+09	0.
5	13.5	5.000e+10	2.000e+09	2.000e+09	2.000e+09	2.000e+09	2.000e+09	0.
6	16.5	2.000e+09	2.000e+09	2.000e+09	2.000e+09	2.000e+09	2.000e+09	0.
7	19.5	2.000e+09	2.000e+09	2.000e+09	2.000e+09	2.000e+09	2.000e+09	0.
8	22.5	2.000e+09	2.000e+09	2.000e+09	2.000e+09	2.000e+09	2.000e+09	0.
9	25.5	2.000e+09	2.000e+09	2.000e+09	2.000e+09	2.000e+09	2.000e+09	0.
10	28.5	2.000e+09	2.000e+09	2.000e+09	2.000e+09	2.000e+09	2.000e+09	0.
11	31.5	2.000e+09	2.000e+09	2.000e+09	2.000e+09	2.000e+09	2.000e+09	0.
12	34.5	2.000e+09	2.000e+09	2.000e+09	2.000e+09	2.000e+09	2.000e+09	0.
13	37.5	2.000e+09	2.000e+09	2.000e+09	2.000e+09	2.000e+09	2.000e+09	0.
14	40.5	2.000e+09	2.000e+09	2.000e+09	2.000e+09	2.000e+09	2.000e+09	0.
15	43.5	2.000e+09	2.000e+09	2.000e+09	2.000e+09	2.000e+09	2.000e+09	0.
16	46.5	2.000e+09	2.000e+09	2.000e+09	2.000e+09	2.000e+09	2.000e+09	0.
17	49.5	2.000e+09	2.000e+09	2.000e+09	2.000e+09	2.000e+09	2.000e+09	0.
18	52.5	2.000e+09	2.000e+09	2.000e+09	2.000e+09	2.000e+09	2.000e+09	0.